Environmental influences on banana shrimps of the Sofala Bank, Mozambique Channel

Bernardino Sérgio Malauene

A thesis presented in fulfillment of the requirement for the degree of

Doctor of Philosophy

Faculty of Science, Department of Biological Sciences

University of Cape Town

South Africa

December, 2014

Environmental influences on banana shrimps of the Sofala Bank, Mozambique Channel

By

Bernardino Sérgio Malauene

Submitted in fulfillment of the requirements for the degree of

Doctor of Philosophy

in the Faculty of Science, Department of Biological Sciences, University of Cape Town

South Africa in December, 2014.

Thesis supervisors:

Ass. Prof. Coleen L. Moloney

Marine Research Institute and Department of Biological Sciences

University of Cape Town (UCT), Private Bag X3, Rondebosch 7701, Cape Town, South Africa

Dr. Michael J. Roberts

Oceans and Coasts Research - Department of Environmental Affairs

Bayworld Centre for Research and Education, PO Box 52126, Cape Town 8002, South Africa

Dr. Francis Marsac

Institut de Recherche pouré le Développement (IRD) - UMR 212 EME (Exploited Marine Ecosystems)

International Centre for Education, Marine and Atmospheric Sciences over Africa (ICEMASA)

UCT - Department of Oceanography, Private Bag X3, Rondebosch 7701, South Africa

Dr. Pierrick Penven

IRD - UMR 6523 LPO (LMI ICEMASA, CNRS, IFREMER, IRD, UBO)

Laboratoire de Physique des Oceans, Centre IRD de Bretagne, BP 70, Plouzane - France

Dr. Christophe Lett

IRD - UMI 209 UMMISCO

Centre de Recherche Halieutique Méditerranéenne et Tropicale, BP 171, Sète Cedex - France

Declaration

I hereby declare that this thesis is my own work and effort, both in concept and execution, with normal guidance and assistance from my supervisors.

Each significant contribution to, and quotation in, the above from the work (s), of other people has been attributed, and has been cited and referenced.

Neither the substance nor any part of the above thesis has been submitted in the past, or is being, or is to be submitted for a degree at this university or at any other university.

_____

Bernardino Sérgio Malauene

Cape Town, 15 December 2014

Dedication

I would like to dedicate this thesis my little daughter Zoe Malauene, “my zoea larva”. She has missed her father while I was busy in the processes of writing up this thesis.

Acknowledgments

This PhD thesis was both a joy and challenge to write; a joy because I grew up eating these shrimps and I hope that this work will contribute on sustainability of this resource so that the next generations also have the chance to taste it; and a challenge because it is a multidisciplinary study. There are persons and organizations, however, who have made the challenge much easier and I would like to kindly thank.

To the organizations that provided financial support for this study, international flight between Mozambique, South Africa and France, international conferences and symposiums, etc. I would like to express my sincere gratitude to; in alphabetical order: French Agence Inter-établissements de Recherche pour le Devéloppement (AIRD-DPF) through Campus France and the International Center for Education, Marine and Atmospheric Sciences over Africa (IRD-ICEMASA); Marine Research Institute (MA-RE Institute) at UCT and Mozambican Ministry of Science and Technology (MCT-PDRHCT) with assistance from the World Bank.

To my supervisors Ass. Prof. Coleen Moloney, Dr. Michael Roberts, Dr Francis Marsac, Dr Pierrick Penven and Dr. Christophe Lett. I am very grateful for your support and constant feedback during the development of this thesis, especially for sharing your knowledge, discussion of the results, suggestion "spot-on" and revision of the manuscript. I am fortunate to have you all as supervisor. Thanks for taking a chance on me as one of your student.

To Dr Atanasio Brito (shrimp ecologist and chief scientist at the Mozambican fisheries research institute – IIP) for especial collaboration and discussion on the Sofala Bank penaeid shrimps ecology. Thank for all you have done.

To Dr Nicolas Bez (IRD, France) and Dr Claire Saraux (IFREMER, France) for the discussion and suggestion on Chapter 2, especially on geostatistical. I appreciated and thank you.

To Dr James Penn (Director Emeritus of the Western Australian Fisheries and Marine Research Laboratories) for personal discussion and encouragement. Thank you for your especial time.

To Dr Genito Maure (Universidade Eduardo Mondlene, Mozambique and Climate System Analysis Group (CSAG) at UCT) and Izidine Pinto (CSAG) for the introduction to the self-

organizing map. Oh, and you have become my friend and family by sharing a flat during this thesis in Cape Town. I appreciate it – and thank you for everything.

To the CSAG/Oceanography high performance computer (CORE) at UCT, which is a wonderful initiative and without it, I would probably still be running simulation on my laptop. Thank to Dr Chris Jack, Rodger Duffett and Phillip Mukwenha for the technical support on CORE. Regarding technical support, I also thank Jerome Guiet for the help on the ROMS and Philippe Verley on Ichthyop. You deserve my gratitude for your effort to maintain this tool freely available and updated for the community.

To Carol Hartley and Welly Qwabe for proof reading and English grammar review. I am thankful.

To the IIP, especially the Director Paula Afonso and the former Director Domingos Gove for allowing me to go in study leave for this PhD thesis and continuous help. Thank for the *in-situ* data. Especial thanks to the people who are responsible for collecting and maintain the Sofala Bank data: to Lizette Palha de Sousa for the commercial logbook shrimp data, Silvia Abdula for the annual research survey shrimps data, and Emidio Andre for the CTDs. You are doing a great job, thank you.

To the Centre de Recherche Halieutique Méditerranéenne et Tropicale, IRD - Universite Montpellier II - Ifremer in Sète, France, especially the director Philippe Cury for hosting and giving me a working space during my stays in France. To Pascal Cauquil for hosting me on my second stay in Sete. Oh, and you took me to the mountain to see the snow and ski for first time at the age ... I am thankful for your friendship and everything you did.

To all my colleagues who have shared their special time with me in quasi-daily basis. In Prof Moloney's lab at UCT many thanks to Dr Hilkka Ndjaula, Ricardo Oliveros, Louis du Buisson and Grea Groenewald; at the UCT Oceanography Dept. to Dr Issufo Halo, Dr Yonss Jose, Dr Fialho Nehama, Dr Charine Collins, Obadias Cossa and Pavs Pillay (Ma-Re Institute); and in the research center in Sète to Robert Bauer, Daniel Grados and Marion Cuif.

To Gilly Smith for the assistance on the administrative and paper work for the university (re)registrations, study visa applications and etc. I appreciated and thank you.

Last but not least, to my beloved family and friends for the valuable personal support, my mother Vitoria Malauene, my father Bernardo Malauene, my sister Leopoldina and my brothers Heitor, David and Nelson. To Juliana Come, my wife, when I first told that I want to do this thesis you supported me. Thanks for your continuous support and encouragement. "Obrigado meu amor". Thank also to all my friends, there are many and I won't bore you with names.

Contents

Environmental influences on banana shrimps of the Sofala Bank, Mozambique Channel

By Bernardino Sérgio Malauene

Thesis submitted in fulfillment of the requirements for the degree of Doctor of Philosophy in the Faculty of Science, Department of Biological Sciences, University of Cape Town South Africa, December, 2014

Thesis Supervisors: Ass. Prof. Coleen Moloney, Dr Michael Roberts, Dr Francis Marsac, Dr Pierrick Penven and Dr Christophe Lett

Abstract

The Sofala Bank in the western Mozambique Channel is an essential habitat for shallow-water penaeid shrimps. It supports an important multi-sector and -species fishery, with *Fenneropenaeus indicus* and *Metapenaeus monoceros* (banana shrimp) being the two main target species. Over the past decade this valuable resource has been declining, which has been attributed to environmental changes, but no conclusive evidence has been found. This PhD thesis aims to understand the interactive roles of biophysical processes on recruitment of banana shrimps, particularly their larvae on the Sofala Bank. It is hypothesized that shrimp larvae can be advected offshore by passing mesoscale eddies to regions where they are unable to survive and are thus lost. In the absence of both physical and biological observations, a modelling approach is used. A high-resolution, nested, coastal, Regional Ocean Modeling System (ROMS) of the Sofala Bank is developed. In general, the model agrees well with available observations and literature. The ROMS outputs and self-organizing map analysis indicate that the shelf circulation, structure and river plumes are strongly influenced by the highly energetic offshore eddy activity. A biophysical, individual-based model (IBM) coupled to the ROMS was developed for early life stages of banana shrimps on the Sofala Bank. The IBM uses spawning patterns identified from analyses of both commercial and research survey data. Simulations indicate that shrimp larvae are lost offshore by entrainment in mesoscale eddies at inter- and intra-annual scales and eddies therefore are unlikely to produce a continuous declining in the catch. In contrast, these eddies induce onshore transport of larvae, promoting coastal settlement, compared with periods without eddies. Locations for simulated larval coastal settlement are identified: northern, central and southern. The roles of tides and larval diel vertical migration in influencing simulated larval settlement success was not conclusive; further research considering a selective tidal stream is needed. Simulated larvae were sensitive to low lethal temperature and river plumes. A conceptual model for the Sofala Bank circulation and another for the banana shrimps, early life history dynamics are proposed based on the results of this thesis.

Chapter 1

Introduction

Seafood is an important source of high-quality nutritious food and animal protein for much of the world's population (FAO, 1997), especially in developing countries (FAO, 2000). Fisheries provide livelihoods for local communities and foreign income for countries that export worldwide (FAO, 1997). Shrimps are considered the most valuable commercial seafood product traded worldwide (FAO, 2010, 2012). According to the FAO (2012), the wild shrimp catch of the world remains stable. However intra- and inter-annual variability in catch per unit effort of penaeid shrimps has been reported in some tropical and sub-tropical shallow waters around the world (López-Martínez et al., 2005; Diop et al., 2007).

Off the Mozambique coast, the Sofala Bank ($16 - 21°$S) is a key natural habitat for penaeid shrimps in the Western Indian Ocean (Ivanov and Hassan, 1976). It supports an important multi-sector and multi-species shallow water shrimp fishery, based on six species, of which the two most important are the closely related *Fenneropenaeus indicus* and *Metapenaeus monoceros*. These so-called "banana shrimps" contribute $> 80\%$ of the total catch (de Sousa et al., 2008). Sofala Bank shrimps are the main component of Mozambican export fisheries (de Sousa et al., 2006, 2013). For example, they contributed 55 million USD to the GDP in 2007 (de Sousa et al., 2008). The annual catch has been declining from typical historical levels of > 7000 tons from $2004 - 2006$ to a critical low level of ~ 2000 tons in 2012 (de Sousa et al., 2013). This decrease is thought to be related to low levels of recruitment, which was first attributed

to environmental factors (de Sousa et al., 2008, 2009). Recently, under continued low recruitment, a combination of detrimental environmental factors and overfishing has been proposed as the cause of poor recruitment, which is a major concern (de Sousa et al., 2013). However, no conclusive evidence of either overfishing or environmental factors has been found on the Sofala Bank.

Shrimp catch each year depends to a large extent on recruitment of juveniles into the fishery (Baxter, 1963; Ehrhardt and Legault, 1999; Diop et al., 2007). This is mainly driven by the level of spawning (Penn and Caputi, 1986; Gracia, 1991; Ye, 2000), and by environmental factors that influence larval transport and dispersal (Ehrhardt and Legault, 1999). Currents can transport shrimp larvae either shoreward or offshore (Penn, 1975; Rothlisberg et al., 1983). The Mozambique Channel circulation is dominated by mesoscale eddies (Sætre and da Silva, 1984; de Ruijter et al., 2002; Schouten et al., 2003) and rings (Halo et al., 2014). These features, and especially dipole eddies, can potentially provide mechanisms for the generation of high velocity offshore-directed boundary currents (Roberts et al., 2014; Ternon et al., 2014). Many studies have shown that eddy-induced currents can transport coastal biotic and abiotic material offshore (Quartly and Srokosz, 2004; Omta et al., 2009; Tew-Kai and Marsac, 2009; Kolasinski et al., 2012; Jose et al., 2014; Malauene et al., 2014; Roberts et al., 2014). It is hypothesized that shrimp larvae similarly can be transported to offshore regions where they are unable to survive. Therefore, they cannot contribute to recruitment into the fishery. In the absence of observations, a high-resolution ocean model of the Sofala Bank shelf that takes into account the offshore features is developed. This model is used here to set up a biophysical, dispersal model to test hypotheses about larval transport and dispersal. Ultimately, this information can be used to help implement adaptive management of the fishery.

Thesis objectives and hypotheses

The aim of this thesis is to extend understanding of the interactive roles of physical and biological processes on recruitment of penaeid shrimp populations in tropical, shallow-water, low productivity ecosystems. The impacts of currents, temperature, salinity and river plumes on shrimp populations will be investigated together with biological aspects of behavior, mortality,

shelf retention and settlement. The Sofala Bank, where the Mozambican shrimp fishery takes place, is selected as the study area. The objectives and hypotheses (note that the hypotheses are numbered related to the number of the chapter where they are addressed) of the thesis are to:

- identify and characterize the main areas and timing of spawning of banana shrimps on the Sofala Bank, using biological data from research surveys and commercial fisheries. It is hypothesized that: ($H_{2.1}$) spawning will not be uniformly distributed over the entire bank and ($H_{2.2}$) the timing and locations of spawning will be related to environmental factors (temperature, salinity and chlorophyll-a);

- investigate the influence of offshore eddies on: (1) the circulation of the Sofala Bank, (2) river plumes and in addition (3) investigate the effect of river plumes on the shelf circulation. It is hypothesised that: ($H_{4.1}$) while passing along the shelf break, anticyclonic eddies cause a poleward shelf current whereas cyclonic eddies cause an equatorward current, ($H_{4.2}$) the direction and size of the river plumes are influenced by offshore eddy activity and ($H_{4.3}$) the river plumes should influence the coastal and shelf circulation by changing the salinity, temperature and currents;

- investigate shelf retention and transport of simulated larvae of banana shrimps on the Sofala Bank, in relation to environmental processes such as eddies and temperature. It is hypothesised that: ($H_{5.1}$) banana shrimps spawn in locations that facilitate larval retention and ($H_{5.2}$) simulated larvae die when encountering cooler temperature than 20°C according to the available literature on physiological response reviewed in the introduction chapter.

- investigate transport and coastal settlement of simulated larvae of banana shrimps along the Sofala Bank, in relation to environmental processes (offshore eddies, tides and river plumes) and diel vertical migration. It is hypothesised that: ($H_{6.1}$) simulated larval coastal settlement is directly related to shelf retention, ($H_{6.2}$) larval settlement is not uniformly distributed over the entire coast of the Sofala Bank and ($H_{6.3}$) high settlement is not randomly distributed, but related to tides, which transport shrimp larvae towards

the coast, resulting in large transport success during spring tides.

Thesis outline

This PhD thesis has seven chapters. In the current Chapter, the next sections present a description of current understanding of the oceanography of the Sofala Bank and the Mozambique Channel, the biology of the penaeid shrimps and the description of the shrimp fishery and catch on the Sofala Bank. In Chapter 2 the main areas and timing of spawning of banana shrimps on the Sofala Bank are identified and characterized in relation to geographical and environmental variables. The hypotheses $H_{2.1}$ and $H_{2.2}$ are tested here. Chapter 3 presents the configuration and the implementation of a high-resolution ocean model (ROMS) for coastal applications on the Sofala Bank and adjacent offshore waters. It evaluates the performance of the model by comparing simulations and observations. Chapter 4 uses the model results together with self-organizing maps to describe the likely impact of offshore eddies on the shelf circulation and variability of river plumes. The effect of the buoyant plume on the nearby circulation is investigated. This Chapter tests hypotheses $H_{4.1}$ to $H_{4.3}$. In Chapters 5 and 6 an individual-based model configuration using ICHTHYOP and incorporating outputs of the Sofala Bank ROMS model is developed. Chapter 5 investigates the role of highly energetic and complex offshore eddy activity on shelf retention and long-distance dispersal of simulated larvae. In this Chapter the effect of cool, lethal temperatures on shelf retention is presented and hypotheses $H_{5.1}$ and $H_{5.2}$ are tested. Chapter 6 focuses on simulated larval settlement along the coast and, in the absence of *in-situ* data, uses model results to identify potential best locations for settlement success. Small-scale processes and features relevant to coastal larval settlement, like diel vertical migration, tides and rivers, are assessed and discussed. This chapter tests hypotheses $H_{6.1}$ to $H_{6.3}$. Finally, Chapter 7 synthesizes and concludes the work of the thesis as a whole. It proposes an updated conceptual model of biophysical processes influencing banana shrimps, makes recommendations for the management of the national shrimp fishery in Mozambique, and suggests areas for further research.

1.1 Background

1.1.1 Study area

The Sofala Bank is located on the central Mozambique Channel between Madagascar and the African mainland, on the western side of the channel between 16°S (near Angoche) and 21°S (north of Bazaruto archipelago; Fig. 1.1). The continental shelf is generally shallow and wide, with an average depth $20-30$ m and the 200 m isobath is found far offshore except in the north where the 200 m is isobath close to the coast (Fig. 1.1). The Sofala Bank is characterized by strong semi-diurnal tides (Chevane, 2013) and it is a world's "hotspot" for internal tides and wave generation (da Silva et al., 2009). The bank is a transition zone between two surface water masses (Sætre and da Silva, 1982; de Ruijter et al., 2002; Johnesen et al., 2008): the warm tropical surface water to the north and the relative cool sub-tropical surface water to the south.

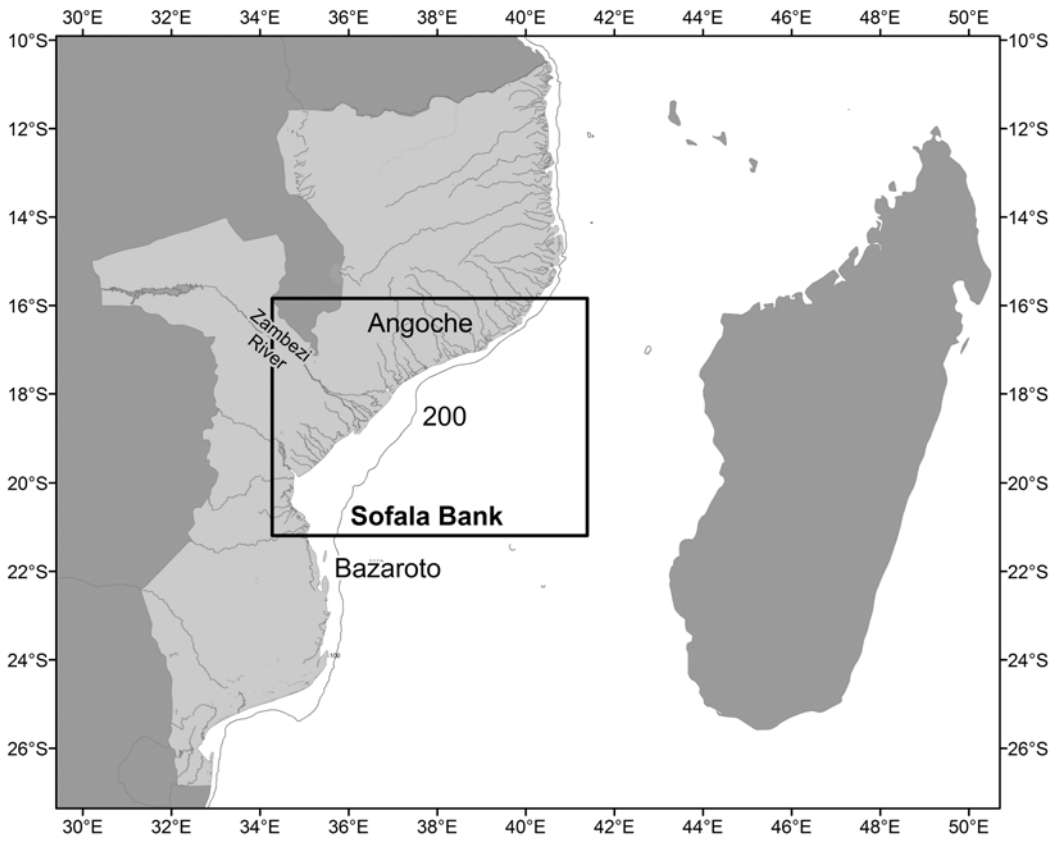

Figure 1.1: Map of the Mozambique Channel with the Sofala Bank study area outlined by the black box.

Atmospheric variables: The climate is characterized by two main seasons, winter and summer that influence the sea surface temperature and salinity. Winter is relatively cool and dry between May and October, whereas summer is warm, humid and rainy between November and April. Wind is another important factor influencing coastal circulation. Wind in the Mozambique coast is dominated by two regimes: the southeast (SE) trade winds and the East Africa monsoon (Sætre and da Silva, 1982). The Sofala Bank, again, is the transition zone between the two wind regimes. The SE trade winds dominate in the south with prevailing easterly winds all year-round. The north is influenced by the southern extension of the East African monsoon. The monsoon exhibits seasonal variability with two distinct regimes: (1) the southwest monsoon associated with strong ($> 10\,\mathrm{m}\cdot\mathrm{s}^{-1}$) winds during winter and (2) the northeast monsoon characterized by relative weak ($< 8\,\mathrm{m}\cdot\mathrm{s}^{-1}$) northeasterly winds during summer (Sætre and da Silva, 1982; Malauene et al., 2014).

Eddies and circulation in the Mozambique Channel: The Mozambique Channel, on a global scale, is an extremely energetic region, in which the circulation is dominated by trains of intermittent, passing mesoscale eddies (Sætre and da Silva 1982, 1984; Biastoch and Krauss 1999; de Ruijter et al. 2002; Lutjeharms 2006; Tew-Kai and Marsac 2009). Recently Halo et al. (2014) demonstrated that indeed these mesoscale vortices actually have properties of rings rather than eddies. They stated that the difference between eddies and rings is in the shape of their vorticity, which is close to a bell profile for the cyclonic and the small anticyclonic eddies while for large anticyclones rings is characterized by a plateau in the core of the vortex. Most of the eddies are formed within the channel in relation to baroclinic instabilities of the flow (Halo 2012; Halo et al. 2014). Although cyclonic eddies also occur, the majority of these mesoscale features are anticyclonic in nature (Fig. 1.2). Both model and observational studies have proposed that, on average, about four to six large anticyclonic eddies are found per year (de Ruijter et al. 2002; Schouten et al. 2003; Backeberg et al. 2008; Halo et al. 2014). They have diameters of approximately $300 - 400$ km (Backeberg et al. 2008). They propagate southwards at approximately $3 - 6\,\mathrm{km}\cdot\mathrm{day}^{-1}$ with currents reaching up to $2\,\mathrm{m}\cdot\mathrm{s}^{-1}$ at their edges (Schouten et al. 2003). The average net southward water volume transport has been estimated to be approximately 14 Sv at the narrow section of the Mozambique Channel at $\sim 17°\mathrm{S}$ (Ridderinkhof and de Ruijter 2003; Lutjeharms 2006), but varies between $9 - 20$ Sv

depending on the study and method used.

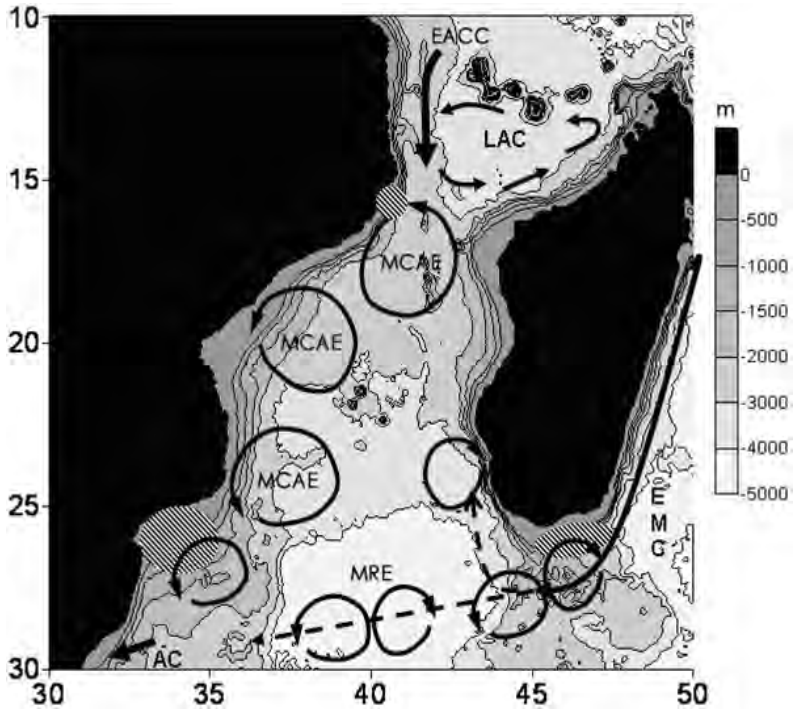

Figure 1.2: General circulation in the Mozambique Channel superimposed in the bathymetry (Tew-Kai and Marsac 2009). Where EACC is the South Equatorial Current; MCAE are the Mozambique Channel anti-cyclonic eddies; EMC is the East Madagascar Current; MRE is the south east Madagascar dipolar eddies and AC is the Agulhas Current. The white area with black points represents the lee eddy off Angoche and Maputo Bight.

***Productivity*:** Primary production is important for feeding larvae of the banana shrimps. Chlorophyll gives the first indication of biological production in the ocean. In the case of the Mozambique coast, highest chlorophyll-a (Chl-a) levels are observed in the upwelling cell near Angoche, on the northernmost limit of the Sofala Bank (Nehring et al., 1987; Malauene et al., 2014). In contrast, the general Mozambique Channel has relatively low (0.3 $\text{mg} \cdot \text{m}^{-3}$) Chl-$a$ concentrations (Omta et al. 2009). Studies using satellite observation (Tew-Kai and Marsac, 2009) and biogeochemical models (Jose et al., 2014) have shown that Chl-a concentration is usually higher on the shelf compared to offshore. There is a weak seasonality in the surface Chl-a concentration in the central ($16-24°$S) Mozambique Channel compared to the north and south due to strong eddy influences (Tew-Kai and Marsac, 2009; Omta et al., 2009). Offshore mesoscale eddies interact with the continental shelf and advect coastal production offshore (Tew-Kai and Marsac, 2009; Omta et al., 2009; Lamont et al., 2014; Jose et al., 2014; Malauene et al., 2014; Roberts et al., 2014). This was supported by a study using natural isotope tracers that

found two sources of productivity: (1) active autochthonous, local upwelled (i.e. new) production within the cyclonic eddies and (2) allochthonous coastal (i.e. old) production advected by eddies (Kolasinski et al., 2012). The phytoplankton surface community structure is dominated by prokaryotes (Barlow et al., 2014), however diatoms were also found near the shelf and eddy boundaries, supporting offshore entrainment of coastal production. Similarly, mesozooplankton ($> 200\,\mu$m) are advected and redistributed offshore by eddies (Huggett, 2014). Although microzooplankton ($< 200\,\mu$m) were misampled by the former study's 200 μm mesh multi-net, the author thought that they may also be present in larger numbers. Overall, although the Mozambique Channel is characterized by low productivity (oligotrophic) waters, the mesoescale eddies play an important ecological role in redistributing and enhancing productivity.

Rivers: There are a number of rivers draining into the marine ecosystem of the Sofala Bank, the major being the fourth largest African watershed−the Zambezi River (Fig. 1.1). The minor rivers contribute with small amounts of freshwater inputs. The Zambezi River discharge rate is an average of 3000 $m^3 \cdot s^{-1}$ (Gammelsrod, 1992), with large loads of sedimentary organic matter inputs. The freshwater runoff is seasonal in relation to the rain season, with the maximum runoff ($60 - 90\%$) between January and March and the minimum in October (Sætre and da Silva, 1982). The freshwater runoffs from the Zambezi River generate a buoyant plume (Fig. 1.3), which influences the dynamics of the Sofala Bank (Nehama, 2012). Consequently, it is thought to influence the yield of the shrimp fishery (Gammelsrod, 1992) through dispersal and recruitment of larvae. It has been proposed that increased river runoff, which reduces salinity and alters temperature, reduces net growth rates, distribution and abundance of *Litopenaeus setiferus* in estuarine nursery areas of southeastern Louisiana (Rozas and Minello, 2011). In contrast, a study by Galindo-Bect et al. (2000) suggested that decreases in freshwater discharge of the Colorado River in the Gulf of California potentially decreased *Litopenaeus stylirostris* landings. These results suggest that river inputs can have negative or positive impacts on the shrimps. On the Sofala Bank, freshwater runoff is thought to have a positive impact on coastal shrimp species (*F. indicus* and *M. monoceros*), whereas species having more oceanic affinities are negatively impacted (de Sousa et al. 2008). However, thus far no conclusive evidence has been found. In general, studies are limited on the impacts of river runoff, such as from the Zambezi, on Sofala Bank shrimp populations.

Figure 1.3: Plume of Zambezi River. (NASA Earth Observatory true color image by Robert Simmon, using Landsat 8 data from the USGS Earth Explorer captured on August 29, 2013 and available at http://visibleearth.nasa.gov/view.php?id=82361.)

1.1.2 The biology of penaeid shrimps

Penaeid shrimps are members of the order Decapoda (De Grave et al., 2009), which is a group of crustaceans that have ten legs. They are characterized by their unique shape and the number of teeth on the rostrum. The natural distribution of penaeid shrimps is widespread, occurring in shallow and inshore, tropical and sub-tropical waters (roughly between 40°N and 40°S), with influence of freshwater river runoff. Six species of penaeid shrimp are native to the Sofala Bank: *Fenneropenaeus indicus* formerly *Penaeus indicus*, *Metapenaeus monoceros*, *Penaeus japonicus*, *Penaeus monodon*, *Penaeus semisulcatus* and *Penaeus latisulcatus* (Ivanov and Hassan, 1976). *Fenneropenaeus indicus* and *M. monoceros* are related species, are the most important commercially and together are called "banana shrimps" (de Sousa et al., 2006). Over the past few (~ 4) years two invasive non-native species of penaeid shrimp (*Metapenaeus dobsoni* and *Parapenaeopsis sculptilis*) have been observed on the Mozambique coast, first at Maputo Bay and then on the Sofala Bank (Atanásio Brito and Luísa Simbine, personal communication). Correctly, the idea that the non-native species can compete with the commercially important depleted native species is becoming a major concern.

There are two groups of penaeid shrimps, distinguished on the basis of the female thelycum, an organ that receives and stores the spermatophore from the male during mating (Dall et al., 1990). The first group "open-thelycum" occurs on the Atlantic coast of North, Central and South America, and the second group "closed-thelycum" occurs off the Indo-West Pacific (Australia and Asia), the eastern part of the Mediterranean Sea and East Africa, including the Sofala Bank (Primavera, 1985; Yano, 1995). All the penaeid shrimps of the Sofala Bank belong to the closed-thelycum group.

Typically, mating of penaeid shrimps occurs deep offshore at night, lasting a few minutes during which the male transfers the spermatophore to the female (Radhakrishnan, 2007). The females carry the spermatheca (sperm packs) during ovarian maturation, dispensing the sperm during spawning. The process of fertilization is external (Kongkeo, 2005; Radhakrishnan, 2007). Females of banana shrimps have four ovarian maturation stages: I−immature; II−developing; III−mature and IV−spawning (Cristo and Mascarenhas, 1986; López-Martínez et al., 2005). After final maturation of ovaries, closed-thelycum females of penaeid shrimps spawn (Fig. 1.4; Primavera, 1985; Yano, 1995). They can mature and spawn several times in the life-history (Primavera, 1985). Fecundity of penaeid shrimps is high, with more than a half million eggs per female. For example, females of *Fenneropenaeus indicus* ranging $14 - 18$ cm total length can produce about one million eggs (Jayawardane et al., 2002). The eggs are immediately fertilized by the sperm, into the water (Fig. 1.4). Yano (1995) suggested a schematic relationship between mating and spawning in penaeid shrimps with a closed-thelycum (Fig. 1.4).

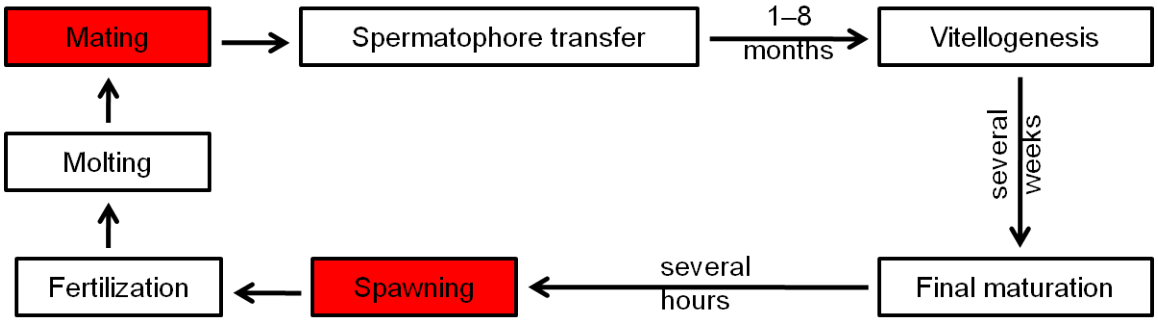

Figure 1.4: Temporal sequence of mating and spawning in a typical closed-thelycum penaeid shrimp (Yano, 1995)

All Sofala Bank shrimp species have a full life cycle within one year, typical of the Penaeidae family (Fig. 1.5). Adult shrimps lay eggs/spawn deep offshore near the shelf slope where salinity is high. For *P indicus* this generally occurs in a depth less than 50 m (Dall et al., 1990). On the Sofala Bank, it is thought that spawning is clumped in deep waters, where females with eggs are found throughout the year. Eggs of penaeid shrimps are tiny, being less than 500 μm in diameter; for example, *F. indicus* eggs average $250-300$ μm (Jayawardane et al., 2002). These tiny eggs are light and less dense than seawater, therefore they have positive buoyancy and float in the water column (Fig. 1.5). Penaeid eggs hatch $8-15$ hours after they were spawned. It has been shown that eggs of cultured *F. indicus* fertilize and hatch within $8-12$ hours after spawning (Radhakrishnan, 2007), for *P. semisulcatus* after 14 hours (Ronquillo et al., 2006) and for *P. monodon* after $12-15$ hours (Kongkeo, 2005).

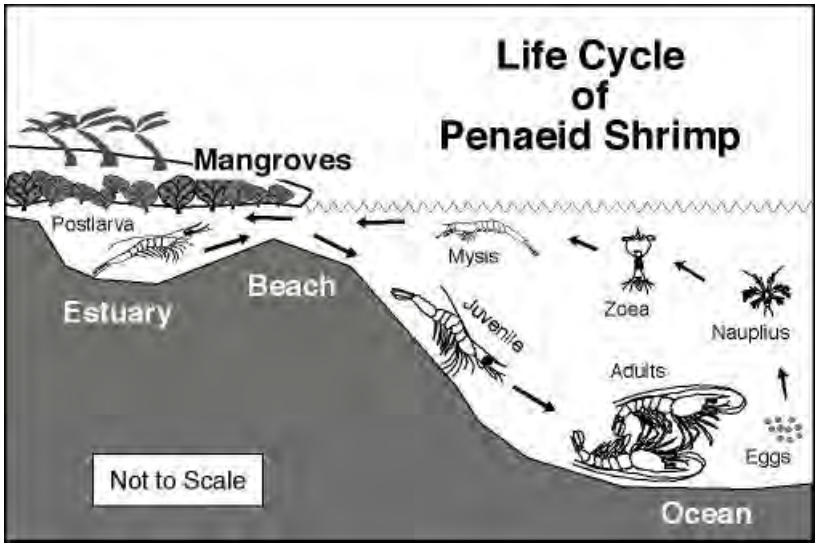

Figure 1.5: Typical life cycle of penaeid shrimps.

The larvae pass through a series of pelagic larval stages (developmental stages); in the case of *F. indicus* there were six naupliar, three protozoeal, and three mysis stages (Table. 1.1) (Laxminarayana et al., 1995; Radhakrishnan, 2007). A similar number of stages has been reported for other penaeid shrimp species, for instance, *P. monodon* (Kongkeo, 2005) and *P. semisulcatus* (Ronquillo et al., 2006). Similarly to many marine organisms, larvae, penaeid shrimp larvae have limited swimming ability or control of their movements. The nauplius has positive buoyancy and rises to the upper layer (Fig. 1.5). Protozoea and mysis larval stages display diel vertical migration (in response to light), in which they rise to the surface at night

(Dall et al., 1990; Rothlisberg et al., 1995; Anger, 2001). At the surface where the currents are strong compared to the bottom, the protozoea and mysis are advected by currents. Early-postlarvae (postlarvae I) are transported towards their coastal and estuarine nursery areas by tidal and wind-driven currents. As they approach coastal shallow areas they become epibenthic, settling on the bottom (Rothlisberg et al., 1983). At that instant the postlarvae shift from diel vertical migration (nocturnally active) to tidal vertical migration (tidally active). They are active during the flood-tides (selective tidal stream transport), either during the day or night (Rothlisberg et al., 1995). Thus, epibenthic behaviour and selective tidal stream transport progressively carry the postlarvae into estuaries during the first three hours of the flood-tide (Rothlisberg et al., 1995; Calderon-Aguilera et al., 2003). Benthic juveniles and sub-adults migrate seaward back to oceanic water. Adults of penaeid shrimp occur offshore, for *F. indicus* at depths of $\sim$ 30 m but also up to 90 m (Radhakrishnan, 2007). On the Sofala Bank, such adults occur at depths up to 60 m, where recruits are mostly caught by the fishery from April-August (de Sousa et al., 2009). It has been proposed that the size distribution of juvenile and adult shrimp on the Sofala Bank follows the bathymetry, where large shrimps are found in deep water (Brito et al., 1998). It has been proposed that the abundance of *F. indicus* (and *P. japonicus* and *P. monodon*) on the Sofala Bank decreases as depth increases from 10 to $35-45$ m, whereas *M. monoceros* (and *P. latisulcatus*) increase in abundance with depths up to 45 m (de Sousa et al., 2006).

Table 1.1: Duration and size range of each larval stage (e.g. Nauplius I) of *F. indicus* reared at $27-32$°C and salinity $32-33$. Adapted from Laxminarayana et al., 1995; Radhakrishnan, 2007.

Phase	Molting cycle (instar)	Total length (µm)	Average duration (hours)	Cumulative duration (days)
Nauplius	I	280 – 310	4	0,0
	II	290 – 320	4	0,2
	III	300 – 330	7	0,3
	IV	340 – 380	12	0,6
	V	350 – 410	15	1,1
	VI	430 – 540	18	1,8
Protozoea	I	880 – 910	30	2,5
	II	1400 – 1550	30	3,8
	III	2410 – 2730	30	5,0
Mysis	I	3070 – 3650	30	6,3
	II	3390 – 3580	30	7,5
	III	3430 – 4170	30	8,8
Postlarva	I	4550 – 5360	27	10,0

Egg development depends principally on maternal effects, relying on nutrients transferred from the female (Racotta et al., 2003). The nauplii are non-feeding larvae, obtaining their energy from remaining parts of their egg yolk-sacs (Anger, 2001; Radhakrishnan, 2007). The protozoea and mysis stages are generalist feeders, eating microplankton ($20-200\ \mu m$ size) consisting of both phytoplankton and zooplankton as well as suspended detritus. On the other hand, small fish and filter feeders can prey upon them (Anger, 2001). Postlarvae feed on benthic detritus, polychaete worms and small crustaceans (Kongkeo, 2005; Radhakrishnan, 2007). Adult shrimps are opportunistic omnivores; they forage or graze on plant detritus, micro-algae, decaying animals and live animals from both the water column and the seabed (Dall et al., 1990).

The pelagic larval stages of penaeid shrimps have a short duration (Dall et al., 1990). They quickly develop from floating fertilized eggs, hatching, growing and moulting through their many stages to the first postlarval stage over a relatively short period. For *F. indicus* that pelagic larval duration is estimated between 10 and 15 days (Laxminarayana et al., 1995; Radhakrishnan, 2007), depending on ambient (natural or reared) and environmental conditions. Detailed duration and size ranges of each stage of reared larvae of *F. indicus* are presented in Table. 1.1. The pelagic larval duration for reared *M. monoceros* was $11-12$ day (Kumlu et al., 2001). For other penaeid species, however, a similar short duration has been reported: $10-12$ days for *Litopenaeus setiferus* (Diop et al., 2007), $10-14$ days for *Litopenaeus stylirostris* (Calderon-Aguilera et al., 2003; Marinone et al., 2004), and $10-15$ days for *P. monodon* (Kongkeo, 2005) and *P. semisulcatus* (Ronquillo et al., 2006).

1.1.3 Effect of temperature and salinity on penaeid shrimps

Numerous factors (pH, salinity, temperature, oxygen concentration, light, heavy metals, pesticides, petroleum hydrocarbons and miscellaneous pollutants) have ecological effects on marine organisms (Anger, 2001), with temperature and salinity being among the most prominent (Ponce-Palafox et al., 1997; Anger, 2001; Zacharia and Kakati, 2004). Temperature directly affects the growth and development of penaeid shrimps during all stages of their life cycle (Kir and Kumlu, 2008). It can increase physiological responses throughout the entire biokinetic temperature range. Most importantly, temperature can be lethal–when out of the tolerance

range of the shrimps. Therefore, in this section emphasis is given to the temperature tolerance range, especially for larval stages (Table. 1.2). The temperature range and the optimum temperature vary between species and can be site-specific (Table. 1.2). In summary, penaeid shrimps are generally eurythermal, i.e. capable to adapt to a wide range of ambient temperatures ($20-30°C$). The optimum temperature range is generally $> 25°C$, whereas temperatures $< 20°C$ can cause them to be lethargic (Anger, 2001).

Table 1.2: Comparison of temperature between different penaeid shrimps and location.

Species	Temperature (°C)			Location	Reference
	Range	Optimum	Lethal		
F. indicus	–	21-27	–	Reared	Radhakrishnan, 2007
P. vannamei	20-30	28-30	–	Reared	Ponce-Palafox et al., 1997
P. chinensis	–	27-35	<20	Reared	Miao and Tu, 1995
P. merguiensis	20-30	28-30	–	Australia	Staples and Heales, 1991
P. semisulcatus	21-30	–	>30	Australia	Jackson et al., 2001
P. japonicus	–	–	–	Taiwan	Main and Fulks, 1990
P. japonicus	–	–	–	Korea	Main and Fulks, 1990
P. japonicus	–	–	–	Japan	Main and Fulks, 1990

Penaeid shrimps have an estuarine and a marine phase in their life cycle and thus get exposed to a wide range of salinity from $5-40$ (Kutty et al., 1971; Parado-Estepa et al., 1987; Dall et al., 1990; Radhakrishnan, 2007). For most penaeid shrimps, low salinities (< 20) may have higher impact on the oceanic larval stages (< 15 days old) than on the estuarine postlarvae (> 15 days old) (Racotta et al., 2003). This is because shrimp reproduction and subsequent larval development occur offshore in stable, high salinity oceanic waters (Dall et al., 1990). The optimum salinity for spawning, hatching and development of larvae of *F. indicus* range from $30-35$ (Kumlu and Jones, 1995; Laxminarayana et al., 1995; Radhakrishnan, 2007), while mortality (5% day^{-1}) is observed at salinities above 35 (Kumlu, 1998). On the other hand, reared postlarvae of *F. indicus* do not survive rapid salinity changes (greater than ± 10 per day, Kumlu and Jones, 1995). Larvae of *M. monoceros* perform better in high oceanic salinity than in low salinity (< 22), while an abrupt salinity drop (but not increase) of over 10 causes mortality (Kumlu et al., 2001). Early larval stages of *P. semisulcatus* tolerate salinities ranging from $20-35$ (Jackson et al., 2001; Kir and Kumlu, 2008), however, protozoeae were mostly found naturally (e.g. in Autralia) associated with salinities ranging from $28-35$ (Jackson et al.,

2001), while salinities < 20 cause an increase in larval mortality (Kir and Kumlu, 2008). The high mortality in low salinity waters might be related to the increased metabolic requirements of osmoregulation (Parado-Estepa et al., 1987; Anger, 2001; Rozas and Minello, 2011).

1.1.4 Effect of currents and circulation on larval dispersal

Offshore−inshore dispersal and transport of larvae, estuarine settlement and supply/recruitment of postlarvae are affected by interactions between larval behaviour and many physical processes of the ocean: tides and tidal currents, internal waves, along- and cross-shelf flow, freshwater river discharges, river plumes, buoyancy-driven currents, geostrophic currents, eddies and others (Queiroga and Blanton, 2004). Pelagic larvae are transported from offshore towards their coastal and estuarine nursery areas by wind-driven and tidal currents. Tidal currents are sheared in the vertical, i.e. tidal flow decreases with an increase in depth, with strong flow at the surface and weak flow near the sea bed (Rothlisberg et al., 1983; Hill, 1991). Similarly to the Sofala Bank, tides are semi-diurnal in Western Australia (Penn, 1975). This author proposed that in Western Australia tidal currents show a day-night seasonal cycle dominated by nocturnal flood-tide flow in one half of the year and nocturnal ebb-tide flow in the other half. A similar result was obtained in the Gulf of Carpentaria, Australia (Rothlisberg et al., 1983).

It has been suggested that penaeid larvae use diel vertical migration to enhance their net horizontal transport in one direction by interacting with the tidal regime and vertically sheared tidal currents (Penn, 1975). The distance and direction, however, depend on the tidal regime (Rothlisberg, 1982; Rothlisberg et al., 1983). The proposed mechanism is that during the day larvae rest and save energy in the deep layers where the tidal current is weak, whereas during the night larvae migrate to the upper layers. When this coincides with the nocturnal flood-tide flow, larvae are transported greater distances towards shore at night than offshore during the day, even against the surface currents. For example, larvae of *P. latisulcatus* in Western Australia were transported > 80 km distances (Penn, 1975) and in the Gulf of Carpentaria up to $70 - 100$ km within 2 weeks (Rothlisberg, 1982). Another study by Rothlisberg et al. (1983) found biggest inshore distances (up to 165 km) for penaeid larvae with nocturnal vertical

migration that rest during the day, and smallest distances (50 km) for larvae that do not rest. Such an inshore transport was consistent with the period (peak in March) of high recruitment of postlarvae into the nursery area off the Gulf of Carpentaria. Rothlisberg (1982) and Rothlisberg et al. (1983) noticed offshore transport of larvae during the nocturnal ebb-tidal flow season, consistent with a period of low recruitment of postlarvae into the nursery area off the Gulf of Carpentaria. Brito and Pena (2007) found a high peak of recruitment of juvenile *F. indicus* and *M. monoceros* in Pugue estuary off Beira Bay, from February−March. Whether this peak was caused by the interaction between diel vertical migration and the tidal cycle is unknown.

Postlarvae enter their estuarine nursery areas using selective tidal stream transport (Hill, 1991; Rothlisberg et al., 1995; Queiroga et al., 2007). The proposed mechanism only relies on postlarvae being epibenthic (settle on the bottom, Rothlisberg et al., 1995), rather than displaying pelagic or vertical migratory behaviour. Postlarvae become epibenthic in response to relative pressure changes as they approach the shore (i.e. a 2 m tide in a 10 m water column compared with a 2 m tide in a 20 m water column, Rothlisberg et al., 1995). It has been proposed that during the flood-tide in the estuary, freshwater flows seaward at the surface while saline seawater moves shoreward at the bottom. Postlarvae are carried into the estuary by the saline water (Calderon-Aguilera et al., 2003). When the tide turns to ebb (seaward flow), salinity decreases and this causes postlarvae to settle to the bottom (Calderon-Aguilera et al., 2003), avoiding being displaced seaward. Queiroga et al. (2007) reviewed the processes for recruitment of crustacean postlarvae into two estuaries of Portugal, and found that the higher the tidal amplitude the larger the recruitment into the estuary.

Onshore transport in the early larval stages, i.e. before postlarvae, far from the estuaries or near the coast has not been demonstrated. Tides in the Sofala Bank region are semi-diurnal (as in Portugal and some areas off Australia), with big amplitudes, up to 4 m. It is hypothesized ($H_{6.3}$) that tides play a role in transport of shrimp larvae towards the coast of the Sofala Bank, with large transport success occurring during spring tides.

Mesoscale eddies have been long identified as key mechanisms in transporting larvae of marine organisms (Fiedler, 1986; Griffiths and Wadley, 1986). Criales and Lee (1995) suggested that larvae of pink shrimp (*Farfantepenaeus duorarum*) are transported towards the coast by small-

scale eddies generated by the persistent Tortugas gyre. Studies on interactions between the panaeid shrimp larvae and mesoscale eddies are scarce. Therefore, our general understanding of the processes involving mesoscale eddies is limited. Particularly, the role that offshore passing eddies of the Mozambique Channel play on the penaeid shrimp larvae of the Sofala Bank is still unknown. In the case of non-penaeid shrimps, offshore mesoscale eddies could entrain and trap coastal larvae (in the Hawaiian waters, Lobel and Robinson, 1986). A recent study by Sánchez-Velasco et al. (2013), based on abundance of fish (129 taxa) larvae, identified two main larval habitats in a cyclonic eddy in the Gulf of California: the eddy core habitat and the eddy edge habitat. This study found that the eddy edge habitat had larger larval abundance and biodiversity than the core habitat. The larvae are subsequently transported with the rotational eddy propagation. It has been suggested that these larvae can be transported to far offshore waters from which it could be difficult for postlarvae to reach the coastal nursery ground in the southern and central California, with negative effects on recruitment success (Nieto et al., 2014). In contrast, other studies suggest that since mesoscale eddies are highly productive, they could support larvae, without impact or with a positive effect on recruitment in the southern California (Logerwell et al., 2001). On the other hand, other studies suggest that eddies could favor transport of larvae towards the coastal nurseries (Criales and Lee, 1995; Sponaugle et al., 2005). It is also possible that eddies from the Florida Current could promote along-shore transport of larvae (Limouzy-Paris et al., 1997). These previous studies differ from the Sofala Bank environment by the presence of well defined current systems. The Sofala Bank, central Mozambique Channel, is a highly energetic eddy field of the world (Tew-Kai and Marsac, 2009). It is therefore appropriate to use this region to investigate the role mesoscale eddies play in transport and dispersal of larvae of the worldwide commercially important penaeid shrimps.

1.1.5 Sofala Bank shrimp fishery

Penaeid shrimps support one of the most important fisheries in Mozambique, in which the main fishing ground occurs in shallow ($20-60$ m) waters of the Sofala Bank. The Sofala Bank fishery consisted of three sectors: artisanal, semi-industrial and industrial. The industrial sector historically covered almost all of the Sofala Bank fishing grounds, except the area off Beira,

at depths ranging from $\sim$ 10 m to 60 m. The industrial fleet is composed of large trawlers averaging $>$ 20 m in length (e.g. Fig. 1.6B) (73 trawlers in 2007 and 70 in 2008; de Sousa et al., 2009). They use four otter trawl nets in a quad-configuration, with a total head-ropes length of 80 m (de Sousa et al., 2013). These industrial trawling vessels have freezing capacity and most can spend up to three months at sea. The semi-industrial fishery takes place in inshore waters using intermediate-sized ($10-20$ m) mechanical trawling vessels (e.g. Fig. 1.6C). The catch is stored on ice and each fishing trip lasts $3-7$ days. This fleet operates in two main areas (de Sousa et al., 2009), one at the northernmost limit of the bank near Angoche (8 trawlers in 2007 and 2008) and another to the south of 20°S off Beira (18 trawlers in 2007 and 15 in 2008). For both industrial and semi-industrial fleets, there is a decreasing trend in numbers of vessels engaged in fishing over the past $\sim$ 6 years from $>$ 80 to $\sim$ 50 vessels due to economic constraints, such as high fuel prices (de Sousa et al., 2013). A mesh size regulation (6 mm) is in place for the industrial and semi-industrial fishing sectors, allowing shrimp larvae and juveniles to escape from the nets. An annual seasonal closure of the fishery is applied to these two fishing sectors from November−February, to protect the spawners and recruitment (Brito and Pena, 2007). The semi-industrial and industrial fleets are also not allowed to fish within three nautical miles of the nearest land.

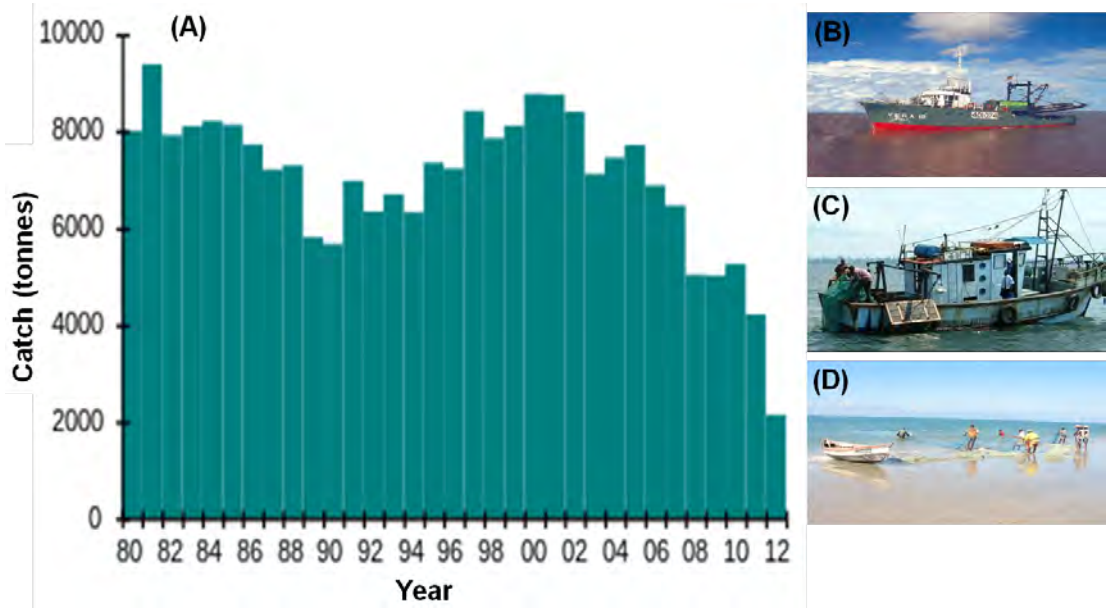

Figure 1.6: (A) Historical total (combined all six species and all three sectors) catches of penaeid shrimp on the Sofala Bank from 1980−2012, adapted from (de Sousa et al., 2013). (B) industrial trawling vessel, (C) semi-industrial ice vessel and (D) artisanal fishing boat (Photos from Lisette Palha de Sousa).

The subsistence, artisanal fishery operates within three nautical miles, covering almost the entire coast, including estuarine areas. They use small boats of < 10 m (e.g. Fig. 1.6D) and hence do not spend > 1 day at sea. Although shrimp is by-catch in some artisanal fishing with fish as the main target, the artisanal catch accounts for $\sim 20\%$ of the total shrimp catches (de Sousa et al., 2013). The seasonal closure does not apply to this sector, which fishes year-round using trawl nets from the beaches (de Sousa et al., 2009). In contrast to the semi-industrial and industrial fleets, the mesh size regulation is not enforced for the artisanal fishery. So, it potentially catches juvenile shrimps in the estuary nursery ground, with possible impacts on the shrimp population and the entire fishery.

The shrimp catch of the Sofala Bank comprises all six native penaeid species, with the banana shrimps (*F. indicus* and *M. monoceros*) being the main target and together accounting for $80 - 90\%$ of the total catch (Brito and Pena, 2007; de Sousa et al., 2009). Historically, the total, annual catch of the industrial fishery (including the semi-industrial fleet in which the catch is stored on ice) was more than 7000 tons (de Sousa et al., 2006). However, over the past ~ 10 years a declining trend has been observed (Fig. 1.6A; de Sousa et al., 2013). Although, the annual catch tended to stabilize between 2008 and 2009 at the level of ~ 5000 tons, which was lower than the historical low catch observed in 1990 (de Sousa et al., 2009). The catch continued to decrease, reaching a critical low level of ~ 2000 tons in 2012, i.e. a drop of $> 60\%$ in two years (de Sousa et al., 2013). A similar decline has been reported in other penaeid shrimp stocks along the eastern coast of Africa and in Madagascar. For example, off Kenya, in Malindi-Ungwana Bay a decrease in the shrimp catch had been observed, which led the Kenyan Government to ban the commercial trawl fishery in the bay (Munga et al., 2013). This decrease, which is still poorly understood on the Mozambican coast, is currently the major concern of the fishery sector and the government. It is a hope that the present study will contribute to understanding the processes involved in the variability of tropical shrimp stocks, and make recommendations that help management of this worldwide valuable resource.

Chapter 2

Spawning areas of banana shrimps on the Sofala Bank

Abstract

The characterization of spawning patterns of marine organisms and their space and time variability is key to understand the dynamics of stocks and implement appropriate spatial management, especially for short-lived species like banana shrimps (*Fenneropenaeus indicus* and *Metapenaeus moneceros*) on the Sofala Bank. This chapter analyzes commercial data during 2000–2003 and annual research survey data during 2003–2010 to identify the main areas and timing of spawning of banana shrimps on the Sofala Bank. These spawning areas and times are characterized in relation to environmental factors. Both species spawned year-round, with periods of increased spawning activity. The proportion of mature females of *M. monoceros* showed a tendency to decrease with cool winter temperatures ($r = 0.48, p = 0.08$), whereas that for *F. indicus* was independent of temperature, although rising temperatures stimulated and promoted maturation and spawning of this species. There was a spawning migration from shallow to relatively deep water for *M. monoceros*, but not for *F. indicus*. Spawning of both species overlapped in shallow ($<$ 25 m depth) waters, whereas *M. monoceros* spawning extended further offshore to $\sim$ 40 m depth. Three main spawning areas were identified on the bank: (1) northern, (2) central and (3) southern. All three spawning areas were adjacent to a river. The northern and central areas were more consistent than the southern area. The Sofala Bank has favourable summer conditions (temperature, salinity and chlorophyll-a) for ovarian maturation and spawning of banana shrimps. The maps and descriptions of the main spawning areas provided by this study can be used to assist in management of this important fishery.

2.1 Introduction

Spawning of banana shrimps on the Sofala Bank occurs all year-round, with two increases, one in March/April and another one in August/September (de Sousa et al., 2006, 2009). Spawning areas of banana shrimps on the Sofala Bank, however, are not yet well known. Over approximately four decades, the shrimp fishery has been managed on the generic concept described by Dall et al. (1990) that spawning occurs offshore. More accurate knowledge about timing and location of spawning (and other essential habitat properties) is important for two main reasons: (1) ecological−to understand the processes controlling the dynamics of stocks, i.e. patterns of larval dispersal, retention and settlement, natural mortality of the early life stages, and stock-recruitment relationship; (2) management − to implement integrated management of human activities in order to ensure protection of essential life-history stages, like spawners, eggs and larval habitats for biodiversity and fisheries. In Western Australia, for example, decreased recruitment of tiger prawns into the fishery was linked to depleted spawning stocks (Penn and Caputi, 1986), and this led to the adoption of management measures to ensure protection of the spawning habitat. The fishery recovered (Penn et al., 1997).

Many of the world's coastal and marine areas are sites of potential increasing human activity, like inshore, onshore and offshore oil and gas exploration in east Africa (Berg et al., 2012; Ledesma, 2013; Turok, 2013). Oil and gas are among the fastest-growing sectors in the coastal and marine regions of Mozambique (Law, 2011). Pollution related to oil and gas activities is widely recognized to negatively influence marine ecosystems and their functioning, with impacts on organisms from early life stages (fertilized eggs and pelagic larvae) (Holdway, 2002; Jiang et al., 2010) to the adult population (Jiang et al., 2010). The recently introduced oil and gas activity on the Mozambican coast overlaps historically important fishery grounds, such as the penaeid shrimp fishery on the Sofala Bank. The Ramsar Advisory Mission expressed concern about future inshore oil and gas drilling explorations causing damage to the mangrove forest in the Marrameu Complex, Zambezi Delta (Pritchard et al., 2009); it is believed that Sofala Bank shrimps utilize this mangrove as a nursery. Seismic surveying for oil and gas also influences fish spawning habits, therefore information on spawning grounds is used to determine seismic exclusion areas to protect these habitats (Coull et al., 1998). Although the government

and stakeholders participate in the environmental impact assessment process, without accurate knowledge on essential habitats like nursery and spawning grounds, it is not possible to advise on the best locations for inshore or offshore exploration and exploitation drilling, and thus protect these vital habitats for fisheries, food security and the economy.

The objective of this chapter is to use research survey data and commercial data to identify and characterize the main areas and timing of spawning of banana shrimps on the Sofala Bank. It is hypothesized that: ($H_{2.1}$) spawning will not be uniformly distributed over the entire bank; instead, times and patches of high spawning activity will be observed, as is the case for many living organisms; and ($H_{2.2}$) the timing and patches of spawning will not be randomly distributed but will be related to environmental factors (temperature, salinity and chlorophyll-a). On the basis of information from related species (Chapter 1), banana shrimps should be associated with warm, low salinity and nutrient rich waters, related to freshwater inputs from local rivers. Temporal and spatial distribution patterns of mature (i.e. spawning) females are analyzed using statistical approaches and a geographical information system (GIS). The characterization of the identified spawning areas is conducted in relation to geographical (latitude and bottom depth) and environmental (temperature, salinity and chlorophyll) variables.

2.2 Data and methods

2.2.1 Fishery data

Research survey data from 2003 to 2010 were obtained from the annual biomass and fishing pre-season cruises carried out on the Sofala Bank by the *Instituto Nacional de Investigação Pesqueira* (IIP). In these surveys, a stratified random sampling scheme was adopted each year by fixed fishing strata (Fig. 2.1). Thus, the sampling stations might change from one year to another, but the strata do not. The surveys were limited to periods from late-January to early-February every year, during the closed season that protects recruitment of juveniles into the fishery. They were carried out on board commercial, industrial bottom-trawling vessels with four nets in a quad-configuration. The average duration of each trawl was 30 minutes and the average speed was 3 knots ($\sim$ 1.5 m s^{-1}). The research surveys covered the entire bank from 16 to 21°S and depths ranged from $\sim$ 7 to 60 m (Fig. 2.1A). A total of 44 stations was sampled from 2003 to 2006, increasing to 55 stations from 2007 to 2010.

The sampling protocol consisted of selecting samples from each part (top, bottom and sides) of the catch (from the four nets pooled together; Figs. 2.1B and C), identifying the species and separating by sex, according to the keys of de Freitas (1972) and Fischer et al. (1990), then measuring the carapace length (L_C- using a dial caliper) or total length (L_T-using ruler for each specimen; Fig. 2.1D) (Brito and Pena, 2007; Brito and Abdula, 2007). Adult female ovarian maturity stages were determined following a microscopic scale of four stages according to Cristo and Mascarenhas (1986) and López-Martínez et al. (2005) (Table 2.1). Therefore, maturity stages I and II were combined as "immature" and considered to be non-spawning, whereas stages III and IV were combined as "mature" and considered to be ready or about to spawn. Before 2007, all four female maturity stages were reported, but from 2007 only the two combined maturity stages, i.e. immature and mature, were reported. The research survey data provided the following information per species (*F. indicus* and *M. monoceros*) of banana shrimps: starting time (day and hour) and position (latitude and longitude) of the catch, catch (weight and number of individuals) and, for each individual, its sex (male or female), carapace length (mm) and gonadal maturation stage (immature or mature).

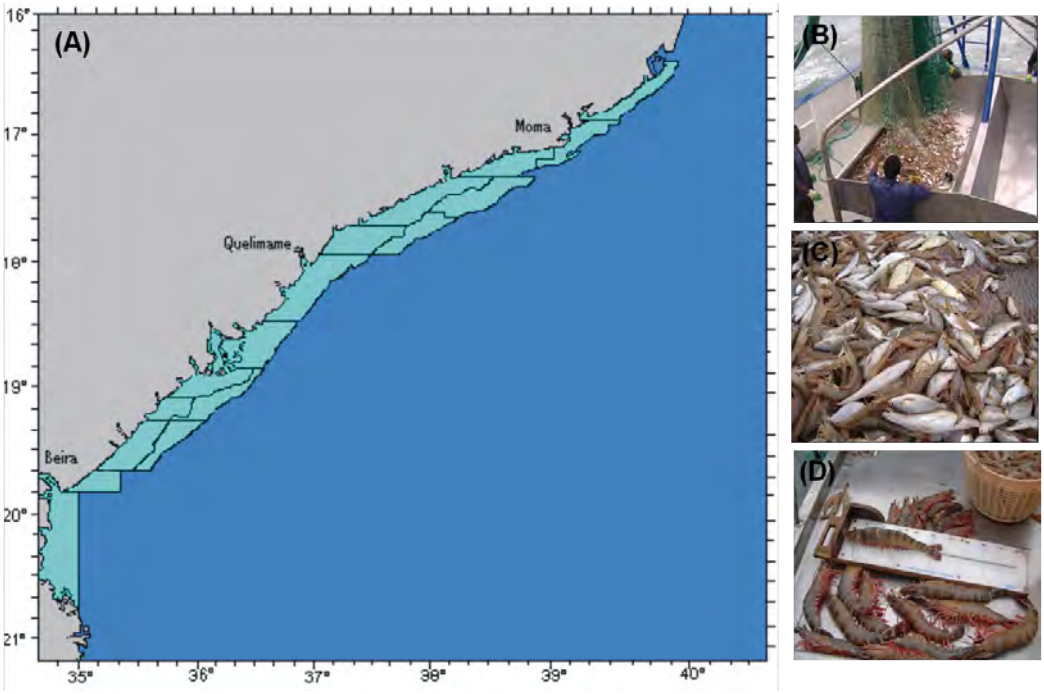

Figure 2.1: (A) Map of the Sofala Bank showing irregular strata (light blue) used in the annual January/February research cruise surveys 2003 – 2010. (B) catch landing, (C) typical shrimp catch including and fish bycatch, and (D) onboard sampling procedure, *P. monodon* on the table and *F. indicus* in the basket. Adapted from Brito and Abdula (2007).

Table 2.1: Female penaeid shrimps ovarian maturation stages. Adapted from Cristo and Mascarenhas (1986); Kumlu et al. (1999) and López-Martínez et al. (2005).

Stages	Description	Observation
I	Ovaries are slim or relatively big, in the abdomen, fine and transparent but distinguishable from other organs; germ cells visible and visible nucleus	Stages I and II considered as immature or none-spawning
II	Ovaries are big, opaque, visible nucleus with ovum	
III	Ovaries are stout and coarse, opaque, cephalothorax, ovum with vitellus	Stages III and IV considered as mature or spawning
IV	Ovaries are flaccid and slim, opaque, germ cells visible, residue maturity ovum	

Commercial fisheries are an important source of data, which are used to understand the dynamics of exploited species, particularly when research data are scarce. The Sofala Bank commercial shrimp fleet provides logbook (catch and effort data) reports to the Mozambican Government. These data are more readily available from the largest catching sector, the industrial fishery (de Sousa et al., 2006), than from the semi-industrial and the artisanal sectors. As a consequence, this study focuses on data from the major industrial company, which manages about 70% of the fishing fleet and is the largest contributor to the total catch on the Sofala Bank.

The exact locations of the trawl tows, although recorded in the logbooks, were not available in the processed data format extracted from the IIP database for this study. In the database, tows falling within a pre-defined, stratified, square grid of 10 × 10 miles (Fig. 2.2A) were pooled. Information about the duration of each trawl haul is recorded in the logbooks, with an average duration estimated between three and four hours. Data were provided as catch (kg) by size categories for a mix of the two banana shrimp species for the fishing season (March-November) from 2000 to 2003. Accordingly, a daily averaged abundance index (kg h^{-1}) by size categories per strata was computed for the same period.

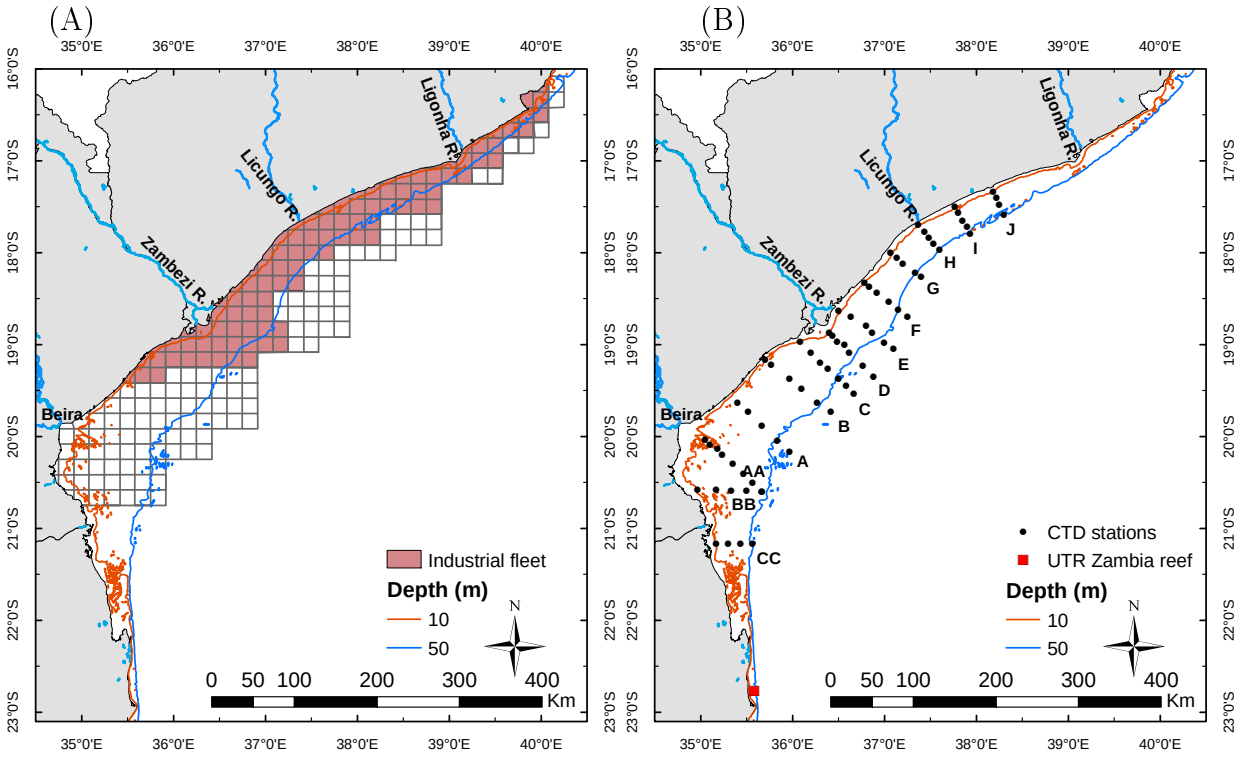

Figure 2.2: Map of the study area showing (A) the stratified sampling used in the commercial shrimp trawl vessel logbook on the Sofala Bank. Grid size 10 × 10 miles. The pink filled boxes/strata refer to the area covered by the industrial fleet in the study between March and April, from 2000 to 2006. (B) CTD stations sampled between January and February 2003 – 2008. and the UTR location.

Commercial landings were also used for biological studies. Once a month, two boxes (containing 2 kg each) of each of the size-categories of banana shrimps to be landed in the Port of Beira were randomly chosen and taken to the IIP laboratory in Beira for detailed biological sampling. At the laboratory, each individual in these boxes was subjected to the same sample processing protocol as described for the research cruise data. The data consisted of number of individuals per species, sex of each individual, carapace lengths and female ovarian maturation stages

(stage I–IV) for *F. indicus* and *M. monoceros*. Since only two boxes per size category were available each month, it is possible that these data came from (1) different strata each month or (2) the same stratum/tow. Therefore, the extent to which they are representative of the entire Sofala Bank area and population is unknown. What is known is that they came from the area where the industrial fleet operates (Fig. 2.2A). These data were all processed by IIP, and fishing seasons' data from 2000 to 2003 were made available to this study.

2.2.2 Environmental data

For environmental characterization of banana shrimp spawning distributions, temperature (°C), salinity and chlorophyll-a concentrations (as determined by fluorescence in mg m^{-3}) were used. Oceanographic data were independently collected as part of the IIP annual pre-season survey on the Sofala Bank. In total, 73 fixed oceanographic stations distributed along 13 cross-shelf transects were sampled between January and February from 2003 to 2008 (Fig. 2.2B). Note that the environmental stations do not cover an important fishing ground to the north of 17°S. At each station, the water column was vertically sampled every 1 m to the sea bottom during the downcast of a CTD-Seabird 19. The CTD is sent to Sea-Bird Electronic Ltd for calibration on a regular basis and the same instrument was used throughout the study period. The CTD data were loaded onto a computer in ASCII (.cnv) format using the Seabird Seasave software. The data were subjected to quality checks to remove erroneous data and then imported into a standard spreadsheet.

Although the oceanographic and fishery data came from the same cruise survey each year, they were not always taken at the same stations. Consequently, for most of the locations, the environmental data do not coincide with biological data. The environmental variables were interpolated for each biological station. The nearest station approach was not robust because of differences in the distances between stations. Thus, interpolated regular gridded data were produced. Since spawning of the two banana shrimp species occurs at the sea bottom, bottom values were calculated for each environmental variable per station as the average of all observations in the last 5 m depth at the station. These values were converted to horizontally-

interpolated, regularly-spaced gridded data at 0.2° spatial resolution, using the inverse distance interpolation method of Surfer golden Software version 8.

An underwater temperature recorders (UTR−model Seamon mini temperature recorder, accuracy ±0.01°C), deployed to the south (Zambia reef UTR site, Fig. 2.2B) of the Sofala Bank at a depth of 18 m was used. The 18 m depth is reasonable when compared to the Sofala Bank averaged depth (∼ 15 m). The UTR recorded hourly measurements of temperature from October 2002 to September 2007. These hourly data were averaged to obtain daily and seasonal time series, which were analyzed. In this study, seasons are defined as summer (January−March), autumn (April−June), winter (July−September) and spring (October−December).

2.2.3 Data analysis

Spawning areas of marine organisms are commonly identified by presence of either mature females or eggs (Ye, 2000; Niamaimandi et al., 2008; Ellis et al., 2012). Penaeid shrimps spawn soon after final maturation (Dall et al., 1990; Yano, 1995), thus mature females are often used as an indication of spawning. In the present study, in absence of *in-situ* banana shrimp egg and larval data, only mature females ready to release eggs were considered to indicate spawning. Commercial data from 2000 − 2003 were used to determine the spawning period, so that months with high percentages of mature females were considered as spawning months (Kumlu et al., 1999; de Sousa et al., 2006; Brito and Pena, 2007; Amanat and Qureshi, 2011).

Research data from the annual surveys 2003 − 2010 were used to determine the spawning area. A persistent spawning area was determined by two criteria: (1) the proportion of mature females at a station was greater than 50% (Niamaimandi et al., 2008), and (2) shrimps visited the area frequently throughout the years. Spawning locations were mapped as single points using the GIS and each map provides composite information for the eight years (research data January/February 2003 − 2010), instead of snapshots by year, in order to minimize the number of maps. Composite maps were chosen rather than averaged maps because the station positions change from year to year on the stratified random sampling scheme.

Centres of gravity are widely used to summarize spatial locations of marine populations (Woillez

et al., 2007) or habitats. For the purpose of the present study, a centre of gravity analysis is used to summarize locations of spawning areas for the banana shrimps on the Sofala Bank and to investigate spatial changes (shifts or movements) in spawning areas over the years. The centre of gravity (CG_{lon} and CG_{lat}) was computed as the mean of geographical coordinates (lon and lat) weighted (w) by the number of shrimps at station (i) for every station (n) of the surveyed year (t), as defined by equations (2.1 and 2.2):

$$CG_{lon,t} = \frac{\sum_{i=1}^{n} lon_i \cdot w_{i,t}}{\sum_{i=1}^{n} w_{i,t}} \tag{2.1}$$

$$CG_{lat,t} = \frac{\sum_{i=1}^{n} lat_i \cdot w_{i,t}}{\sum_{i=1}^{n} w_{i,t}} \tag{2.2}$$

The centres of gravity were obtained for both *F. indicus* and *M. monoceros* at each identified spawning area per year and then mapped in the GIS for visualization. Interannual changes in the spawning area were determined by the trajectory and distance (km) between the centres of gravity of consecutive years.

Single parameter quotient (SPQ) analysis has been used worldwide to characterize spawning habitat preference/avoidance in relation to geographical and environmental variables, especially for sardine and anchovy (van der Lingen et al., 2001; Twatwa et al., 2005; Bernal et al., 2007; Ibaibarriaga et al., 2007; Oozeki et al., 2007; Zwolinski et al., 2010). In the present study, SPQ analysis was used to investigate each banana shrimp spawning (i.e., mature female) preference or avoidance in relation to each geographical (latitude, longitude and logarithmically-transformed bottom depth) and each environmental (temperature, salinity and fluorescence) variable. All these data were derived from the annual January/February research survey from 2003 to 2010, but environmental data for 2009 and 2010 were not available. In addition, the environmental data did not cover a small area to the north of 17°S, and this northernmost section was not included in the environmental characterization of spawning habitat. Each explanatory variable

(geographical and environmental) was converted into a categorized discrete variable with equal size classes or bins, and then, within each class (i), the number of stations (N_i) and the total number of mature females (A_i) were determined. The quotient (Q_i) number was defined as the proportion of mature females divided by the proportion of stations per class for all classes (n) (Ibaibarriaga et al., 2007):

$$Q_i = \frac{A_i / \sum_{i=1}^{n} A_i}{N_i / \sum_{i=1}^{n} N_i} \tag{2.3}$$

The SPQ analysis was performed using the R package shachar developed by Bernal et al. (2007) and freely available at `http://sourceforge.net/projects/ichthyoanalysis/` (last visited in July 2014). The statistical significance was set at a 95% confidence level. Spawning avoidance or preference for an explanatory variable class value is interpreted using confidence limits according to Bernal et al. (2007); significant avoidance is defined by the quotient value (or curve) below the lower confidence limit, tolerance between the confidence limits, and significant preference above the upper confidence limit. This method was chosen rather than simple preference as $Q > 1$ or avoidance $Q < 1$ (van der Lingen et al., 2001) because it considers the tolerance range.

Spearman's rank correlation was used to evaluate the strength of the relationship between female ovarian maturation stages of each banana shrimps species and both intra- and inter-annual temperatures derived from the UTR at the Zambia reef site. The nonparametric measure was chosen because of the relatively short data set (i.e. 10 months for the intra-annual variability and 8 years for the inter-annual variability). Spearman's rank correlation was also used to compare temperatures and movement in the centres of gravity of mature banana shrimps on the Sofala Bank. A Mann-Whitney U test was used to evaluate the differences in distributions between immature and mature females of each banana shrimp species, and also differences in distributions between *F. indicus* and *M. monoceros* for each of the two female stages.

2.3 Results

2.3.1 Temporal variability of female ovarian maturity stages

All four female ovarian maturity stages of the two species, *F. indicus* (Fig. 2.3A) and *M. monoceros* (Fig. 2.3B), were found in all the months during both closed (January and February) and fishing (March to November) seasons in $2000-2003$. Generally, the percentage of monthly mature (stages III and IV) females was higher for *F. indicus* (Fig. 2.3A) than for *M. monoceros* (Fig. 2.3B), except in November and March when they were about the same. Mature females of *F. indicus* comprised $> 40\%$ of the samples in all months. They exhibit a bimodal distribution, with two increased percentages of mature females, one observed in March ($\sim 55\%$) and the other in August ($\sim 70\%$), while the lowest percentages ($\sim 40\%$) occurred in May (Fig. 2.3A). The correlation between the monthly averaged temperature at the Zambia reef UTR site and mature *F. indicus* was not significant ($r = -0.48$, $p = 1$, Fig. 2.3A). In contrast, there was a significantly positive correlation between temperature and immature *F. indicus* females in stage I ($r = 0.68$, $p = 0.014$). Mature females of *M. monoceros* displayed increased percentages ($>$ 30%) in spring and summer (September−March) and decreased percentages ($< 30\%$) in autumn and winter (April−August) (Fig. 2.3B). Mature females of *M. monoceros* were positively correlated with seasonal temperatures at the Zambia reef UTR site ($r = 0.77$, $p = 0.081$, Fig. 2.3B), whereas there was no correlation between temperature and stage I females ($r = 0.16$, $p = 0.33$).

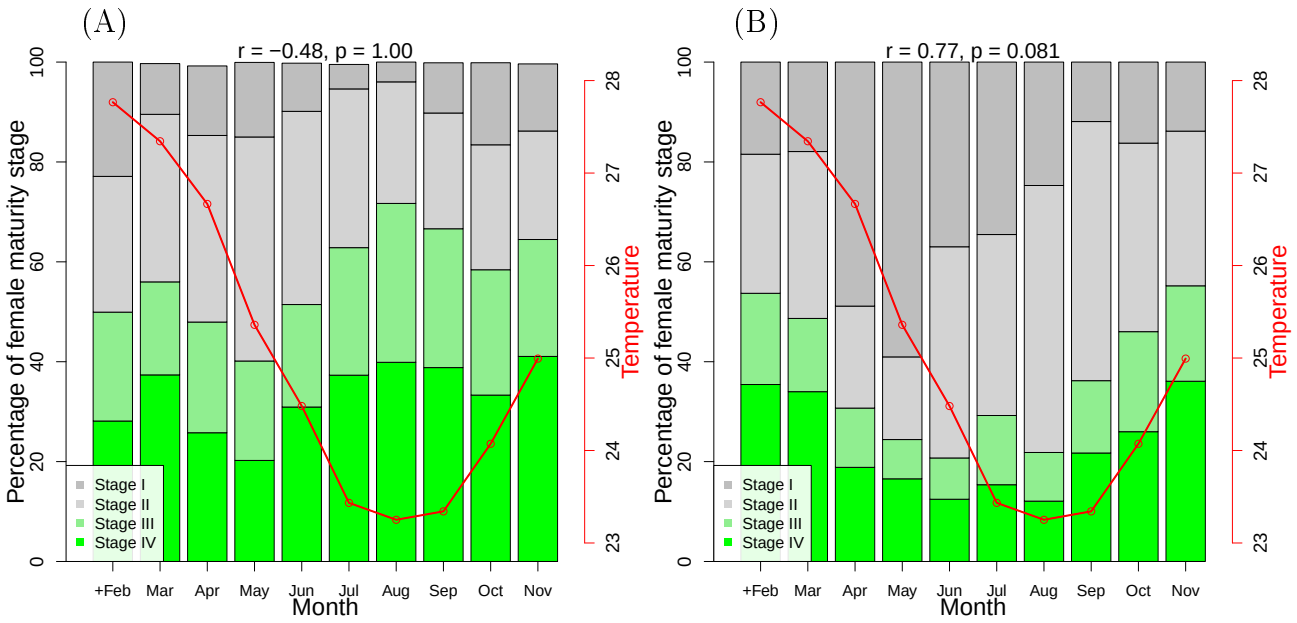

Figure 2.3: Mean (averaged monthly among years) percentage of female ovarian maturity stages for (A) *F. indicus* and (B) *M. monoceros* from commercial fishery data, fishing seasons 2000 – 2003. Note: +Feb refers to closed season data averaged from annual January/February research survey data 2003 – 2010 and added to extend the analyses to summer time. Red line indicates monthly averaged temperature at the Zambia reef UTR site from 2003 to 2011. r and p indicate relationship between mature females and temperature.

Both immature and mature females of the two banana shrimp species were found every year (2003 – 2010) during the January/February fishing pre-season survey. The percentages of mature females fluctuated from one year to another, ranging between 40% and 65%, with the largest values in 2006 and the lowest in 2010 (Fig. 2.4A). There was no significant correlation between mature females of *F. indicus* and the preceding winter-averaged temperatures (Fig. 2.4A). For *M. monoceros*, the percentages of mature females varied between 35% and 65%, with the largest values obtained in 2003 and 2007 and the lowest in 2009 and 2010 (Fig. 2.4B). There was also a low value of mature *M. monoceros* in 2005 and 2006. Mature females of *M. monoceros* were significantly positively correlated with the preceding year's averaged winter temperatures (Fig. 2.4B).

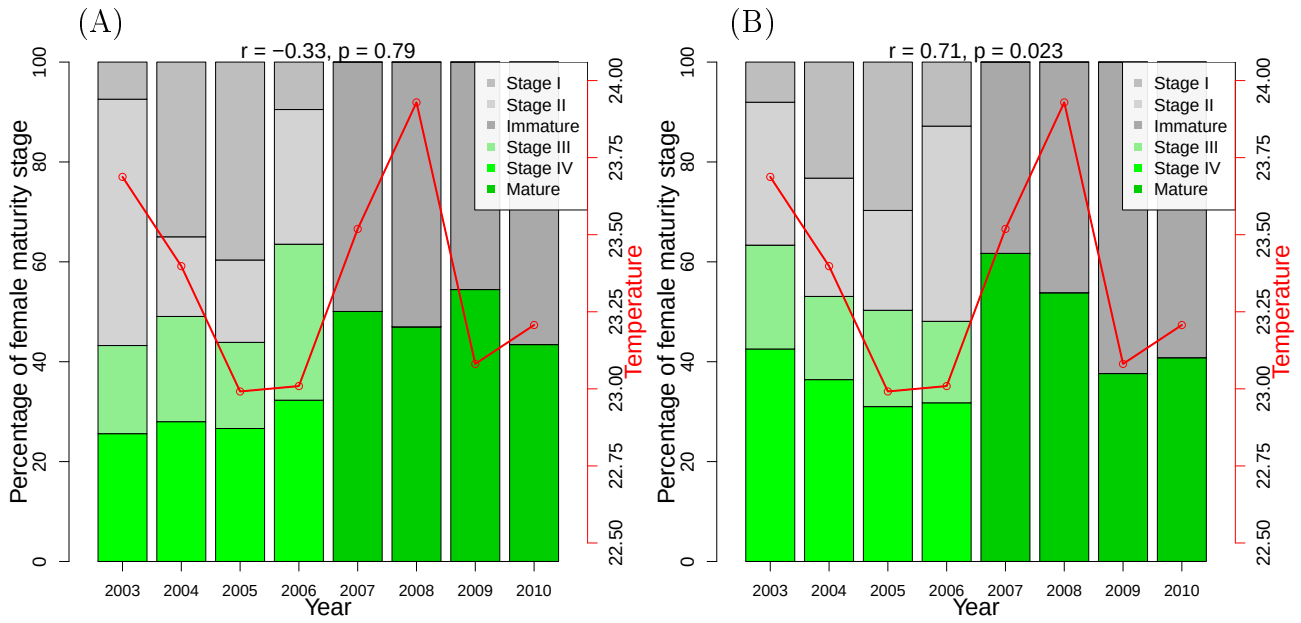

Figure 2.4: Interannual variability of the percentage of female ovarian maturity stages for (A) *F. indicus* and (B) *M. monoceros* from research surveys during the closed fishing season, January/February 2003 – 2010. Grey–immature (stages I and II) and green–mature (stages III and IV). Red line indicates the preceding winter (Jul, Aug and Sep 2002 – 2009) averaged temperature at the Zambia reef UTR site. r and p indicate relationship between mature females and temperature.

2.3.2 Spawning distribution

Comparison of the occurrence (presence/absence) of immature and mature females of *F. indicus* (Fig. 2.5A) and *M. monoceros* (Fig. 2.5B) shows many stations with zero catch (none, in Table. 2.2). Immature and mature females of *F. indicus* generally occurred at the same locations (Table. 2.2) in the coastal and inshore waters of the bank (Fig. 2.5A). There was no difference in the depths of occurrence of the two female stages (Mann-Whitney $U = 9812$, $Z = -0.083$, $p = 0.933$, $N_{immature} = 139$, $N_{mature} = 142$), with depths ranging between 8 and 25 m (boxplot in Fig.2.5A). Only a few locations scattered over the bank had only immatures or only matures for this species (Fig. 2.5A, Table. 2.2).

For *M. monoceros*, locations with occurrence of both immature and mature females were also most frequently observed (Fig. 2.5B; Table. 2.2). There were a few stations where only immature females were observed, restricted to waters shallower than 25 m depth. In contrast, there were some stations with only mature females, mainly on the offshore edge of the Sofala Bank, just north of 17°45′S (Fig. 2.5B). There was, however, no difference in the depth distributions

731 between immature and mature *M. monoceros* (Mann-Whitney $U = 15998.5$, $Z = -1.58$, $p =$
732 0.114, $N_{immature} = 183$, $N_{mature} = 193$).

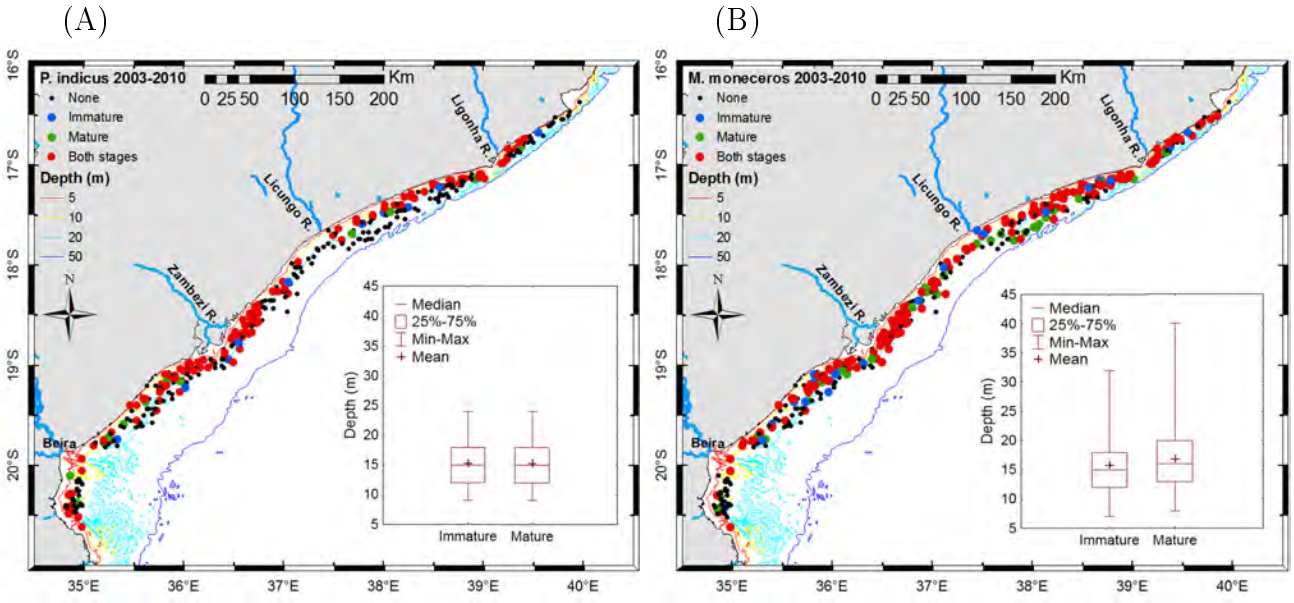

Figure 2.5: Composite maps showing presence/absence of immature and mature females for (A) *F. indicus* and (B) *M. monoceros* from research surveys for January/February 2003 – 2010. Boxplots show the distribution of the station depths (m) for immature (blue+red) and mature (green+red) female stages.

Table 2.2: Percentage of stations with zero (none), only one or both maturity stages of female *F. indicus* (*P.i*) and *M. monoceros* (*M. m*). Total number of stations = 170.

	Stage (%)					Species (%)			
Species	None	Immature	Mature	Both	Stages	None	*F. i.*	*M. m.*	Both
F. i. (Fig. 2.5A)	60	3	4	33	Immature (Fig. 2.6A)	46	6	18	30
M. m. (Fig. 2.5B)	43	7	10	40	Mature (Fig. 2.6B)	43	6	20	31

733 Comparison of occurrence (presence/absence) of *F. indicus* and *M. monoceros* shows many
734 stations with zero for immature (Fig. 2.6A, Table. 2.2) and mature (Fig. 2.6B, Table. 2.2) fe-
735 males. Immature females of both *F. indicus* and *M. monoceros* occurred frequently at the same
736 locations (Fig. 2.6A, Table. 2.2). Immature as well as mature *F. indicus* occurred sporadically
737 alone over the bank, particularly to the south of 20°S (Fig 2.6A and B). Immature females of
738 *M. monoceros* were found alone at some stations (Table. 2.2) to the north of 17°30′S (Fig.
739 2.6A). There was no difference between the depths where immature females of *F. indicus* and
740 *M. monoceros* were found (Mann-Whitney $U = 11939.5$, $Z = -0.941$, $p = 0.345$, $N_{P.indicus} =$

139, $N_{M.monoceros} = 183$).

For mature females, the two banana shrimp species co-occurred in some locations (Fig. 2.6B, Table. 2.2). Mainly *F. indicus* were observed on the southernmost portion of the bank, whereas *M. monoceros* occurred on the northernmost portion (Fig.2.6). There was a relatively large number of stations with only mature females of *M. monoceros* (20% of the stations, Table. 2.2). These stations were particularly located on the offshore edge of the Sofala Bank, to the north of 17°45′S (Fig. 2.6B). There were differences in the depths of occurrence of mature females of the two species (Mann-Whitney $U = 11361$, $Z = -2.372$, $p = 0.018$, $N_{P.indicus} = 142$, $N_{M.monoceros} = 193$), with mature females of *M. monoceros* found deeper than those of *F. indicus* (boxplot in Fig. 2.6B).

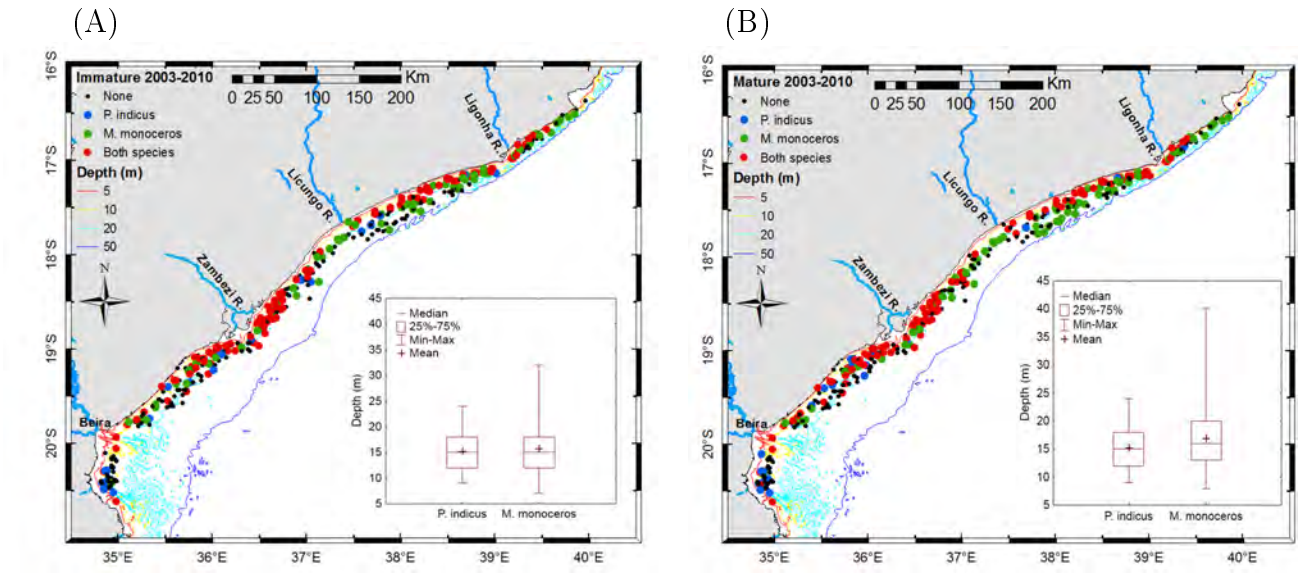

Figure 2.6: Composite maps showing presence/absence of *F. indicus* and *M. monoceros* for (A) immature females and (B) mature females from research surveys for January/February 2003−2010. Boxplots show the distribution of the station depths (m) for *F. indicus* (blue+red) and *M. monoceros* (green+red).

Mature females of the two banana shrimp species were widely distributed and abundant (number in quartiles) on the Sofala Bank (Fig. 2.7). However, two major discontinuity regions were apparent, one off the Licungo River around 17°45′S and another around 19°30′S. As a result, three main spawning areas can be identified (by presence of mature females > 50%, i.e. 3rd and 4th quartiles): (1) northern−off the Ligonha River (north of ∼ 17°45′S), (2) central−off the Zambezi River (between ∼ 18°S and ∼ 19°30′S) and (3) southern−off the Bay of Beira (off the Búzi and Pungué Rivers, south of ∼ 19°45′S).

For the northern spawning area, although the distribution of mature *M. monoceros* (Fig. 2.7B) extended further north than *F. indicus* (Fig. 2.7A), there was no station with > 50% of mature females on the northernmost portion of the Sofala Bank, to the north of the Ligonha River (Fig. 2.7A and B). Results of the analyses of centres of gravity of mature females show that all in this area were found to the south of the Ligonha River mouth every year for both species (Fig. 2.8). In the central spawning area, dense aggregations of mature females > 50% were found to the north of the Zambezi River mouth, and only a few to the south for the two species, especially for *M. monoceros* (Fig. 2.7A and B). In the southern spawning area, there were only a few stations with > 50% of mature females spread over the area for *F. indicus* (Fig 2.7A), while for *M. monoceros* there were nearly no stations with mature females in the 4th quartile (Fig 2.7B). In this spawning area, the centres of gravity of the two species were also found spread over the entire area, with a large distance range (Fig. 2.8).

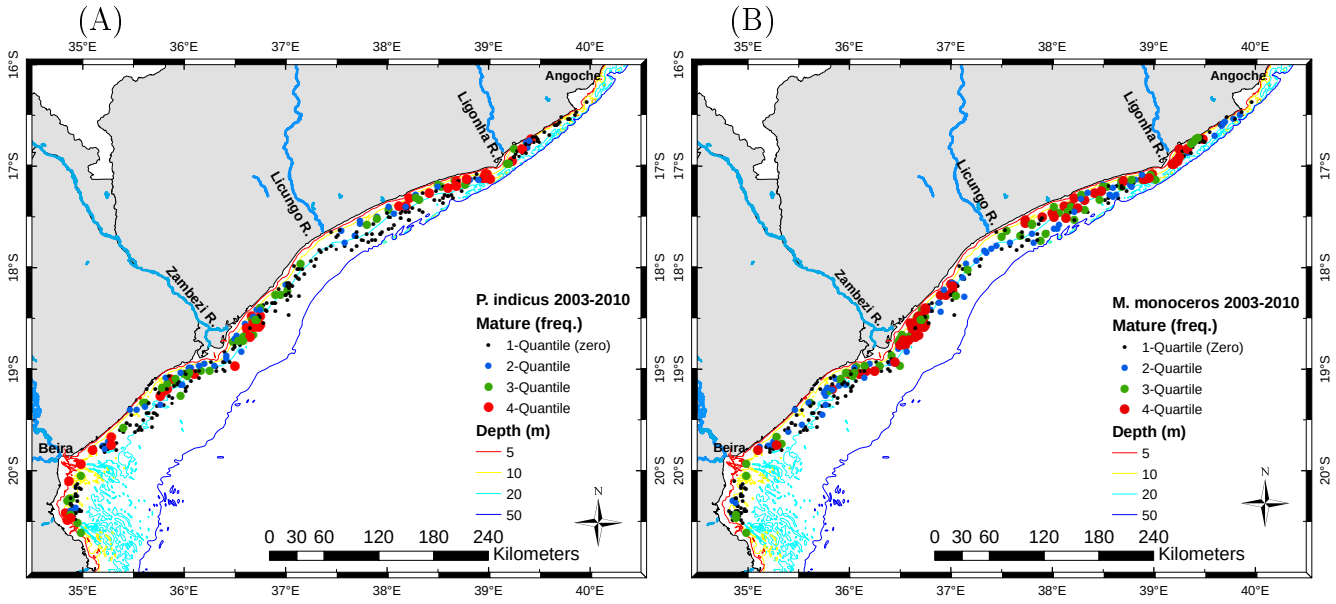

Figure 2.7: Composite maps of numbers (quartiles) of mature females for (A) *F. indicus* and (B) *M. monoceros* on the Sofala Bank from the research surveys in January/February 2003 – 2010.

There was no clear pattern in spawning area variability in all three spawning areas (Fig. 2.8). Following the trajectory of the centres of gravity throughout the years, it appeared that they moved both southward and northward with no apparent pattern (Fig. 2.8A). Similar results were obtained for the distances between consecutive years, in which there was no trend. The distance increased and decreased across the years for *F. indicus* (Fig. 2.8B) and *M. monoceros*

(Fig. 2.8C). For mature females of *M. monoceros*, however, the variation in the distances between the centres of gravity in the northern and central areas were synchronized (Fig.2.8C).

The smallest change in the centre of gravity ($\sim$ 4 km for *F. indicus* and $\sim$ 6 km for *M. monoceros*) was observed in the central spawning area, while the largest change (78 km for *F. indicus* and 97 km for *M. monoceros*) was observed in the southern spawning area (Fig. 2.8). The northern and central spawning areas exhibited relatively small range variability in the location of the centres of gravity from one year to the next. In contrast, large variability in the centres of gravity among the years was observed on the southern spawning area, especially for *M. monoceros* (Fig. 2.8A and C). Generally, *F. indicus* showed a smaller change in centres of gravity than *M. monoceros*, mainly in the central and northern spawning areas (Fig. 2.8). There was no relationship between temperature and change in the centres of gravity for both banana shrimps in any of the three spawning areas.

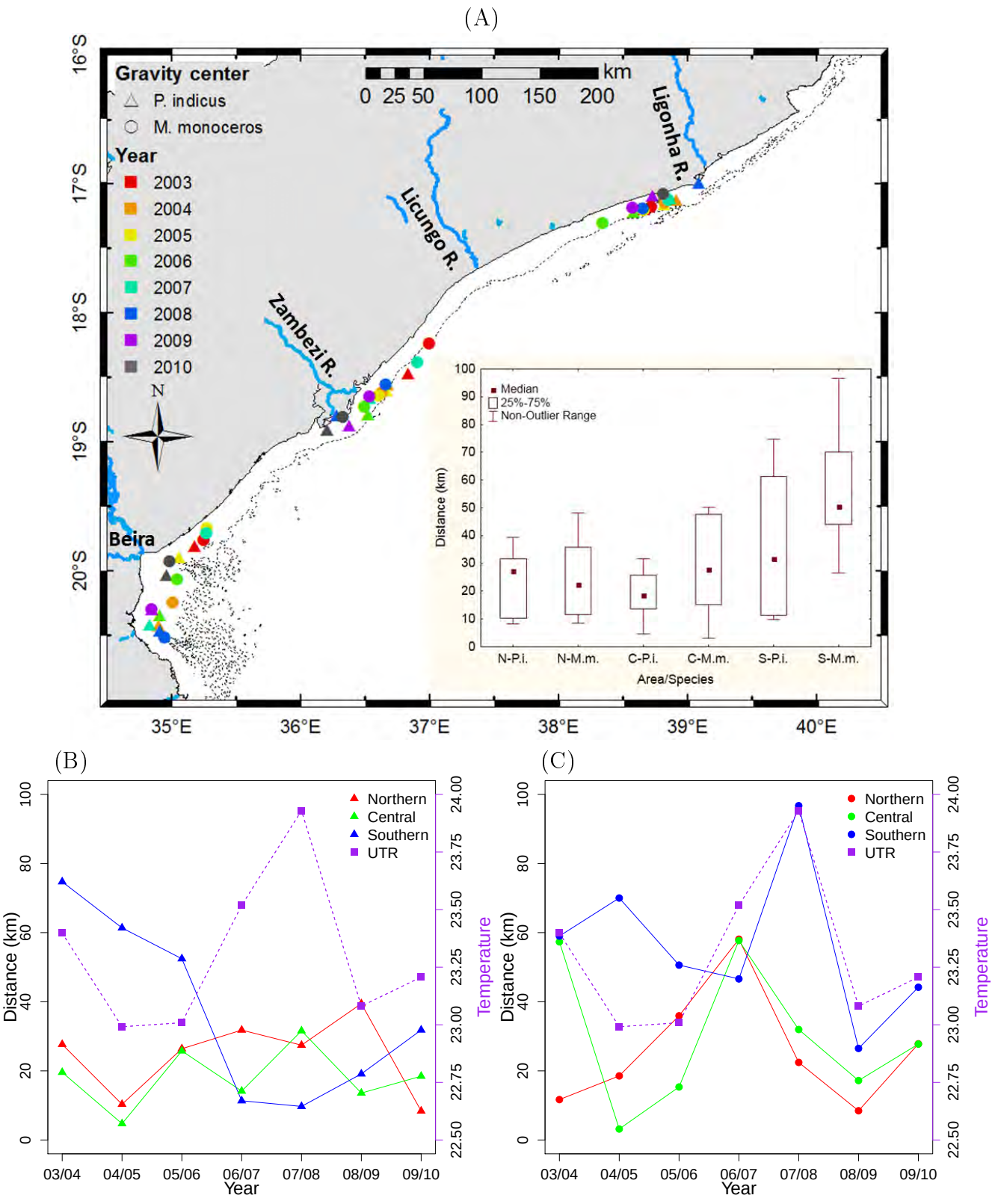

Figure 2.8: (A) Annual distribution of centres of gravity for *F. indicus* (triangle) and *M. monoceros* (circle) from 2003 to 2010 (color). Boxplots show distances (km) between centres of gravity in consecutive years in the three spawning areas indicated as: (N-P.i.) northern area for *F. indicus*, (N-M.m.) northern area for *M. monoceros*, (C-P.i.) central area for *F. indicus*, (C-M.m.) central area for *M. monoceros*, (S-P.i) southern area for *F. indicus* and (S-M.m) southern for area *M. monoceros*. The distances between centres from one year to another are shown for (B) *F. indicus* and (C) *M. monoceros*. Dashed line indicates the (Jul, Aug and Sep) winter-averaged temperature at the Zambia reef UTR site (18 m depth).

2.3.3 Spawning habitat characterization

Mature females of *F. indicus* were found to avoid three latitude regions on the Sofala Bank: (1) $\sim 19°30'$S, (2) $\sim 18°30'$S and (3) $\sim 16°45'$S (Fig. 2.9A). There were three regions of latitudinal tolerance (between the confidence limits and with quotient value >1): (1) northern; (2) central and (3) southern latitudes, with significant preferences for the northern and central latitudes.

For *M. monoceros* mature females, there were also three regions of latitudinal tolerance (northern, central and southern), with significant preferences for the northern and central latitudes (Fig. 2.9B). Similar to *F. indicus*, mature females of *M. monoceros* show a significant avoidance at $\sim 19°30'$S, separating the southern and central spawning areas. However, in contrast to *F. indicus* (Fig. 2.9A), for *M. monoceros* (Fig. 2.9B) there was no significant avoidance at $\sim 18°30'$S, whereas a significant avoidance was apparent on the southernmost portion of the bank to the south of $20°30'$S.

Mature females of *F. indicus* were tolerant of shallow waters, ranging from 7 to 35 m depth, whereas there was a significant avoidance for deeper waters of > 35 m depth (Fig. 2.9C). Mature females of *M. monoceros* appeared to tolerate the full range of observed depths from 7 to 45 m, with no significant preference or avoidance (Fig. 2.9D).

There was no avoidance for all three environmental covariates (Fig. 2.10). Temperature tolerances covered the full range from 23 to 30°C, with significant preference for mid-range temperatures ($\sim$ 27.75°C) for the two species (Fig. 2.10A and B). Salinity tolerances also covered the full range, with significant preference for mid-salinity ($\sim$ 34.7) (Fig. 2.10C and D), which corresponds to oceanic salinity, rather than coastal. Fluorescence tolerances also covered the full range from 2 to 10 mg m^{-3} with no significant preference for a particular concentration (Fig. 2.10E and F). Note that, similar to bottom depth (Fig. 2.9C and D), there was a small number of observations on both edges of all environmental covariates (Fig. 2.10), therefore caution is needed when interpreting these values.

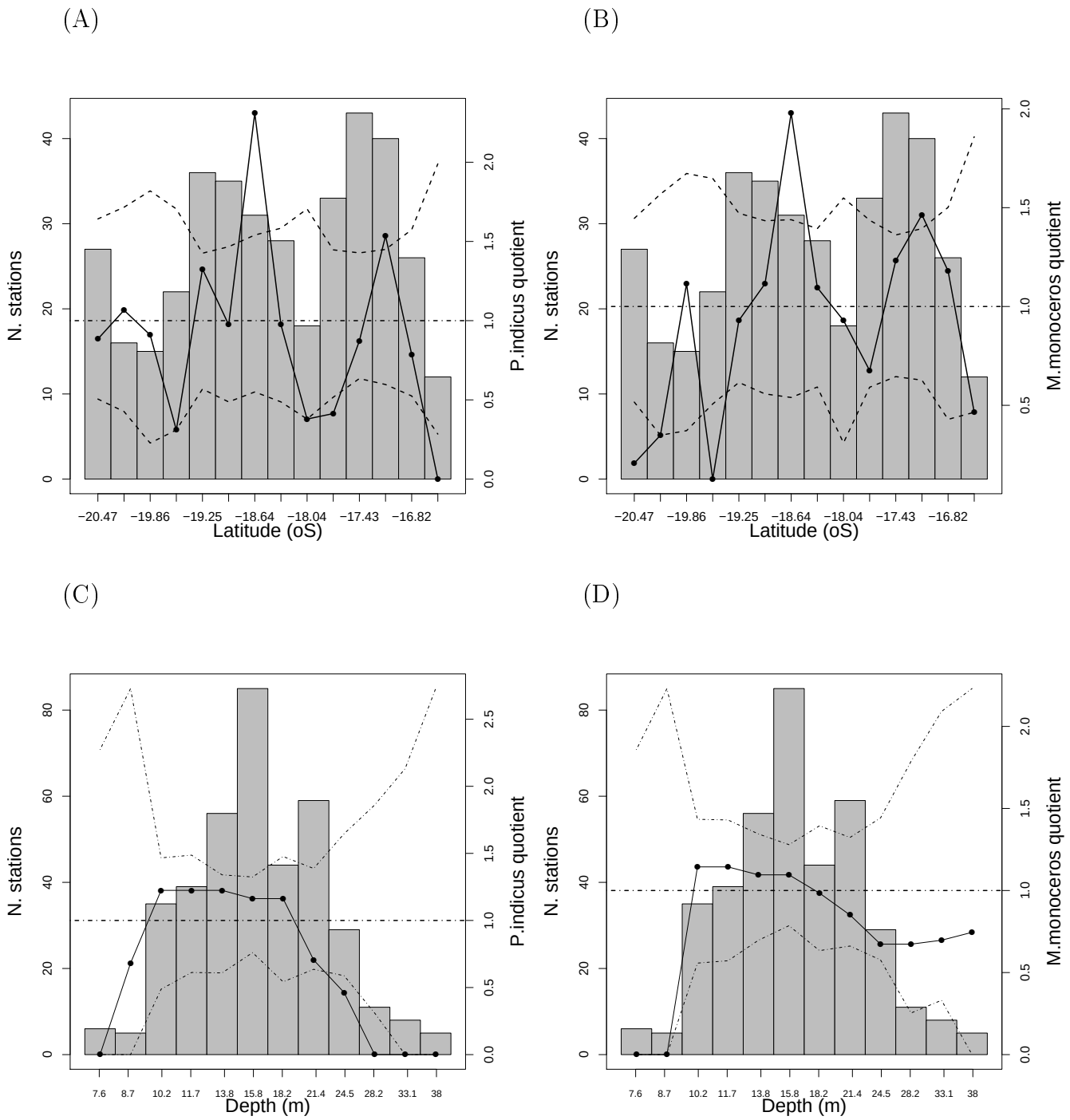

Figure 2.9: Characterization of presence of banana shrimps mature females in relation to geographical covariates. Quotient plot (solid line) of number of mature females of (A) *F. indicus* relative to latitude, (B) *M. monoceros* relative to latitude, (C) *F. indicus* relative to bottom depth and (D) *M. monoceros* relative to bottom depth from the research surveys 2003 – 2010. Note that the depth scale is logarithmic (C and D). Dashed lines indicate the 95% confidence interval of mature females and histograms represent the number of sampled stations in each covariate bin.

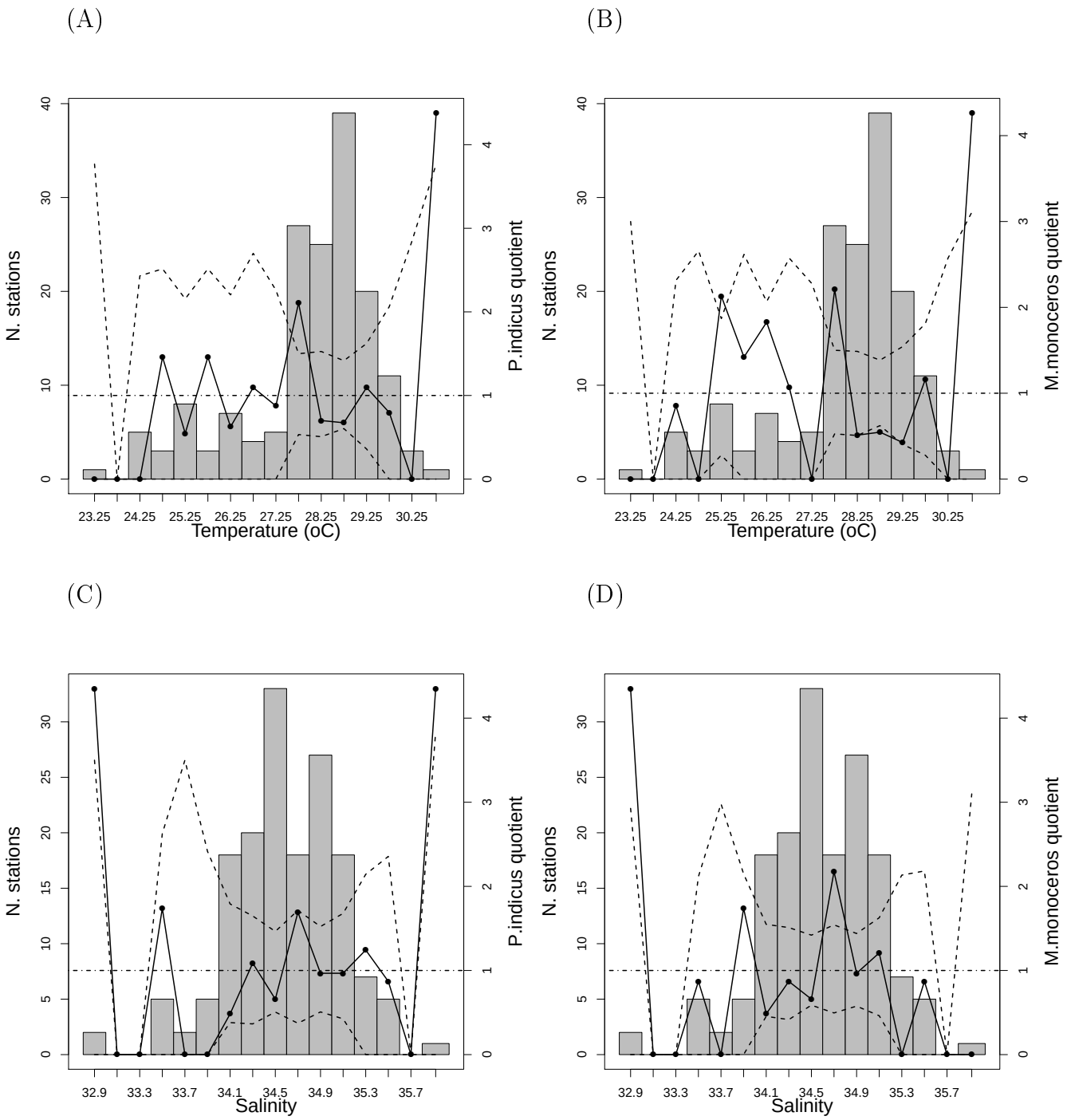

Figure 2.10: Same as Fig. 10 but in relation to environmental covariates for (A) *F. indicus* relative to temperature, (B) *M. monoceros* relative to temperature, (C) *F. indicus* relative to salinity and (D) *M. monoceros* relative to salinity.

2.4 Discussion

2.4.1 Inter- and intra-annual spawning variability

The present study confirmed that females of both banana shrimp species spawn year-round on the Sofala Bank (Figs. 2.3), as has been proposed by previous studies (de Sousa et al., 2006, 2008). The present study was able to show that the spawning season includes the closed fishing season, by extending the data sets to the months of January and February. For *F. indicus*, despite small fluctuations between months, there were two periods of increased percentages of mature females: a minor one in late−summer and autumn, and another major one (main effective spawning) in late−winter and spring (Fig. 2.3A). This supports the second hypothesis ($H_{2.1}$), indicating times of increased activity. Similarly, two main spawning periods have been reported for many tropical penaeid shrimps around the world (Badawi, 1975; Crocos and Kerr, 1983; García, 1988; Dall et al., 1990; Crocos and van der Velde, 1995; Ayub and Ahmed, 2002; Qureshi and Amanat, 2014), including other *F. indicus* stocks in the Mozambique Channel. On the eastern side of the channel, on the west coast of Madagascar (Le Reste and Marcille, 1976), to the south, in Maputo Bay (de Freitas, 2011), and further south, in KwaZulu-Natal, South Africa (Forbes and Demetriades, 2005). The secondary, late-summer and autumn increased spawning, is generally irregular (García, 1988; Crocos and van der Velde, 1995). The existence of this secondary increased spawning in autumn was proposed by de Sousa et al. (2006, 2008, 2013), based on the occurrence of the greatest spawning biomass in the first half of the year. Moreover, they observed two peaks of juveniles entering the fishery, one in autumn and another in spring, supporting the idea of two main periods of spawning activity.

There was no clear relationship between the percentage of mature female *F. indicus* and temperature (Fig. 2.3A), suggesting that spawning of *F. indicus* does not depend on temperature. However, when the temperature started to warm from minimum winter values, the percentage of mature females of this species suddenly increased, suggesting that the first rise in temperature triggered maturation and, therefore, spawning of *F. indicus* (Fig. 2.3A). García (1988) and Dall et al. (1990) reported that some penaeid shrimps developed a long-term adaptation to the annual temperature cycle, such that maximum reproduction coincides with rising tem-

peratures from late winter to early spring, with potential favourable summer conditions for egg and larval development. Indeed, in the present study, the number of immature females of *F. indicus* increased significantly with increasing temperatures (stage I in Fig. 2.3A), supporting the spring temperature induction for maturation and spawning. Increasing temperatures have been extensively reported to induce or improve maturation and spawning of some wild and domestic (cultured) penaeid shrimps around the world, including *P. duorarum* (Cripe, 1994), *P. merguiensis* (Hoang et al., 2002), *P. semisulcatus* (Aktaş et al., 2003) and *Litopenaeus vannamei* (Kumlu et al., 2011).

For *M. monoceros*, spawning decreased in winter and increased in summer (de Sousa et al., 2006, 2008), supporting the hypothesis ($H_{2.1}$) indicating some seasonal differences. The present study revealed that, in contrast to *F. indicus*, spawning of *M. monoceros* was significantly correlated with annual temperature cycle, as cool winter temperatures decreased spawning, whereas warm spring and summer temperatures increased spawning (Fig. 2.3B). This supports the second hypothesis ($H_{2.2}$) for this species, that timing of increased spawning is clearly related to temperature. Similarly, other studies reported that winter temperatures below 25°C inhibit ovarian development and spawning of some penaeid shrimps, for instance *P. esculentus* (Crocos and Kerr, 1986), *P. stylirostris* (Robertson et al., 1991), *P. semisulcatus* (Aktaş et al., 2003; Turkmen, 2007) and *Rimapenaeus constrictus* (da Costa and Fransozo, 2004). Reviewing maturation and reproduction of some closed thelycum penaeid shrimps, Primavera (1985) reported high maturation and spawning rates with increased egg and larval production at temperatures above 26°C for tropical penaeid species.

Although there were some spawning fluctuations for both species of banana shrimps on the Sofala Bank, there was no month with zero or nearly zero mature females in the fishing seasons 2000−2003, i.e. there was no spawning off-season. Off-seasons have been reported for some penaeid species during the winter in temperate and subtropical regions, especially when temperature falls below 16°C (Penn, 1986; García, 1988; Dall et al., 1990; Minagawa et al., 2000; Hossain and Ohtomi, 2008). For some other species, the threshold is temperatures below 20°C (Dredge, 1985; Aktaş and Kumlu, 1999; Kumlu et al., 1999; Aktaş et al., 2003). In Turkey, *P. semisulcatus* and *M. stebbingi* do not spawn at all in winter, while during the summer percent-

ages of mature females were at times $> 75\%$ (Kumlu et al., 1999). In the tropical Sofala Bank, temperatures below 20°C rarely occur.

Caution should be exercised when interpreting these results (Fig. 2.3), because of limited spatial coverage of biological samples taken from landings data. It is important to note that only a few landings data were made available and it is possible that (1) they came from different locations each month, introducing bias to the comparisons, and (2) they came from the same location, but the extent to which they are representative of the entire Sofala Bank is unknown. Besides this limitation, these data still provide unique and important useful insights on intra-annual variability in reproductive biology, including ovarian maturation and spawning of banana shrimps on the Sofala Bank.

Spawning of both banana shrimp species fluctuated in the years from 2003 to 2010 on the Sofala Bank (Fig. 2.4). Consistent with intra-annual temperature variation, for *F. indicus* there was no correlation between inter-annual fluctuations in spawning and temperature (Fig. 2.4A). However, the rise in temperature from the preceding winter lows in 2005/2006 and 2009 to the comparatively high winter temperatures that followed in 2007 and 2010 corresponded with higher than usual increases in *F. indicus* female maturation rates. This inter-annual increase has a similar effect to the annual trigger caused by the rise from the winter low temperatures. This further supports the hypothesis that rising temperatures induce ovarian maturation and spawning of *F. indicus*, with subsequent favorable conditions for larval development (Cripe, 1994; Hoang et al., 2002; Aktaş et al., 2003; Kumlu et al., 2011). In contrast, numbers of mature females of *M. monoceros* were strongly correlated with winter temperatures of the preceding year (Fig. 2.4B), indicating that years with severe winters produced low maturation and spawning, whereas mild winters yielded high spawning. It is suggested that immature females of *M. monoceros*, which leave nursery areas during cold winters, do not reach maturity and spawning in spring-summer, therefore resulting in a low reproductive output season. These findings further support the hypothesis ($H_{2.2}$) that low temperatures are not favourable for *M. monoceros* maturation and successful spawning of this species depends on winter temperatures. Similar results of winter temperatures affecting spawning have been reported for other penaeid shrimp species around the world, including *Penaeus merguiensis* on the Australian Queensland

coast (Dredge, 1985), *Litopenaeus setiferus* in the South Carolina Atlantic Ocean (DeLancey et al., 2005) and *Parapenaeus longirostris* in the Moroccan Atlantic Ocean (Benchoucha et al., 2008). DeLancey et al. (2005) found that cool winter temperatures delayed maturation while warm temperatures promoted ovarian development and spawning of *L. setiferus*.

2.4.2 Reproductive strategy

It is known that penaeid shrimps have two types of offshore migration (Dall et al., 1990): (1) juvenile migration – juveniles migrate from the inshore nursery ground to join the offshore adult population, and (2) spawning migration – adults migrate offshore as they mature through ovary developmental stages. It has been shown that juvenile males outnumber females for both species in the Pungué estuarine nursery ground off Beira, Sofala Bank (Brito and Pena, 2007). In contrast, the present study found that, at the spawning grounds, adult females outnumber males for both species (Fig. A.1), supporting juvenile migration into the adult population (Dall et al., 1990). Males, which dominate in the estuaries, stayed there while females migrated offshore and dominated the spawning ground. However, the confidence interval for mature females of both species is large at shallow depths in the SPQ analysis (Fig. 2.9C and D), because of small sample sizes. There seems to be avoidance of shallow waters, also suggesting offshore migration into the adult grounds.

Although there were a few stations scattered over the entire bank with only one of the two female stages, with no particular pattern, both immature and mature females of *F. indicus* generally occurred together at most of the stations (Table. 2.2, Fig. 2.5A). There was no difference between depths (< 25 m) of occurrence of the two stages, indicating that there is no spawning migration from immature to mature females of *F. indicus* on the Sofala Bank. This is in agreement with García (1988), who reported that spawning (adult) migration is not important for some penaeid shrimps. For *M. monoceros*, however, although immature and mature females also occurred together at most of the stations (Table. 2.2), there were more stations with only mature females than stations with only immature females (Fig. 2.5B). Although not statistically significant, immature females of *M. monoceros* tended to be found

relatively shallower (< 30 m depth) than mature females (~ 40 m depth), indicating spawning migration, although this needs further investigation.

Generally, mature females of both banana shrimp species were found at the same stations (31%) in the onshore waters below 25 m depth (Fig. 2.6B), indicating that they co-occur at some locations in shallow waters. This finding is supported by both species generally being caught by the fishery in the same hauls (de Sousa et al., 2006, 2008, 2009, 2013). On the other hand, there was a significant difference between the depths of occurrence of mature *F. indicus* and *M. monoceros* (Fig. 2.6B), indicating that, although they overlap in the shallow waters (< 25 m), the mature *M. monoceros* extend deeper (up to 40 m), especially to the north of 17°45′S. The SPQ analysis also indicated that mature *F. indicus* avoided waters > 25 m depth (Fig. 2.9C), whereas mature *M. monoceros* did not. Indeed *M. monoceros* tolerate a full range of depths, including waters > 25 m (Fig. 2.9D). Similar differences in depth of spawning between closely related penaeid shrimp species have been reported in other regions around the world. For instance, in the northern Gulf of Mexico, *Penaeus setiferus* spawning occurs in shallow waters between $10 - 30$ m depth, while *Penaeus aztecus* spawning extends to > 30 m depth (Turner and Brody, 1983). This is in agreement with catch rates of adult *F. indicus* decreasing with depth, while those of *M. monoceros* increase (de Sousa et al., 2006, 2008, 2009, 2013). Similarly, off Kenya, in Malindi-Ungwana Bay, *F. indicus* were more abundant in shallow waters, whereas *M. monoceros* occurred in both shallow and deep waters (Munga et al., 2013).

These differences between depths of spawning of the two banana shrimp species may be explained by different substrata preference in relation to their burrowing capabilities (Williams, 1958; Dall et al., 1990). *Fenneropenaeus indicus*, which does not burrow, prefers substrata with high ($> 80\%$) mud content, where turbid water provides protection from predators. *Metapenaeus monoceros* however, which burrows completely for protection, has a wider range of substratum preferences from relatively low to high ($30 - 90\%$) mud content (Dall et al., 1990). The depositary mud content decreases with increasing depth seaward (Forbes and Demetriades, 2005), supporting overlap between *F. indicus* and *M. monoceros* in shallow muddy areas, while other *M. monoceros* extend deeper in less muddy areas. Other evidence in support of a muddy preference for both species is the fact that most mature females of both species were found in

954 regions with low autochthonous production (chlorophyll-*a* as determined by CTD fluorescence).
955 This is possibly because of low photosynthesis rates due to suspended organic matter and thus
956 limited light penetration in turbid coastal environments (Valiela, 1995).

957 Spawning of banana shrimps on the Sofala Bank is often reported as occurring offshore (de Sousa
958 et al., 2006, 2009, 2013). However, spawning of both species occurs within 50 m depth, thus
959 spawning onshore or on the continental shelf is more appropriate and the term "offshore" should
960 be avoided for these species. Offshore migration is only acceptable as a relative term, indicating
961 migration away from the shallow inshore/coastal nursery grounds to relatively deeper spawning
962 grounds. True deep offshore (> 100 m or even > 200 m depth) migration and spawning has
963 been observed for other penaeid shrimp, especially deep-water shrimp, for example, *Parapenaeus*
964 *longirostris* on the north Atlantic Moroccan coast (Benchoucha et al., 2008).

965 With regards to the latitudinal extent of spawning, there were a few stations with only mature
966 *F. indicus* females on the southernmost limit of the bank, in contrast with some stations with
967 only mature *M. monoceros* females, which were found at the northernmost limit (Fig. 2.6B).
968 These findings suggest that spawning of *F. indicus* has a more southwards distribution, while
969 spawning of *M. monoceros* happens more northwards. That is supported by the SPQ analysis
970 for latitude, which indicates mature *F. indicus* avoided the northernmost latitudes (Fig. 2.9A),
971 possibly due to a narrow shelf and consequently unfavourably deep water conditions.

972 2.4.3 Identifying and characterizing the dominant spawning areas

973 Dall et al. (1990), in a comprehensive review of the biology of penaeid shrimps, observed that
974 only few spawning areas have been identified and mapped. These authors also noted that
975 spawning is generally assumed to coincide with overall distribution of adults on the offshore
976 fishing grounds; their observation is still true today. Niamaimandi et al. (2008), however,
977 identified six main spawning areas for *Penaeus semisulcatus* in limited parts of the Bushehr
978 fishing ground of Iran, based on high densities of mature females. Similarly, in the present study,
979 three locations with elevated densities of mature females were identified as main spawning areas
980 for both banana shrimp species on the Sofala Bank (Fig. 2.7). All three spawning areas are near

an estuarine river: the Ligonha River for the northern area, the Zambezi River for the central area and both the Pungué and Buzi Rivers in Beira Bay for the southern area, supporting the hypothesis ($H_{2.2}$) that spawning of banana shrimps occurs near rivers. However, no preference for low salinity associated with freshwater inputs was found (Fig. 2.10C and D). Instead, relatively high oceanic salinity (~ 34.75) was preferred for spawning of both species, especially for *M. monoceros*. This preference agrees with the well-established concept that most shrimp species spawn in oceanic waters away from the estuary inlets (Dall et al., 1990). Therefore, the relationship with rivers is not directly associated with the brackish estuarine water; another possible explanation is substratum preference and its organic matter content. It has been shown that depository mud patches are found in the vicinity of the river mouths (Forbes and Demetriades, 2005). Such muddy patches have elevated allochthonous production carried by the rivers and other organic matter content from nearby mangrove forests (Williams, 1958; Hughes, 1966; Downing et al., 2000; Cloern et al., 2014). Vast mangrove forests occur on the Sofala Bank (Barbosa et al., 2001; FAO, 2005; Giri et al., 2011; Fatoyinbo and Simard, 2013), in which the spatial distribution is not homogeneous (Fatoyinbo et al., 2008). The sediment organic matter (detritus) content in mud and mangrove is believed to be the bulk food source for penaeid shrimps (Hughes, 1966; Dall et al., 1990; Primavera, 1998). This rich organic matter is carried by the rivers, explaining the observed spawning grounds adjacent to the rivers. By analogy, the mangrove free-region near the Licungo River (17°45′S Fatoyinbo et al., 2008) suggests the absence of mud, supporting the absence of adult mature shrimp and spawning in this region (Figs. 2.7 and 2.9).

It is well known that juvenile shrimps utilize riverine estuaries and mangrove creeks as nursery grounds (Hughes, 1966; de Freitas, 1986; Primavera, 1998; Rönnbäck et al., 2002; Macia, 2004), and then migrate to the continental shelf adult population (Dall et al., 1990). Thus, it is hypothesized that the association between the identified spawning areas and the adjacent rivers is related to the distance that juveniles can travel from the estuarine nurseries to the spawning grounds. More research, for instance on river discharge rates, sediment transport and substratum type, and mangrove distribution, is needed to clarify the role of rivers in the distribution of the spawning areas.

It has been proposed that spawning areas of marine organisms may be subject to change over years (Coull et al., 1998; Ellis et al., 2012). In the present study, there was little variability in the centres of gravity of mature females of both banana shrimp species in the northern and central spawning areas from year to year (Fig. 2.8), suggesting consistent spawning in these two regions during the study period. Similar results were obtained from the SPQ analysis in relation to latitude, showing spawning preference for the northern and central latitudes for both species (Fig. 2.9). In contrast, there was a relatively large inter-annual change in the spawning centres of gravity in the southern area (Fig. 2.8). There was no preference for spawning in the southern latitudes for both species (Fig. 2.9). These findings indicate that the southern spawning area might be less suitable than the other two areas. This is in agreement with low recruitment of juveniles into the adult population and subsequent low catches in this region (de Sousa et al., 2006, 2013).

Over the past decade, many studies have reported shifts (especially poleward) in the geographic distribution of marine organisms, in response to global climate change and warming (Harley et al., 2006; Snover, 2008; Hoegh-Guldberg and Bruno, 2010; Sorte et al., 2010; Burrows et al., 2011; Doney et al., 2012; Poloczanska et al., 2013). Recently, the Mozambique Channel, including the Sofala Bank, was identified among others as an ocean warming hotspot for climate change impacts (Hobday and Pecl, 2014). In the present study, there was no clear evidence of any shift in spawning distribution of banana shrimps on the Sofala Bank. The movements of the centres of gravity fluctuated both southwards and northwards with no prevailing direction in all three areas (Fig. 2.8A). Similarly, there was no trend or relationship between distances of consecutive years' spawning centres of gravity and temperature (Fig. 2.8B and C). However, the relatively short (8-year) time span might not be enough to demonstrate climate effects; a longer time series is needed.

It has been shown that some penaeid shrimps display seasonal variability in the depth of spawning (Vance et al., 1998; Benchoucha et al., 2008). However, this is mainly observed in temperate regions where the depth of the thermocline fluctuates with seasons, forcing the shrimps to change depths (García, 1988). Caution should be exercised when interpreting the spatial spawning patterns discussed here, because neither biological nor environmental spatial

data used in this study cover the whole annual cycle. It should be noted that the data were limited to summer (with no seasonality) during the January/February annual surveys of 2003−2010. Accepting that both banana shrimp species spawn all year-round and, indeed, spawning is relatively high during the summer, it is reasonable to use these summer data to identify and characterize the spawning areas. Similarly, spawning areas of many marine organisms around the world have been identified from annual data with no seasonal variation, for example, > 10 commercial fish species in the United Kingdom by Ellis et al. (2012). With the aim of extending the spawning area analysis throughout the year, it was hypothesized that shrimp size could be used as an indicator of spawning, given that shrimps increase in body size as they mature (Amanat and Qureshi, 2011). This would allow extra data (i.e., size−categorised commercial logbook data during the fishing season March – November) to be used. Although the mean sizes of females of both shrimp species increased with ovarian maturity stages (Appendix A), the size ranges of all four maturity stages overlapped (Fig. A.2). Moreover, the size at first maturity for both species (Fig. A.3) was found within all four stage size ranges (Fig. A.2). These findings may be explained by the fact that penaeid shrimps reproduce several times (Dall et al., 1990). In their reproductive cycle, individuals in stage IV return to stage II after spawning, so "small" individuals for the first time in stage II, III and IV are found mixed with "large" individuals that had spawned before. These findings led to the rejection of the hypothesis that the size class of banana shrimp females may be used as a strict indicator of spawning. Hence, no extra spatial data are available to cover a full year.

In the 1970s, just before the main development of the large shrimp fisheries in the East African region, it was demonstrated that the Sofala Bank has favourable conditions for penaeid shrimps and hosts the largest stock in the region (Ivanov and Hassan, 1976). Overall, in this chapter no avoidance for any environmental variable by the shrimps was observed (Fig 2.10), supporting the idea that their spawning on the Sofala Bank is not limited by environmental (summer) conditions like temperature and salinity.

The three spawning areas are relatively small compared with the entire Sofala Bank fishing ground, as described by the combined (both species) distribution of hauls from the captains' logbooks (de Sousa et al., 2013). This finding supports the hypothesis $H_{2.1}$ that spawning of

banana shrimps is not uniformly distributed. The spawning areas, however, coincided with locations of the highest levels of fishing effort combined for the main fleets (de Sousa et al., 2006, 2008, 2009) and for all fleets (de Sousa et al., 2013). This may explain why spawning biomass decreases continuously throughout the fishing season, soon after it opens in March, to low levels late in the season in November, especially for the shallower *F. indicus* (de Sousa et al., 2006, 2008). These results clearly show that these essential spawning grounds need protection and effective management; spawning stock overfishing might occur and could lead to low recruitment of juveniles entering the fishery and, consequently, to low fishing yields.

In summary, both species of banana shrimp spawn year-round on the Sofala Bank. The present study elaborates for the first time on the relationships between timing and location of banana shrimp spawning and environmental factors on the bank. Spawning of *M. monoceros* decreases significantly with cool winter temperatures. For *F. indicus* spawning is independent of temperature, although rising temperatures from winter to spring or from year to year stimulate and promote maturation and spawning of this species. The main banana shrimp spawning areas on the Sofala Bank comprise three locations: (1) northern, (2) central and (3) southern, with the northern and central locations being more consistent than the southern. All three spawning locations are related to rivers, possibly associated with substratum type and food availability. More data are needed to clarify patterns of spawning of banana shrimps on the Sofala Bank, particularly regarding river discharge rates, sediment transport, substratum type and organic matter content in the sediment. The Sofala Bank has optimum summer conditions for maturation and spawning of banana shrimp.

This study assists the management of these commercially important resources by providing maps of the essential spawning grounds that may be considered in environmental impact assessment processes for integrated coastal and marine developments on the Sofala Bank. For ecological purposes, these identified spawning areas will be used in the next chapters (5 and 6) as release areas to set up an individual based-model to investigate and understand patterns of larval dispersal of banana shrimps on the Sofala Bank and possible factors influencing it. The understanding of larval migration into the nursery area is a key point in the spawner-stock/recruitment issue (García, 1988; Ospina-Álvarez et al., 2013).

Chapter 3

A circulation model of the Sofala Bank

Abstract

A coastal ocean circulation model of the continental shelf of the Sofala Bank and the adjacent deeper ocean was simulated for ten years, with climatological forcing. The split-explicit, free-surface, topography-following vertical (50) σ-layers coordinate Regional Ocean Modeling System (ROMS) is used. The three-dimensional, high-resolution model configuration consisted of two-way nesting, with a coarse Parent grid at ~ 6 km resolution and a fine Child grid at ~ 2 km resolution. Simulations were forced with monthly climatology surface winds, fresh-water and heat fluxes included in the ROMSTOOLS. For some experiments, tides (ten main constituents) and monthly climatology river (four, including the Zambezi) forcing were integrated. For the large-scale lateral open boundary conditions the South-West Indian Ocean Model was used, based on the offline one-way nesting. The model results are shown in comparison with available observations and published works. The model overestimates the eddy kinetic energy and root mean square of SSH of AVISO observations by 50% and underestimates the offshore extent of the Zambezi River plume by 50%. The discrepancy of the tidal amplitude between the model and the Beira tide gauge (percentage error 20%) is related to position in the estuary, which was not resolved by the model. However, all the known current, hydrography and water mass structures were identified by the model. This model is useful to understand the oceanography of the Sofala Bank shelf, particularly the influence of the Mozambique Channel mesoscale eddies. The model is used in different applications for the Sofala Bank, including coupling with biological models.

3.1 Introduction

The circulation in the Mozambique Channel is dominated by passing mesoscale eddies and rings (Chapter 1). During their displacement, eddies have been observed to alter the physical environment of the southern part of the Mozambique Channel by entraining coastal waters into the pelagic region, creating temporary and localized currents (Roberts et al., 2014). However, their impact on the shelf waters of the Sofala Bank is presently unknown as even basic knowledge on the oceanography of the Sofala Bank is limited.

Similarly to other regions around the world, in the Mozambique Channel ocean modelling has been used to understand the ocean circulation and structures, particularly when the observational data are scarce. Recent modelling studies include: the effect of the presence of Madagascar in driving the Mozambique Channel eddies (Penven et al., 2006b); the general circulation and the Mozambique eddies (Segtnan, 2006; Backeberg and Reason, 2010; Quartly et al., 2013; Halo et al., 2014); eddy influences on biological production (Jose et al., 2014); Zambezi River plume (Nehama, 2012); and general tides of the Sofala Bank (Chevane, 2013). Most of these studies, except Nehama (2012) and Chevane (2013), focus on the open waters with regional application, while little attention is given to the coastal and shelf regions. Nehama (2012) focused on the coastal river plume dynamics, but his model lacked the Mozambique eddies that are important for ecosystem function (Weimerskirch et al., 2004; Quartly and Srokosz, 2004; Omta et al., 2009; Tew-Kai and Marsac, 2009; Tew-Kai et al., 2009; Jose et al., 2014). Chevane (2013) model focused on coastal tides, but lacks fine-resolution and river inputs that are responsible for coastal stratification, influencing shelf dynamics (da Silva et al., 2009).

The aim of this chapter is to set up a high-resolution ocean model of the Sofala Bank shelf which takes into account the offshore features and to evaluate model results by comparison with observations and the literature. The "Regional Ocean Modeling System" (ROMS, Shchepetkin and McWilliams, 2005) version AGRIF (Debreu et al., 2012) is used. ROMS is a descendant of the S-Coordinate Rutgers University Model (SCRUM, Song and Haidvogel, 1994; Hedstrom, 1997) that superseded the Semi-spectral Primitive Equation Model (SPEM, Haidvogel et al., 1991). The AGRIF version of ROMS (ROMS_AGRIF or just ROMS) was developed at the

IRD, France, and it is freely available at http://www.romsagrif.org. ROMS has been widely used in continental shelf and oceanic studies in different regions of the world (e.g. Di Lorenzo et al., 2005; Marchesiello et al., 2003; Veitch et al., 2009, 2010; Penven et al., 2006b), including the western Indian Ocean and Mozambique Channel (e.g. Segtnan 2006; Halo et al. 2014; Jose et al. 2014). The ROMS model of the Sofala Bank (hereafter ROMS-BSM) is primarily for coastal application, as it includes tides and river discharge. The results from the ROMS-BSM will be used in the following chapter as physical forcing for the biological model, which uses the IBM "Ichthyop software" (Lett et al., 2008).

3.2 Model and data

3.2.1 ROMS for simulating ocean dynamics

ROMS is a split-explicit, free-surface, topography-following vertical sigma(σ)-coordinate, and curvilinear horizontal σ-coordinate ocean model designed for regional applications (Shchepetkin and McWilliams, 2005). The σ-coordinate allows the resolution of interactions between bottom topography and ocean dynamics (Marchesiello et al., 2003), which is important for the Sofala Bank. Moreover, ROMS is a three-dimensional regional model which solves the incompressible, hydrostatic and Boussinesq primitive equations (seven) described by Haidvogel et al. (1991).

The updated version of ROMS used in this study uses a third-order, upstream advection scheme for tracers, which has been split into a fourth-order advection scheme associated with a rotated biharmonic diffusion (Shchepetkin and McWilliams, 2005). This higher-order precision reduces dispersive property errors and enhances model effective resolution of smaller scale processes (Marchesiello et al., 2003). The rotated diffusion operator is designed for numerical stability and is able to preserve low dispersion and diffusion capabilities, while preserving water mass characteristics (Marchesiello et al., 2009). Vertical mixing is computed through a nonlocal K-profile parameterization scheme (Large et al., 1994). Bottom friction is parameterized using a quadratic bottom drag term. The split-explicit mode decomposition of ROMS allows longer time steps for the slower 3D baroclinic mode (Marchesiello et al., 2009) and shorter time steps for the fast 2D barotropic mode. This time step ($\triangle t$) should be adjusted to preserve the Courant Friedrichs Lewy (CFL) stability criterion (equation 3.1):

$$\frac{\triangle x}{\triangle t} > C \tag{3.1}$$

where $\triangle x$ is the horizontal grid resolution, $\triangle t$ the model time step and C the fastest propagating wave speed (for example, the external gravity wave propagation [$c_g = \sqrt{gH}$, where g is the gravitational acceleration and H is the scale height] resolved by the 2D fast mode). A complete description of ROMS is presented by Shchepetkin and McWilliams (2005).

3.2.2 Model configuration design and forcing

The circulation on the Sofala Bank should be influenced by the offshore mesoscale eddy activity, as well as tides and river flows. For this reason a model domain that encompasses the entire Sofala Bank was chosen between roughly 14−24°S (Fig. 3.1A) and includes a broad and shallow continental shelf, a continental shelf break, a continental slope and deep ocean (i.e. offshore adjacent waters). The model uses a structured regular square grid in the horizontal plane with a resolution set to 6.36 km ($^1/_{16}$°). This model domain has a total of 114×194 horizontal grid points. To minimize the number of grid points lying on the land mask, an oblique Mercator domain that follows the coastline is used (Fig. 3.1A). The oblique domain was rotated so that the u-component of the model currents flows approximately in the along-shore direction and the v-component in the cross-shore direction.

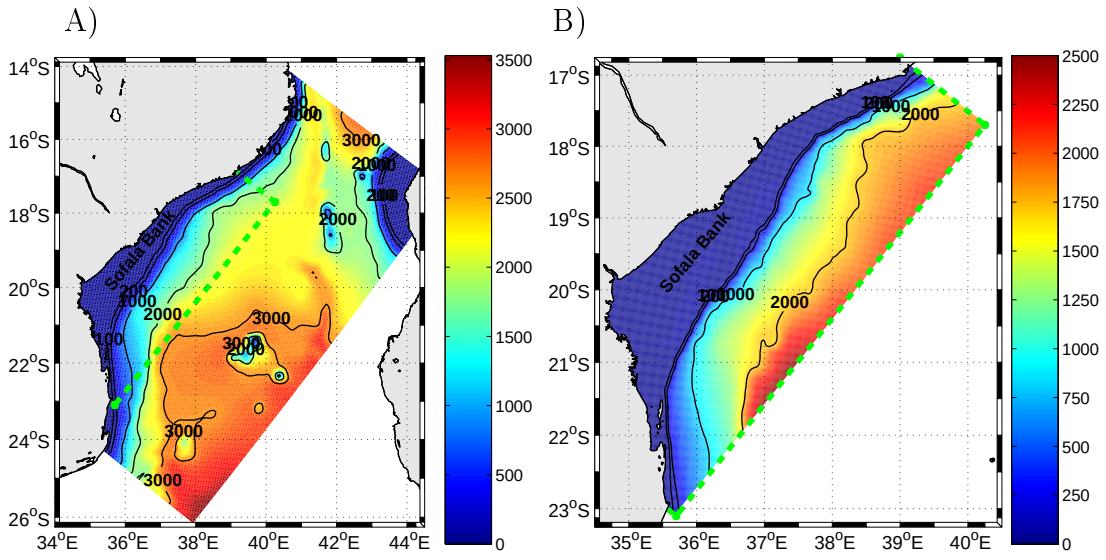

Figure 3.1: Oblique model domains used for the ROMS model of the Sofala Bank (A) at 6 km resolution (Parent) and (B) nested at 2 km resolution (Child). Color (blue-red) shading indicate depth and isobaths are plotted for 100, 200, 500, 1000, 2000 and 3000 m (black lines). The green dashed-line outlines the Child domain.

The model topography was derived from the General Bathymetric Chart of the Oceans (GEBCO) One Minute Grid data set (Jakobsson et al., 2008). The GEBCO One Minute Grid bathymetry (available at `http://www.gebco.net/data_and_products/gridded_bathymetry_data/`) was interpolated to the model grid using ROMSTOOLS (Penven et al., 2008) and smoothed for numerical accuracy using an r-smoothing factor (Haidvogel and Beckmann, 1999) kept to 0.25 according to the following equation:

$$r = \frac{\nabla h}{h}, \tag{3.2}$$

where r is the smoothing factor, h the depth of the bathymetry and ∇h the depth gradient.

The minimum depth was set to 30 m at the coast. The model bathymetry is in agreement with that described in chapter 1, i.e. a wide continental shelf in the central Sofala Bank which becomes narrow to the north and south edge (Fig. 3.1).

The model has 50 vertical σ-layers N with enhanced resolution toward the surface. The vertical σ-coordinate control stretching parameter at the surface is defined by $\theta_s = 5.5$ and at the bottom $\theta_b = 0$. The vertical transition depth layer between the horizontal surface levels and the bottom terrain-following levels Hc is 10 m. The bottom friction coefficient is determined by a logarithmic law and the bottom roughness (zob) is 0.01 m.

Surface forcing and lateral open boundary conditions

Monthly climatologies are used for the surface forcing. Sea surface wind stress from the Quick Scatterometer (QuikSCAT) satellite with a grid resolution of $1/2^\circ$ is used. These wind data show that the model domain is a transition region between the dominating SE trade winds in the south and the seasonal East African monsoon wind in the north (Fig. 3.2). During the dominant SE trade winds from April to September, the wind forcing is relatively weak in the coastal region of the central Sofala Bank ($\sim 20^\circ$S), although strong winds are apparent to the north of 16°S. The influences of monsoon winds are evident by weak winds to the north of $\sim 20^\circ$S during the austral spring and summer from October−March (Fig. 3.2). Such monsoon winds exhibit directions different from the southeastern (SE) trade winds, generally being northeasterly (NE) (spring in Fig. 3.2). The overall regime of the wind forcing is consistent with that of the observed winds described in chapter 1.

For surface fresh-water and heat fluxes, COADS (Comprehensive Ocean-Atmosphere Data Set) monthly climatology is used at a grid resolution of $1/2^\circ$ (Da Silva et al., 1994). Sea surface temperature (SST) from Pathfinder satellite observations at a high horizontal resolution of

1220 $\sim$ 9 km (Casey and Cornillon, 1999) was used as an alternative for the lower resolution $^1/_2°$
1221 SST from COADS of the correction of the sensitivity of the surface heat flux to SST (Barnier
1222 et al., 1995). The global atlas of surface marine data from COADS and SST-Pathfinder are
1223 included in ROMSTOOLS (Penven et al., 2008) available at `http://www.romsagrif.org`. The
1224 horizontal grid resolutions for all surface variables used here were interpolated onto the model
1225 grid (resolution $\sim$ 6 km). Time in days for the monthly climatology data sets correspond to
1226 the middle of each month.

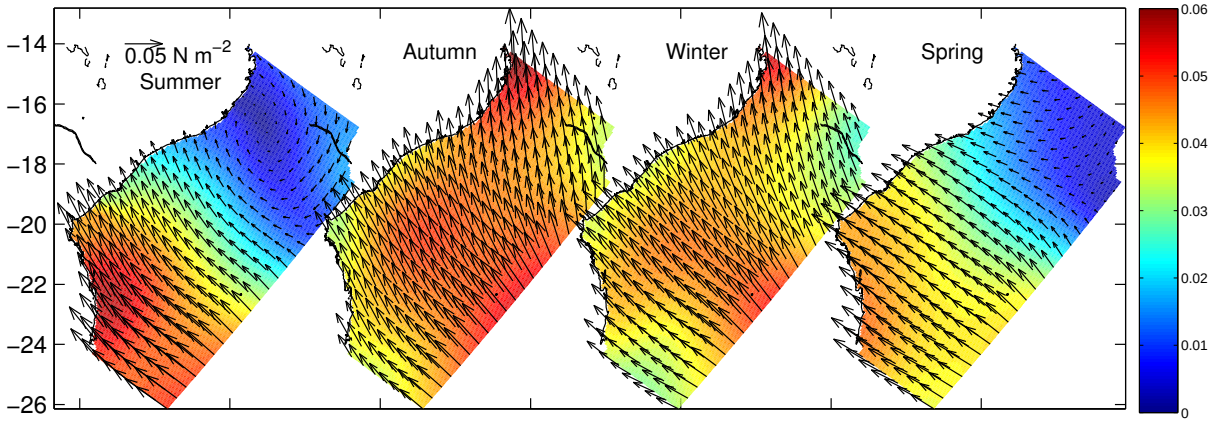

Figure 3.2: Seasonal mean sea surface wind stress and direction vectors (N m^{-2}) derived from QuikSCAT at a grid resolution of 1/2° for summer (January, February and March), autumn (April, May and June), winter (July, August and September) and spring (October, November and December). Color shading (color bar) indicates wind stress magnitude.

1227 The lateral boundaries are open everywhere except at the coastal side to the west of the
1228 domain. To avoid numerical instabilities at the lateral open boundaries, a "sponge" layer (the
1229 area directly influenced by the adjacent outer region) with enhanced diffusion/viscosity based
1230 on a classical Laplacian operator is applied. The width of the sponge layer (x_sponge) is 60
1231 km. The explicit lateral viscosity is zero everywhere in the domain except in the sponge layers
1232 (x_sponge), where it increases smoothly from the interior to the maximum value of 500 m^2 s^{-1}
1233 close to the boundaries.

1234 For lateral open boundary conditions the model configuration used outputs from the South-
1235 West Indian ocean Model (SWIM, Halo 2012; Halo et al. 2014) employing the one-way (also
1236 called ROMS-to-ROMS or off-line) nesting technique (Mason et al., 2010). SWIM is a model
1237 configuration of ROMS_AGRIF with a horizontal grid resolution of 1/5° in the south west
1238 Indian Ocean, which encompasses the entire Mozambique Channel (Halo, 2012; Halo et al.,

2014). The SWIM model outputs have been evaluated using *in-situ* moored current meter array data of the Long-term Ocean Climate Observation (LOCO) program (de Ruijter et al., 2002; Ullgren et al., 2012), and satellite-derived sea surface altimetry (Halo, 2012; Halo et al., 2014). With this one-way nesting, SWIM provides important information such as mesoscale eddy activity of the Mozambique Channel and other remote forcing for our coastal model, but there is no feedback from our model to SWIM. The set of boundary conditions used include sea surface elevation, barotropic and baroclinic velocity components, temperature and salinity.

Tidal forcing derived from TPXO6.2 was also integrated into the lateral open boundaries. TPXO6.2 is a Global Inverse Tide Model data set with a horizontal resolution of $1/4° \times 1/4°$ (Egbert and Erofeeva, 2002), and is also included in the ROMSTOOLS (also available at `http://www.esr.org/polar_tide_models/Model_TPXO62.html`). Ten tidal primary constituents (M2, S2, N2, K2, K1, O1, P1, Q1, Mf and Mm) propagate into the model using the open boundary condition method described by Flather (1976). Chevane (2013) has demonstrated that the model tides are comparable to *in-situ* observed tides collected by a coastal tide gauge off the Bay of Beira. To avoid instabilities, particularly from tidal currents, a ramp-up time of 2 days was applied at the initialization of the model simulation.

The model was run for a period of 10 years with a time step of 300 s (Courant number = 0.22) and an output averaged for each 3 days. To minimize the computation time, the model was run using MPI parallelization with 24 processors, requiring 7 days to complete the 10 year simulation.

3.2.3 Nesting (Parent+Child) configuration design and forcing

Because the aim of this chapter is to set up a model to investigate the shelf dynamics on the Sofala Bank in relation of offshore remote features such as the eddies, there is a need to zoom from the deep ocean into the coastal region with depths below 200 m. The two-way nesting (Debreu et al., 2012) capability of ROMS_AGRIF is well suited for this purpose. Such a two-way nesting allows several (in this case two) grids to be created at different resolutions, with a regional fine resolution grid (Child grid) embedded into a coarser grid (Parent grid)

(Penven et al., 2006a; Debreu, 2008; Debreu et al., 2012). The nesting approach increases the regional horizontal resolution, improving the representation of small-scale coastal features that are hardly represented in the coarser grid alone. In two-way nesting, the Child grid uses information from the Parent grid for its lateral boundaries and then the solution of the Child grid is transferred back to update the solution of the Parent grid (Debreu et al., 2012). This includes information about river discharges.

The $\sim$ 6 km ($1/16^{\circ}$) resolution grid domain described in the previous sections was used as the Parent grid. Grid and time refinement of ROMS_AGRIF allows high spatial and temporal resolution. In this model the spatial and temporal coefficient of refinement (r_{coef}) used to define the Child grid was a factor of one third the Parent grid. (i.e. Child resolution is the Parent resolution divided by three and the Child time step is the Parent time step divided by three.) Thus the Child grid resolution is 2.12 km ($1/48^{\circ}$) and the Child model time step is 100 s (Courant number = 0.18). The Child domain has a total of 144×360 horizontal grid points. This Child domain, although smaller than the Parent in area, still covers the entire Sofala Bank, including the continental shelf and slope (Fig. 3.1B). The estuaries and the Zambezi delta are not included in the model, only the river mouths are located in the land/sea mask boundary.

The Child grid bathymetry (Fig. 3.1B) was interpolated from the original GEBCO data set, allowing for a more detailed topography. The Child grid minimum depth was set to 15 m to avoid the drying of grid cells at the shore, particularly during tide simulations. Note that the tide model simulation was unstable when a minimum depth was set to 10 m due to drying of the inter−tidal region to the south of Beira Bay. The Child model has 50 vertical σ-layers and the vertical grid parameters are those of the Parent model ($\theta_s = 5.5$, $\theta_b = 0$ and $Hc = 10$).

Child model surface forcing and initial conditions were interpolated in space and time from the Parent model. The two-way nested (Parent + Child) model simulations were also run for a period of 10 years with an output averaged every 3 days. Because of the Child grid, which requires a high demand of computation time, the number of processors used in the MPI parallelization approach was increased to 48 for the simulation with two-way nesting. The total time required to complete a 10 year two-way nesting simulation was approximately 12 days. Additionally, for simulations with tides, higher frequency outputs were written for the Child

grid, with sampling every hour for one year (model year 5).

3.2.4 River model configuration

Knowledge of river inputs and plume behaviour are important for understanding the circulation and biogeochemistry on the Sofala Bank. Four rivers were included in the model simulations: the Licungo, Zambezi, Pungué and Buzi Rivers (Fig. 3.3). Because the river mouths of the Pungué and Buzi Rivers are located close to each other in the Bay of Beira (Fig. 3.3) they were considered as one river and their flows added together (referred to as "Beira-Bay River").

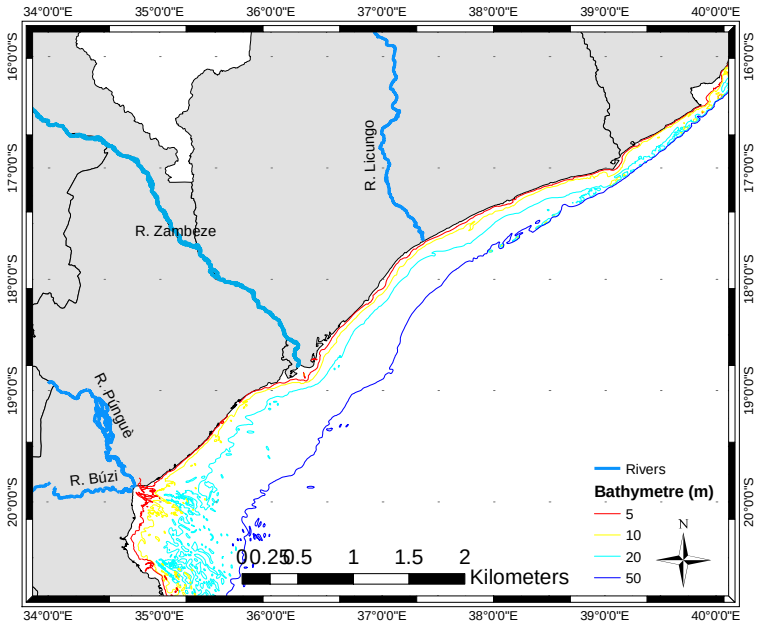

Figure 3.3: Map of the Sofala Bank showing the four rivers included in the model simulation: Licungo River, Zambezi River, Pungué River and Buzi Rive. Note that the letter R. on the map refers to river.

These rivers were included in the model as three point sources of momentum (realistic river flow Q) and tracers (temperature and salinity) lying at the land and sea boundary (i.e. the rivers flow from the land mask into the sea). The effect of estuaries was not considered as this is a shelf model. River forcing was incorporated into both the Parent and Child grid. The vertical distribution of the river flow was set to be exponential so that most of the flow is placed in the upper surface layers, decreasing to near zero at the bottom of the river source point. Because the river flow rates ($m^3\ s^{-1}$) were made available to this study as a monthly averaged climatology

by the Mozambican National Directorate of Water (DNA), the river forcing was introduced as a constant monthly flux (Fig. 3.4). The ROMS source code was modified to allow the input of monthly river flow. The tracer input of the rivers consisted of averaged temperature (28°C) and salinity (20) derived from the Mozambican Fisheries Research Institute (IIP) annual cruise surveys between January-February 2003 to 2010 (Chapter 2).

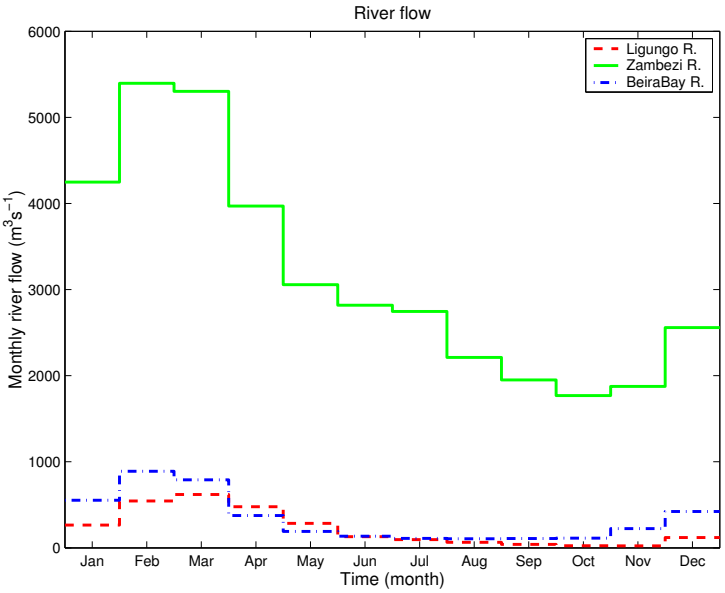

Figure 3.4: Monthly flow ($Q = m^3 s^{-1}$) for the Licungo (red), Zambezi (Green) and Beira-Bay (Pungué + Buzi, blue) rivers. Data from the National Directorate of Water.

Fresh water plume index

The extent of the river plumes on the Sofala Bank can be determined by the salinity, ranging between $28 - 34$ (typical of the frontal zone) observed during the IIP's annual cruise surveys. The plume index (also called fresh water thickness, h_f) is determined by vertical integration of the salinity anomaly ($(S_0 - S)/S_0$), relative to a reference salinity (S_0) (Hetland, 2004; Horner-Devine, 2009):

$$h_f = \int_{-H}^{\eta} \frac{S_0 - S}{S_0} dz \tag{3.3}$$

where $-H$ is the bottom depth and η the free surface. The reference salinity at the Sofala Bank was set to $S_0 = 34.5$.

3.2.5 Data for model evaluation

The accuracy of the model solutions was assessed, where possible, by comparisons with observations (satellite and *in-situ* data) and knowledge gained from available literature. Because of the scarce observational data in this region, most of the evaluation was performed for the large-scale Parent grid using statistical approaches such as the long-term and seasonal means. In the evaluation of the model, emphasis is placed on accurate reproduction of the seasonal variability and mean state of currents, temperatures and salinities, tides and eddy dynamics. A summary of datasets used in the model evaluation is presented in Table 3.1.

Table 3.1: Summary of satellite and *in-situ* datasets, and literature that were used to evaluate the model solutions. Note that "res." refers to resolution.

Model	**Observation**			
ROMS-BSM	**Data**	**Source**	**Spatial res.**	**Temporal res.**
Mean SSH	MDT	CNES-CLS09 (Rio et al., 2011)	1/4°x 1/4°	mean 1993-1999
	ADT	AVISO	1/4°x 1/4°	mean 1993-1999
Surface currents	Geostrophic current	CNES-CLS09 (Rio et al., 2011)	1/4°x 1/4°	mean 1993-1999
		AVISO	1/4°x 1/4°	mean 1993-1999
Mean SST	SST	MODIS	4 x 4 km	mean 2002-2012
		CARS	1/2°x 1/2°	annual climatology
		Pathfinder	9 x 9 km	annual climatology
		WOA2009	1°x 1°	annual climatology
Mean SSS	SSS	CARS	1/2°x 1/2°	annual climatology
		WOA2009	1°x 1°	annual climatology
Mean vertical currents	Current	LOCO (Ullgren et al., 2012)	Irregular section $\sim 16°$S	Mean 2003-2009
Mean vertical Temperature	Temperature	LOCO (Ullgren et al., 2012)	Irregular section $\sim 16°$S	Mean 2003-2009
		CARS	$1/2° \times 1/2°$	annual climatology
Mean vertical Salinity	Salinity	LOCO (Ullgren et al., 2012)	Irregular section $\sim 16°$S	Mean 2003-2009
		CARS	$1/2° \times 1/2°$	annual climatology
Monthly Temperature	Temperature	UTR	Irregular (station at $\sim 17°$S)	weakly 2003-2007
			Irregular (station at $\sim 22°$S)	weakly 2003-2007
SSH	Tides	Tide gauge station (INAHINA)	Irregular (near Beira)	Hourly for two months

Analysis and statistics

A statistical measurement for the agreement between a model and observation or between two models is the correlation coefficient (r) and coefficient of determination (R^2) (Liu et al., 2009b). In the present study, the correlation coefficient was determined for the comparison between simulated and observed tides at the Beira tide gauge.

Another widely used statistic to assess model accuracy is simply the difference (bias) between two models (M_{diff}), computed by subtracting one model value (M_1) from the other (M_2); defined by the expression $M_{diff} = \frac{1}{n}\sum(M_2 - M_1)$, where n is the number of model data pairs (Lehmann et al., 2009). Since mesoscale eddies are not expected to occur at exactly the same time (and space) in the two distinct model simulations due to chaos; a long-term mean ($\overline{M}$) is used to calculate the difference, therefore $n = 1$ and the expression becomes $\overline{M}_{diff} = \overline{M}_2 - \overline{M}_1$. The smaller the absolute values of the difference the better the agreement between the two, while zero difference indicates a perfect match between the two. Difference or bias is preferable rather than root mean square error (RMSE) because the square loses the bias signal and therefore it is difficult to assess an under- or overestimation. Moreover, Lehmann et al. (2009) have demonstrated that RMSE can be problematic in highly energetic mesoscale eddy regions, such as the study area.

3.3 Results and discussion

3.3.1 Model sensitivity and Spin-up time

A set of sensitivity experiments using different initial conditions and parameters showed that the model ocean dynamics in the Mozambique Channel are highly sensitive to the initial conditions and parameter choices, especially offshore (not shown). For example, by changing parameters such as the viscosity in the sponge layer from 500 to 1000 $m^2\ s^{-1}$ and/or the bottom roughness from 0.01 to 0.001 m, the model solution diverges rapidly from the reference run. Based on these sensitivity experiments, the best solution was found to use a viscosity of 500 $m^2\ s^{-1}$ and a bottom roughness of 0.01 m, which are used here for the reference configuration described in the data section. Such sensitivity to initial conditions (and parameters) is characteristic of nonlinear dynamic systems and was defined as chaos (Lorenz, 1963). Chaos has been widely studied in oceanic and atmospheric sciences (Sharifi et al., 1990; Zeng et al., 1993; Huang and Dewar, 1996; Feliks, 2004). A chaotic system is not considered disordered but rather ordered without periodicity (Lorenz, 1963; Zeng et al., 1993). As a result, a statistical approach has been adopted for investigation of the behavior of the model results. It is also important to note that the model solutions are unreliable at the edges of the model domains (lateral open boundaries).

A set of six model experiments was carried out for case studies. Note that initial conditions, forcing and reference parameters were all kept the same for all six experiments (as described in the data section, reference configuration). A summary of the six experiments and those parameters that were changed is shown in Table 3.2. Although some of the experiments (such as E1 and E5) are not discussed in detail in this study, they were included in Table 3.2 because the approach used was to progressively evolve from a simple to complex configuration by adding layers of complexity and analyze the results one at time. i.e. before the tide simulation (E2) was carried out a simulation without tide (E1) was undertaken – as was the case for the river simulation (E6).

Table 3.2: Summary of the six model experiments and parameters that were varied.

ROMS-BSM Experiment (E)	Temporal Resolution		Spatial resolution		Tide	River
	Frequency	Period	Parent	Child		
E1 Base 1	3-day mean	1-10 years	6 km	n/a	–	–
E2 Base with tide	3-day mean	1-10 years	6 km	n/a	√	–
E3 Nesting	3-day mean	1-10 years	6 km	2 km	–	–
E4 Nesting w tide	3-day mean	1-10 years	6 km	2 km	√	–
	hourly mean	year 5	n/a	2 km	√	–
E5 River	3-day mean	1-10 years	6 km	2 km	–	√
E6 River w tide	3-day mean	1-10 years	6 km	2 km	√	√
	hourly mean	year 5	n/a	2 km	√	√

The spin-up time was defined by the volume−averaged salinity, which was the last to reach an equilibrium stability. The model surface−averaged kinetic energy, volume−averaged kinetic energy and volume−averaged temperature reached equilibrium stability after about one year (Figs. 3.5A, B and C). The volume−averaged density also reached an equilibrium stability at one year (not shown), but the volume−averaged salinity took longer, reaching the equilibrium state only after three years (Fig. 3.5D). This implies that the spin-up time required for the model (E2) to reach equilibrium is three years and the model results from the first three years (year 1 to 3) are therefore excluded from the analyses in this study, i.e. years 4 to 10 were used. The model annual, seasonal and monthly averages were computed for these seven years $(4-10)$. All other experiments (E1, E3, E4, E5 and E6) also had a similar spin-up time of three years (not shown).

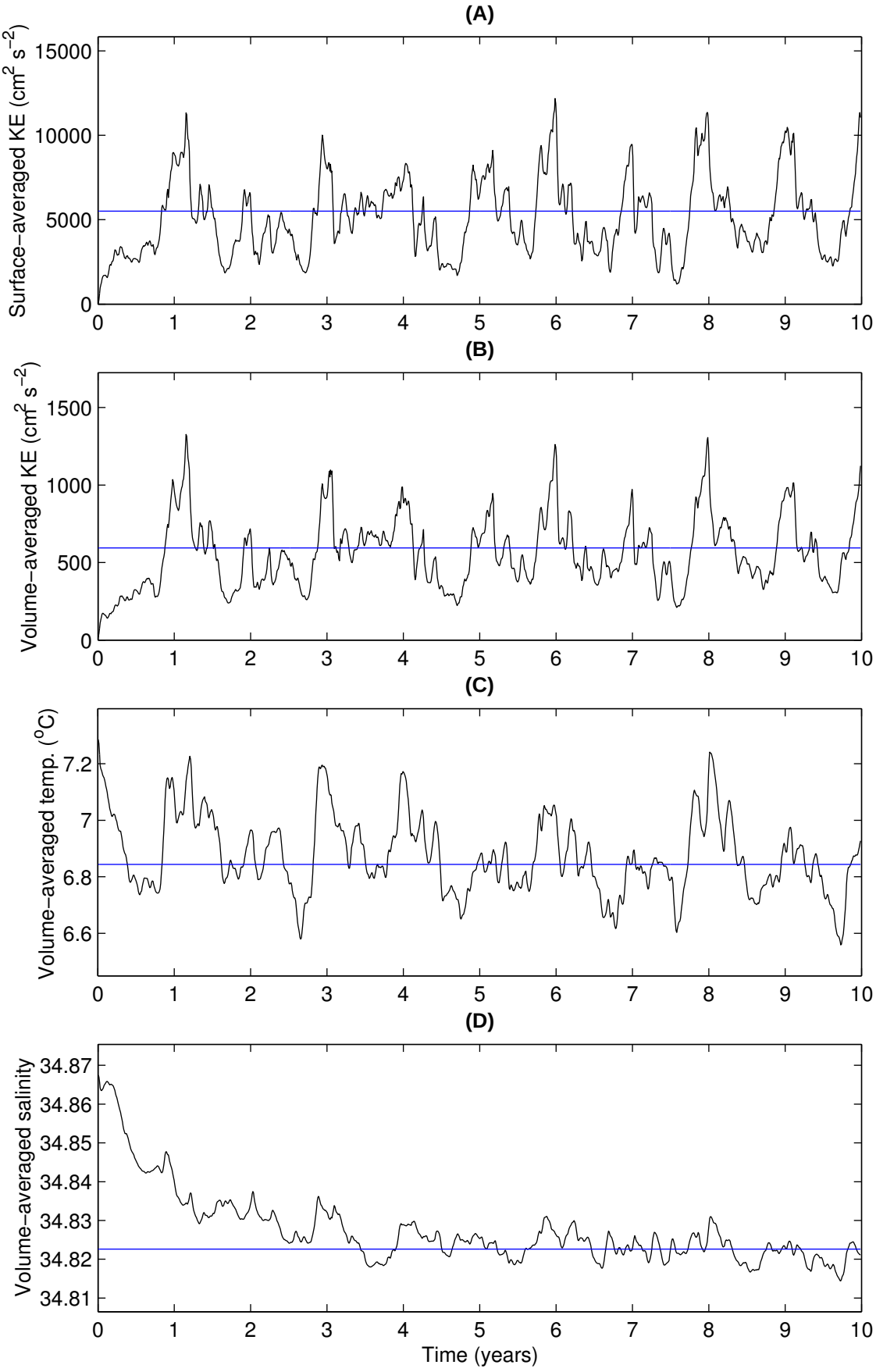

Figure 3.5: Results of the base experiment with tide (ROMS-BSM-E2, E2 in Table 3.2) showing 10-year time series of the Parent model for (A) surface-averaged kinetic energy (KE) (B) volume-averaged kinetic energy, (C) volume-averaged temperature (temp.) and (D) volume-averaged salinity. Blue line indicates the averaged.

3.3.2 Mean state (circulation and hydrography structures)

It is important to note that, because of the scarcity of observational data, the mean state is used for model comparisons investigating the large scale domain of Sofala Bank (Parent model before nesting, E2). Nesting of the Parent and Child models is investigated by taking into consideration knowledge gained from the Parent model before nesting.

3.3.2.1 Annual mean SSH and circulation

Mean sea surface height

The model long-term mean (climatology) SSH was generally positive, ranging from 0 to 55 cm (Fig. 3.6A). A homogeneous and low mean SSH ($<$ 10 cm) was apparent at the continental shelf within the 200 m isobath. A high mean SSH ($>$ 50 cm) is apparent from the northernmost limit of the domain to $\sim$ 20°S in the middle of the channel. Offshore there is a low SSH ($<$ 20 cm) centered at $\sim$ 40°E and $\sim$ 22°S. A strong west-east gradient (closely-spaced contours) of mean SSH is apparent over the Mozambican continental slope, following the bathymetry between the 200 and 2000 m isobaths (Fig. 3.6A). This mean SSH gradient is an indication of the presence of a mean "Mozambique Current". A similar strong mean slope SSH gradient was found in simulations of a NEMO (Nucleus for European Modelling of the Ocean) model of the Mozambique Channel at different horizontal resolutions from 1997 to 2001 (Quartly et al., 2013).

Comparisons between mean SSH from model, CNES-CLS09 and AVISO altimetry shows qualitative agreements (Fig. 3.6), in particular, the low SSH on the continental shelf of the Sofala Bank, the high SSH (red spectrum) from the northernmost limit, the offshore low SSH centered at $\sim$ 40°E and $\sim$ 22°S and finally the west-east SSH gradient over the slope with SSH isolines following the 200 and 2000 m isobaths. Quantitatively, the mean SSH derived from the model (Fig. 3.6A) had a stronger west-east slope SSH gradient compared to observations from the CNES-CLS09 (Fig. 3.6B) and AVISO (Fig. 3.6C) data. This is probably because of the high-resolution ($\sim$ 6 km) of the model solution compared to both the global, coarser resolution ($\sim$ 25 km) and smoothing of CNES-CLS09 and AVISO (Quartly et al., 2013).

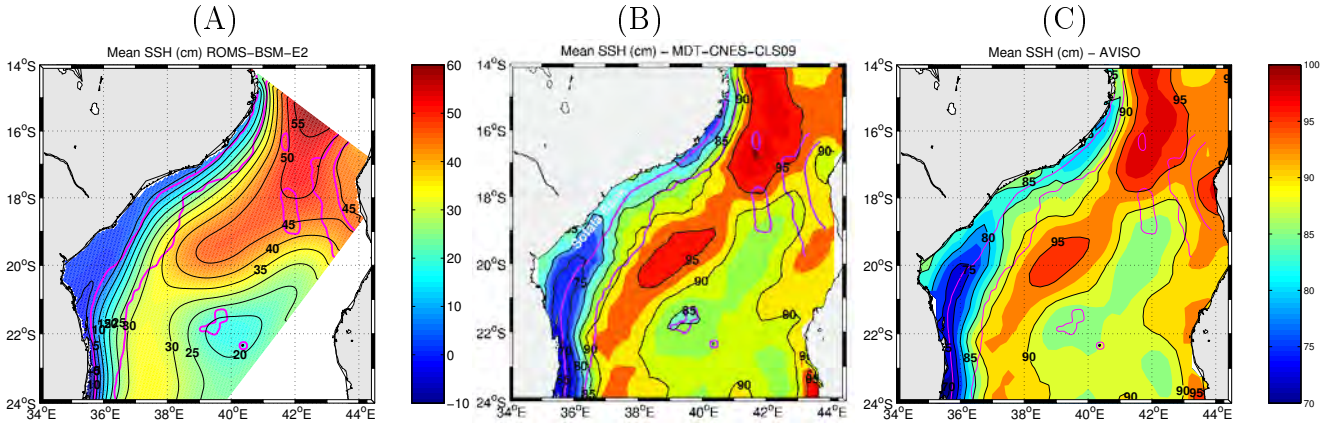

Figure 3.6: Comparison between the long-term mean SSH (color shading and contour) (A) derived ROMS-BSM-E2 solution from model years $4-10$, (B) mean dynamic topography from MDT-CNES-CLS09 for the period $1993-1999$ and (C) absolute dynamic topography derived from AVISO also from $1993-1999$. Note that the absolute values from the model (ROMS-BSM-E2) have different orders of magnitude than the two observations (MDT-CNES-CLS09 and AVISO) and are plotted with a different color-bar for better visualization. Pink lines indicate the 200 and 2000 m bathymetry contours.

Mean eddy kinetic energy and root mean square of SSH

Mean eddy kinetic energy (EKE) and root mean square (RMS) computed from SSH have been extensively used as an indicator of mesoscale eddy variability in different regions of the world, including the Mozambique Channel (Halo, 2012; Halo et al., 2014; Jose et al., 2014; Penven et al., 2014). High eddy variability is indicated by either high EKE (Halo, 2012; Jose et al., 2014; Penven et al., 2014) or high RMS (Halo, 2012; Halo et al., 2014; Penven et al., 2014) or both. Simulated (ROMS-BSM-E2) maximum EKE are apparent in two centres (Fig. 3.7A), one between $21-22°$S and 38°E, and the other between $19-20°$S and 39°E. Comparison with observed mean EKE derived from AVISO also showed two centres of maximum energy (Fig. 3.7B), with locations consistent with the model, but the observational values were smaller. The maximum energy from the model (3000 cm^2 s^{-2}, Fig. 3.7A) was double that of AVISO observations (1500 cm^2 s^{-2}, Fig. 3.7B), suggesting that the model overestimated EKE by some $\sim 50\%$.

Comparisons between RMS derived from the model (Fig. 3.7C) and the AVISO observations (Fig. 3.7D) show that the model exhibits a high value of RMS between $37-38°$E and 22°S, which is in agreement with observations. The maximum model RMS values ($\sim$ 35 cm) were

larger than the observations (~ 20 cm), suggesting that the model overestimates RMS and thus the eddy variability by $\sim 50\%$. This model overestimation of the mean eddy variability (EKE and RMS) is gained from the SWIM climatology model used here for the lateral open boundary conditions employing one-way nesting (model and data section). According to Halo (2012) and Halo et al. (2014), the SWIM model overestimated the Mozambique Channel eddy variability relative to AVISO by about $40-50\%$. The authors demonstrated that such overestimation is due to the fact that the model reproduces the eddies with larger diameter and higher amplitude than AVISO. This is also true in our model, where the amplitude of mean SSH ranged 55 cm (i.e. $0-55$ cm, Fig. 3.6A) compared to 25 cm in AVISO (i.e. $70-95$ cm, Fig. 3.6C). This could explain the high EKE and RMS in the model solutions.

Differences in model-observation EKE have been reported in many similar ocean model studies around the world, including SWIM, an independent ROMS model of the Mozambique Channel (Segtnan, 2006; Jose et al., 2014). However, it should be noted that algorithms deriving geostrophic currents from SSH are known to be problematic (Maximenko et al., 2009), by exclusion of the centrifugal force and thus bias the eddy variability like geostrophic currents and EKE (Maximenko and Niiler, 2006; Penven et al., 2014). Recently Penven et al. (2014) proposed three methods for the inclusion of inertia when deriving currents from SSH that could improve both the model and satellite altimetry results. They demonstrated that their iterative method could reduce the error RMS from geostrophic SSH of the SWIM model and, most importantly, increased the satellite altimetry geostrophic EKE ($1400-1800$ cm^{-2} s^{-2}). This could make the EKE model-observation more comparable and may be used in the future.

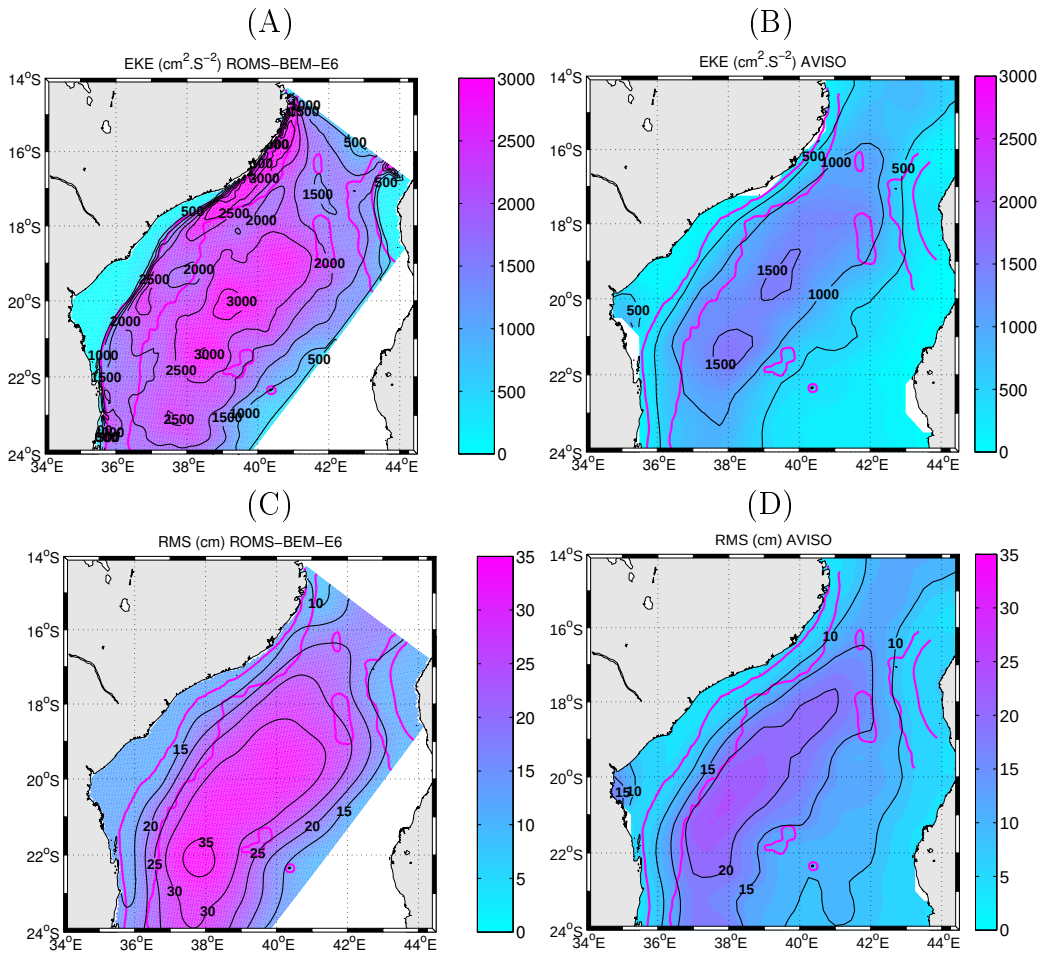

Figure 3.7: Comparison between mean EKE (cm^2 s^{-1}) for (A) ROMS-BSM-E2 from model-year 4 to 10 and (B) AVISO for the period 1993 to 1999, and RMS (cm) for (C) ROMS-BSM-E2 and (D) AVISO for the same periods. Pink lines indicate the 200 and 2000 m bathymetry contour.

Mean surface current

The model mean surface current shows a strong (up to 100 cm s^{-1}) alongshore, poleward, surface current on the slope between the 200 and 2000 m isobaths (Fig. 3.8A). This coincides with the sharp gradient of mean SSH (Figure 3.6), indicating that the model produces a mean "Mozambique Current" that flows poleward (Quartly et al., 2013). This may be related to southward propagating eddies associated with baroclinic instabilities in the Mozambique Channel. Prior to 2000, it was thought that a permanent western boundary current existed along the Mozambican shelf (Schouten et al., 2003; DiMarco et al., 2002). However, it is known that anticyclonic eddies commonly found here produce strong poleward flow along the shelf edge (Sætre and da Silva, 1984; Biastoch and Krauss, 1999; de Ruijter et al., 2002; Schouten et al., 2003; Rid-

derinkhof and de Ruijter, 2003; Lutjeharms, 2006; Backeberg et al., 2008; Hancke et al., 2014; Penven et al., 2014), i.e., an eddy corridor. The long-term average of these poleward intermittent flows suggests a mean "Mozambique Current" on the slope (Fig. 3.8A). The model mean surface "Mozambique Current" is in qualitative agreement with observations of mean currents distributed in the CNES-CLS09 products (Fig. 3.8B), but do not match the mean geostrophic currents derived from AVISO mean dynamic topography (Fig. 3.8C). In particular, there are differences between the two observations (AVISO and CNES-CLS09) with respect to the well distinguished slope mean "Mozambique Current". The velocities (called "geostrophic currents") distributed in the CNES-CLS09 are actually drifter derived mean velocities (with a filtering of the Ekman component) and are not in geostrophic balance with the mean dynamic topography in the same product (M.-H Rio, personal communication, 2013), provided CNES-CLS09 velocities show a mean "Mozambique Current" (Fig. 3.8B) while AVISO (which used CNES-CLS09 MDT) presents no clear "Mozambique Current" (Fig. 3.8C). There are low velocities in both the inner- and outer-sides of the mean current for both the model and observation (Fig. 3.8), which agrees well with the similar model study by Quartly et al. (2013).

Quantitatively the modeled mean surface current was faster (up to 100 cm s^{-1}) than the observations (up to 70 cm s^{-1}) for mean surface current from CNES-CLS09 and mean geostrophic currents from AVISO (Figure 3.8), indicating that the model overestimates the surface current. This is particularly evident on the slope – possibly because of the strong gradient in model mean SSH, which determines the current velocity. Again, this could be explained by the higher horizontal resolution of the model compared with the coarser resolution of both observations. Quartly et al. (2013) demonstrated that the model resolution affects the mean "Mozambique Current". Increasing the resolution of numerical models will generally improve their ability to represent realistic aspects of the physical flow currents, making them better able to simulate pulses (Quartly et al. 2013). On the other hand, the AVISO mean slope surface current is observed to be weak, nearly zero, at the center region between $17 - 19°$S. These results indicate a serious mismatch between CNES-CLS09 and AVISO velocities. Maximenko and Niiler (2006) proposed that geostrophic currents derived from altimetry overestimate the velocities in cyclonic eddies while underestimating those in anticyclonic eddies (compared with surface drifters). Since the Mozambique Channel circulation is dominated by large anticyclonic ed-

dies (Sætre and da Silva, 1984; Biastoch and Krauss, 1999; de Ruijter et al., 2002; Schouten et al., 2002, 2003; Ridderinkhof and de Ruijter, 2003; Lutjeharms, 2006; Backeberg et al., 2008; Hancke et al., 2014; Penven et al., 2014), like in Maximenko and Niiler (2006), it is assumed that AVISO altimetry underestimates the mean "Mozambique Current". Recently, differences in surface velocities derived from AVISO altimetry and *in-situ* observations (S-ADCP and surface drifters) were observed in the Mozambique Channel, indicating that AVISO altimetry underestimated the geostrophic velocities by some $\sim 30\%$ (Ternon et al., 2014). This difference is consistent with the difference observed between both AVISO and CNES-CLS09 and our model velocities.

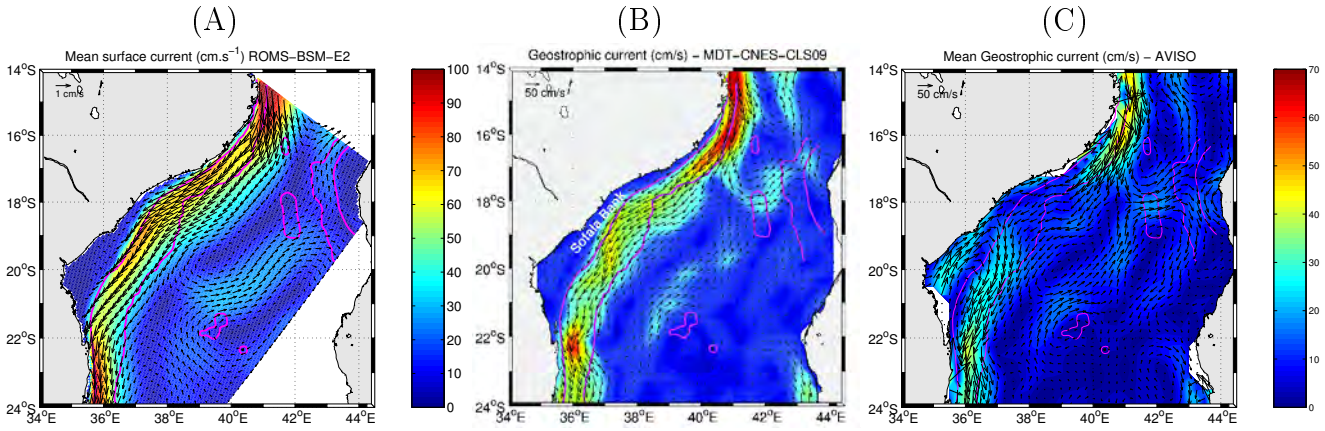

Figure 3.8: Same as in Fig.3.6, but for surface currents (cm s^{-1}).

Vertical mean horizontal current

Vertical sections of velocity along cross-shelf transects located at the latitude of the coast near 16°S and 20°S are shown in Fig. 3.9. It is seen that the 7-year modeled long-term mean alongshore current component at $\sim$ 16°S is in agreement with the 6-years *in-situ* current observation at nearly the same place (Ullgren et al., 2012). In particular the following three documented currents are reproduced by the model (Fig. 3.9):

- a strong slope mean poleward surface current on the western side of the section,
- a weak mean equatorward surface current on the eastern side of the transect, and
- a mean equatorward undercurrent – the Mozambique Undercurrent, over the slope below (1500 m depth) the mean poleward surface current.

This mean 6-year dataset from the mooring at 16°S (Ullgren et al., 2012) is the longest record in the region and was updated from the 4.2-year (Ridderinkhof et al., 2010) and 1.5-year (Ridderinkhof and de Ruijter, 2003) previously plotted time series. All show similar vertical-current structures. A snapshot of observed an Lowered Acoustic Doppler Current Profiler (L-ADCP) transect also shows the three current structures corroborating the model, particularly the Mozambique Undercurrent (de Ruijter et al., 2002). The model-based study by Quartly et al. (2013) also found similar vertical current structures at the same region using NEMO at a coarser (1/4°) resolution, but the undercurrent appeared distorted when they used a higher-resolution (1/12°). In contrast, the present model-based study using a finer-resolution (1/16°) shows a clear Mozambique Undercurrent that matches the observations (de Ruijter et al., 2002; Ullgren et al., 2012), confirming that our model represents the vertical currents reasonably well.

Further south at $\sim$ 20°S off Beira, where the continental shelf is relatively wider than at $\sim$ 16°S, an additional (fourth) mean current is apparent on the shelf (Fig. 3.9B). This mean, weak equatorward coastal current indicates that the model is reproducing the Sofala Bank coastal counter-current (i.e., opposed to the mean poleward surface current, Sætre and da Silva, 1984). The upper layer mean currents (coastal equatorward current, slope poleward current and offshore equatorward current) match the surface current structures depicted in Fig. 3.8. Quantitatively, the model vertical velocities (Fig. 3.9A) are approximately similar to those of the LOCO observations (Fig. 3.9C). This result suggests that the differences in the absolute values of the surface velocity between model (Fig. 3.8A) and observations (CNES-CLS09, Fig. 3.8B) was due, perhaps in part, to underestimation of CNES-CLS09 instead of only an overestimation by the model. This is possibly explained by the coarse global spatial resolution of the CNES-CLS09 data products. Another possible explanation is the bias when deriving geostrophic currents from altimetry (Maximenko and Niiler, 2006; Maximenko et al., 2009; Penven et al., 2014); altimetry is included in the CNES-CLS09 product (Rio et al., 2005, 2011).

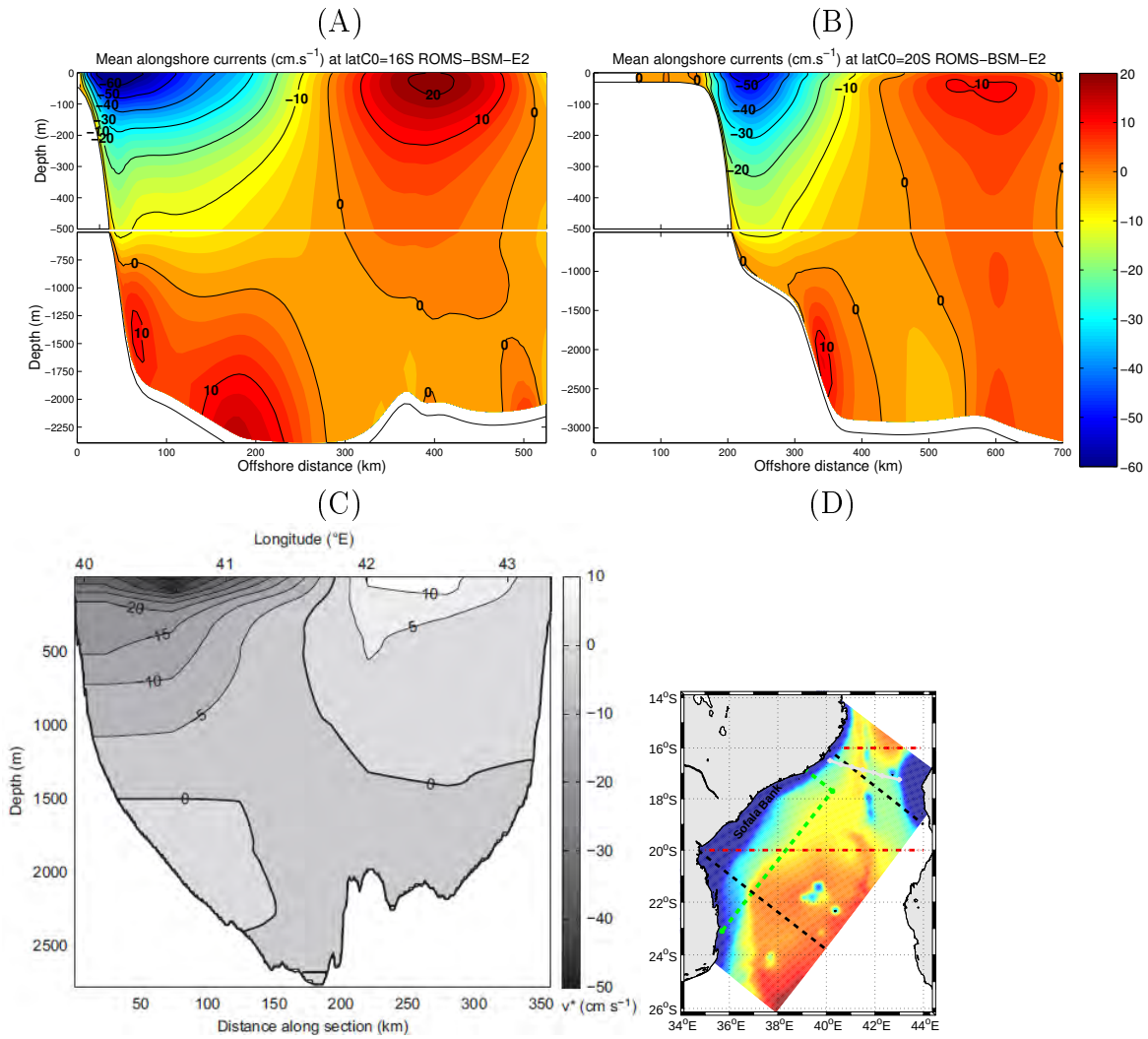

Figure 3.9: Comparison between long-term mean alongshore velocity (u, cm.s^{-1}) for ROMS-BSM-E2 from model year 4 to 10 on the cross-shelf transect at latitude of the coast (latCO) of (A) 16°S and (B) 20°S, and (C) the mean alongshore velocity (cm.s^{-1}) for the Long-term Ocean Climate Observation (LOCO) transect at $\sim$ 16°S for the period 2003 to 2009 (Ullgren et al. 2012). (D) The model domain with bathymetry (color shading, blue[red] for shallow[beep]) illustrating the locations of transects for (black dashed lines) ROMS-BSM-E2 to the north and south, (white solid line) the LOCO section and (red dash-dot line) CARS to the north and south. The green dashed line outline the Child domain. Note the all the three transect to the north are outside of the Child domain.

3.3.2.2 Annual mean hydrography (temperature, salinity and water masses)

Horizontal structures

The long-term mean model sea surface temperatures (SST) show warm surface water with an overall north-south gradient, which decreases from a maximum of 28°C in the north to a minimum of 25°C in the south (Fig. 3.10A). This large-scale north-south SST gradient agrees well with SST observations from MODIS, Pathfinder, CARS and WOA2009 (Fig. 3.10). A west-east SST gradient is also apparent, with temperature increasing from the western boundary of the channel to the east. This is generally in good agreement with observations, except WOA2009, which has no data close to the coast (Fig. 3.10).

The model captured a cool (~ 25.5°C) water lens over the continental shelf between the inner-shelf (~ 50 m isobath) and the shelf-break (~ 200 m isobath), surrounded by relatively warm water on both inner and outer sides (Fig. 3.10A). This cool water lens on the Sofala Bank shelf is in agreement with observations from mean MODIS SST (Fig. 3.10B). The model, however, overestimates the cool water lens with minimum temperatures cooler than the observations from MODIS. In the case of the model, the cool water lens reached the coast between 17 and 19°S and the coastal warm water was not apparent, which was not the case for the MODIS observations where coastal warm water existed. The offshore edge of this cool water lens for both observations and model follows the 200 m isobath and coincides with the inshore edge of the observed mean "Mozambique Current" (Fig. 3.8). Such a cool water lens is not well represented in the Pathfinder and CARS SST, with the exception of the cool water cell found at $\sim 20-21$°S and ~ 35°30′E, possibly due to the Pathfinder and CARS SST lower resolution than the model and MODIS. Similar to the model and MODIS, a shelf-edge front (depicted by ~ 27°C isotherm) was apparent in Pathfinder (Fig. 3.10C) and CARS (Fig. 3.10D) SST following the 200 m isobath, indicating the cool water lens. Despite the large-scale north-south SST gradient, other SST features are not represented in the coarse resolution WOA2009 SST observations, mainly due to an absence of data close to the coast (Fig. 3.10E).

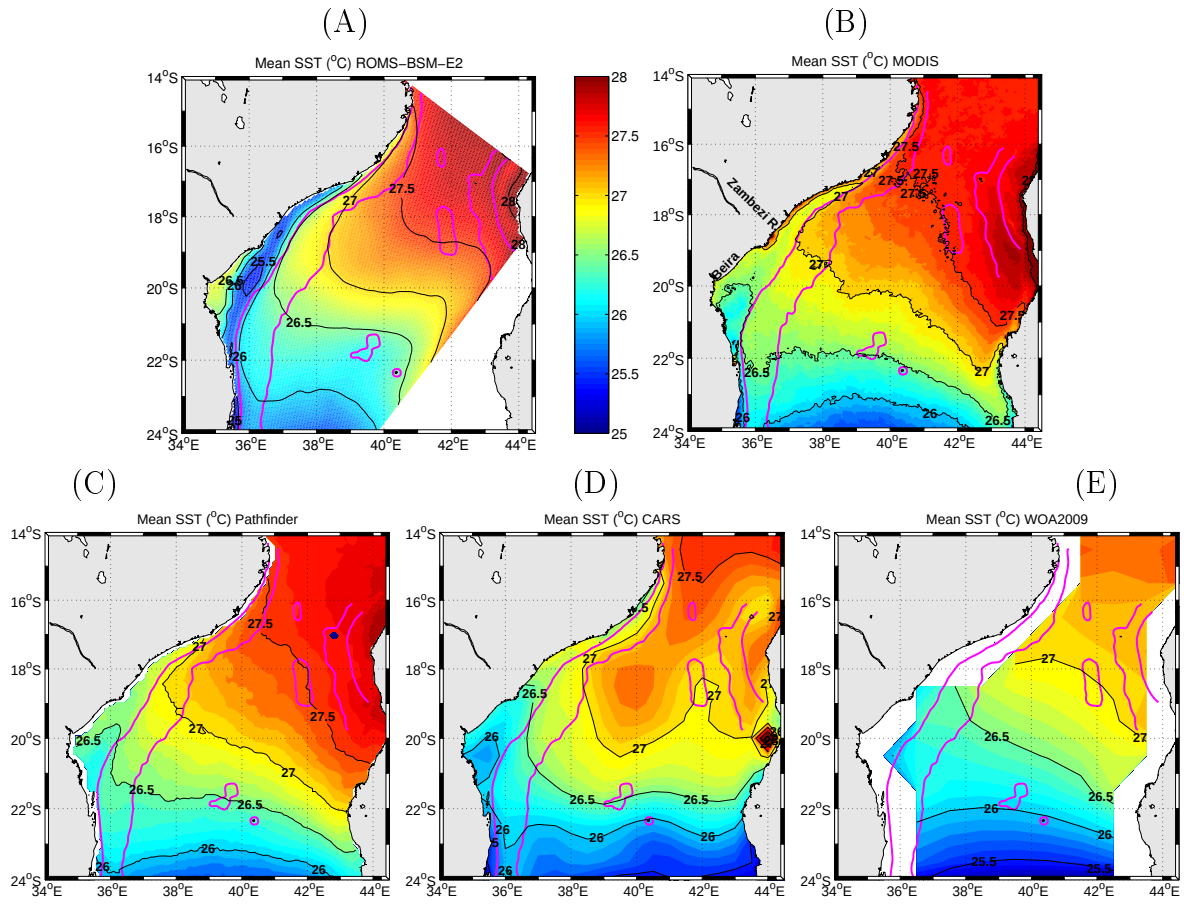

Figure 3.10: Comparison between long-term mean sea surface temperature (SST, °C) for (A) ROMS-BSM-E2, (B) CARS, (C) World Ocean Atlas 2009 (WOA2009), (D) MODIS satellite and (E) Pathfinder satellite. Summary of spatial and temporal resolution of these data is presented in Table 3.1.

The long-term mean model sea surface salinity (SSS) also shows a large-scale north-south gradient of salinity, ranging from 35 in the north to 35.3 in the south (Fig. 3.11A). There is a west-east gradient with relatively low salinity (< 35) found in the coastal region of the Sofala Bank off the Zambezi River delta at $\sim 19°$S. The north-south SSS variation is in agreement with the SSS distribution derived from CARS and WOA2009 (Fig. 3.11). However, the west-east SSS gradient was much weaker in ROMS-BSM-E2 than in CARS observations due to the absence of river inflow in this ROMS-BSM-E2 configuration. Mean SSS derived from WOA2009 shows a strong west-east gradient of salinity ($\sim 19°$S), with low salinity (<35) extending far offshore compared with CARS observations. The lack of data near the coast for the WOA2009 dataset hampers evaluation of the ROMS-BSM-E2 solution, particularly within the 2000 m depth range.

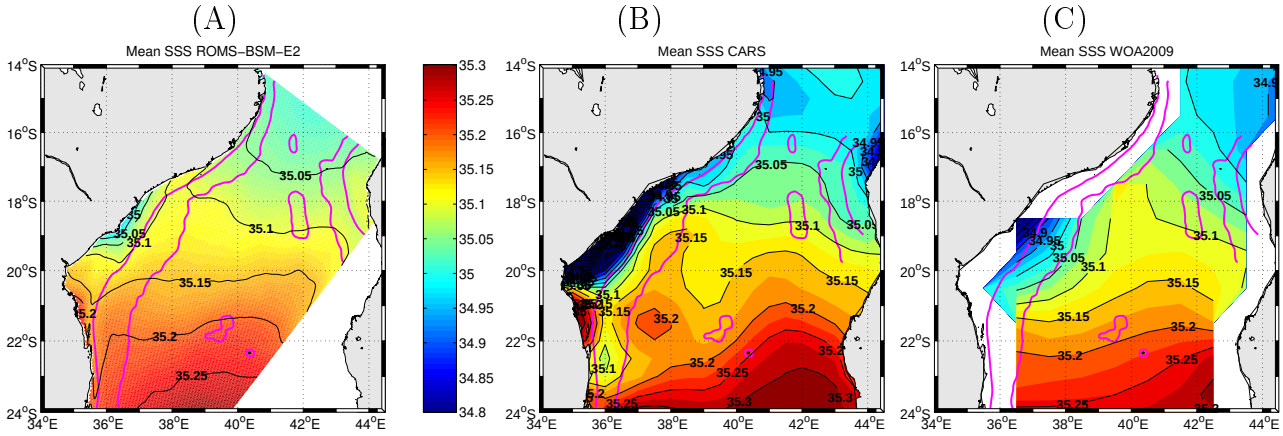

Figure 3.11: Comparison between long-term mean sea surface salinity (SSS) for (A) ROMS-BSM-E2, (B) CARS and (C) World Ocean Atlas 2009 (WOA2009). Summary of spatial and temporal resolution of these data is presented in Table 3.1.

Long-term mean model sea surface densities (not shown) exhibit a pattern similar to the mean model SST (Fig. 3.10A). Similarly, a north-south and west-east gradient of surface density is observed. Furthermore, a lens of high density was observed following the bathymetry (200 m) over the shelf break, as in SST. These suggest that the density is mostly determined by temperature.

Vertical mean temperature and salinity

The model vertical section of mean temperature at $\sim$ 16°S shows a warm (> 26°C) surface water layer in the upper $\sim$ 50 m along the entire transect (Fig. 3.12A). Below the surface layer, a strong thermocline is apparent with temperature decreasing from $\sim$ 25°C at $\sim$ 50 m to 16°C at 250 m. In the upper 500 m, isotherms are found to rise on the slope at the western side of the channel (Fig. 3.12A), indicating the presence of the mean poleward "Mozambique Current". Modeled, upper 500 m vertical temperature structures (Fig. 3.12C) agree with CARS observations (Fig. 3.12C). However, LOCO, which is the longest *in-situ* dataset in the region, did not resolve the thermocline because temperature observations were scarce in the upper 500 m with data only available at one mooring station (Ullgren et al., 2012). In the depths below 500 m the model temperature is observed decreasing from 10°C to a minimum of 2°C at $\sim$ 2200 m (Fig. 3.12A) and agrees with both CARS (Fig. 3.12C) and LOCO (Fig. 3.12E) vertical temperature structures.

For salinity, a subsurface maximum (> 35.2) with a maximum at the eastern side of the transect was found centered at ~ 200 m depth for the model (Figs. 3.12B), is in agreement with the CARS observations (Figs. 3.12D). There were, however, surface brackish waters observed on both extremes of the CARS transect that were not apparent in the model solution due to the absence of freshwater river input in this model configuration. Similar to the isotherms, the isohalines uplift on the continental slope between $250 - 500$ m depth (Fig. 3.12B and D), supporting the presence of the poleward mean "Mozambique Current". As in temperature, LOCO did not resolve salinity in the upper 500 m. There was a salinity minimum (< 34.7) at $\sim 1200 - 1600$ m on the western side of the channel (Figs. 3.12B) that corresponds with the LOCO observations (Figs. 3.12F), but is observed to be relatively shallow (~ 1000 m) in the CARS transect (Figs. 3.12D). This salinity minimum (Fig. 3.12B, D and F) corroborates the presence of an equatorward Mozambique Undercurrent (Fig. 3.9)(de Ruijter et al., 2002).

The principal water masses (Sætre and da Silva, 1982; de Ruijter et al., 2002; DiMarco et al., 2002; Ullgren et al., 2012) are apparent from the model vertical sections of temperature and salinity at $\sim 16°$S (Fig. 3.12). At the surface, warm ($> 26°$C) and fresh (< 34.1) water indicates Tropical Surface Water (TSW) transported by the South Equatorial Current from the Pacific and Indonesian Seas. The subsurface salinity maximum (> 34.2) indicates Subtropical Surface Water (STSW) from the south. Below the thermocline a quasi-linear decrease in both temperature (from $16 - 8°$C) and salinity (from $34.2 - 34.8$) marks the presence of South Indian Central Water (SICW). At intermediate depths, the dominant water mass is the relatively cold ($\sim 4°$C) and saline (> 34.7) Red Sea Water (RSW) originating in the Gulf of Aden. However, on the west side of the transect the salinity minimum (< 34.7) advected from the south by the equatorward Mozambique Undercurrent suggests diluted Antarctic Intermediate Water (AAIW). Below 2000 m, cold ($2°$C) and saline (> 34.8) water indicates North Atlantic Deep Water (NADW) at the bottom.

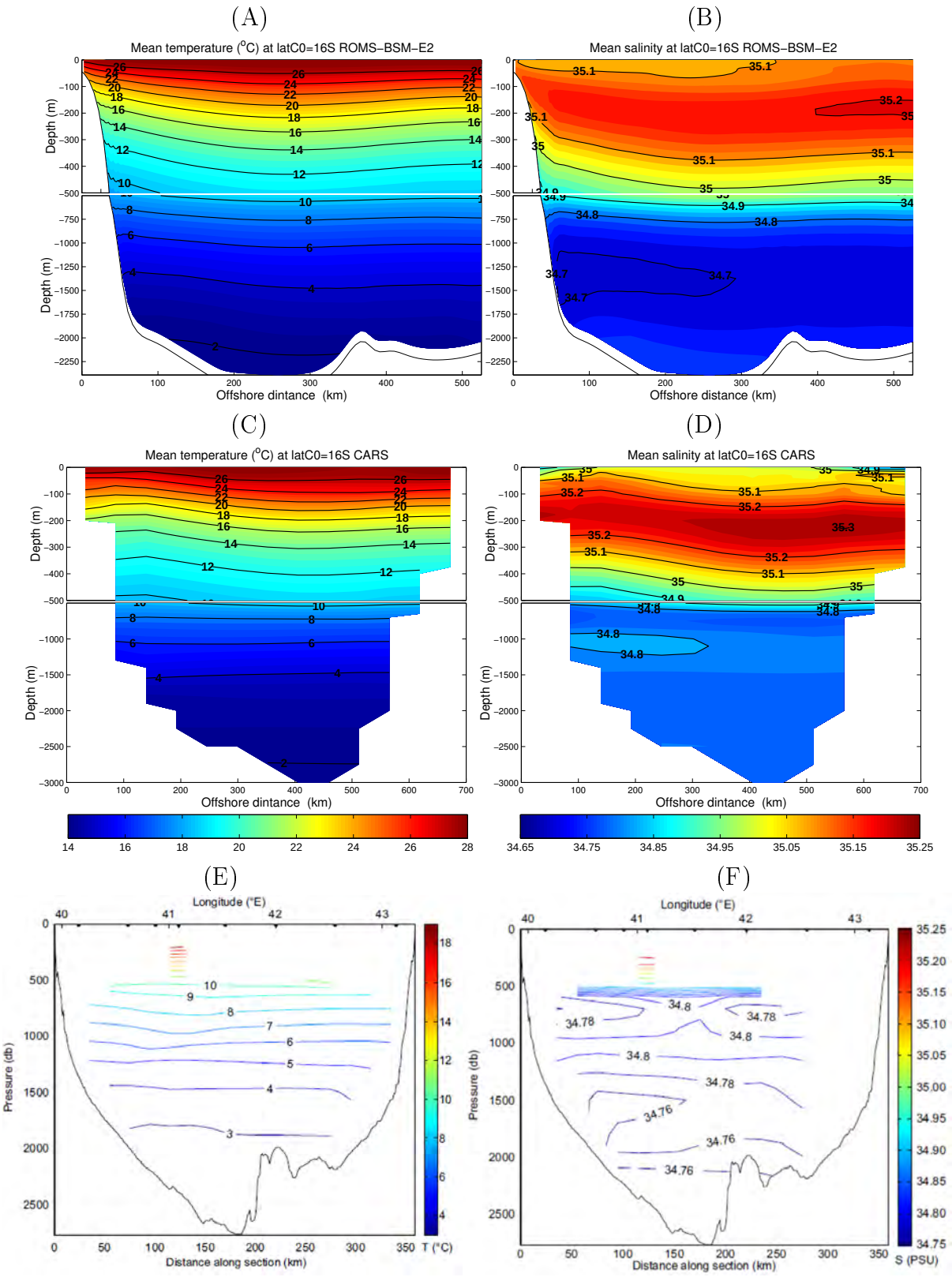

Figure 3.12: Comparison of vertical section of long-term mean (A, C and E) temperature (°C) and (B, D and F) salinity as derived from (A and B) ROMS-BSM-E2, (C and B) CARS and (E and F) LOCO on the cross-shelf transect at the latitude of the coast of 16°S.

The vertical transect further south at 20°S (Fig. 3.13) shows similar patterns of temperature and salinity to those observed at 16°S (Fig. 3.12). However, it is notable that the warm surface water is shallower, with the 26°C isotherm very close to the surface for both model (Fig. 3.13A) and CARS (Fig. 3.13C). For salinity, the fresh surface water (< 35.1) no longer exists and the subsurface salinity maximum reached the surface for model (Fig. 3.13B) and CARS (Figure. 3.13D). These suggest a decreased influence of TSW from the north and an increased influence of STSW from the south due to decreasing precipitation and increasing evaporation at the latitude of 20°S. The salinity minimum in the intermediate depths increased in thickness and covered the full extent of the transect from west to east (Figure. 3.13 right), indicating increased influence of the AAIW from the south. Similar changes in water masses with latitude were observed in previous studies using hydrographic data (de Ruijter et al., 2002, including historical-1960s data DiMarco et al., 2002), supporting our model.

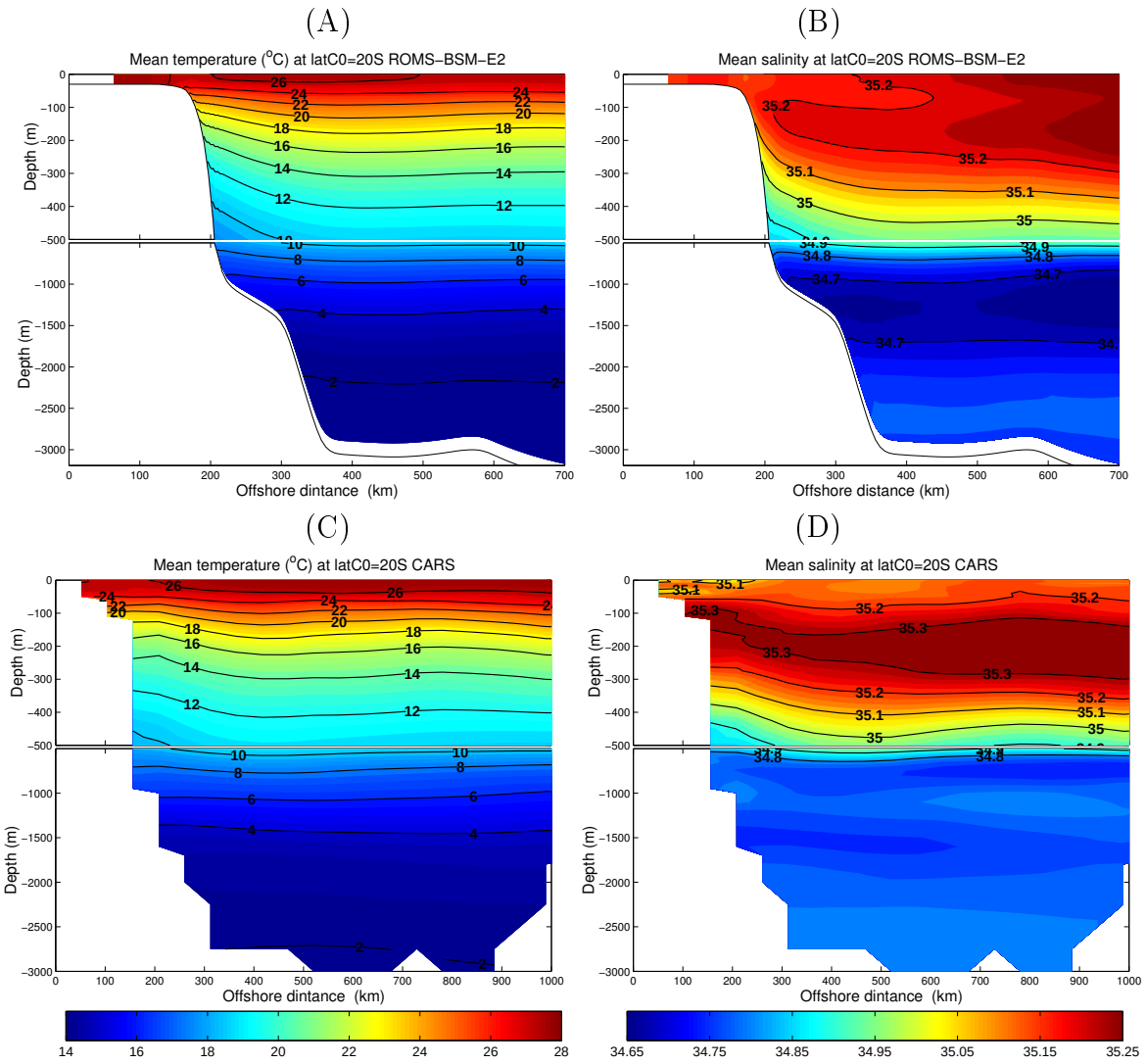

Figure 3.13: Similar to Fig. 3.12A-D, but for cross-shelf transect off Beira Bay at the latitude of the coast of 20°S.

3.3.3 Model sensitivity to nesting, tides and river effect

In this section the sensitivity of the model to the nesting, tide and river simulations is investigated, based on the knowledge gained from the previous sections. Focus is given to the Child grid.

Nesting simulation experiment (Parent and Child grid sensitivity)

In the previous subsection (3.3.2) the annual mean circulation and structures for the large-scale model domain without nesting were presented. Now we must consider both the Parent

and Child grids after nesting and the ability of the model to perform the nesting (Parent and Child grid). Comparison between the Parent model before (Fig. 3.14A) and after nesting (Fig. 3.14B) show that, in the case of the model simulation after nesting, there is coastal warm water between $\sim 17°$ and 19°S and the cool water lens no longer reaches the coast, which was not the case for the simulation before nesting. This coastal warm water agrees well with observations from MODIS SST (Fig. 3.14C). Moreover, the cool water minimum has shifted southward in the case of the simulation after nesting, which is also in better agreement with the observations. These indicate that there are important positive improvements after nesting. Overall there were more small-scale structures such as filaments, fronts and coastal eddies in the simulation with than without nesting, particularly in the Child grid snapshots (not shown). Improvement in shelf dynamics after nesting have been reported in other hydrodynamic modelling studies (Biastoch et al., 2008; Debreu et al., 2012; Zheng and Weisberg, 2012). In two-way nesting the Child domain is embedded in the Parent domain and there is communication (feedback) between the two model grids, as mentioned in the data section. The concept of nesting is not valid without a stable and smooth transition from one model grid to another (Penven et al., 2006a; Zheng and Weisberg, 2012). Most importantly, there is a smooth and stable transition in the sponge layer from one grid to another (white line in Fig. 3.14B), indicating that the nesting is robust.

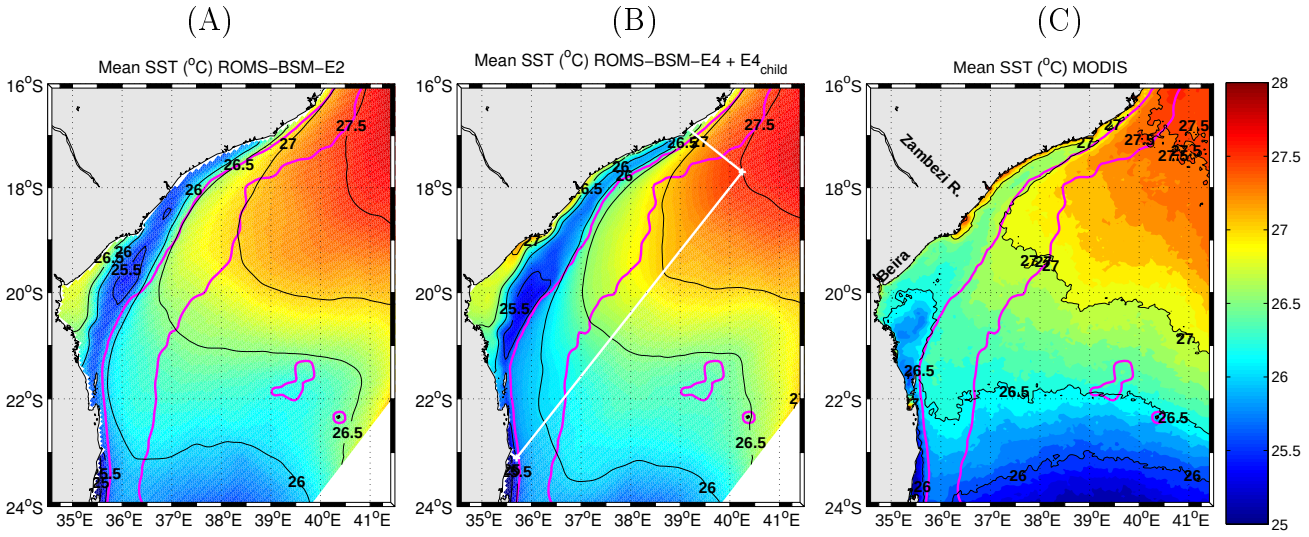

Figure 3.14: Comparison between two-nesting simulation and observation. Mean SST for (A) model before nesting, (B) model after nesting (Parent and Child simulation overlapped, the gray line outline the Child grid) and (C) MODIS observation. Pink lines indicate the 200 and 2000 m bathymetry contour. The white line outlines the Child grid .

Tidal simulation experiment

In the present section we consider tidal simulation with a focus on the Child grid; the tidal simulation on the Parent grid without nesting was discussed by Chevane (2013). The model's ability to perform tide simulations is evaluated with observations from the coastal tide gauge located at Beira. This is the only observational tidal station on the Sofala Bank. Data from the Beira tide gauge is collected by the Mozambican National Hydrography Institute (INAHINA). Data for September and October 1998 were made available for this study. Simulated, high frequency, hourly–averaged SSH at the nearest grid point to the Beira tide gauge is compared with observed tide at Beira (Fig. 3.15A) and agree well in phase, with difference in amplitude. The modeled tidal phase near the Beira tide gauge is in good quantitative agreement, peak to peak, with the observations (Figure 3.15A). There is a strong correlation (r= 0.96) between the two time series. It is seen that the tide is semi-diurnal with two high and two low tides each day, with the one low and another high amplitude day-cycle captured by the model. The modeled tides exhibit a clear spring to neap tidal fortnight cycle (four of the total 25 modeled in one year), with high amplitude in spring and low amplitude in neap that match the observations.

The tidal amplitudes in the model solution are smaller than those observed at the Beira tide gauge, particularly during the spring tides (Figure 3.15A). Tidal range (2 x amplitude) is defined for spring and neap tide separately. The observed neap tidal range is $\sim$ 2 m while for the model it is $\sim$ 1.6 m (Figure 3.15A). The spring tidal range for the observations is $\sim$ 6 m and for the model $\sim$ 4.8 m (percentage error 20%). Chevane (2013), using the coarser (6.3 km) Parent grid before nesting, also found a difference between the modeled tidal range and that observed at the Beira tide gauge. She had attributed this to the inshore location of the Beira tide gauge, which was not resolved by the Parent model. This is also true for the Child model in the present study. The Beira tide gauge is positioned inside the Pungué River estuary, which is not resolved by both Parent and Child model, so some differences between the model and observations should be expected. An estuarine model configuration is needed to resolve the tide at the Beira tide gauge station. Another possible reason for the model-observation discrepancy in tidal amplitude is the bathymetry (Zheng and Weisberg, 2012). In this study, the Child model minimum depth is set to 15 m, resulting in a zone of flat bottom near the coast. The

interaction between the tide and relatively deep, flat bottom, rather than the true shallow depth variation, may affect the amplitude. However, in the case of the Parent grid with minimum depth of 30 m (Chevane, 2013), the tidal amplitude was similar to those with 15 m.

The modeled inshore and offshore (cross-shelf) velocity components near the Beira tide gauge site (Fig. 3.15B) show a good correspondence with tidal elevation (Fig. 3.15A). Velocity also shows a clear spring to neap fortnight cycle, with speed decreasing from a maximum in the spring tide peak to a minimum in the neap tide peak and increasing again to the next spring tide peak (Fig. 3.15B). A similar fortnightly cycle in tidal speed was reported by Gudmundsson (2006). Comparison between model surface and bottom modeled velocities at Beira Bay show that the velocities were slower at the bottom, especially during the spring tides (percentage error 40%) (Fig. 3.15B).

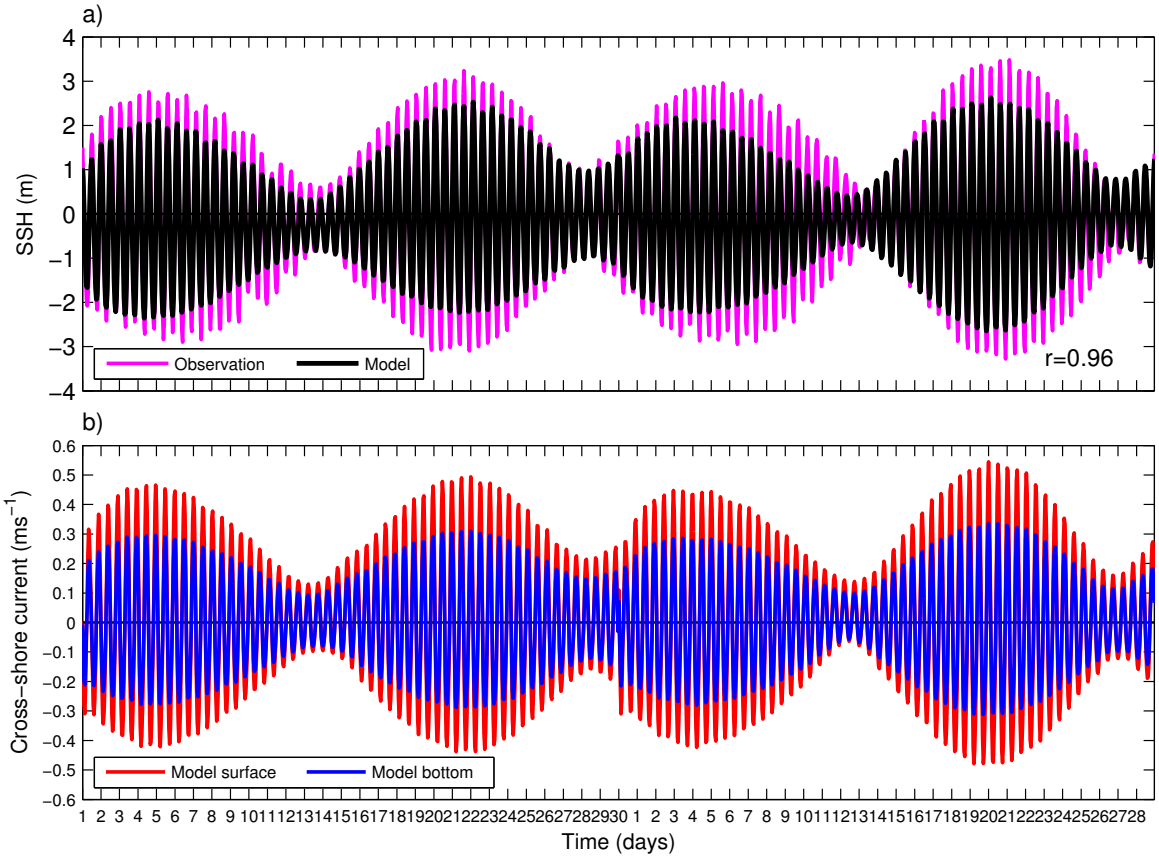

Figure 3.15: Two month time series (a) comparison between tidal elevations (m) observed at the Beira tide gauge (red line), and simulated near Beira tide gauge (black line) and off Zambezi River mouth (blue line). (b) comparison between tidal surface current (m s^{-1}) modeled near Beira (black line) and off Zambezi River mouth (blue line).

Spatial distributions of surface currents during the spring tide are presented in three snapshots

for: (1) ebb condition, with a dominant offshore flow (Fig. 3.16A), (2) near slack water condition, with weak (nearly zero) currents (Fig. 3.16B), and (3) flood condition, with dominant onshore flow (Fig. 3.16C). It appears that when the current is weak there is an equatorward coastal current ("counter-current") (Sætre and da Silva, 1984), which was also shown by Chevane (2013). However, during the strong ebb or flood tidal current this "counter-current" no longer exists, suggesting that strong tidal currents dominate the relatively weak coastal "counter-current".

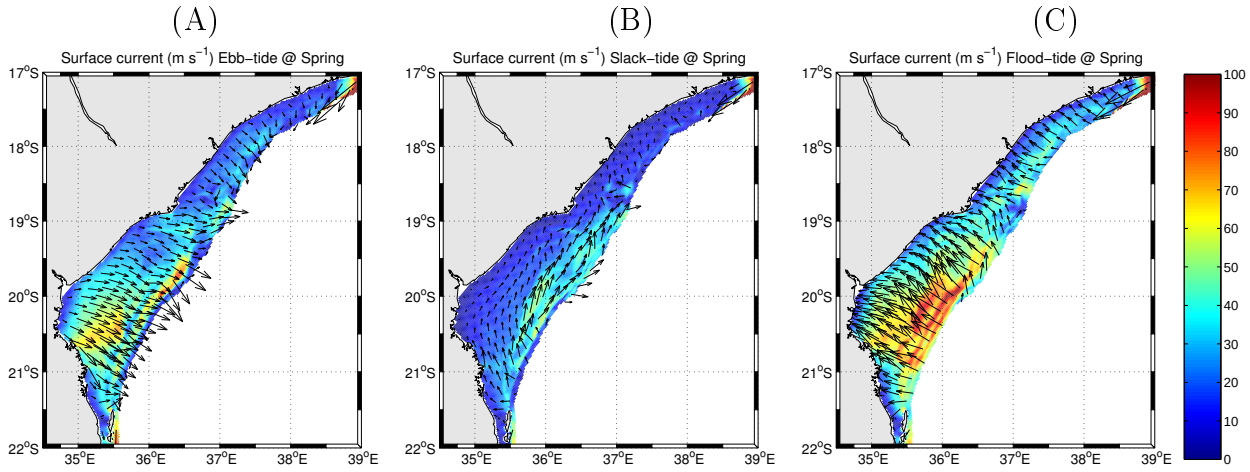

Figure 3.16: Snapshot of hourly surface current to illustrate the tidal-driven current near maximum (A) ebb, (B) slack and (C) flood tide conditions during the spring on 5 January model-year 5 every three hour from 5:00, respectively. Experiment ROMS-BSM-E4.

Similarly to Chevane (2013), high tidal velocities occurred off Beira between $\sim 20-21$°S and ~ 35°E (Fig. 3.16A and C), but in the case of the Parent simulation before nesting, the values were < 70 m s^{-1} (Chevane, 2013), whereas here in the Child simulation the values are up to 100 m s^{-1}. This indicates that the nesting procedure is intensifying the tidal current. Most importantly, small-scale filaments of maximum velocities appeared on the shelf-break (200 m depth) following the bathymetry (Fig. 3.16A and C). These were not apparent in the case of the Parent grid before nesting (Chevane, 2013). These filaments seem to coincide with the surface signatures of the internal waves observed from satellite advanced synthetic aperture radar imagery (da Silva et al., 2009). These authors identified this region between $\sim 20-21$°S near the shelf-break of the Sofala Bank as an important "hotspot" in the world for internal tide and internal wave generation, possibly due to the complex bathymetry in this region. Internal waves and tides are important processes for ecology, influencing pelagic larval transport and

vertical migrations (Pineda et al. 2007; Kaartvedt et al. 2012).

Comparing the mean circulation between the experiment without tides (Fig. 3.17A) and with tides (Fig. 3.17B) indicates negative velocity differences on the continental shelf (Fig. 3.17C). These suggest that the tides account for a decrease in the mean shelf circulation of $\sim$ 40%, particularly off Beira. This can be explained by the nearly zero velocities of the average of the harmonic (sinusoidal) tides (i.e. the difference between the high and low tide currents is $\sim$ zero). The maximum (~ -8 cm s^{-1}) difference occurred near the shelf-beak between $20-21°$S, which coincides with the "hotspot" for internal tide and wave generation (da Silva et al., 2009), indicating the presence of strong barotropic tides. Offshore, the velocity difference between the two experiments ranged from -6 to 2 cm s^{-1} (Fig. 3.17C). Since the offshore currents are strong (Fig. 3.17A and B), such differences account for $< \pm 10$ cm s^{-1} and therefore might be negligible.

SST comparisons between the model simulations without tides (Fig. 3.17D) and with tides (Fig. 3.17E) show that there was a positive SST difference in the inner-shelf (Fig. 3.17G), indicating that the tidal mixing is warming the shallow waters. On the mid-shelf to the shelf-break, negative SST differences were apparent, with a peak of $\sim -0.8°$C (Fig. 3.17G). Such a decrease in SST suggests the presence of the cool water lens (Figs. 3.17D and E), which is consistent with observations from MODIS satellite data (Fig. 3.10B). Chevane (2013) attributed this cool water lens to tidal mixing. The present study, however, demonstrated that, although the cool water lens was enhanced ($< 25.5°$C) for the simulation with tides (Figs. 3.17E), it was still apparent ($< 26°$C) for the simulation without tides (Figs. 3.17E). Therefore tides alone cannot explain the cool water lens, implying that other factors are most likely involved.

This cool water lens (Figs. 3.10A-B and 3.17D-F) coincides with the western edge of the mean "Mozambique Current" (Figs. 3.8A and B) and the internal wave generation hotspot at the shelf-break (Fig. 3.16A and C). It is therefore hypothesized that: ($H_{3.1}$) the cool water lens is limited offshore by the mean "Mozambique Current", such that the current acts as a physical barrier; and ($H_{3.2}$) the cool water lens generation is in part related to the mean "Mozambique Current" associated with passing eddies, i.e., the eddy corridor. Recently, studies have shown coastal (biotic and abiotic) traces from the Sofala Bank being transported offshore, crossing the

shelf-break (Hancke et al., 2014; Jose et al., 2014; Malauene et al., 2014), thus the hypothesis ($H_{3.1}$) suggesting a physical barrier for the offshore propagation of the cool water lens is unlikely.

Vertical sections of temperature for both simulations without tides (Figs. 3.17G) and with tides (Figs. 3.17H) show isotherms rising on the shelf-slope, indicating influence of a southward flow. These findings support the hypothesis ($H_{3.2}$) that eddies or the mean "Mozambique Current" contribute to the cool water lens by setting the deep cool at the mid-depth on the shelf-break (Figs. 3.17G and H). The coastal, warm, well mixed water is seen to move more seaward in the case of the simulation with tides than without. A tidal mixing energy erodes the vertically stratified water column, producing a front between the well mixed, warm coastal water and the stratified oceanic waters on the shelf-break. Moreover, the tidal action on the stratified water generates internal tides and internal solitary waves (da Silva et al., 2009). The internal tides and waves propagating on the shelf induce vertical turbulent mixing that can bring the cool water made available in the frontal region upwards, reaching the surface (Neves et al., 2003). Similarly, two forcing mechanisms of the cool lens, one local or coastal (tidal mixing in this case) and another remote or oceanic (eddies in this case) have been proposed in other shelf regions around the world (Lie, 1989; Geyer, 1995; Kasai et al., 1999; Stabeno et al., 2001; Stockwell et al., 2001; Kachel et al., 2002; Weisberg and He, 2003).

In our case the cool anomaly for the simulation without tides was ~ 0.5°C, whereas for the simulation with the tides it was ~ 1.5°C; this is when the influence of eddies is subtracted from the simulation with the tides, the remaining anomaly is ~ 1.0°C. Hence, the cool water lens of the Sofala Bank is primarily (70%) driven by the tidal mixing (Chevane, 2013), in combination with the Mozambique Channel eddies (30%). The cool water lens was found in all the seasons (not shown), which is acceptable because neither of the identified forcing is seasonal. This cool water lens could be important for biology and ecosystem functioning by supplying deep, cool, nutrient-rich waters into the euphotic zone, although this needs further investigation. A sequence of snapshots shows one event of a cooling during the passage of an anti-cyclonic eddy for the simulation with tides (Fig. C.1). Accepting that the model overestimates eddies compared with AVISO observations, eddies could explain the model-observation of enhanced cooling (Figs. 3.10 and 3.17), such that the more eddies, the cooler the water lens.

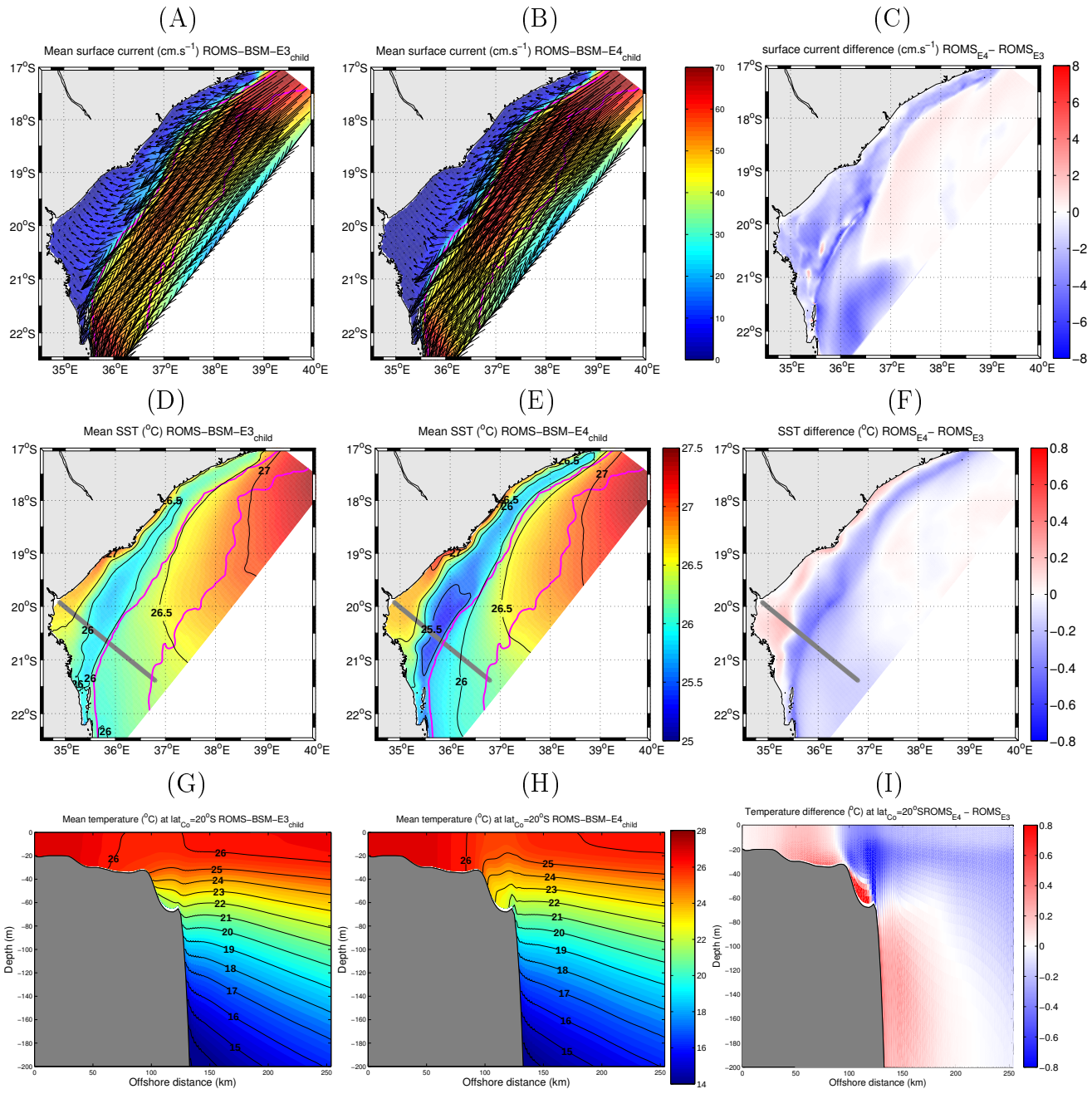

Figure 3.17: Comparison between model experiment (A and D) without tide ROMS-BSM-E3 and (B and E) with tide ROMS-BSM-E4. (A and B) long-term mean surface current (cm s^{-1}) from model years $4-10$ and (C) the mean velocity differences between the two model. Pink lines indicate the 200 and 2000 m bathymetry contours. (D and E) mean sea surface temperature (SST,°C) for the same period and (F) SST differences. (G and H) vertical section of mean temperature (°C) off Beira with latitude of the coast ~ 20°S (gray line in D−F) and (I) the vertical temperature differences.

It has been shown that geostrophic eddies interacting with bottom topography generate internal waves in the deep ocean (Nikurashin and Ferrari, 2010a,b; Nikurashin et al., 2013; Nikurashin and Ferrari, 2013). Similarly, on the coastal Sofala Bank, internal wave generation was found associated with an anticyclonic eddy (da Silva et al., 2009), but these authors focused on barotropic tides, while little attention was given to the eddies. It is hypothesized that in highly energetic eddy regions the role of eddies in the generation of internal waves could be greater than expected. This hypothesis still needs to be tested. A model simulation without eddies could clarify the possible role of eddies in the generation of internal waves. Internal waves are known to generate turbulent mixing (Nikurashin and Ferrari, 2010a,b; Nikurashin et al., 2013; Nikurashin and Ferrari, 2013). Ocean mixing leads to stratification of the ocean by upwelling of dense, deep waters (Wunsch and Ferrari, 2004; Nikurashin et al., 2013). These further support the partly eddy-induced cool water lens.

River simulation experiment

Comparisons between the model experiment without rivers (ROMS-BSM-E4) and with rivers (ROMS-BSM-E6) show that the difference in the mean velocity was relative small (near zero) over the entire continental shelf except for a slight positive difference (> 6 m s^{-1}, red spectrum) near the Zambezi River mouth (Fig. 3.18A). This difference indicates that the effect of the Zambezi River disrupts the shelf circulation in the vicinity of the river mouth, which is in agreement with a previous study (Nehama, 2012). SST differences were zero everywhere except a positive (~ 0.5°C) difference at the Zambezi River mouth (Fig. 3.18B), suggesting a slight increase in water temperatures due to inflow of relatively warm water from the land. However, its influence is found to be very localized to the Zambezi River mouth and probably has a marginal effect on the continental shelf as a whole. For SSS there were large (> -5) negative differences off the Zambezi mouth, with a small one off Beira Bay (Buzi and Pungué Rivers) (Fig. 3.18C). These indicated that the model was capable of reproducing the Zambezi River plume (Nehama, 2012).

Comparisons between the model and observed mean SSS shows that in the case of the experiment with rivers there was clear low mean salinity spread over a large area off the Zambezi River mouth ($\sim$ 19°S) and a relatively small area off Beira Bay (Buzi and Pungué Rivers at $\sim$ 20°S) (Fig. 3.18E), which was not apparent in the experiment without rivers (Fig. 3.18D). More importantly, the low salinity of the experiment with rivers (Fig. 3.18E) is more comparable with observations from CARS (Fig. 3.18F), indicating that the freshwater river inputs are improving the model. Low model salinity off the Zambezi spread over a smaller area than observations from CARS, suggesting that the monthly climatology river inputs are insufficient to accurately reproduce the plume size. However, it should be noted that CARS data are from interpolation over a coarse resolution (Ridgway et al., 2002); thus far it is not showing the small river plume off Beira and probably exaggerates the Zambezi River plume.

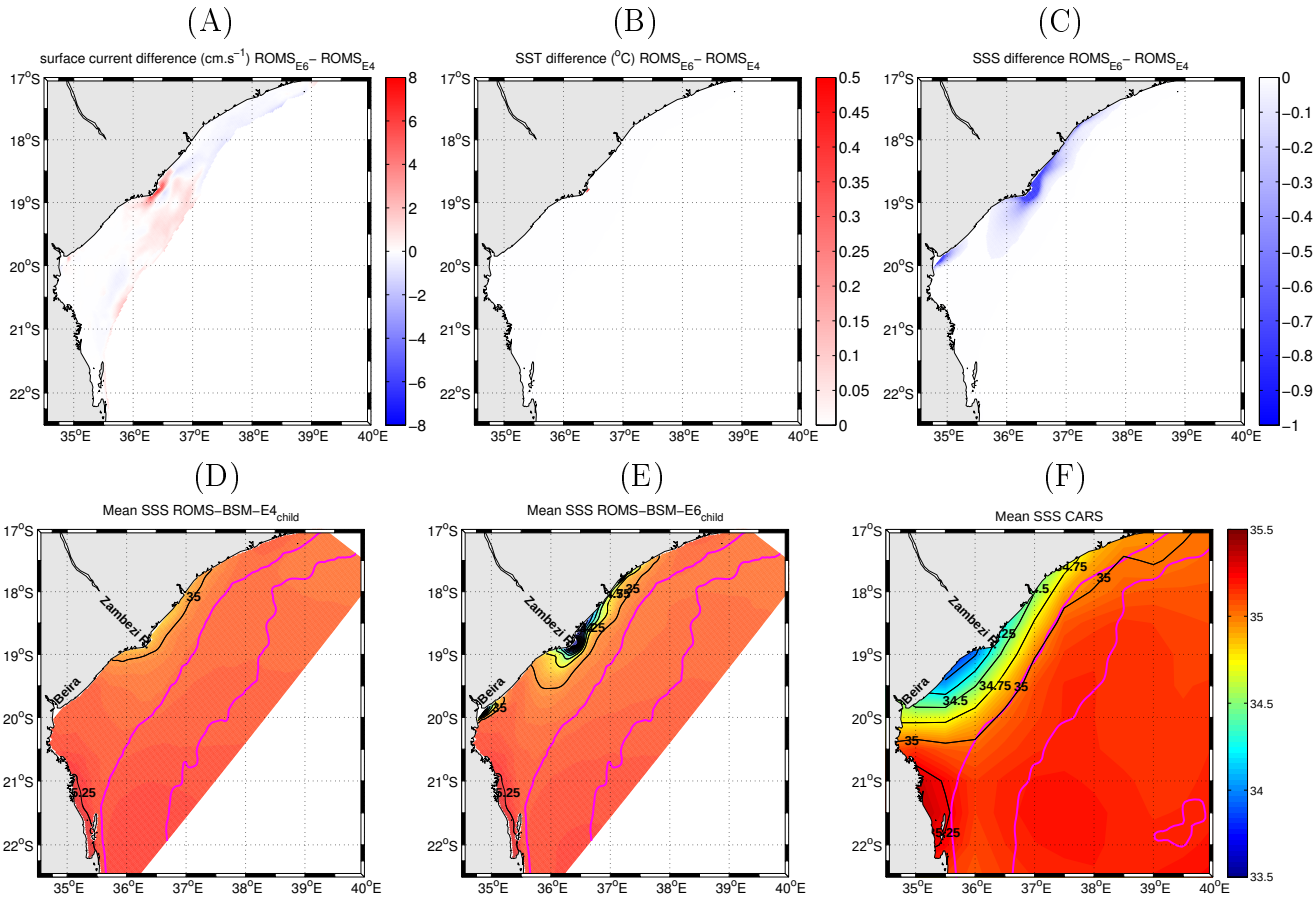

Figure 3.18: Comparison between model experiments with - without rivers and observation from CARS climatology. Difference between model simulation with (ROMS-BSM-E6) and without (ROMS-BSM-E4) rivers for long-term mean (A) surface current (cm s^{-1}), (B) sea surface temperature (SST,°C) and (C) sea surface salinity (SSS) from model year $4-10$. Pink lines indicate the 200 and 2000 m bathymetry contour. (D) mean model SSS without rivers, (E) mean model SSS with rivers and (F) mean SSS derived from CARS climatology.

Comparison between summer climatology SSS from the model (Fig. 3.19A) and CTD observations (Fig. 3.19B) agrees well, although there is an underestimation of the northward extent of the Zambezi River plume by the model. This model underestimation coincides with the relative large standard deviation of the observed SSS (Fig. 3.19C), indicating a large inter-annual variability in the Zambezi River plume that was not captured by the model. As a matter of fact, the monthly climatology river discharge rates used here are somewhat lower than the observed and lack variability in time to accurately reproduce the behavior of the plumes. The vertical section comparison also shows a good agreement between the model and observed mean summer salinity from CTDs (Fig. 3.19D and E), particularly the low surface salinity indicating the buoyant river plume. However, the model underestimates the offshore plume, with the 34.75 isohaline found $\sim$ 20 km offshore of the shore-most edge of the section for the model (Fig. 3.19D), whereas for the CTD observations it was $\sim$ 50 km offshore (Fig. 3.19E). Overall the model reproduces the river plumes reasonably well.

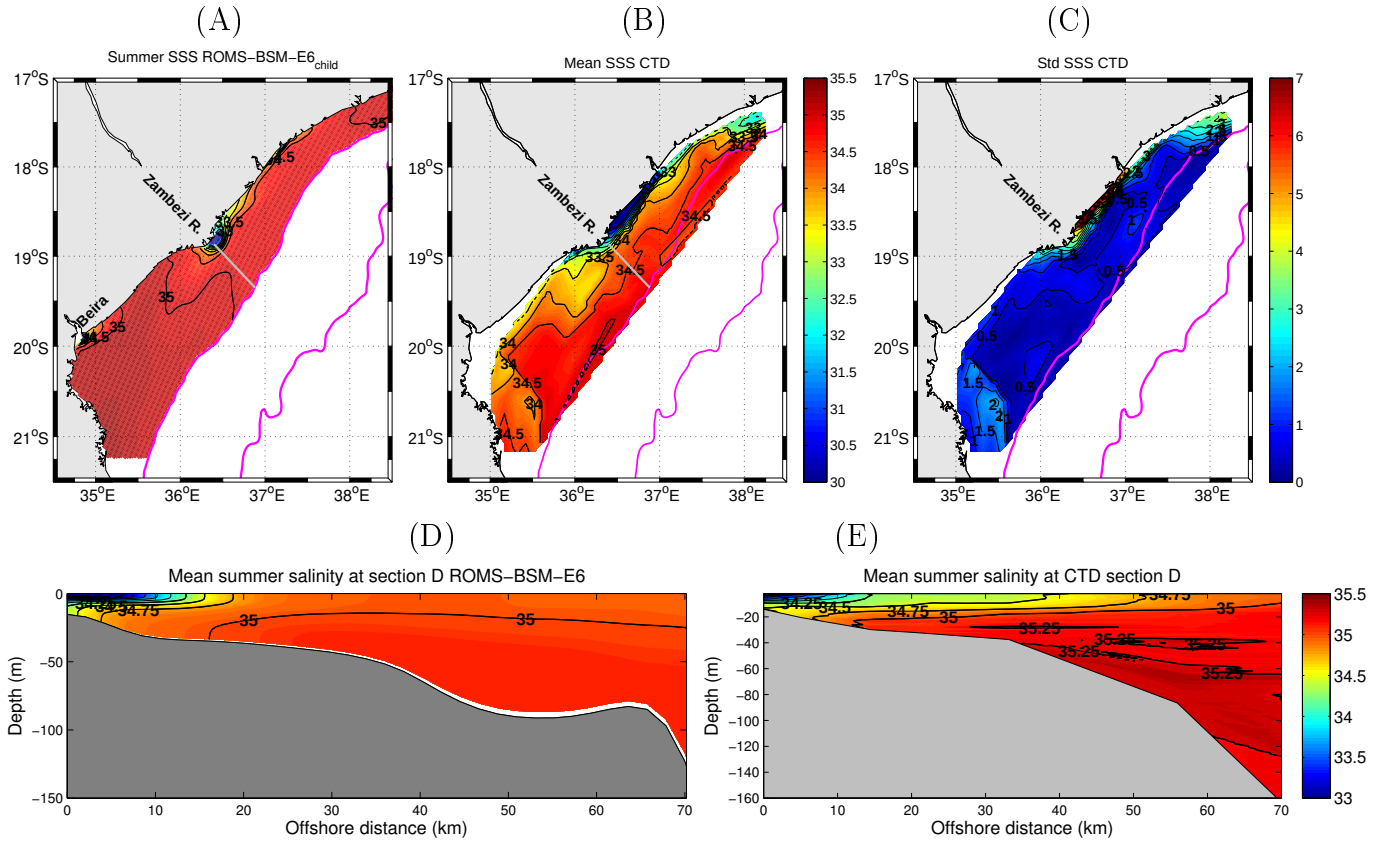

Figure 3.19: Comparison for river experiment between (A and D) model with river inputs averaged for summer year $4-10$ and (B, C and E) CTD observations from the annual January/February cruise $2003-2008$ (Chapter 2). (A and B) surface salinity, (C) standard deviation and (D and E) vertical section at cross-shore transect D off Zambezi River.

3.4 Summary and conclusions

The present chapter describes the implementation of a three-dimensional, high-resolution, climatological coastal ocean circulation model for the Sofala Bank and adjacent deeper ocean. With the two-way nesting, the finer grid is ~ 2 km, which is considerably finer than previous regional models, allowing it to resolve most of the small-scale shelf dynamics. Although there were some differences, the model circulation and structure in general agree reasonably well with the available observations and published studies.

The model was able to reproduce the Mozambique Channel eddies, although it exaggerated the mean SSH amplitude compared with observations (CNES-CLS09 and AVISO), which probably stemmed from the open boundaries (Halo, 2012; Halo et al., 2014). Similarly, the model overestimated the eddy variability as indicated by EKE and RMS relative to AVISO observations, again possibly due to the open boundaries (Halo, 2012; Halo et al., 2014). The model was able to produce the mean and general circulation patterns, particularly the mean poleward surface "Mozambique Current" on the slope (Quartly et al., 2013). This is in agreement with the observations from the CNES-CLS09 but mismatched the geostrophic current derived from the AVISO altimetry. In addition to this, the present study revealed a mismatch between the surface current of the CNES-CLS09 and AVISO derived geostrophic currents, indicating an inconsistency in the treatment of drifter data when computing the mean dynamic topography used in AVISO. The equatorward coastal "counter current" (Sætre and da Silva, 1984) appeared in the model, especially when the tidal current was weak during the slack or neap tides. The model indicates that the strong spring flood and ebb tidal currents dominate the coastal "counter current", which is not apparent during these tidal conditions.

The model was also able to reproduce the vertical patterns of the along-shelf current and agreed with the long-term mean LOCO observations (Ridderinkhof et al., 2010; Ullgren et al., 2012), particularly the Mozambique Undercurrent (de Ruijter et al., 2002). Most importantly, in the surface layer the velocity values of the model and the LOCO were similar. In contrast, both CNES-CLS09 and AVISO were relatively low. This supports the idea that the AVISO altimetry underestimates surface currents (Ternon et al., 2014; Penven et al., 2014). For this

reason, caution needs to be exercised when applying altimetry data, particularly for model-observation comparisons in the Mozambique Channel and in other similar systems around the oceans of the world.

The model also reproduces the sea surface temperature structures reasonably well. One of the major finding of this model is the cool water lens (or tongue) on the shelf, which is in agreement with the MODIS observations. The occurrence of this cool water lens can be explained in part by tidal mixing ($\sim 70\%$), supporting Chevane (2013), and in part by eddies ($\sim 30\%$). Eddies primarily set up the deep cool water at mid-depth on the shelf-slope so that tidal mixing energy and the related front transport the cool water to the surface. In comparison, the other observational data used here (CARS, WOA2009 and Pathfinder) poorly captured the nature of the cool water lens due to resolution issues.

The vertical section of temperature and salinity also agrees with the observations (LOCO, Ullgren et al., 2012). The documented water masses were reproduced by the model, including the subsurface transition from the TSW from the north to the STSW in the south, and in the intermediate depths transition from the RSW from the north to the AAIW transported from the south by the Mozambique Undercurrent (de Ruijter et al., 2002; DiMarco et al., 2002). The bottom temperature agreed with the annual-mean and seasonal UTR observations (Appendix C), but failed to reproduce the summer cool upwelling near Angoche in the north (Malauene et al., 2014). This can be explained by a lack of temporal variability of the climatology winds or problems related to the model edge (boundary). The latitudinal gradient of temperature, with warm water in the north and cool water in the south, were represented in the model both at the surface and in bottom waters.

The two-way nesting procedure was robust and improved the results of the model, as demonstrated for the SST before nesting in comparison with the MODIS observations. The semi-diurnal tides with a clear spring-neap cycle agree with the observations from the nearest tide gauges. The only difference (in the amplitude) can be explained by the fact that the model does not resolve the tide gauge location, which is inside the river. Since this is not an estuarine model, the river inlets were explicitly marked as land to avoid energy dissipation, with potential impacts on the tidal balance (Greenberg et al., 2007). The model was able to reproduce the

internal tides and wave generation "hotspot" at the shelf-break off Beira Bay (da Silva et al., 2009). There were clear velocity filaments following the bathymetry (200 m isobath) that were not as clear in the case of the Parent grid without nesting (Chevane, 2013), confirming that our two-nesting is improving the model outputs. The model indicated that the internal wave generation "hotspot" could be in part explained by the interaction of passing eddies with bottom topography. Until now, this has been poorly understood due to limited observational data. However, it has been observed in other parts of the world (Nikurashin and Ferrari, 2010b,a; Nikurashin et al., 2013). The river inputs improved the results of the model when compared to the simulation without rivers. This also agreed with observations from the CARS and CTDs. The buoyant plume (Nehama, 2012), however, was slightly underestimated, probably because the climatology river inputs lacked temporal variability.

A major limiting factor in the model was the use of climatological surface forcing, like wind, which lacks temporal variability that could accurately reproduce some coastal ocean dynamics and made it difficult to compare model-observations at the inter-annual synoptic scale (true calendar). In other words, comparison of the model with a few snapshot observations is not sufficiently reliable nor robust, thus relying on seasonal and/or mean state comparisons. Future improvements may be obtained through inter-annual synoptic surface forcing. Another limitation identified is the open boundary forcing. The values provided by the climatological SWIM overestimated the Mozambique Channel eddy variability depicted by EKE and SSH RMS (Halo, 2012; Halo et al., 2014). In the one-way nesting, the performance of the inner model (the present model in this case) depends on the outer model (SWIM in this case) (Penven et al., 2006a; Mason et al., 2010). The overestimation of the SWIM EKE and SSH-RMS propagates throughout our model (Fig. 3.7), indicating the need to improve the lateral open boundary forcing. Nonetheless, this one-way nesting with SWIM was still useful to obtain approximate Mozambique eddies, which were missing in other models of the region (e.g. Nehama, 2012). Overall, this coastal ocean circulation model of the Sofala Bank may be used to improve our understanding of ocean circulation and structure patterns in the region, and applied for interdisciplinary studies.

Chapter 4

The influence of eddies and rivers on the shelf circulation of the Sofala Bank

Abstract

The influence of offshore mesoscale eddy activity and river discharges on the shelf circulation and hydography of the Sofala Bank are investigated. Seasonal and quasi-synoptic (short) time scales are considered. In the absence of observational data, a modelling approach is followed. Self-organizing maps are used for pattern recognition and identification. The Mozambique Channel eddies and river plumes, especially from the Zambezi, were identified to be important features. It was found that the offshore eddies strongly modulate the shelf circulation. The plume of the Zambezi River is bi-directional in response to opposing effects of the Coriolis force and the nearby offshore anticyclonic eddies. Variability in size of river plumes occurs on a seasonal basis, related to seasonal variability in river discharges. Model data show that river discharges impact the ocean circulation within the buoyancy-driven plumes. During northward plumes there was a strong equatorward current with a coastal anticyclonic recirculation near the river mouth. During southward plumes there was a poleward current.

4.1 Introduction

The Mozambique Channel is dominated by mesoscale eddies which tend to propagate southwards along the shelf edge on the western side of the channel (Chapter 3; Lutjeharms 2006; Halo 2012; Halo et al. 2014). Given their strong current, it is thought that these eddies influence the shelf circulation. Previous studies have shown that, during the poleward passage of a large anticyclonic eddy near Angoche at the northernmost limit of the Sofala Bank (16°S), a strong poleward current forms along the shelf edge (Lutjeharms, 2006). This current appears to detach from the coast, moving offshore, and apparently generating a cyclonic lee eddy to the south off Angoche (Ridderinkhof and de Ruijter 2003; Lutjeharms 2006). High chlorophyll-a (Chl-a) levels have been associated with this cyclonic eddy (Nehring et al. 1987; Tew-Kai and Marsac 2009). More recently Malauene et al. (2014) demonstrated that Mozambique Channel eddies advect coastal productivity offshore into the channel near Angoche.

Major rivers of the world are known to provide large loads of nutrients (exogenous production) to the adjacent shelf regions. For example, a highly productive ecosystem is linked to the river plume of the Columbia (Hickey et al. 2010) and Mississippi Rivers (Lohrenz et al. 1999). Locally enhanced productivity is similarly observed on the Sofala Bank (Malauene et al., 2014), a region influenced by the Zambezi River, which is the largest on the east coast of Africa. Apart from the supply of nutrients, it has also been demonstrated that large river plumes significantly influence the shelf circulation, hydrography and ecology (García-Berdeal et al., 2002; Hickey et al., 2005; Liu and Weisberg, 2005; MacCready et al., 2009; Liu et al., 2009a,b). River plumes advect coastal material over large distances, both cross- and along-shore (McCabe et al. 2009). Recently, the plume of the Zambezi River has been the subject of a process-oriented model study (Nehama 2012). This study demonstrated that the buoyancy-driven plume of the Zambezi River flows northward or southward depending on the ambient flow. However, the model did not include the Mozambique Channel eddies, which could affect the observed plume variability. Understanding the impact of offshore eddy activity and river plumes on the shelf circulation could be important in improving our knowledge of shelf and coastal productivity and ecosystem functioning.

The aims of this chapter are to (1) investigate the influence of offshore eddies on the shelf circulation of the Sofala Bank, (2) assess the impact of offshore eddies on river plumes and (3) investigate the effect of river plumes on the shelf circulation. Analyses using self-organizing maps analysis (SOMs, Kohonen, 2001) of model simulation outputs of the Sofala Bank are used; this is the first time that SOMs are used to analyze Mozambique Channel eddy activity. Therefore, some time is spent in affirming the reliability of this technique in a highly nonlinear, energetic system. The model simulations are used to test the hypothesis that ($H_{4.1}$) anticyclonic eddies cause a poleward shelf current, whereas cyclonic eddies cause an equatorward shelf current. It is further hypothesized that ($H_{4.2}$) the direction and size of the river plumes are influenced by offshore eddy activity, with northward plumes driven by cyclonic eddies and southward plumes by anticyclonic eddies, and the offshore excursion of the plume depending on eddy proximity to the shelf and its magnitude. It is also hypothesized that ($H_{4.3}$) the river plumes should influence the near-coastal and shelf circulation by changing the salinity, temperature and current. Understanding these processes is important for understanding dispersal and transport of shrimp eggs and larvae on the Sofala Bank (Chapters 5 and 6).

4.2 Data and methods

As indicated in Chapter 3, few observational data on the circulation of the Sofala Bank are available. This chapter uses data generated by the two-way nested coastal-ocean circulation model of the Sofala Bank (ROMS-BSM model, including simulations with river inputs E6 in Table 3.2; Chapter 3). The ROMS-BSM model generated a time series of 840 images (matrices) per model grid (Parent and Child), for each of the selected variables of salinity, SSH and current vectors (u and v components). This amounted to a large dataset of 5040 images, i.e. 3 (variables) $\times$2 (grids) $\times$7 (years) $\times$360 (days) $\div$3 (3 days averaged outputs). The SOM analysis (Kohonen, 2001) is used on this large dataset.

Self-organizing maps

SOM is an unsupervised artificial neural network classification method, which projects complex multi-dimensional input data (images) into low-dimensional (two-dimensional) output maps. It preserves the geometric properties and spatial relationships (topological) within the input images (Kohonen, 2001). SOM is also a non-linear cluster analysis, which groups similar input data into a set of output units (so-called patterns), based on competitive training (or learning). The unit showing the smallest Euclidian distance is the "winner" and best represents the input data, i.e., the best matching unit (BMU). The relative frequency of occurrence of similar input data in each unit or pattern is given as a percentage. Note that unsupervised SOMs means that no pattern was preselected; they were randomly generated and distributed during the training process. SOMs were used for these analyses because the approach has been demonstrated to have advantages over other traditional linear methods, such as empirical orthogonal function analysis (Richardson et al., 2003; Liu and Weisberg, 2005; Liu et al., 2006).

In this study, SOMs are applied to model 3-day averaged outputs of SSH and salinity between year 4 to 10 to identify and extract patterns of mesoscale eddies and variability in river plume on the Sofala Bank. The SOMs training parameters were chosen according to Liu et al. (2006) and included: a rectangular neural lattice of ''flat sheet'' shape, linear initialization, ''ep'' neighborhood function with radius of 1, and the "batch" algorithm. These parameters define

the feature extraction performance of the SOM. A sensitivity test with small (3×3) and large (3×4) map sizes was conducted before selecting the SOM map size. For both the SSH anomaly and river plume, the 3×4 SOM map size, which gives 12 patterns, was chosen. Larger map sizes are known to produce detailed patterns, whereas smaller maps produce general structures but with less information (Vesanto et al., 2000; Liu et al., 2006, 2008). The time of each pattern in the original input dataset is shown as a time series of BMUs. The relative frequency of occurrence of each pattern is computed based on the BMU time series and is given as a percentage in the SOM maps. The SOMs analyses were performed using R package Kohonen (Wehrens and Buydens, 2007).

Prior to SOMs training, the model SSH outputs were reprocessed by producing a SSH anomaly (subtracting the seven-year long-term mean). The shelf region ($<$ 200 m isobath) was masked and not included in the SSH analysis. Salinity was converted into a river plume index, computed as defined by equation 3.3 (Chapter 3). In this case, the offshore region ($>$ 200 m isobath) was masked. To investigate the influence of the offshore eddies on the Sofala Bank circulation, averaged original surface shelf current velocities during the period of each SSH SOM pattern, based on its BMU time series, were produced. Attention was given to the (i) eddy rotation, (ii) eddy strength and (iii) eddy proximity to the Sofala Bank. In the case of the influence of offshore eddies and ambient circulation on plume structures (direction and size), averaged surface shelf currents and offshore SSH during the period of each SOM plume pattern were produced.

4.3 Results

4.3.1 Eddy variability and influence on the shelf circulation

Offshore eddy variability patterns using SOM

The SOM maps show mesoscale eddy variability, highlighting anticyclonic and cyclonic eddies (Fig. 4.1A). In the seven-year simulation it is clear that the anticyclonic eddy patterns dominate the SOM maps. The temporal evolution of the SOM patterns show that these eddies propagate southward (Fig. 4.1A). An example of eddies moving southwards is given by the sequence of patterns from 12→1→5→10→11 at the beginning of the BMU time series (Fig. 4.1B). In pattern 12, an anticyclonic eddy is apparent to the south at $\sim$ 21°S and 38°E with another anticyclone observed entering the study domain from the north. Both anticyclonic eddies were separated by relatively low SSHA. In pattern 1, the southern anticyclone had moved southward, whereas the northern anticyclone, once developed, also moved south. The low SSHA between the two anticyclones also developed into a cyclonic eddy. In pattern 5, the southern anticyclone completely exited the study domain to the south, with the one to the north continuing to move southward and the cyclone spreading over a large area. In pattern 10 the anticyclonic eddy to the north had moved westward. Finally, in pattern 11, the anticyclone to the north had decayed in the middle of the domain. Another example of a train of eddies moving southward and westward is shown by following the patterns (10→7→12→4→5→9→12) in November of model year 5 to March of model year 6 (Fig. 4.1B). Although some of the pattern is repeated during this long event, the pattern sequence is not the same.

The BMU time series shows that there is no seasonal cycle in the SSHA SOM patterns (Fig. 4.1B). Interannual variability is, however, apparent as some patterns were not observed in certain years. For instance, there was no pattern 1 in year 5, pattern 2 in year 7, pattern 4 in year 8, pattern 6 in year 10, and pattern 8 and 9 in year 4. Only model years 6 and 9 had all 12 patterns (Fig. 4.1B).

In terms of pattern identification, the 12 SOM patterns of SSHA can be grouped in five general eddy categories:

1. **Poleward passage of an anticyclonic eddy (eddy corridor) -** This consisted of pattern 3 only (Fig. 4.1A). Most of the time, pattern 3 emerged after a large anticyclonic eddy (patterns 1, 7, 10 and 12) and before a decaying anticyclonic eddy (pattern 6, 8, 11), indicating the passage of strong anticyclonic eddies on the continental slope to the western side of the Mozambique Channel.

2. **Anticyclonic eddy offshore -** This category consisted of patterns 7, 9 and 12 (Fig. 4.1A), in which a large and strong anticyclonic eddy is located in the central region off the Sofala Bank. There were also some cyclonic eddies surrounding it, but those had weak negative SSHAs. In the case of pattern 9, the eddy was far from the shelf (200m isobath), whereas in pattern 12 it was close to the shelf.

3. **Cyclonic eddy offshore -** This category consisted of patterns 1 and 5 (Fig. 4.1A), where a cyclonic eddy occurred off the central Sofala Bank. There were also anticyclonic eddies, but in both patterns the cyclonic eddies were located closest to the central Sofala Bank.

4. **Eddy dipole -** This category consisted of patterns 4 and 10 (Fig. 4.1A). In the case of pattern 4, there was a cyclonic eddy to the north, showing a cyclonic (anticyclonic) eddy pair dipole. In contrast, for pattern 10 there was an anticyclonic eddy to the north, indicating an anticyclonic (cyclonic) eddy pair dipole.

5. **Eddy generation and decay -** This category consisted of patterns 2, 6 and 11 (Fig. 4.1A), with weak positive and negative SSHAs. The BMU time series shows that these at times precede (e.g. patterns 2 $\rightarrow$ 1, 2 $\rightarrow$ 5, 6 $\rightarrow$ 5, 12 (weak SSH northern) $\rightarrow$ 1 and 12 (weak SSH northern) $\rightarrow$ 4) or follow (e.g. patterns 5 $\rightarrow$ 11 and 10 $\rightarrow$ 11) well developed eddy patterns (Fig. 4.1B).

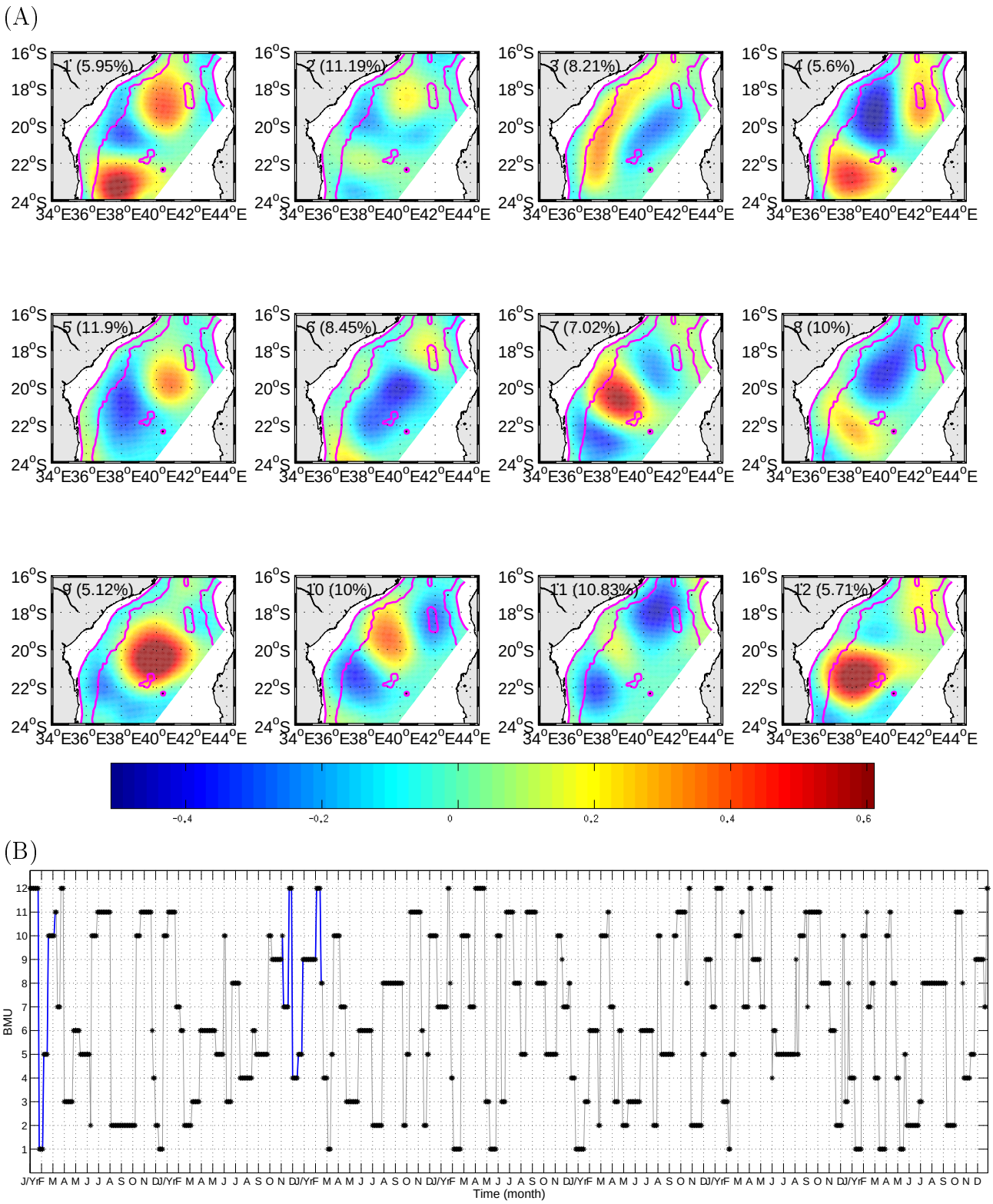

Figure 4.1: (A) 3x4 SOM maps for the SSH anomaly for model years $4-10$. The numbers $1-12$ (in the top left corner) indicate the SOM patterns and the percentage (in brackets) the frequency of occurrence of each pattern. Blue (negative SSHA) indicates cyclonic eddies and red (positive SSHA) anticyclonic eddies. The shelf region within the 200 m depth was masked prior to running the SOM. (B) shows the temporal evolution (variability) of each SOM pattern as a time series of the best matching unit (BMU) for the same period. Blue lines highlight two sequential event of anticyclonic eddies propagating southward.

Offshore eddy influence on the shelf circulation

Various patterns of simulated mesoscale eddy variability, such as anticyclone, cyclone and dipoles, have been identified in the preceding section, using SOMs. The following subsections investigate the influence of these patterns on coastal circulation, especially in relation to eddy rotation, strength and proximity to the shelf. Composite-averages of coastal currents, corresponding to the occurrence of selected patterns of simulated offshore eddy variability, are analyzed here.

Effect of an anticyclonic eddy

The averaged surface current relative to the close proximity of an anticyclone (Fig. 4.2) shows that there is a relatively strong southward current extending over much of the shelf, except off Beira ($\sim 20°$S), where there is a weak, nearly zero, current. When the anticyclone is closer to the shelf, the strong southward flow extends over the shelf close to the coast (e.g. pattern 7 in Fig. 4.2A). In the case where the anticyclone is found further offshore, a narrow and strong southward flow is observed along the shelf-break, whereas on the inner-shelf there is a relatively weaker circulation (e.g. pattern 9 in Fig. 4.2B).

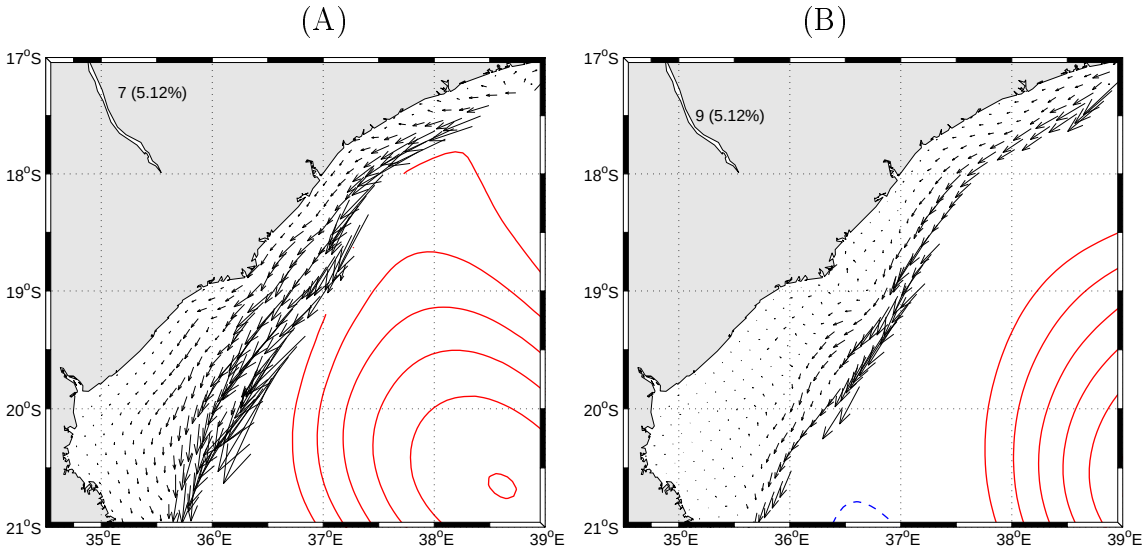

Figure 4.2: Averaged surface currents for the proximity of an anticyclonic eddy to the shelf for (A) the eddy is close and (B) the eddy is farther offshore. Contours in 10 cm intervals indicating (red) anticyclonic and (blue) cyclonic eddy as in SSHA SOM maps, Fig. 4.1A. The number in the upper left corner indicates the SOM pattern and its frequency of occurrence. Note here the domain has been cropped from the SOM map and the current outside the 200 m isobath masked to improve visualization of the shelf circulation.

Effect of a cyclonic eddy

Relative to the close proximity of a cyclonic eddy (Fig. 4.3), the surface shelf current tends to flow northward. In the case when the cyclone is strong, there is a strong northward flow extending over the shelf and reaching the coast (Fig. 4.3A). In Fig. 4.3B, the cyclone is in an early stage of development and therefore weak. As a result, there is a relatively strong northward flow on the shelf-break, with a relatively weak flow on the inner shelf (Fig. 4.3B).

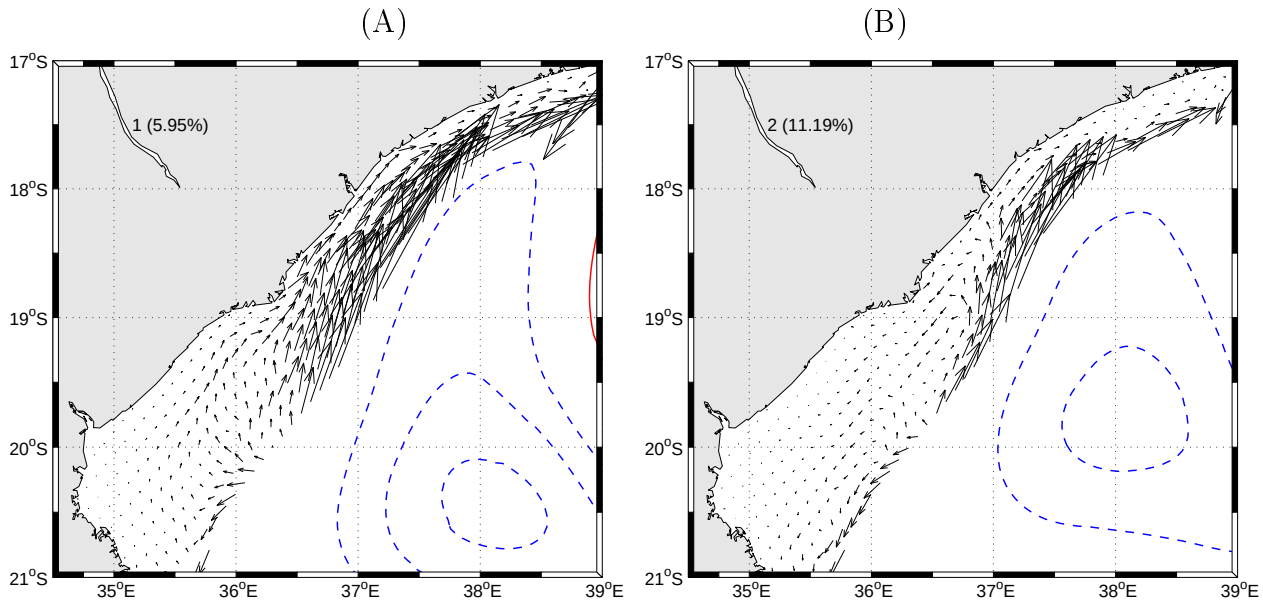

Figure 4.3: Same as Fig. 4.2 but relative to a cyclonic eddy (A) strong (pattern 1) and (B) weak (pattern 2) off the central Sofala Bank.

Effect of an eddy dipole

Fig. 4.4A shows the case of a cyclonic−anticyclonic eddy pair dipole, with the cyclone to the north. There are averaged surface current vectors on the shelf-break, which diverge between the two eddies ($\sim 19°30'$S), one northward and the other southward, corresponding with their eddy rotation (Fig. 4.4A). In the case of the anticyclonic−cyclonic eddy dipole, with the anticyclone to the north (pattern 10 in Fig. 4.1B), currents over the shelf are found to flow southward on the north and northward on the south (Fig. 4.4B). These currents converge on the central shelf, resulting in a strong offshore current exiting the Sofala Bank between the two opposite eddies (Fig. 4.4B).

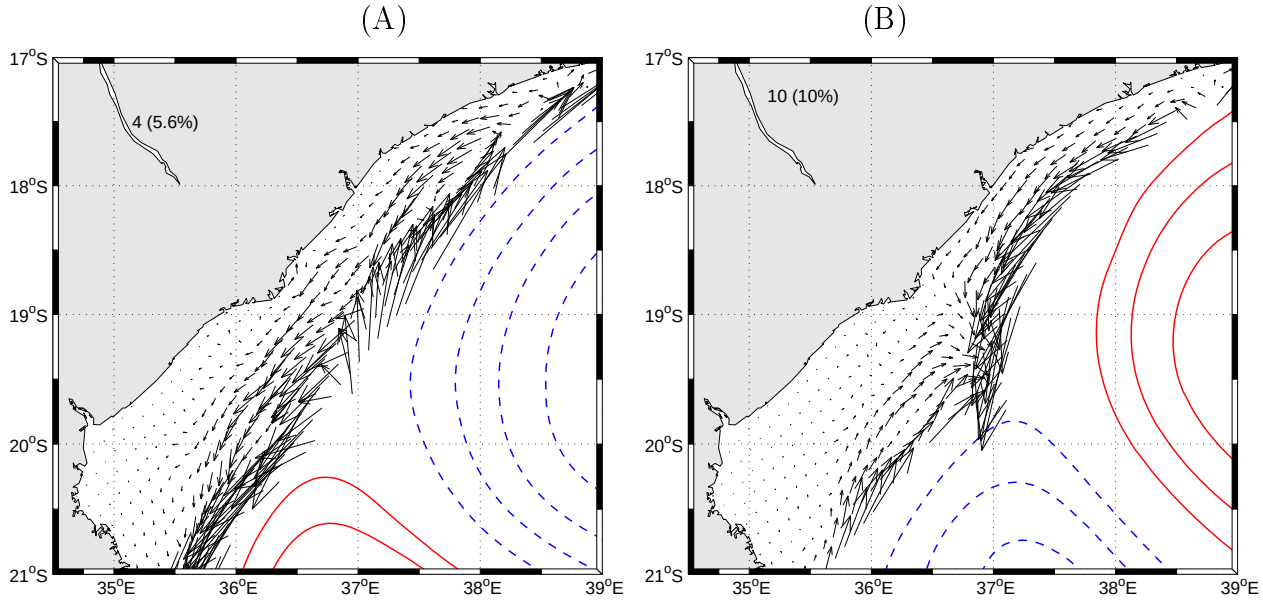

Figure 4.4: Same as Fig. 4.2 but relative to dipole pair of eddies (A) cyclone−anticyclone (pattern 4) and (B) anticyclone−cyclone (pattern 10).

4.3.2 River plumes and circulation

River plume variability patterns using SOM

Twelve patterns of river plume variability were identified using 3 × 4 SOMs of the plume index derived from model salinity outputs. In the model, there are plume associated with three river systems, i.e. the Licungo (∼ 18°45′S), Zambezi (∼ 19°S) and Beira Bay (Pungué and Buzi,∼ 20°S) (Fig. 4.5A). As expected, the Zambezi River plume strongly dominates by spreading over a much larger area compared to the other two (Fig. 4.5A). This is due to its much larger river discharge rate, which is > 5 times larger than the others (Fig. 3.4). The Zambezi plume generally extends far north to the Licungo River mouth at ∼ 18°45′S (Fig. 4.5A), resulting in the joining of the two plumes. The Licungo River plume, however, becomes apparent when the Zambezi plume does not extend so far north (green line at ∼ 18°45′S in Fig. 4.5A patterns 9 and 10). Both the plumes of the Licungo and Beira Bay Rivers were very localized near their river mouths, suggesting a small influence on the continental shelf.

From this analysis, it is clear that the dominant mode of plume variability is along the coast to the north of the river mouth (i.e. downstream), especially for the Zambezi River. The

12 patterns of river plume variability, however, can be summarized into three more general categories according to the direction of spread and structure:

Northward – This consists of patterns 3, 4, 6, 8, 11 and 12 (Fig. 4.5A), in which the Zambezi River plume is found to flow northward. In this mode a long narrow plume structure is apparent, with brackish water confined to the coastal region, particularly in the far-field (far from the river mouth). This long, narrow, coastal plume extends more than 150 km to the north of the Zambezi River mouth (from $19 - 18°30'$S), beyond the Licungo River mouth ($18°45'$S). Off the Licungo River, the Zambezi plume is superimposed with the local plume originating from the Licungo River, making it difficult to distinguish the two river plumes.

Southward – This consists of patterns 1, 2, 5 and 7 (Fig. 4.5A), which show that, at times, the Zambezi plume flows southward. The southward plume becomes detached from the coast with a more offshore excursion and little along-shore mode of variability.

Small-Bulge – This consists of patterns 9 and 10 in Fig. 4.5A, when there is an accumulation of freshwater runoff close to the Zambezi River mouth, resulting in a plume "bulge". This accumulated, buoyancy-driven plume expands offshore with some alongshore spread. Pattern 9 (Fig. 4.5a) shows the most offshore spread of the Zambezi plume ($>$ 50 km from the coast), but the frequency of occurrence (2.38%) is the smallest. The small-bulge pattern 10, however, accounts for the maximum frequency of occurrence ($\sim$ 22.26%) and is found over a long period ($>$ 60 consecutive days) during late winter and spring each year (Fig. 4.5B). This period coincides with the season of low river discharge rates (Fig. 3.4).

The BMU time series (Fig. 4.5B) shows that the Zambezi River plume is frequently bi-directional, with consecutive northward and southward orientations observed at quasi-synoptic (few days) time scales, particularly during summer and autumn. There is a seasonal cycle in the plume variability (Fig. 4.5B), with patterns 1, 2, 3, 4 and 7 most of the time occurring during summer–autumn (January–May), whereas patterns 9 and 10 occurred during late winter–spring (September–December).

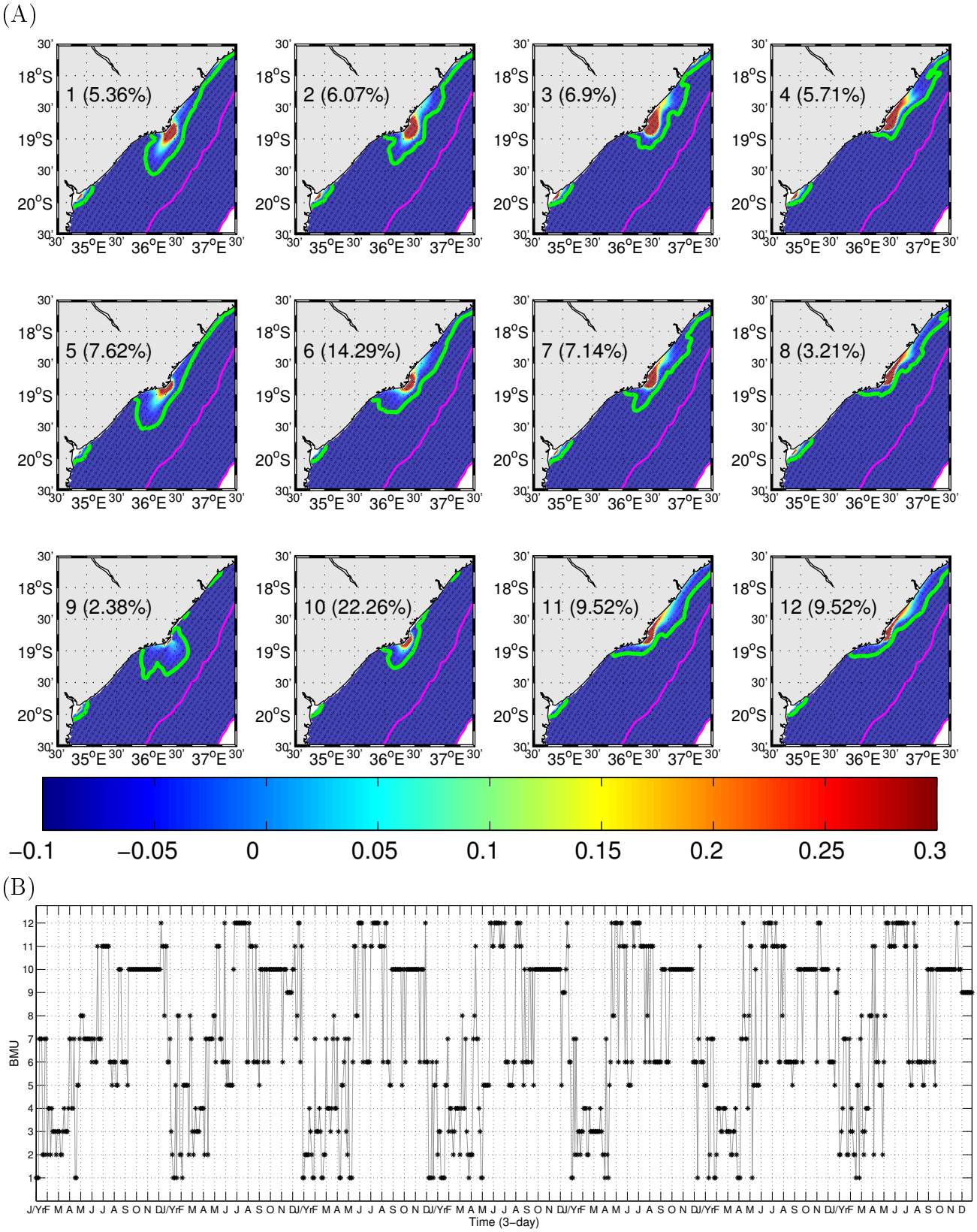

Figure 4.5: (A) 3×4 SOM maps highlighting 12 patterns of river plumes (color shading outline by green line) on the Sofala Bank. There were derived from plume index of salinity from model years $4 - 10$. The number in the upper left corner indicates the SOM pattern and its frequency of occurrence (percentage). (B) Corresponding BMU time series for river plume variability for the same period.

A clear seasonal cycle is apparent in salinity over the Sofala Bank, with high salinity during the summer and spring, and relatively low salinity during autumn and winter (Fig. 4.6). There is also seasonal variability in the river plume, indicated by river brackish water (Fig. 4.6), with the biggest plume apparent during summer and autumn while the smallest plume appeared during spring. During summer, the coastal northeastward incursion of the Zambezi plume was very narrow and close to the coast near $\sim 18°$S (off Quelimane), then relatively far away from the coast near the Licungo River mouth ($\sim 17°45'$S) (Fig. 4.9). Southward−oriented plumes were not apparent in the seasonal average. The Beira Rivers also show seasonal plume variability, with relatively large plumes during summer and small plumes during winter (Fig. 4.6).

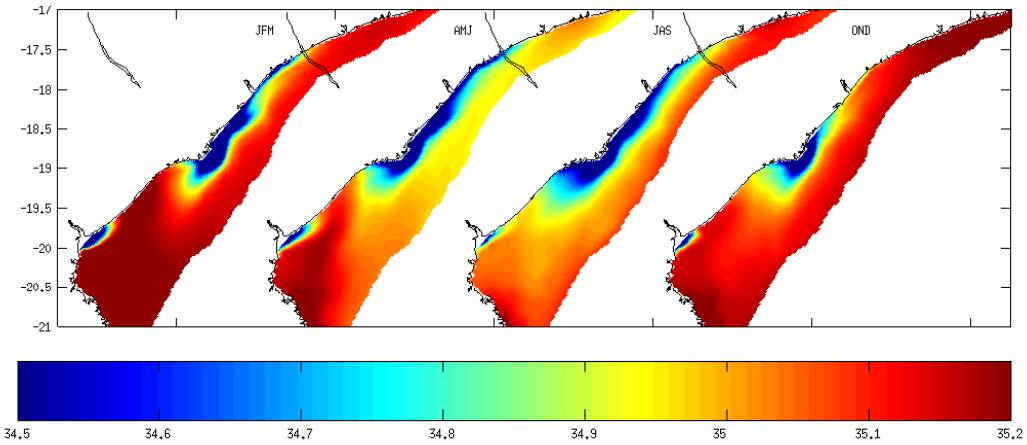

Figure 4.6: Seasonally averaged salinity (color shading) derived from experiment ROMS-BSM-E6 using model years $4-10$. The letters indicate the months of each season (JFM) summer, (AMJ) autumn, (JAS) winter and (OND) spring.

Influence of offshore eddies and shelf circulation on the plume

Averaged SSH during each SOM pattern of river plumes shows that only the southward plumes (patterns 1, 2 and 5) are related to a well defined eddy, an anticyclone in these cases (Fig. 4.7). Comparison between eddy activity during plume patterns 1 and 2 shows that the former was related to a strong anticyclone close to the shelf. In contrast, the latter was related to a slightly weaker and farther offshore anticyclone, causing a slightly shorter southward plume incursion. In the case of the most offshore plume spread (pattern 9), there are weak (nearly zero) and far offshore SSHAs. There was only one northward plume (pattern 12) related with a cyclonic feature.

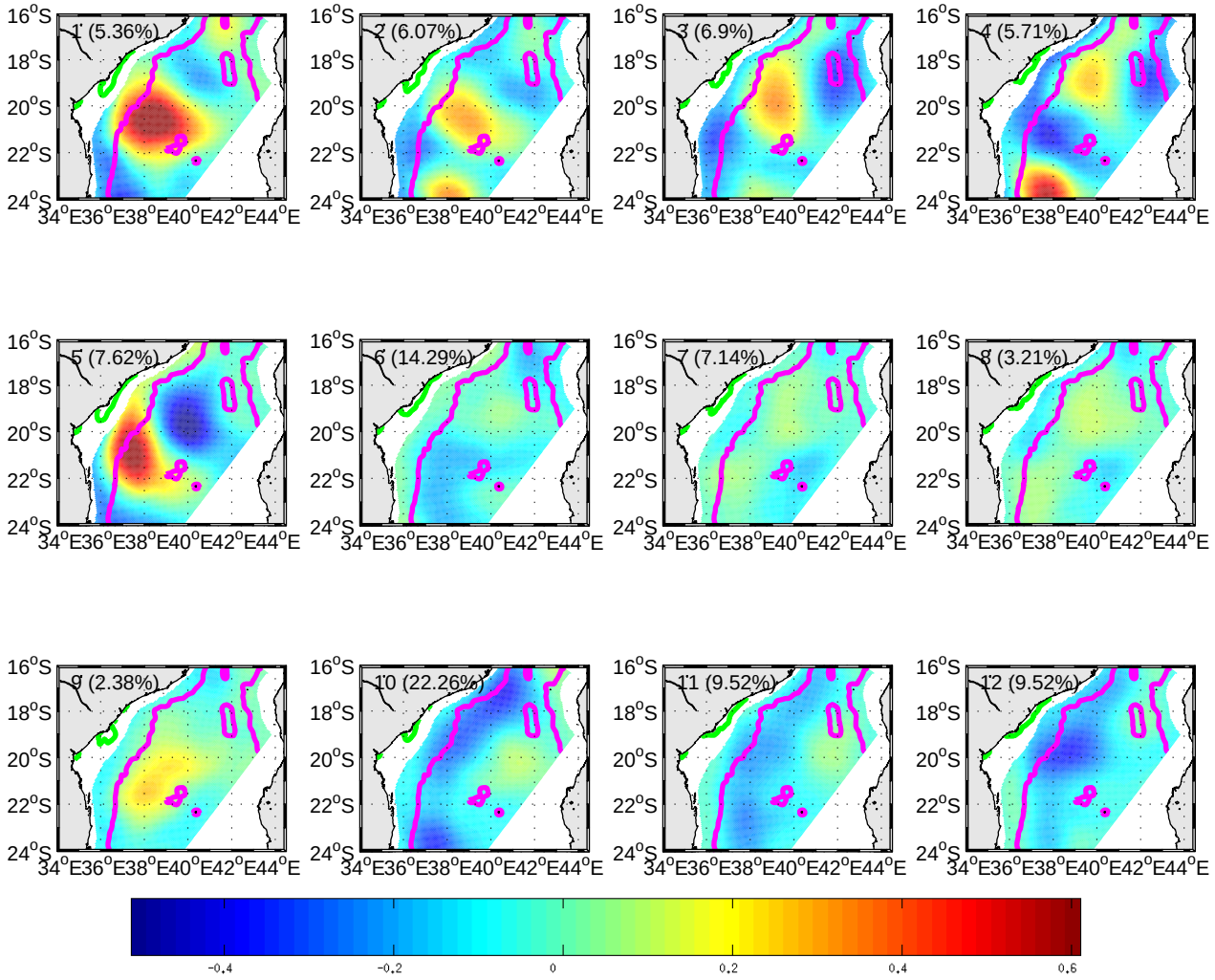

Figure 4.7: Averaged SSHA for eddy activity during each of the plume SOM patterns (green line) depicted in Fig. 4.5A. The number in the upper left corner indicates the SOM pattern and its frequency of occurrence (percentage). Note that the domain is larger than the SOM plume maps and the area inside the 200 m isobath is masked for better visualization.

The southward plumes are found during strong poleward currents on the shelf (Figs. 4.8A and B). Comparison of the current field during plume patterns 1 (Fig. 4.8A) and 2 (Fig. 4.8B) shows that the most southward intrusion is found in pattern 1, which is linked to a strong southward current, while for pattern 2 it is slightly less southward, linked to a relatively weak current. In the case of the small-bulge plume, there are weak shelf currents (Fig. 4.8C). There was a small anticyclonic eddy within the bulge plume right on its southernmost limit (green line), centred at $\sim 19°30'$S and 36°E.

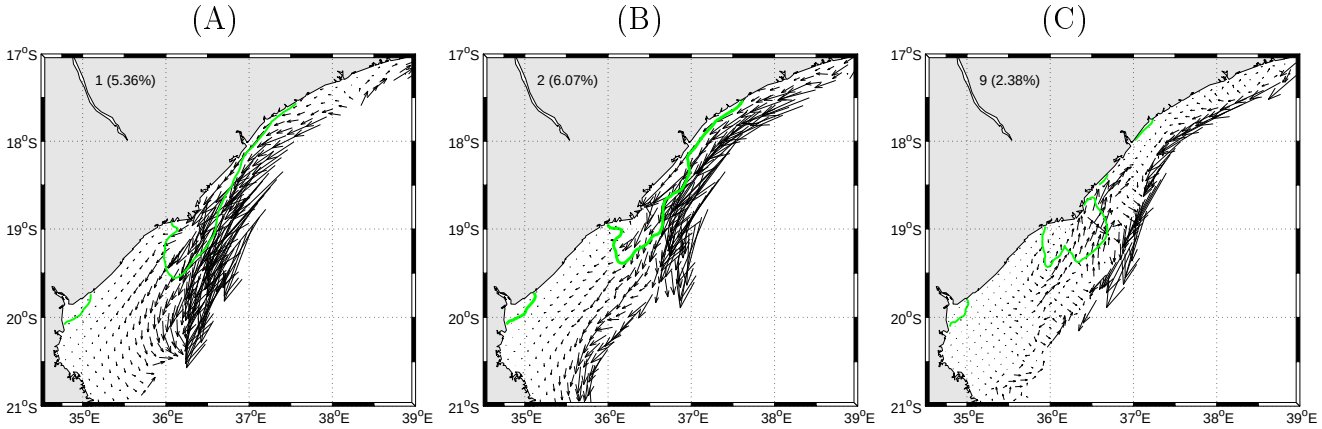

Figure 4.8: Examples of averaged surface shelf current during (A and B) SOM plume patterns 1 and 2 for southward plumes and (C) pattern 9 for the small-bulge strucuture. The number in the upper left corner indicates the SOM pattern (depicted in Fig. 4.5A) and its frequency of occurrence (percentage). Note that the domain is larger than the SOM maps and the area outside the 200 m isobath is masked for better visualization of the shelf circulation.

Plume influence on the shelf circulation

Within the buoyant Zambezi and Beira plumes, there are relatively strong currents compared with adjacent waters outside the plumes (Fig. 4.9). It is apparent that the Zambezi plume radiates current in all directions from the river mouth. During the summer and autumn, when the discharge rate is large, there is a strong offshore and northeastward current near the Zambezi River mouth, which is opposite in direction to the ambient current outside the buoyant plume (Figs. 4.9A and B). Note that there is a small coastal anticyclonic circulation just north of the Zambezi River at 18°45′S, especially in summer (Figs. 4.9A). During winter and spring, there is a strong southward current inside the Zambezi plume (Figs. 4.9C and B). In winter, there is a weak northeastward coastal current to the north of the Zambezi River mouth (Figs. 4.9C) and, in spring, the northeastward current no longer exists while there is influence of a southward current from outside the buoyant plume (Fig. 4.9D).

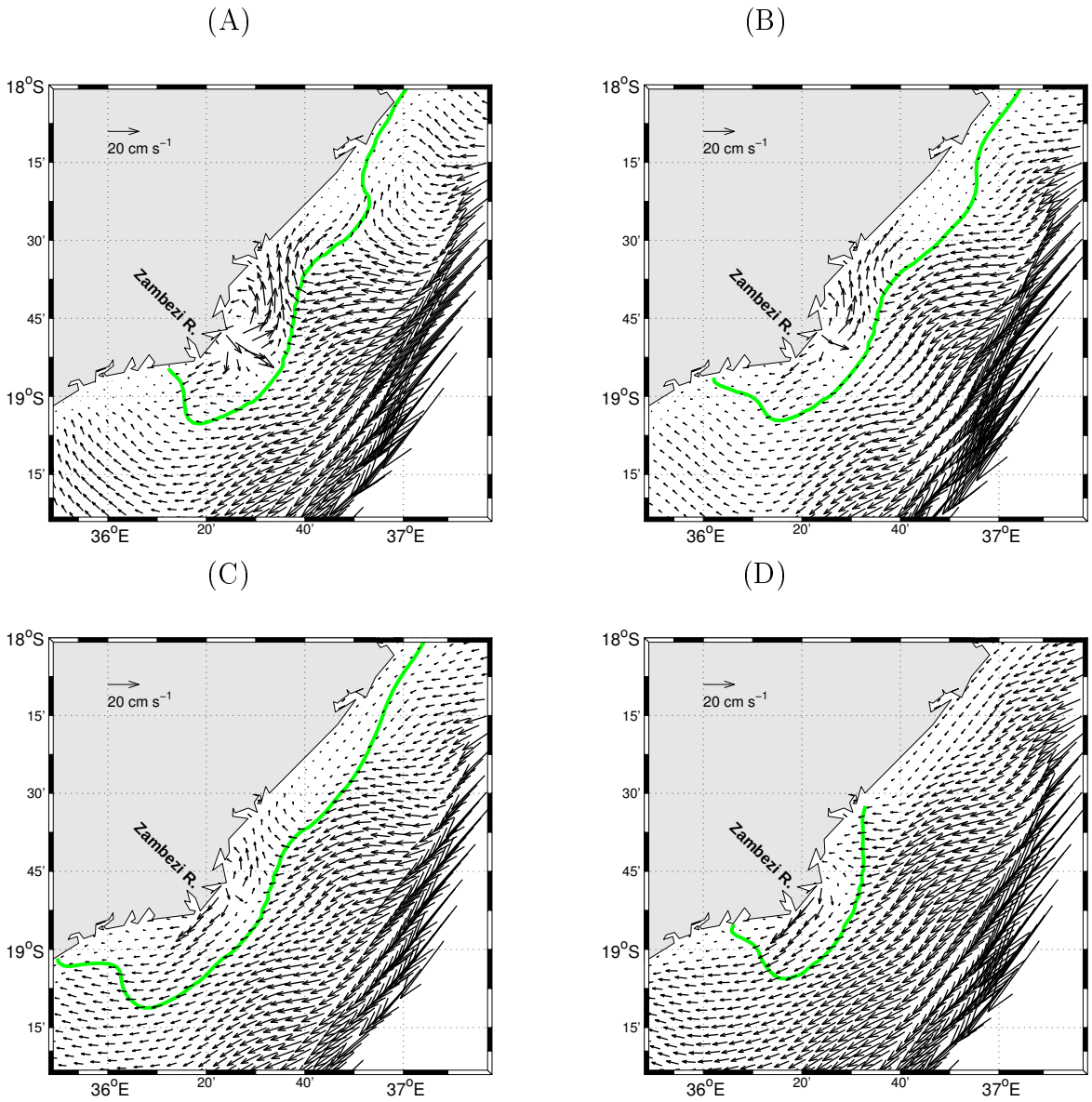

Figure 4.9: Seasonally averaged surface currents (m s^{-1}) and river plumes (green line) derived from experiment ROMS-BSM-E6 model years 4−10 for (A) summer, (B) Autumn, (C) winter and (D) spring at the Zambezi River.

Fig. 4.10 clearly shows that the simulated, small Beira rivers plume is uni-directional, i.e. northward. The size of the Beira plume decreases from summer to spring (Fig. 4.10), with corresponding seasonal decreases in the river volume discharge rates (Fig. 3.4). Similarly to the Zambezi River plume, the Beira plume also has a strong current inside the buoyant plume relative to the adjacent weak ambient circulation outside (Fig. 4.10). During large volume discharges (summer−autumn), there was a dominant northward flow and an associated small coastal anticyclonic rotation within the Beira plume.

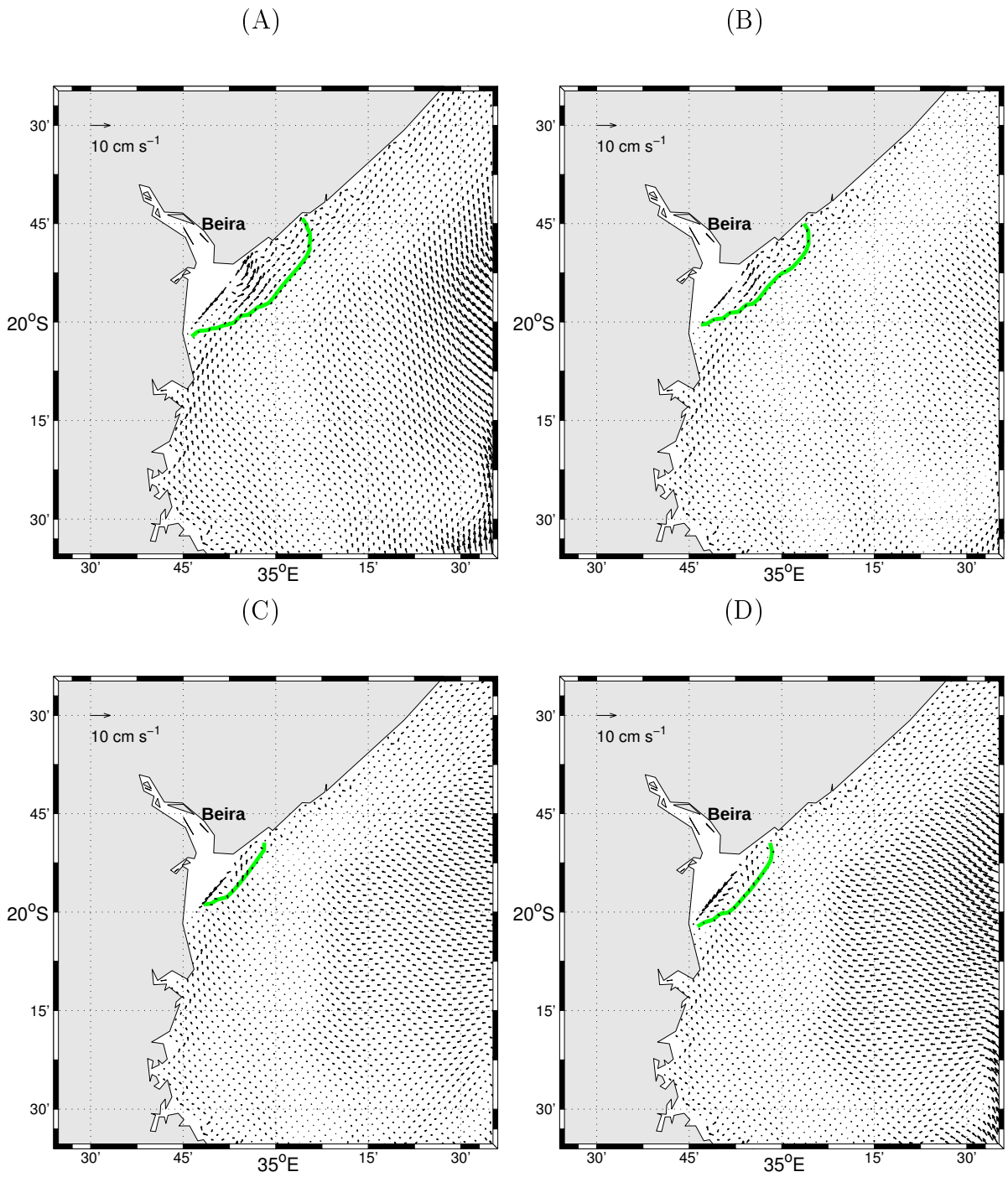

Figure 4.10: Same as Fig. 4.9, but for the Beira rivers (Pungué and Buzi) plume.

4.4 Discussion

The high resolution nested ROMS model of the Sofala Bank has been evaluated in the preceding chapter, and agrees reasonably well with observations. In the absence of *in-situ* observations, the following sections discuss the application of these model outputs to investigate the influence of the offshore, southward passing mesoscale eddy activity and river discharges on the circulation of the Sofala Bank.

Offshore eddy variability

The 3×4 SOM maps of SSH captured both cyclonic and anticyclonic eddies, with the latter being dominant in terms of amplitude (Fig. 4.1A). The numbers of cyclonic eddies were relatively large compared to the anticyclones, which is in agreement with a previous study (Halo et al., 2014). Most importantly, the temporal evolution of the SOM patterns (BMU times series) captured the southward propagation of these eddies (Fig. 4.1B), which also agrees with previous studies (de Ruijter et al., 2002; Ridderinkhof and de Ruijter, 2003; Lutjeharms, 2006; Tew-Kai and Marsac, 2009; Backeberg and Reason, 2010; Halo, 2012; Halo et al., 2014). This provides confidence that SOMs can be used to track eddies – although it should be noted that there are other methods to track eddy trajectories, such as the automatic eddy detection and track scheme described by Halo et al. (2014).

The SOM maps also showed eddy pair dipoles, with two configurations according to their counter-rotations: one with the cyclone to the north, i.e. cyclone-anticyclone (pattern 4), and the another with the anticyclone to the north, i.e. anticyclone-cyclone (pattern 10). Similarly, recent studies using satellite altimetry observations demonstrate that the southward propagating train of cyclonic and anticyclonic eddies result in eddy dipoles along the western slope of the Mozambique Channel (Malauene et al., 2014; Roberts et al., 2014). In addition, the latter study showed that, at times, they can result in tripoles, similar to patterns 7 and 10 in the present study (Fig. 4.1A). Previous studies, based on complex and extended empirical orthogonal function analyses of satellite altimetry, showed a regular variability of the mesoscale pattern, dominated by dipoles or tripoles in the central Mozambique Channel, explaining 10%

(Tew-Kai and Marsac, 2009) and $\sim 15\%$ (Schouten et al., 2003) of the variance. In the present study, the contribution of SOM patterns 7 and 10 produces a frequency occurrence of $\sim 17\%$, which is similar to those of the previous studies.

Halo et al. (2014), using an automatic eddy detection algorithm for SSH derived from satellite observations and models, demonstrated that both cyclonic and anticyclonic eddies are locally generated in the central Mozambique Channel. In the present study, at times weak positive and/or negative SSH anomalies emerged before relatively strong and well defined anticyclonic and/or cyclonic eddies, indicating the early start up phase of an eddy. This confirms that both anticyclonic and cyclonic eddies are locally generated in the Mozambique Channel (Halo et al., 2014). In contrast, there were weak SSH features after strong SSH variations, indicating that some eddies could dissipate (decay) near the Sofala Bank.

Effect of eddies on the circulation

Mesoscale eddies have long been recognized to laterally transfer properties and momentum (vorticity) to the region (Holland and Rhines, 1980; Bell and Pratt, 1992; Vandermeirsch et al., 2003; Waterman and Jayne, 2011). However, studies that have emphasised the effect of offshore eddies on the adjacent shelf circulation or interactions between them were conducted in regions where there is a western boundary current to the west of the eddy activity. For example, the Gulf Stream current system in the North Atlantic Ocean is influenced by offshore, meso-scale eddies (Schmitz, 1984; Cronin and Watts, 1996) and the Kuroshio Current system in the North Pacific Ocean is modulated by the westward propagating offshore meso-scale eddies, with more intrusion associated with cyclones (Qiu and Miao, 2000; Cai et al., 2002; Qiu and Chen, 2010; Jin et al., 2010; Yin et al., 2014). In contrast, the highly energetic eddy field of the Mozambique Channel occurs in the absence of a permanent western boundary current. Although there are studies on eddy dynamics, including interaction with productivity, the effect of the eddies on the shelf circulation, particularly on the Sofala Bank, is not well known.

The present study revealed that the offshore eddies in the Mozambique Channel strongly modulate the shelf circulation on the Sofala Bank, supporting the hypothesis ($H_{4.1}$) that eddies can induce instantaneous circulation over the adjacent shelf. As shown in patterns 7 and 9 (Fig. 4.2), there is a strong poleward surface shelf current during the presence of an anticyclonic eddy off the central Sofala Bank. A similar anticyclonic eddy-induced current was found in the South China Sea, where the western boundary Kuroshio Current is generally weak (Cai et al., 2002). In contrast, an equatorward current (opposite to the net flow transport) is found during the presence of a cyclonic eddy off the shelf (e.g. patterns 1 and 2, Fig. 4.3). This indicates that the eddy rotation (polarity) plays an important role in modulating the short-term variability of the flow direction.

The eddy (both cyclone and anticyclone) proximity to the shelf (200 m isobath) also plays an important role in Sofala Bank circulation, with eddies close to the shelf strengthening currents over most of the shelf (e.g. pattern 7 Fig. 4.2A). In contrast, eddies farther offshore have less influence on the inner-shelf, but do produce strong currents on the shelf-break (e.g. pattern 9 Fig. 4.2B), indicating a westward diminishing influence of offshore eddies on the adjacent shelf circulation. This implies that, for eddies far offshore, the transferred energy is dissipated before it reaches the inner shelf. A recent study by Roberts et al. (2014), analyzing shipboard acoustic Doppler current profiler (S-ADCP) transects further south (at $\sim 20°$S off Pomene), has shown a poleward surface current decreasing in intensity from the edge of an offshore anticyclonic eddy towards the coast. A similar westward diminishing eddy impact is observed in relation to the eddy strength, such that strong eddies intensify the shelf circulation up to the coast (e.g. pattern 1 Fig. 4.3A). In contrast, weak eddies have less impact on the inner shelf, but their influence over the shelf-break should not be neglected (e.g. pattern 2 Fig. 4.3B). This implies that, in the case of a weak eddy, the transfered energy is insufficient to cross the shelf-break into the near shelf.

The dipole pairs of eddies also impact the shelf circulation, with two opposite shelf current directions depending on the counter-rotation relative to the dipole. The eddy dipole with the anticyclone to the north induces poleward currents on the north of the dipole axis and equatorward on the south. These currents converge at the central shelf, resulting in a strong offshore

current between the two eddies. Snapshots of coastal S-ADCP also show a similar pattern of shelf circulation associated with the same type of eddy dipole (Roberts et al., 2014; Ternon et al., 2014). In these observational studies as in the present model study the contribution of the anticyclonic eddy dominates the cyclone counter-part. This possibly occurs because anti-cyclonic eddies are generally larger and stronger than the cyclones in the Mozambique Channel (Halo et al., 2014). In contrast, the eddy pair dipole with the cyclone to the north induce a strong current towards the shore between the two eddies, which is consistent with observations (Fig. 5A in Ternon et al., 2014). Once the current reaches the shelf, it diverges towards the north and south. This eddy dipole may play a role in cross- and along-shore transport and redistribution of matter properties implications for coastal fisheries and water quality. For example, over the past five years two non-commercial important shrimp species invaded the Sofala Bank, outcompeting valuable shrimps in the area. It is not known if an eddy dipole with a strong inshore current contributed in bringing the invasive shrimp to the Sofala Bank. However, such eddy dipoles has been receiving less attention than eddy dipoles with strong inshore current, i.e. eddy dipoles with the anticyclone to the north.

River plume variability

The 3×4 SOM maps of river plume variability, derived from seven years of model salinity, confirmed the nature of the bi-directional plumes, especially of the Zambezi River (Fig. 4.5). This is consistent with the previous study by Nehama (2012) using a similar model and EOF analysis, although the bi-directional plume (using 3×3 SOMs) was not as distinct as found in the present study. Another study, using a similar SOMs approach for the Columbia River plume, also extracted the bi-directional variability in summer (Liu et al., 2009a), supporting the present study. A subsequent study by Burla et al. (2010), using EOF, supported the bi-directional plume for the Columbia River. However, they recognized that the SOM of Liu et al. (2009a) was robust and provided more detailed bi-directional plume structure than their EOF. This has also been demonstrated in other studies comparing (linear) EOF and (nonlinear) SOM results (e.g. Liu et al., 2006; Falcieri et al., 2014). The reason for this was that the EOF cannot accommodate detailed variability because of the orthogonality constraints.

SOMs showed that there was a seasonal variability in the plume structure, with a large plume in summer-autumn becoming smaller in spring (Fig. 4.5B), with the seasonality in river discharge (Fig. 3.4). Nehama (2012), using CTD salinity data during near-peak river discharge season (summer) in $2004 - 2007$, consistently found large plume structures, supporting the findings here. Similar results to those of SOMs were obtained with seasonally averaged salinity (Fig. 3.4), indicating this is a consistent pattern. Again, SOMs gave more detailed plume structures, i.e. the lowest frequency ($\sim 2\%$; patterns 9), small, bulge-like winter plume was not apparent on the winter mean. In addition, SOMs revealed a frequent oscillation between northward and southward plumes during summer and autumn, when the river input was high (Liu et al., 2009a; Hickey et al., 2010), which was also not captured by the seasonal mean.

Are the river plumes influenced or influencing the shelf circulation?

The dominant plume direction of the Zambezi River is northward (Figs. 4.5 and 4.6). This can be explained by the effect of the Coriolis force (Garvine, 1987), which for the southern hemisphere deflects the freshwater outflow to the left of the river mouth. Then, this force presses the northward branch of the plume attached to the coast, maintaining it within the 50 m isobath (Nehama, 2012). There was no clear relationship between the northward plume and offshore eddies, supporting the notion that the Coriolis force was the main driving force. The present study revealed that, in contrast, the southward plume direction was linked to an offshore anticyclonic eddy (Fig. 4.7), supporting the hypothesis ($H_{4.2}$) that anticyclonic eddies cause a southward plume direction. Moreover, the southward plume and the anticyclonic eddy-induced baroclinic current over the shelf are in the same direction (Fig. 4.8A and B). This suggests that the offshore anticyclonic eddies can erode the northward plume and reverse it to the south of the river mouth and the Coriolis force maintains the southward branch detached from the coast. Hickey et al. (2005) have demonstrated that, in order for a bi-directional plume to occur, a baroclinic current that dominates the Coriolis rotational tendency is required to deflect the plume in opposite direction of the Coriolis tendency (Hickey et al., 2005). In their case, it was a wind-driven current. For the Zambezi River, however, it has been shown that winds play a minor role in the plume variability (Nehama, 2012).

The most seaward extent of the plume was found to be linked to weak and far offshore anticyclonic eddy activity (Fig. 4.7, pattern 9), with associated weak shelf currents (Fig. 4.8, pattern 9). This supports the hypothesis ($H_{4.2}$) indicating that far eddies and weak currents facilitate offshore excursion of the plume. It is proposed that the weak shelf circulation allows freshwater to accumulate in the vicinity of the river mouth and then spread further offshore (Fong and Geyer, 2002). Once the plume reaches the shelf-break, it is advected toward the south by a weak offshore anticyclonic eddy.

Eddies, however, had no clear effect on the small plume in pattern 10, which was observed during an elongated, weak negative averaged SSH near the shelf-break (Fig. 4.8). Negative SSH (i.e. cyclonic eddy) induces an equatorward current, as has been discussed in the previous section. For this reason, the plume was expected to flow equatorward, but instead it is southward. Caution, however, needs to be exercised when interpreting the plume in pattern 10 in relation to averaged SSH. This pattern occurs for a long consecutive period (22.26% accounting for ~ 3 months). It is possible that the averaged SSH during the long-period of pattern 10 comprised imagery with different SSH fields, which influenced the comparison. On the other hand, this stable pattern 10 coincides with the relatively small discharge volume in spring. This supports the notion that the seasonal variability in river discharge is a main driver for seasonality in the size of river plumes, which is true for both the Zambezi and Beira plumes.

Interestingly, off Beira ($\sim 20°$S) the mean circulation is generally very weak, independently of the eddy activity, suggesting that this region is not influenced by offshore eddies. Therefore, the hypothesis ($H_{4.1}$), that eddies influence the shelf circulation is not supported off the semi-enclosed Beira Bay. Two possible explanations could be proposed: (1) the wide and shallow shelf makes it difficult for the eddies to penetrate, and the energy dissipated by eddies is converted to generate internal waves at the slope-shelf interface (generating turbulent mixing that contributes to the cool water lens; Chapter 3) and (2) the strong tidal currents there (Chapter 3) dominate the influence of far offshore eddies. As result, the Beira plume is unidirectional and the hypothesis ($H_{4.2}$) indicating offshore eddies influence the plume direction is not supported in the case of Beira.

Comparison between the model simulations with and without river inputs has been treated in the preceding chapter (3), which showed that rivers are impacting the coastal current circulation within the buoyant plume. The present chapter emphasizes that circulation within the plume differs from the outside ambient circulation. There was firstly a strong seaward current that immediately deflected to the left and set up a strong northward current on the seaward edge of the plume. This northward plume flow was opposite to the ambient current on the outside. As the Coriolis force presses the plume towards the coast, the flow splits (at $\sim$ 18°30′S in Figs. 4.9A and B) and sets up a narrow coastal northward current that weakens further north, while another part recirculates into a coastal anticyclonic eddy near the river mouth. This pattern of plume circulation is consistent with the bulge plume circulation that was described initially by Chao and Boicourt (1986), based on idealized model-based studies. It has been recently supported in the Columbia River plume by Horner-Devine (2009), based on both *in-situ* and satellite observational data. For the southward plume, a stronger southward current was observed inside the plume than outside. Differences in the current direction and speed within or without the buoyant plume confirm that the river inputs disrupt coastal circulation near the river mouth, supporting the hypothesis ($H_{4.3}$) that river plumes influence the coastal circulation by changing the salinity and current.

In summary, this chapter has demonstrated that self-organizing maps are useful statistical tools for analyzing highly complex and energetic eddy regions like the Mozambique Channel – supporting the applications of SOMs in other similar regions of the world, e.g., in the South China Sea (Liu et al., 2008) and in the East China Sea (Jin et al., 2010; Yin et al., 2014). Together with the Sofala Bank ROMS outputs (current vectors), it is shown that the shelf circulation is strongly modulated by the offshore eddy field. The coastal impact depends on the eddy strength and proximity of the eddy to the shelf. The model supports a bi-directional Zambezi plume, with the northward plume direction mainly driven by the Coriolis force and the southward direction by anticyclonic eddies. In contrast, the Beira plume, which is some distance from and protected from the influence of offshore eddies, is predominantly uni-directional to the north. In addition, the river outflow influences the coastal circulation, with the currents being relatively stronger within the buoyant plumes than in adjacent waters, and at times in opposite direction. Although it is difficult to assess tides using 3-day averaged outputs, high

frequency tides were included on the Sofala Bank − ROMS model forcing, which implies that they play lesser roles than the eddies in forcing the general shelf circulation of the Sofala Bank. Winds have been demonstrated by Nehama (2012) to play a smaller role than the background current in forcing the Sofala Bank shelf circulation. Therefore, it is suggested that offshore passing eddies play a vital role in modulated the shelf circulation and structure on the Sofala Bank.

Chapter 5

Factors influencing retention and transport of banana shrimp larvae

Abstract

An individual-based model was used to investigate the influence of environmental processes on transport and shelf retention of simulated larvae of banana shrimp on the Sofala Bank. Results of 5-year simulations indicate that most larvae (at times $> 95\%$) were retained on the shelf. No seasonal cycle was apparent, but occasionally events of decreased shelf retention (loss) were observed. Lost larvae were transported offshore or to the south by the complex mesoscale eddy field. An anticyclonic eddy SOM pattern was correlated with low larval retention at lags of $5-12$ days. In contrast, eddies also promoted larval shelf retention, depending on their variability. High retention was correlated with cyclonic/anticyclonic eddy dipoles, with a strong shoreward current, at lags of $7-15$ days. Most larvae retained on the shelf traveled ~ 100 km. The others, lost far offshore or to the south, traveled longer distances, up to 1600 km in 15 days, with a small peak in the distribution at ~ 650 km. For the inshore sites, there was no difference in shelf retention for larvae released in the areas where spawning occurs or not, as determined from Chapter 2. Similarly, there was no difference in shelf retention for simulated larvae released inshore or offshore to the south of $\sim 19°15'$S. To the north of $\sim 19°15'$S, shelf retention was significantly higher for the inshore than for the offshore release areas. Central and northern areas contributed little to the simulated shelf retention, yet promoted dispersal because they are more exposed to the offshore eddies. Simulated larval shelf retention was consistently high off Beira Bay, which is protected from the eddies. Simulated larval retention was sensitive to assumed low lethal temperatures, with potentially massive larval mortality in winter months. Cool (cyclonic) eddies also appeared to affect larval survival at times, even during summer.

5.1 Introduction

Larval supply is a key determinant for adult population dynamics of many marine organisms with pelagic larval stages (Levin, 2006). Thus, understanding patterns of marine larval retention and transport is pivotal to appraising the variability in the population structures. Larval retention and transport of marine organisms are controlled by complex environmental processes (Pineda et al., 2007). Eddies have been reported to control larval retention and transport in many marine ecosystems (Bailey et al., 1997; Adams and Flierl, 2010; Vaz et al., 2013). Those studies, however, focused on fish larvae, mainly in oceanic regions, while little attention has been given to coastal regions, especially for penaeid shrimp larvae. The few studies that have investigated the influence of eddies on coastal populations considered sub-mesoscale eddies (Robins et al., 2013; Tian et al., 2009b), locally generated by winds or tides, rather than offshore mesoscale eddies.

The present study was conducted on the Sofala Bank, a shallow water shelf in the western Mozambique Channel. The circulation in the Mozambique Channel is dominated by both cyclonic and anticyclonic mesoscale eddies (Sætre and da Silva, 1984; Biastoch and Krauss, 1999; de Ruijter et al., 2002; Schouten et al., 2003) and rings (Halo, 2012; Halo et al., 2014; Penven et al., 2014). These eddies strongly influence the shelf water structure and circulation on the Sofala Bank (Chapters 3 and 4). The Sofala Bank hosts the largest population (and stock) of shallow water penaeid shrimp in the southwestern Indian Ocean (east Africa) (Chapter 1). These penaeid shrimps support one of the most important fisheries along the Mozambican coast. The most important target species are *Fenneropenaeus indicus* and *Metapenaeus monoceros*, called "banana shrimps" (de Sousa et al., 2008). The impact of offshore mesoscale eddies on retention and transport of banana shrimp larvae on the Sofala Bank is, as yet, not known. Recent studies, however, showed that the Mozambique Channel eddies can advect coastal production offshore (Jose et al., 2014; Malauene et al., 2014). Therefore, a reasonable assumption is that these eddies can also transport banana shrimp larvae offshore, thus decreasing larval retention.

This chapter aims to investigate shelf retention and transport of simulated larvae of banana shrimp on the Sofala Bank, in relation to environmental processes (mesoscale eddies and tem-

perature). The main hypothesis, that banana shrimp larvae are transported offshore by passing mesoscale eddies, thus decreasing larval shelf retention, is tested here. There is a lack of in-situ data for larvae at sea and models can provide a good way of understanding complex, biophysical relationships as well as informing field sampling programs. Modelling approaches have been widely used to study larval transport of marine organisms (Mullon et al., 2002; Levin, 2006; Paris et al., 2007; Pineda et al., 2007; Lett et al., 2007; Jones et al., 2009; Xu et al., 2013). In this study, a biophysical Lagrangian model is used and simulations consisted of following the trajectories of virtual shrimp larvae. The numbers of successfully retained simulated larvae were quantified for analysis and discussion. Larval transport and dispersal are defined according to Pineda et al. (2007): larval transport is the translocation of a larva between points (all points from the beginning to the end) and larval dispersal is the spread of larvae from a release point (or area) to a retention point (or area), i.e., straight line from the beginning to the end point. The release areas were defined based on spawning areas identified in Chapter 2. Retention (hereafter called shelf retention) was defined as the ratio of the number of larvae found within the shelf (i.e., inside the 50 m isobath) of the Sofala Bank at the end of the simulation to the total number of larvae released.

It has been proposed that marine organisms naturally spawn in locations that facilitate transport and retention of larvae or offspring (e.g. Putman et al., 2010). Similarly, here it is hypothesised ($H_{5.1}$) that banana shrimps spawn in locations that promote larval retention on the Sofala Bank. Temperature, especially cool water, is known to influence survival of penaeid shrimps (Dall et al., 1990). The low temperature at which–penaeid shrimp larvae elsewhere become lethargic is known (Chapter 1). The effect of temperature on simulated shelf retention of banana shrimp larvae on the Sofala Bank is investigated. It is hypothesised ($H_{5.2}$) that larvae die when encountering cooler temperature than 20°C.

5.2 Model, data and methods

Individual-based models (IBMs) are useful tools to investigate the biological and physical (bio-physical) interactions affecting larval dynamics, because they incorporate biotic and abiotic processes at different spatial and temporal scales (Lett et al., 2008). An IBM is used here to simulate shelf retention, transport and dispersal of banana shrimp larvae (i.e., combined *F. indicus* and *M. monoceros*) on the Sofala Bank in relation to offshore circulation. The IBM was developed using the Ichthyop model, coupled to a down-scaled model from the deep ocean to the coast of the Sofala Bank, using the Regional Ocean Modeling System (ROMS, Shchepetkin and McWilliams, 2005). Detailed descriptions and results of the Sofala Bank model (ROMS-BSM) are discussed in chapters 3 and 4. Because this chapter focus on the influence of the offshore eddies on the simulated larval shelf retention and long-distance dispersal, only outputs from the large domain (Parent grid when using nesting) basic experiment with tides (ROMS-BSM-E2, Table 3) were used.

Tides, although leveled out (smoothed) on the 3-day averaged outputs, were incorporated in the configuration. The data consisted of a 3-day averaged climatology of 3D velocities (m s^{-1}), temperature (°C) and salinity fields for five years, from model year four, after the spin-up time (Chapter 3).

The IBM simulations were developed using Ichthyop version 3.1 (Lett et al., 2008), a java tool freely available at `http://www.ichthyop.org`. Ichthyop-3.1 is a Lagrangian transport model that tracks the trajectories of virtual eggs and larvae, computed by spatial integration of the equation of motion (equation 5.1):

$$\Delta X = \Delta U \times \triangle t \tag{5.1}$$

where X is the position vector (x, y, z), U the velocity vector $(u, v, w$ as ROMS outputs) and t the time.

5.2.1 Ichthyop base experiment

Simulations consisted of randomly releasing 30000 virtual banana shrimp eggs within the release areas and tracking their trajectories during 15 days. This period of larval transport was chosen in order to involve the maximum duration of the passive pelagic larval stage of penaeid shrimp, i.e. before they begin active swimming. It is known that penaeid shrimps develop from eggs to first postlarvae within that period (of 15 days) and postlarvae start to develop swimming and walking legs (Chapter 1), and therefore are no longer considered passive entities.

Because banana shrimps spawn all year round (Chapter 1 and 2), and in order to investigate the possible seasonal variability of larval retention and transport, eggs were released every 3 days (release frequency) for a period of five years (ROMS outputs year four to eight). Shrimp eggs have been shown to go quickly to the surface (Dall et al., 1990) and to hatch a few hours (8−12 h) after spawning (Laxminarayana et al., 1995; Radhakrishnan, 2007). For these reasons, the virtual eggs were released near the surface between zero and 10 m depth.

During their transport, simulated larvae could either stay on (or come back to) the Sofala Bank retention area (considered as successfully retained) or leave it (considered as lost). In Ichthyop, individuals are characterized by their state variables: age (days), position (longitude (°E), latitude (°S) and depth (m)) and status (alive or dead). Ichthyop outputs are NetCDF files containing all the state variables for each simulated larva, recorded every 4 hours within the 15 days of the pelagic larval duration.

Release areas and scheme

Nine release areas were defined for all simulations (Fig. 5.1): (1) northern, (2) north-central inshore, (3) central inshore, (4) south-central inshore, (5) southern inshore, (6) north-central offshore, (7) central offshore, (8) south-central offshore and (9) southern offshore. The northern, central and southern release areas coincide with the three actual main spawning areas for banana shrimp identified on the Sofala Bank, respectively (Chapter 2). The northern release area is adjacent to the Licungo River in the area of influence of the Angoche upwelling (Malauene

et al., 2014), hence it has elevated autochthonous production (marine primary production). The central release areas are adjacent to the Zambezi River, which is the largest source of freshwater river inflow onto the Sofala Bank (Fig. 3.4). This area has elevated allochthonous production (production carried by the river or production from rivers). The southern areas are adjacent to Beira Bay, with two rivers, the Pungué and Buzi. The north-central and south-central release areas, although non-spawning areas, were also considered in the simulations.

Spawning release of banana shrimps on the Sofala Bank generally occurs away from the coast between 10 and 35 m depth (Chapter 2), but adult females can go > 50 m (de Sousa et al., 2006, 2013). Because the objective of the present chapter is to investigate the influence of offshore mesoscale features on shelf retention and transport of shrimp larvae, simulated release areas were extended further offshore, up to the 50 m isobath. All the release areas, except at the northern region, which is narrow, were divided into a shallow inshore area between the 10 and $\sim$ 35 m isobaths, and a deeper offshore area from 35 to 50 m isobaths (Fig. 5.1). Because the ROMS bathymetry was smoothed, actual (model independent) 10, 35 and 50 m isobaths were used to define more accurate release areas. Those were first designed in a geographic information system (GIS), using the above isobaths and the spawning areas depicted in Chapter 2. The GIS shapefiles were then converted to .xml files in R software and imported to Ichthyop.

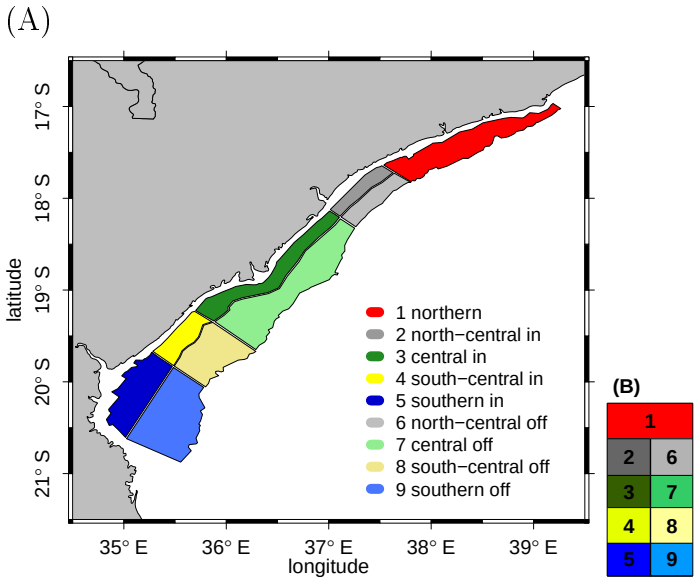

Figure 5.1: (A) Map of the Sofala Bank showing the nine release areas used in the simulations. Dark and light colors indicate the inshore (in) and offshore (off) areas, respectively. Dark red, green and blue are the major spawning areas on the Sofala Bank as identified in Chapter 2 and the light green and blue are their adjacent offshore areas. Both dark and light gray and yellow areas are minor spawning areas. (B) A schematic of all release area.

Movement of eggs and larvae

Movements of eggs and larvae included horizontal and vertical advection, horizontal diffusion and buoyancy (Lett et al., 2008). Horizontal and vertical advection were accomplished by the equation of motion (equation 5.1), using a forward-Euler time-stepping scheme (Lett et al., 2008). The model time step was set to 2400 s (40 min), which meets the CFL criterion (Chapter 3): $\Delta t < {}^{L}/_{U_{max}}$, where Δt is the time step, L is the ROMS grid size (6200 m) and U_{max} the maximum observed current velocity (~ 2 m s^{-1}), thus $\Delta t < {}^{6200\mathrm{m}}/_{2\mathrm{ms}^{-1}} < 3100\,\mathbf{s}$. At each time step Ichthyop interpolates the information (velocities, temperature and salinity) from ROMS and calculates the larva state variables. Larvae were forced to drift at the surface from the first to the last day of the simulation by setting their density at 1 g cm^{-3}, i.e., less than that of sea water. Animations of larval trajectories indicated that simulated larvae remained in the upper surface layer all the time, with only small changes in their depths. Horizontal diffusion was implemented following Peliz et al. (2007).

Shelf retention

The area that covered the entire Sofala Bank shelf from the coast to the 50 m isobath was selected in order to investigate shelf retention of the simulated shrimp larvae (Fig. 5.2). Larvae that were in this area were considered as successfully retained from age 10 days, which is the age they start to reach the first postlarval stage that can settle (Table 1.1 Chapter 1). The simulated larval retention competency time window is $10 - 15$ days after release. Larvae were allowed to enter and exit the shelf retention area until they reached the age criterion for them to be retained. Larvae were set to stop moving when retained in the shelf area, whereas those outside continued to move until the end of the simulation.

5.2.1.1 Mortality experiment

This was the same as the base experiment (described and summarized in Table 5.1), but using threshold values of temperature and the simulations were run for only one year for each

temperature. Six values of temperatures (20, 21, 22, 23, 24 and 25°C) were selected, based on available knowledge (Chapter 1), and it was assumed that simulated larvae died when encountering temperatures lower than the nominated values above. Simulated larvae were considered as successfully retained (survivors) if they had not faced low temperature and were in the retention area (Fig. 5.2).

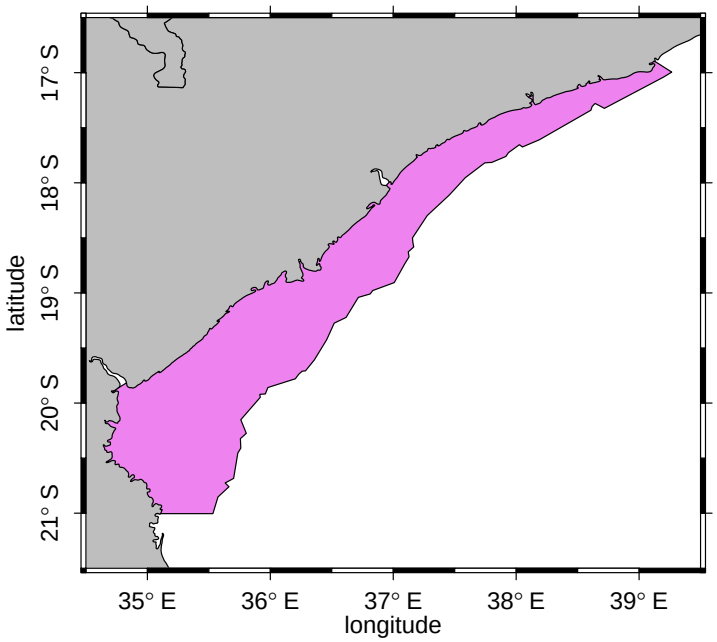

Figure 5.2: Area used in the simulations to investigate larval shelf retention.

Table 5.1: Variables and parameters used in all simulations.

Variables/parameters	Units	Value	Description / Comment
Number of individuals	# eggs	30000	Total number of simulated larvae released.
Release/spawning area	n/a	9	1 northern 2 north-central inshore 3 central inshore 4 south-central inshore 5 southern inshore 6 north-central offshore. 7 central offshore 8 south-central offshore 9 southern offshore.
Release frequency	day	3	Larvae released every three days
Release depth	meter	0−10	All larvae released close to the surface
Retention area (transport success)	n/a	1	Within the 50 m isobath from the coast and the Sofala Bank limit $16-21°$S
Retention age criterion	days	10	Larvae can only be retained after this age
Larval duration	days	15	Maximum simulation period for larval tracking
Time step	seconds	2400	Model time step
Recording frequency	hours	4	Data recorded to output files every 4 hours

5.2.2 IBM output analyses

Distance assessment

To calculate the distance traveled by the simulated larvae between two points, the R function distHaversine of the package geosphere (Hijmans, 2014) was used. This function resolves equation 5.2, based on the Haversine formula (Sinnott, 1984).

$$d = R \times arccos(sin(Lat_1) \times sin(Lat_2) + cos(Lat_1) \times cos(Lat_2) \times cos(Lon_2 - Lon_1)) \quad (5.2)$$

where d is the distance between two points in km, R is the mean radius of the earth ($R = 6371$ km), Lat and Lon are the latitude and longitude of the points.

This formula is widely used to compute small distances. The total distance traveled was obtained by summing all distances between consecutive points along the trajectory of each

larva. Estimates of the total distance traveled are sensitive to the frequency of recording outputs (here 4 h). The distance from origin to final location (displacement) was therefore also computed.

ANOVA and post-hoc test

One-way analysis of variance (ANOVA) was conducted to investigate whether there were differences in the mean percentage of simulated shelf retention among all nine release areas and among the six assumed low-lethal temperatures for the mortality experiments. Where there were significant differences, the post-hoc Tukey test was conducted to assess whether the difference was among all groups. Prior to performing the ANOVA, the assumptions of normality and equal variances were verified. For normality, a visual inspection was conducted on the frequency distributions of retention for all release areas and all temperature values by plotting both histograms and probability plots (Q-Q plots). For equal variance, both visual inspection (by plotting the residuals) and Levene's test ($\alpha = 0.05$) were conducted.

Cross-correlation

Cross-correlation analysis, with a maximum lag of 15 days, was conducted between time series of simulated larval shelf retention and each time series of Euclidian distance to self-organizing map (SOM) patterns (e.g. Fig. 5.3). A similar approach has been used in other biophysical dispersal modelling studies (Cuif et al., 2014). An unsupervised SOM algorithm was computed for SSH anomaly, which represents eddy variability (Chapter. 4). A short Euclidian distance to a particular SOM pattern is interpreted as a high probability of having that particular pattern in the original SSH data set at that particular time. Therefore, when there were negative correlations between time series of shelf retention and Euclidian distances to a particular SOM pattern, that pattern was interpreted as having a positive effect on simulated larval shelf retention and vice versa. Because the Euclidian distances were not normally distributed, the Spearman's rank correlation was used. The statistical significance test for correlation coefficients was set at a 95% confidence level.

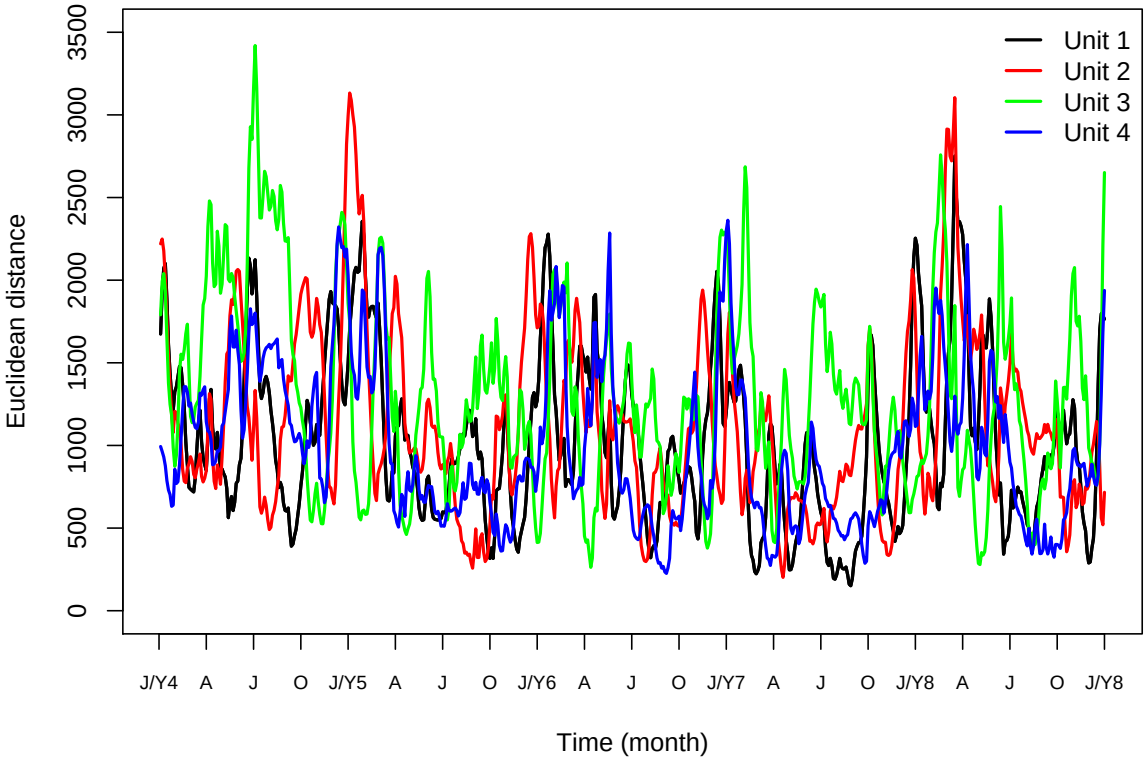

Figure 5.3: Example of time series of Euclidean distances to each 2×2 SOM pattern (units $1 - 4$) for the SSH anomaly from ROMS-BSM-E2 years $4 - 10$.

5.3 Results

5.3.1 Simulated larval shelf retention and transport

Simulated larvae that were successfully retained originated from all nine release areas (Fig. 5.4). There were significant differences in mean simulated larval shelf retention relative to the area where they were released (analysis of variance: $F_{8,1017} = 27.1,\ p < 0.001$). However, not all release areas yielded significantly different mean simulated larval retention (Tukey analysis: Table. 5.2). Fig. 5.4 shows that the lowest mean simulated larval retention was obtained for larvae released from area 1 (northern release area). This mean retention for area 1 was significantly different from all other release areas except for area 6 (north-central offshore) (Table. 5.2A). The highest mean simulated larval retention was obtained from release areas 4 and 5 (south-central inshore and southern inshore release areas, respectively). For the inshore release areas $2-5$, the mean simulated larval shelf retention was high and not significantly different from each other (Table. 5.2A and B). For the offshore release areas, mean simulated larval shelf retention for areas 6 and 7, and also 8 and 9 were not significantly different (Table. 5.2). For inshore−offshore adjacent pairs of release areas, north-central (2 and 6) and central (3 and 7) release areas were significantly different, whereas south-central (4 and 8) and southern (5 and 9) were not (Table. 5.2A and C).

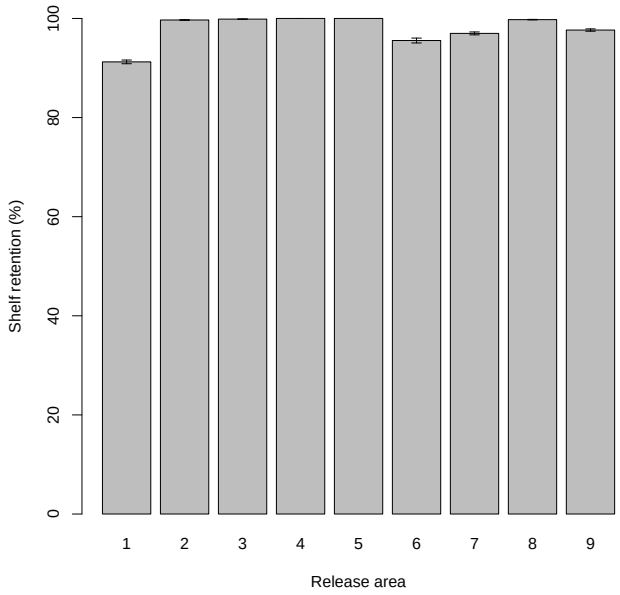

Figure 5.4: Results of base experiment showing mean (± s.e.) percentage of simulated larval shrimp retained on the Sofala Bank for all nine release areas as in Fig 5.1.

Table 5.2: (A) P-values of the post-hoc Tukey test for ANOVA comparing mean shelf retention for all nine release areas. Red values indicate significant differences (P<0.05). B) and C) schematic of the release areas (green) not significantly different and (red) different.

(A)

Release area	1 (91.5%)	2 (99.2%)	3 (99.6%)	4 (100%)	5 (100%)	6 (93.9%)	7 (95.4%)	8 (99.7%)	9 (97.9%)
1		< 0.001	< 0.001	< 0.001	< 0.001	0.128	< 0.001	< 0.001	< 0.001
2	< 0.001		0.998	0.989	0.989	< 0.001	< 0.001	0.999	0.888
3	< 0.001	0.999		0.999	0.998	< 0.001	< 0.001	1.000	0.624
4	< 0.001	0.989	0.998		1.000	< 0.001	< 0.001	0.999	0.291
5	< 0.001	0.989	0.999	1.000		< 0.001	< 0.001	0.998	0.291
6	0.128	< 0.001	< 0.001	< 0.001	< 0.001		0.636	< 0.001	< 0.001
7	< 0.001	< 0.001	< 0.001	< 0.001	< 0.001	0.637		< 0.001	0.070
8	< 0.001	0.999	1.000	0.998	0.995	< 0.001	< 0.001		0.507
9	< 0.001	0.889	0.624	0.291	0.291	< 0.001	0.070	0.507	

(B)

1	
2	6
3	7
4	8
5	9

(C)

1	
2	6
3	7
4	8
5	9

The five-year simulations show that larvae were retained on the shelf all year round and no evidence of association with a particular period of the year was identified (Fig. 5.5). There was no clear seasonal cycle in the simulated larval shelf retention, but occasional intraseasonal variability was observed (Fig. 5.5). Generally, simulated shelf retention was high, however, at times pulses of reduced shelf retention ($< 80\%$) were observed, indicating that sometimes a significant number of larvae were lost from the Sofala Bank.

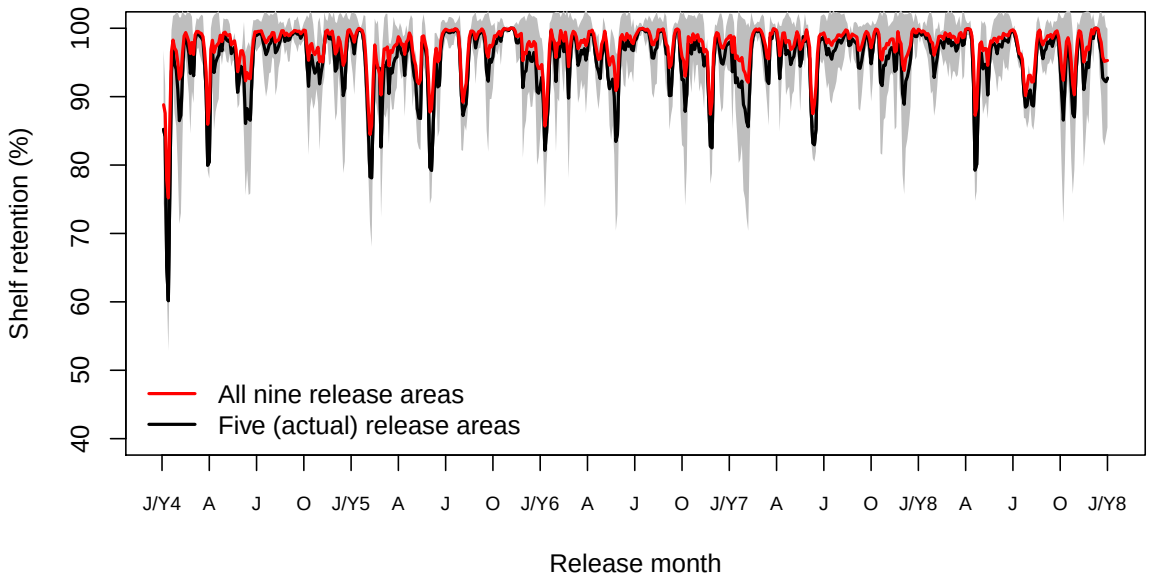

Figure 5.5: Results of the base experiment showing five-year time series of mean percentage of simulated shelf retention from (red) all nine release areas and (black) the five release areas corresponding to the major spawning areas for shrimp on the Sofala Bank (black). Grey shading represents ± s.e. for the five areas. The X- axis label, release month, refers to the start time of each simulation.

A density map (numbers·km^{-2}) of all simulated larvae in the five years shows that most of the larvae (high density) were concentrated on the shelf of the Sofala Bank (Fig. 5.6). This result corroborates the high shelf retention observed in Figs. 5.4 and 5.5. Low densities were observed spread over the entire study domain, i.e., offshore and to the south. Three general patterns were therefore apparent (Fig. 5.6): (1) larvae retained on the shelf, (2) larvae that exited the Sofala Bank at its southernmost limit and (3) larvae transported offshore.

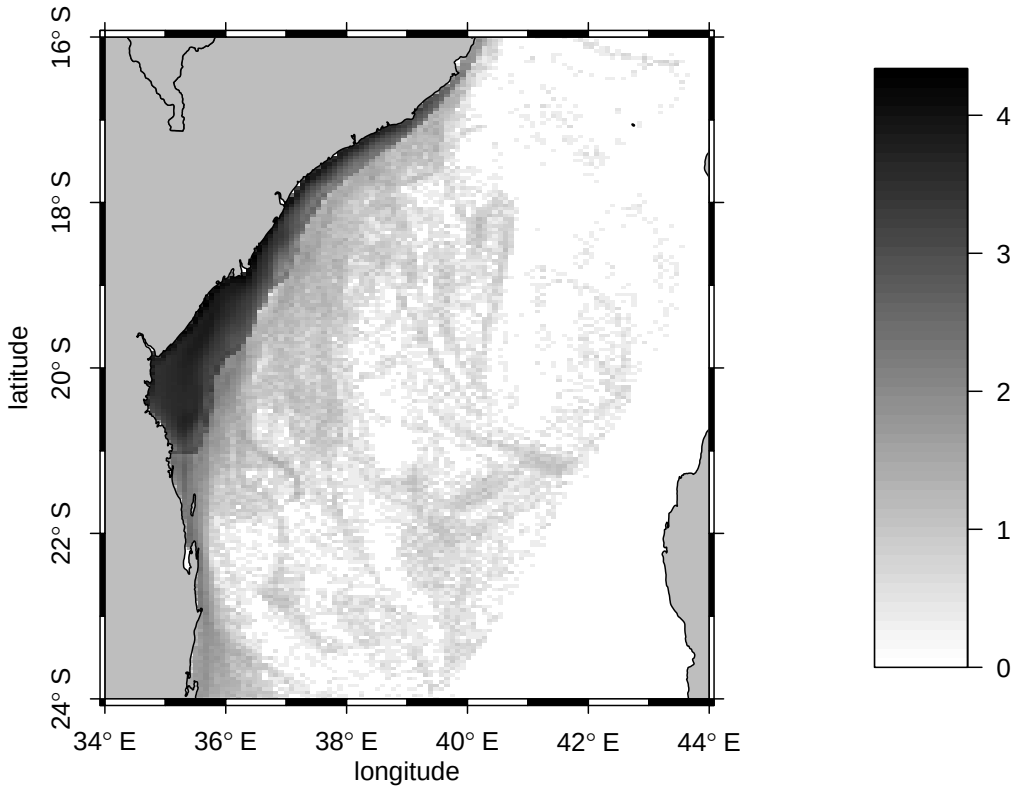

Figure 5.6: Results of base experiment showing log scaled simulated larval density (numbers·km^{-2}) of all shrimp larvae released during the five years. Note that larvae stopped moving as soon as they were considered as retained on the shelf.

Snapshots of trajectories of simulated larvae show that, for a number of simulations, nearly all larvae from all release areas stayed on the shelf during the whole larval period (e.g. Figs. 5.7A and B). At times, however, larvae from the northern and central release areas traveled alongshore for the full extent of the Sofala Bank and then exited the southernmost limit (e.g. Fig. 5.7C). Fig. 5.7D shows an example of larvae released from the central areas being advected to the south, whereas those released from the northern areas stayed on the shelf. Generally, larvae from the southern release areas did not move much (Figs. 5.7 and 5.8), only being transported to the south occasionally (e.g. Fig. 5.7D).

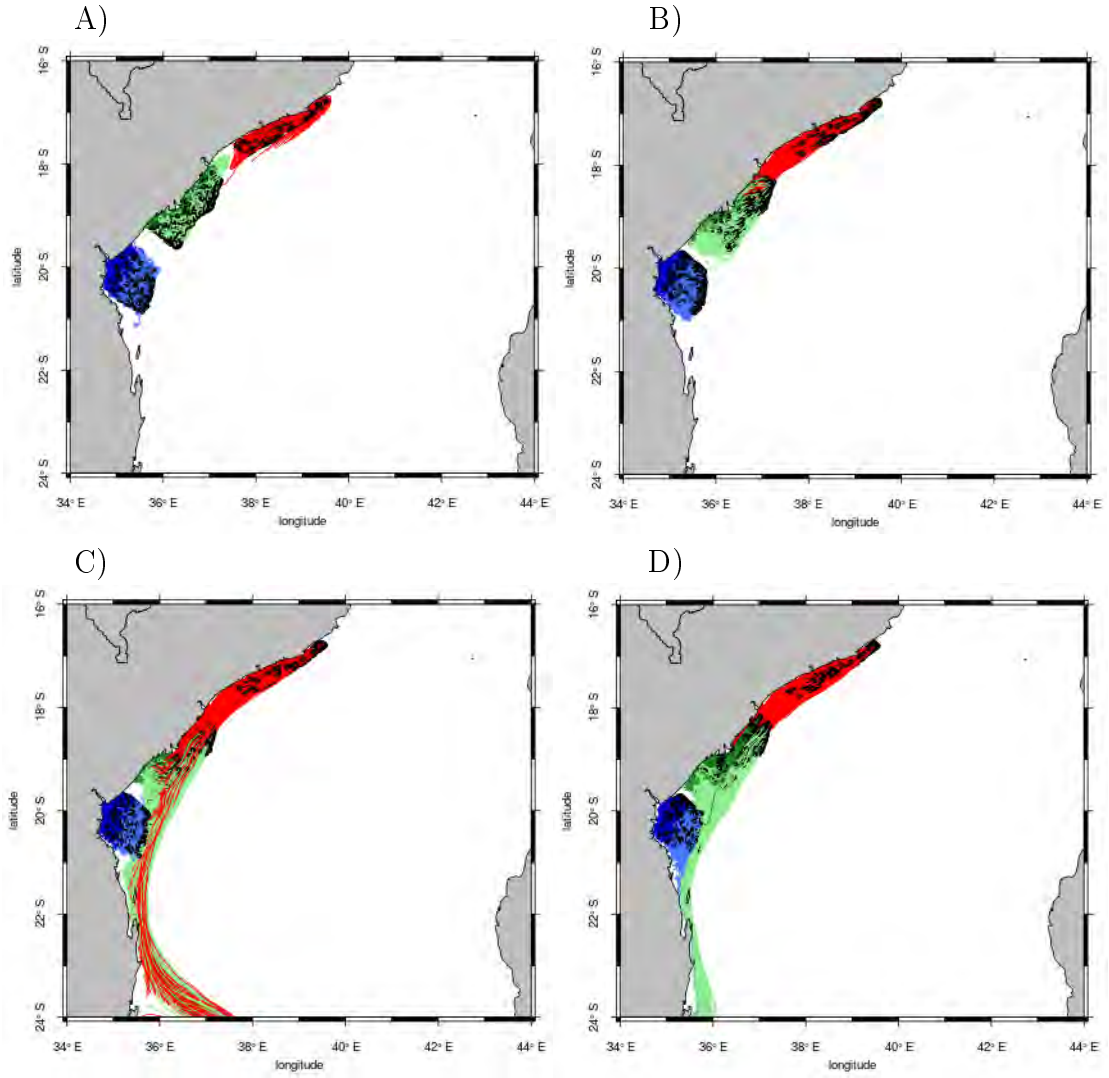

Figure 5.7: Results of base experiment showing snapshots of trajectories of 15000 randomly chosen virtual shrimp larvae released from the northern (red), central (green) and southern (blue) release areas. For green and blue releases areas, dark colors indicate inshore and light offshore. Larvae were tracked for 15 days for simulations starting: (A) 5 July, (B) 5 November, (C) 2 February and (D) 8 May.

Larvae that were transported far offshore were from the northern or central release areas (Fig. 5.8). For the simulation starting on 26 February (Fig. 5.8A), larvae observed offshore were from both northern and central release areas. They appeared offshore along two distinct pathways, one in the north and the other in the centre, depending on their release area. For the simulation starting on 17 March (Fig. 5.8B), larvae found offshore were mostly from the central release area. A few larvae from the northern area were initially transported southwards and then joined the path of larvae from the central release area offshore. Some larvae from the southern release area moved slightly northwards to the central area, but remained on the shelf (Figs. 5.8A and B).

For the simulations starting on 29 May (Fig. 5.8C) and 8 June (Fig. 5.8D), larvae found offshore were only from the northern release area. Fig. 5.8C shows that larvae were first transported offshore into a loop and then some were transported back to the shelf, where they joined the larvae from the other release areas and exited to the south. Fig. 5.8D shows some larvae were entrained in loops and then transported far offshore, almost reaching Madagascar, while others from the central release area exited to the south (Fig. 5.8D).

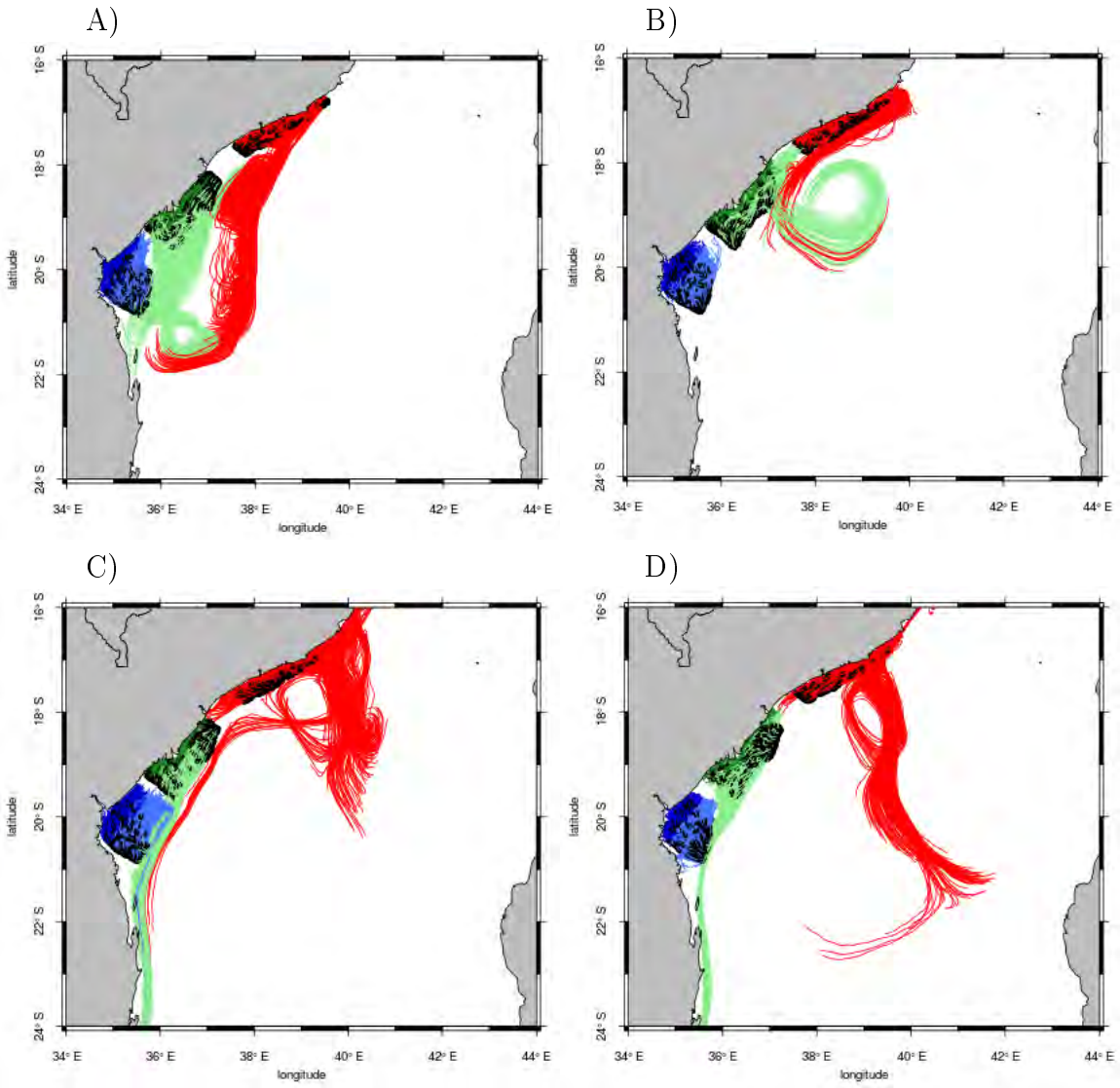

Figure 5.8: Same as Fig. 5.7 but for simulations starting: (A) 26 February, (B) 17 March, (C) 29 May and (D) 8 June.

The distribution of the distance traveled by all simulated larvae was skewed to the right (Fig. 5.9). For the total distance traveled (Fig. 5.9A), the mode was at $\sim$ 100 km and corresponds to most larvae retained on the shelf. The long tail extended up to 1600 km, with a small peak at $\sim$ 650 km. This tail corresponds to the small number of larvae that traveled long distances, like those that appeared close to Madagascar or in loops (Fig. 5.8). The distance from origin to final location had a similar distribution, but with the major mode at $\sim$ 50 km and a second, minor mode at $\sim$ 600 km. The maximum value was $\sim$ 900 km (Fig. 5.9B).

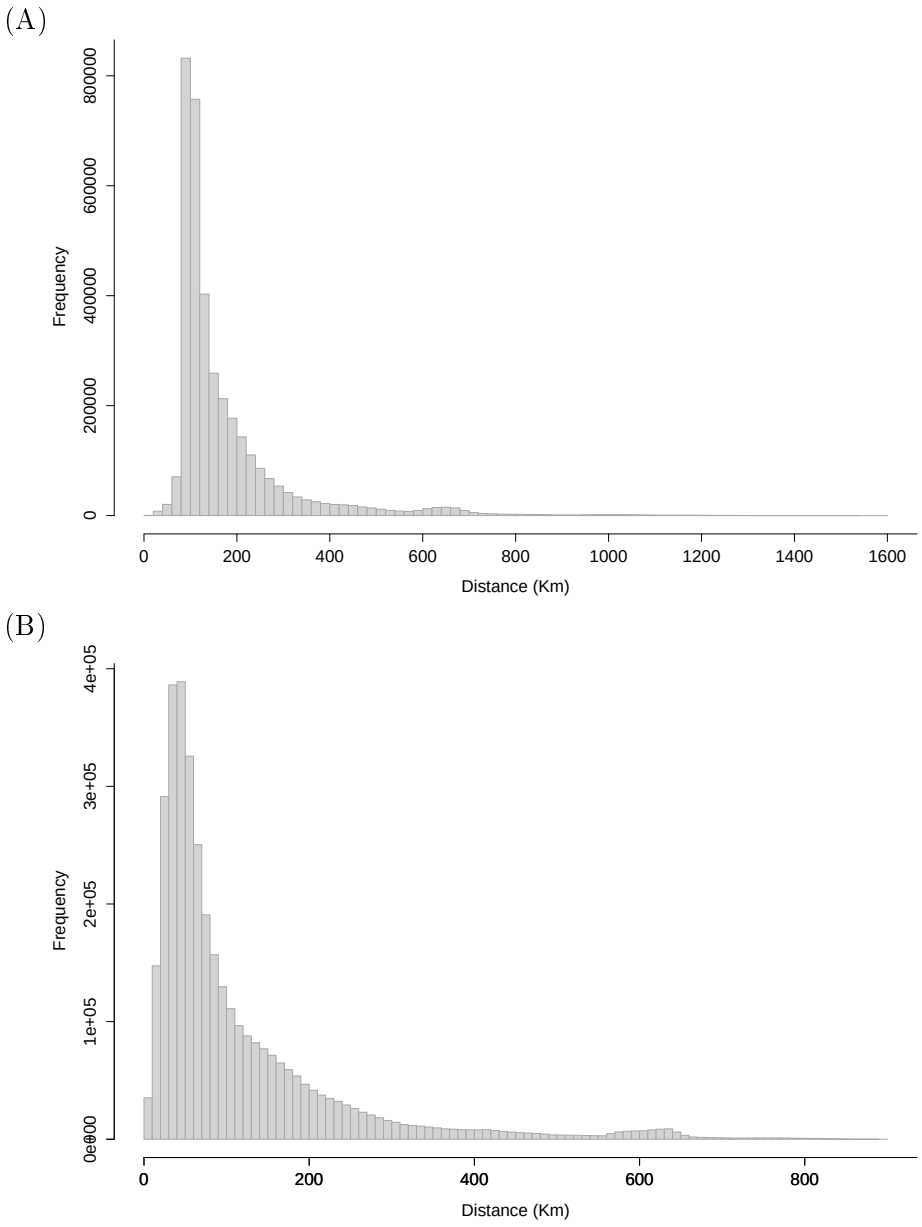

Figure 5.9: Results of base experiment showing frequency distributions of (A) total distance traveled (km) and (B) distance from origin to final location (km) for all simulated.

5.3.2 Influence of oceanic conditions on larval shelf retention

Snapshots of simulated larval distribution superimposed on ocean circulation (Figs. 5.10 and 5.11) were chosen (based on Figs. 5.7 and 5.8) to illustrate the role of offshore eddy activity on simulated larval shelf retention and transport. Where nearly all larvae were retained on the shelf (e.g. Fig. 5.7B), there were essentially no strong eddies near the shelf throughout the simulation, except an anticyclonic eddy far north (Fig. 5.10A).

On the other hand, where larvae exited the Sofala Bank to the south (e.g. Fig. 5.7C), on the first five days of the simulation, larvae were pushed towards the coast by a strong anticyclonic eddy (Fig. 5.10B). The anticyclonic eddy forced the larvae to exit the bank from its southernmost limit. On the tenth and again on the last day of the simulation, the anticyclonic eddy had moved further south, causing more larvae to be transported to the south.

For larvae transported offshore (e.g. Fig. 5.8A), after five days two bands of larvae were moved offshore in the core of two cyclonic features (Fig. 5.11A), one relatively large, centred at $\sim 18°S$, and the other small, centred at $\sim 20°S$. On simulation day 10, the cyclonic eddy to the north had moved southwards towards the other eddy that had moved offshore, dragging larvae with them. On the last day of the simulation the two cyclonic features were completely merged, with the two bands of larvae trapped closely together. Another example of offshore entrainment (Fig. 5.8B) occurred when a few larvae from the northern area were advected offshore by a small cyclonic eddy, centred at $\sim 17°S$ (Fig. 5.11B). On simulation day 10, the cyclonic eddy had dissipated and larvae in the north drifted freely alongshore. Some were advected southwards towards the central area by an anticyclonic eddy, centred at $\sim 19°S$. Here, these larvae and some from the central area were transported offshore by an anticyclonic/cyclonic eddy pair dipole. Once offshore, the larvae were trapped in the edge of the anticyclonic eddy. On simulation day 15, some of the trapped larvae were transported back near the shelf, while others could remain in the eddy circulation until it decayed. In this simulation, there was no eddy close to the southern area, so most of those larvae were retained on the shelf.

Fig. 5.11 gives examples of two different patterns of simulated larval transport (Figs. 5.8C and D), associated with similar eddy circulation (one ~ 5 days after the other). For Fig. 5.11C,

five days after release, some larvae from the northern area were advected offshore by a cyclonic eddy. Five days later, the larvae continued in the cyclonic trajectory and some came back near the shelf and then were transported southwards. On the last day of the simulation, the cyclonic eddy was small, while an anticyclonic feature appeared to the north, and the larvae were spread in the middle of the channel. On the other side, other larvae exited to the south. For Fig. 5.11D, on simulation day 10, only a few larvae continued in the cyclonic trajectory and others were transported cross-shore by the anticyclone/cyclone train of eddies. On the last day of the simulation, under the influence of a series of anticyclonic and cyclonic eddies, larvae were entrained in a filament, almost crossing the entire channel.

SST fields (Appendix. D) showed the same patterns of relationship with simulated larval transport to those observed for SSH in Figs. 5.10 and 5.11, with the larval pathways associated with temperature fronts induced by the eddies (Figs. D.1 and D.2).

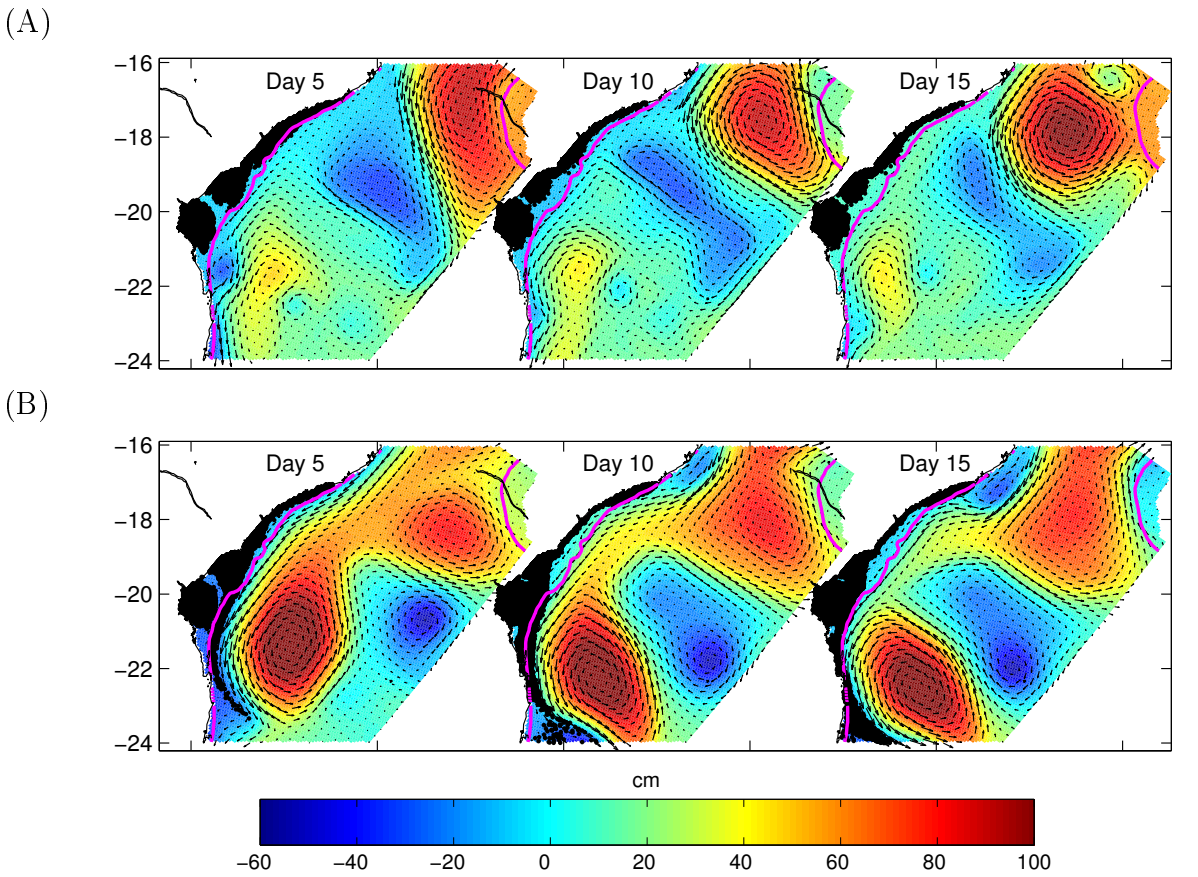

Figure 5.10: Results of the base experiment showing snapshots of larval distribution (black dots) superimposed on the corresponding ROMS−derived surface current vectors (arrows, in cm s^{-1}) and SSH (color shading, in cm) for eddy activity on the Sofala Bank. Labels indicate larvae five, ten and 15 days after release on (A) 5 November and (B) 2 February model year 5.

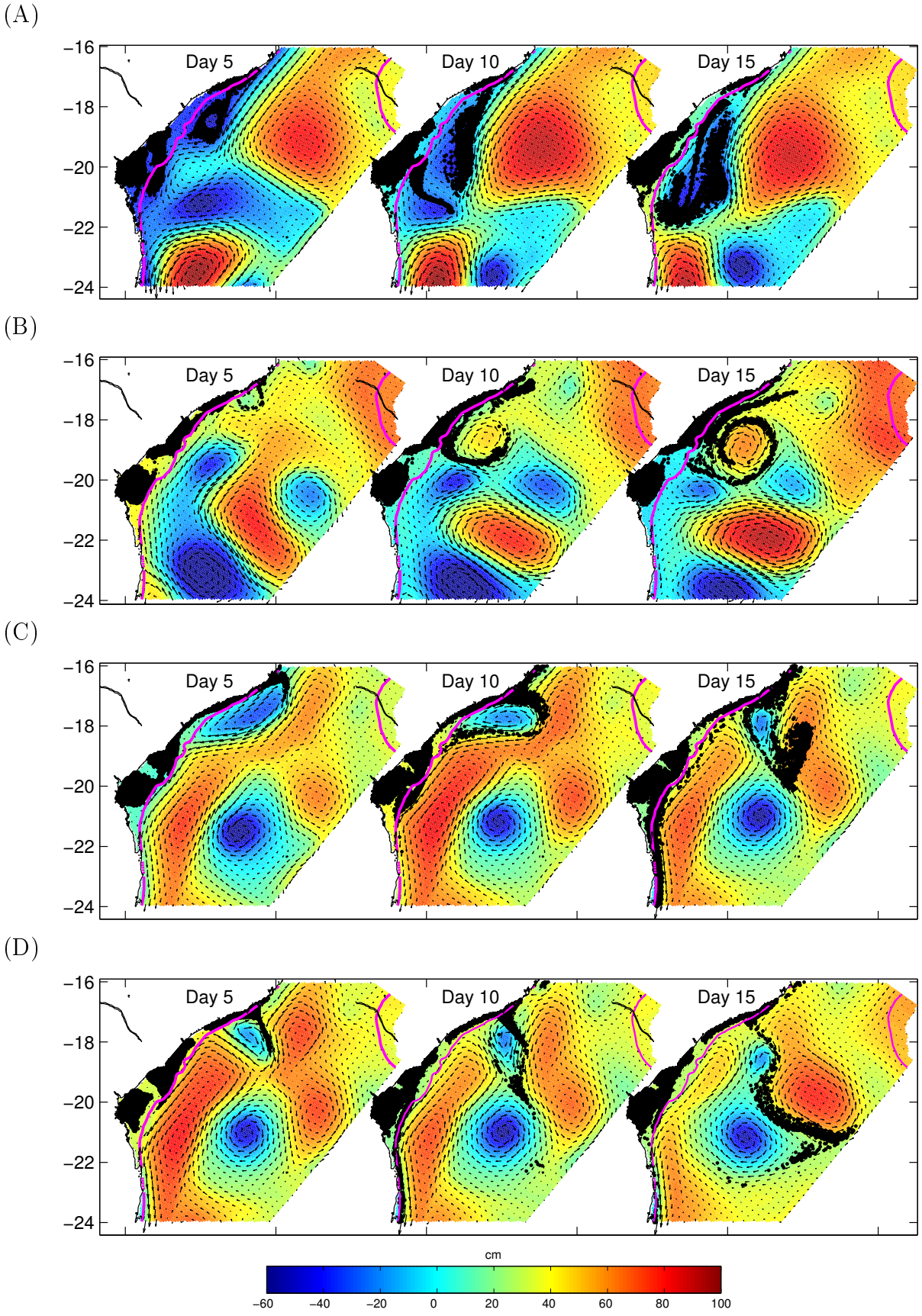

Figure 5.11: Same as Fig. 5.10, but for (A) 26 February and (B) 17 March (C) 29 May and (D) 5 June.

The mean percentage of simulated larvae transported–out the shelf and then back to it was $< 10\%$ (Fig. 5.12). Zero returns coincided with periods of high shelf retention (Fig. 5.5). Peaks of larval return coincided with reduced shelf retention influenced by offshore eddies. There were also events of reduced shelf retention, which were not accompanied by significant return of larvae.

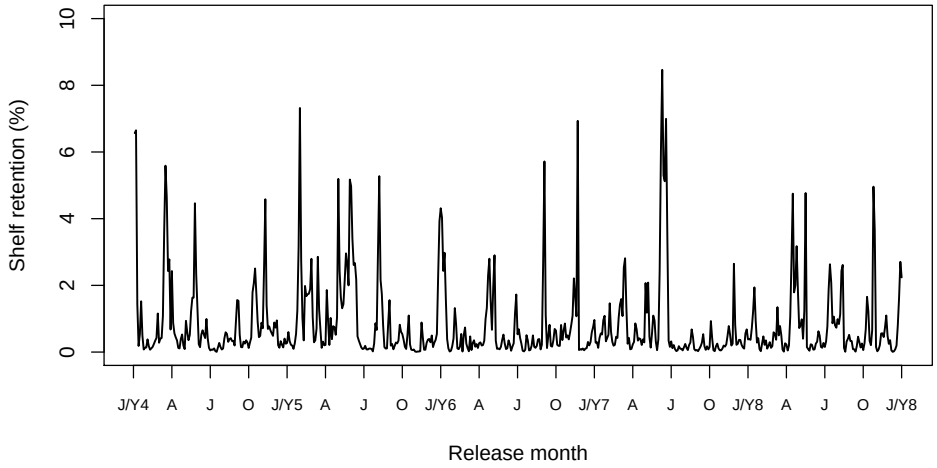

Figure 5.12: Mean percentage of larvae that were transported off the shelf but eventually returned to it, contributing to the total shelf retention.

Four general eddy patterns were identified, using an unsupervised learning algorithm of SOM classification (Chapter 4) for ROMS-derived SSH anomalies (Fig. 5.13A): (1) An anticyclonic/cyclonic eddy pair dipole with the anticyclonic eddy to the north (pattern 1). (2) A cyclonic/anticyclonic eddy pair dipole with the cyclonic eddy to the north (pattern 2). (3) A large and strong anti-cyclonic eddy centred off the shelf (pattern 3). (4) Eddy generation or decay characterized by weak positive SSH anomalies centred off the Sofala Bank and surrounded by weak negative SSH anomalies (pattern 4). All four eddy patterns were also depicted in a larger 3×4 SOM map (Chapter 4).

Cross-correlations between time series of simulated larval shelf retention (Fig. 5.5) and Euclidian distance to eddy SOM patterns (Fig. 5.3) for each of the 4 patterns represented in Fig. 5.13A showed that there were: (1) negative correlations with SOM pattern 2, significant at lags of 7 to 15 days after release (Fig. 5.13B), (2) positive correlations with SOM pattern 3 at lags of 5 to 12 days after release (Fig. 5.13C), (3) no significant correlations for SOM pattern 1 (Fig. 5.13A) or 4 (Fig. 5.13D). Consistently similar results were obtained for 2×3, 3×3 and 3×4 SOM maps (appendix E).

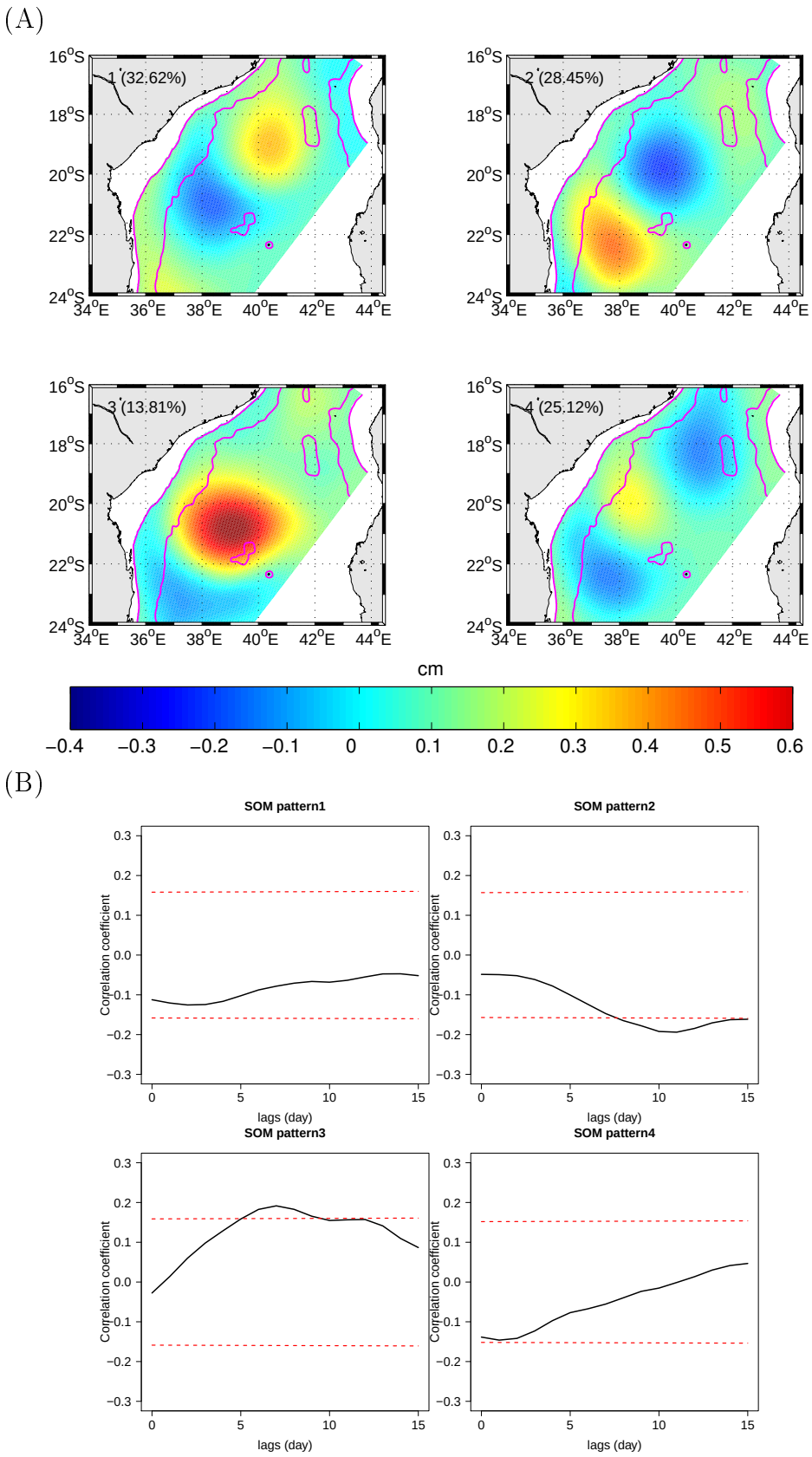

Figure 5.13: (A) 2×2 SOM map for the SSH anomaly from ROMS-BSM-E2 years $4 - 10$. The numbers $1 - 4$ (in the top left corner) indicate the SOM patterns and the percentage refers to the frequency of occurrence of each pattern. Blue (negative SSH anomalies) indicates cyclonic eddies and red (positive SSH anomalies) anticyclonic eddies. The shelf region within the 200 m depth was masked. (B) Correlations at different lag periods (cross-correlations) for time series of simulated larval shelf retention (Fig. 5.5) and each corresponding 2×2 SOM pattern Euclidian distances (Fig. 5.3). Dashed red lines indicate the 95% confidence level corrected for autocorrelation following Cuif et al. (2014).

5.3.3 Influence of temperature on shelf retention of larvae

Simulated shelf retention of banana shrimp larvae varied for different assumed low lethal temperatures (Fig. 5.14 and 5.15) (analysis of variance: $F_{5,714} = 50.02$, $P < 0.001$), but not all lethal temperatures yielded significantly different mean larval shelf retention (Tukey analysis: Table. 5.3). Experiments with lethal temperatures of $20 - 22$°C yielded similar results, with high larval shelf retention, between 85% and 87% (Fig. 5.14 and Table 5.3). The results for the experiment with lethal temperature of 23°C were not conclusive, as they were not different from those for 22°C (Table. 5.3), but were significantly different from all others. The mean simulated larval shelf retention decreased significantly to 61% and to 46% for the simulations with 24°C and 25°C low lethal temperature thresholds, respectively (Fig. 5.14A).

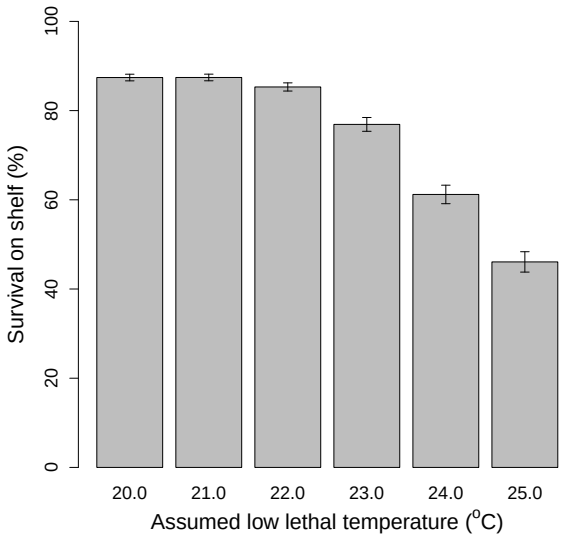

Figure 5.14: Results of the mortality experiment showing the mean (±s.e.) percentage of simulated survivors of shrimp larvae on the shelf for different values of assumed low lethal temperature.

Table 5.3: P-values of the post-hoc Tukey test for ANOVA comparing mean simulated shelf retention for the six assumed low lethal temperatures. Red values indicate significant differences ($P<0.05$).

Low lethal temperature	20°C (87.4%)	21°C (87.4%)	22°C (85.3%)	23°C (76.9%)	24°C (61.2%)	25°C (46.1%)
20°C		1.000	0.989	0.024	< 0.001	< 0.001
21°C	1.000		0.989	0.023	< 0.001	< 0.001
22°C	0.989	0.989		0.132	< 0.001	< 0.001
23°C	0.024	0.023	0.132		< 0.001	< 0.001
24°C	< 0.001	< 0.001	< 0.001	< 0.001		< 0.001
25°C	< 0.001	< 0.001	< 0.001	< 0.001	< 0.001	

Assumed different low lethal temperatures affected the seasonal distribution of simulated larvae retained on the shelf (Fig. 5.15). For assumed low lethal temperatures of 20 to 22°C, there was little change in shelf retention compared with the experiment without temperature-induced mortality (Fig. 5.5). With low lethal temperatures of 23°C, reduced shelf retention occurred mainly in the winter peak between August and September (Fig. 5.15). As the low lethal temperature increased (i.e., warmed), there was decreased larval shelf retention (i.e., massive mortality) during an extended period in winter, from mid-July to mid-September for 24°C and from mid-June to mid-October for 25°C (Fig. 5.15). Simulated larval shelf retention troughs also occurred in summer and autumn, for instance in February and May (Fig. 5.15), suggesting that other factors than seasonal variability in temperature, such as cold eddies, might be involved in larval mortality.

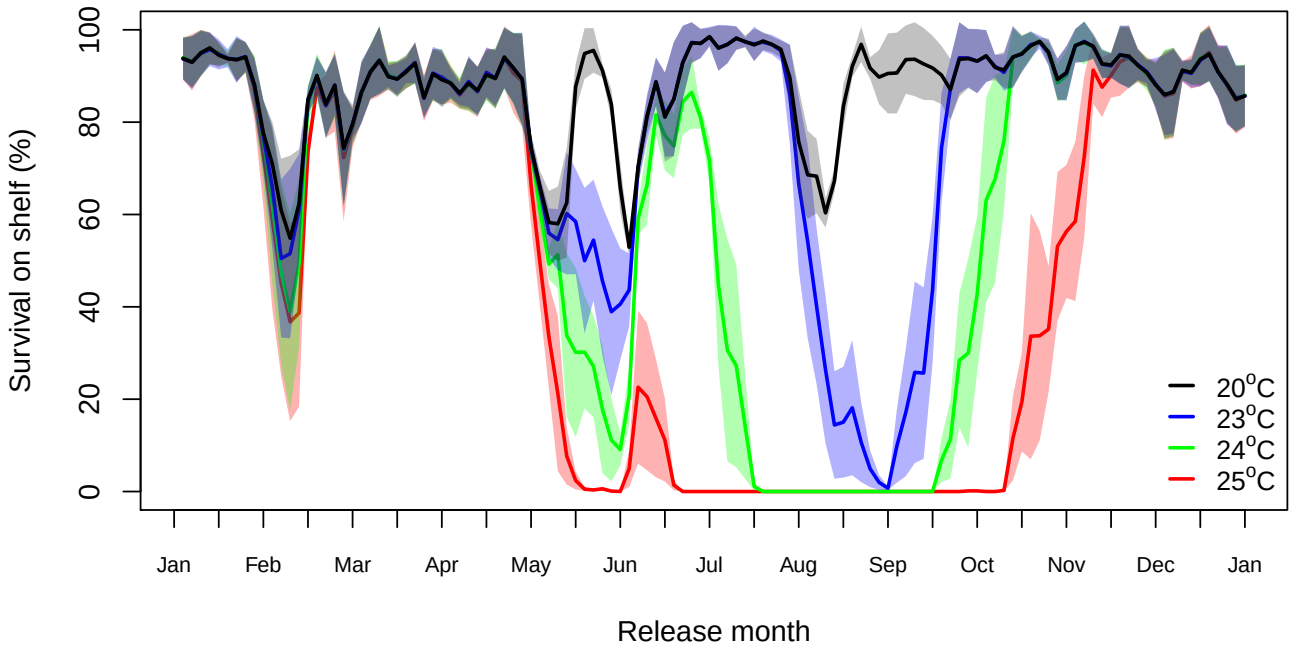

Figure 5.15: Results of the mortality experiment (E2 – 7) showing mean percentage of surviving larvae retained on the shelf over time for different assumed low lethal temperatures for model year 5. Shading indicates ± s.e.

5.4 Discussion

The present model-based study shows that most simulated banana shrimp larvae were retained on the shelf of the Sofala Bank. This simulated larval shelf retention was generally high throughout the five-year simulation (Figs. 5.5 and 5.6). At times, however, there were pulses of reduced shelf retention (Fig. 5.5), which corresponded to simulated larvae being transported offshore or to the south of the Sofala Bank (Fig. 5.6). Early life stages (larvae) of penaeid shrimp, including banana shrimp, disperse from offshore spawning grounds to coastal estuarine nurseries (Jones et al., 1970; Rothlisberg et al., 1983; Dall et al., 1990). Therefore, larvae transported (lost) offshore disrupts their life cycle (Fig. 1.5) affecting the stock-recruitment relationship, with potential implications for the fisheries. When these large pulses of lost larvae coincided with the period of decreased spawning activity the impact can be dramatic and recovery difficult, especially for short-lived species like banana shrimp on the Sofala Bank.

Many factors, including mesoscale eddies, have been proposed to influence larval transport and retention of marine organisms in similar highly energetic regions around the world (Lobel and Robinson, 1986; Bailey et al., 1997; Nakata et al., 2000; Siegel et al., 2008; Adams and Flierl, 2010; Vaz et al., 2013; Porri et al., 2014). Most of these studies focus on fish larvae, for instance, anchovy larvae in the Kuroshio Current system (Nakata et al., 2000) and coral reef fish larvae in the Hawaiian Ridge (Lobel and Robinson, 1986; Vaz et al., 2013). In contrast, little attention has been given to shrimp larvae in coastal areas, especially on the Sofala Bank. Vaz et al. (2013) showed that mesoscale eddies strongly influenced dispersal of oceanic larvae in four distinct ways, which may either enhance or reduce larval retention, depending on the eddy field variability. Their study could not however find a correlation between larval retention and eddy fields due to such a high variability.

Similarly, in the present study, simulated larval shelf retention and transport were influenced by offshore mesoscale eddy activity in different ways (Figs. 5.10 and 5.11). Since the hydrodynamic model used to couple the IBM overestimates the EKE and consequently the number of eddies, caution needs to be exercised when interpreting these results. Here, yet correlations with time lags were found for two eddy patterns identified using the unsupervised SOM algorithm (Fig.

5.13). Note that a negative correlation between time series of shelf retention and (shortest) Euclidian distances to a particular SOM pattern is interpreted as having a positive effect on simulated larval shelf retention and vice versa (data section). (1) There were correlations between high larval shelf retention and cyclone/anticyclone eddy dipole patterns at lags of $7-15$ days. This eddy dipole generates a convergent current between the eddies towards the coast, causing the simulated larvae to stay on the shelf. Besides, this situation might promote larval supply into the coastal and estuarine nurseries. (2) In contrast, there were correlations between low larval shelf retention and anticyclonic eddy patterns at lags of $5-12$ days. On average, $4-6$ large anticyclonic eddies occur in the Mozambique Channel per year (de Ruijter et al., 2002; Schouten et al., 2003; Ridderinkhof and de Ruijter, 2003; Halo et al., 2014). Similar numbers of large events of decreased shelf retention were obtained here (Fig. 5.5), supporting the general hypothesis that anticyclonic eddies induced loss of larvae, and thus low shelf retention. Since the input model overestimated the eddy variability, it is possible that the events of decreased simulated shelf retention are also overestimated. The proposed mechanism for the eddy influencing larval transport is that anticyclonic eddies induce strong coastal currents that entrain larvae offshore (Fig. 5.10B).

Results reported here support the hypothesis that the time of release of larvae relative to the eddy properties (polarity, strength and proximity to the shelf) is important for larval retention and transport (Vaz et al., 2013). This was elaborated in the snapshots of simulated larval distribution, in which, in the first 5 days, only a few larvae were found away from the shelf (Figs 5.10 and 5.11). Moreover, the correlation with eddy influences was significant at longer time lags (5.13). Also note that simulated larvae were considered as retained within the competency window of $10-15$ days, which may explain the lack of significant correlation at small time lags.

There was, however, no correlation with other eddy patterns, for instance the anticyclone/cyclone eddy dipole (pattern 1 in Fig. 5.13A), which was proposed to advect coastal material offshore (Malauene et al., 2014). This is possibly because such an eddy dipole pattern, particularly the anticyclonic eddy to the north, was weak (low SSH anomaly). As a consequence, the current was not strong enough to transport significant numbers of simulated larvae offshore. However, Fig 5.11B shows simulated larvae being advected offshore (Malauene et al., 2014). These

findings prove that eddy strength and proximity to the coast are important factors for larval retention and transport.

The correlations discussed in the previous paragraphs only apply to simulated larval shelf retention and not for larval transport (i.e., trajectories). Larval transport induced by mesoscale eddies is complex and highly variable (Siegel et al., 2008; Blanke et al., 2012; Vaz et al., 2013). Similarly, here the results indicate that the pathways of transported larvae of simulated banana shrimp are indeed complex and highly variable (Figs. 5.7 and 5.8). At times, larvae stayed on the shelf, were transported cross-shore towards the coast or offshore, and/or were transported along-shore to the south. During the study period, neither clear nor stable larval pathways were identified, thus it is difficult to propose or predict transport routes. For example, Figs. 5.8C and D show different larval trajectories resulted from similar eddy fields, one a few days after the other (Figs. 5.11C and D, respectively). Thus, the exact pathway depends strongly on eddy polarity, strength, position and proximity to the coast, which are highly variable factors. However, two generally recurrent patterns were apparent: (1) larvae transported offshore and (2) larvae exited to the south.

In Chapter 2, three inshore areas were identified for banana shrimp spawning on the bank, while other areas were identified as non-spawning. The present chapter tested whether these actual spawning areas were selected naturally because they offer favorable conditions for successful larval retention (Putman et al., 2010), by comparing them with the non-spawning areas. The northern release area (area 1), which is located on the narrow shelf, is notable because it covers both the inshore and offshore sides. This area 1 was significantly different in terms of contribution to the simulated larval retention from the adjacent inshore area 2, but not from the offshore area 6 (Fig. 5.4 and Table 5.2). These findings suggest that area 1 has characteristics more similar to offshore than inshore areas, and will be thus considered together with other offshore areas and apart from inshore areas in the analysis below. Results indicate that, for the inshore side (areas $2-5$), there was no difference in shelf retention of simulated larvae originating from the actual or non-spawning areas, thus the hypothesis ($H_{5.1}$) of Putman et al. (2010) is not supported.

To the north of 19°15′S there were significant differences in mean shelf retention of simulated

larvae released in the inshore and offshore areas, with higher retention for inshore than offshore (Fig. 5.4 and Table 5.2). These results indicate that on the central and northern Sofala Bank, larvae released on the offshore side are more exposed to the eddy activity and corresponding strong currents than those released inshore. Therefore, in this exposed region, offshore released larvae have less chance of being retained on the shelf, promoting dispersal (Figs. 5.8, 5.10 and 5.11). By contrast, to the south of $\sim 19°15'$S, there was no difference in mean shelf retention of simulated larvae released on the inshore or offshore areas (Fig. 5.4 and Table 5.2). This region is semi-enclosed by Beira Bay, and thus less exposed to eddy activity, resulting in a calm environment that promotes larval retention (Figs. 5.8, 5.10 and 5.11), corroborating the high simulated shelf retention found consistently off Beira Bay. These findings prove that larval retention is low in regions exposed to high-energetic circulation and higher in protected regions (Shanks and Brink, 2005; Robins et al., 2013; Porri et al., 2014).

It is suggested that mesoscale eddies are responsible for long-distance dispersal of larvae of marine organisms (Adams and Flierl, 2010; Blanke et al., 2012). Fig. 5.9 shows that simulated larvae were transported long-distances of > 600 km, with a maximum of 1600 km in 15 days. There was a difference between the total distance traveled by simulated larvae and the distance from release to final location (Fig. 5.9). This proves that larvae did not travel in straight lines, but rather in complex trajectories, supporting the hypothesis of eddy-induced long-distance dispersal of simulated shrimp larvae. Moreover, those studies and others proposed that such eddy-induced long-distance dispersal promotes connectivity among distant populations or stocks. Recently, Hancke et al. (2014) reported eddy-induced cross-channel transport of surface drifters in two directions, i.e., westwards and eastwards, between the Mozambique and Madagascar shelves. They hypothesized that this eddy-induced transport plays an important role for connectivity between the two shelves. It should be noticed that their drifters traveled from one shelf to another in 19–30 days, which is longer than the pelagic larval duration (~ 15 days) for the banana shrimp (Chapter 1). Their drifters have a vertical holey-sock drogue (sea anchor at 18 m depth), which may interact with the sea floor (< 20 m), generating a bottom friction that potentially slows down the movement. This is particularly true in coastal shallow waters with $< 15 - 20$ m depth, which is the average depth in the natural habitats of banana shrimp. Thus, caution needs to be exercised when interpreting results reported by Hancke et al.

(2014) on connectivity of shallow water banana shrimp. The present study did not attempt to investigate connectivity between distant populations/stocks. However, here results support the potential eddy-induced long-distance connectivity between Mozambique and Madagascar (e.g. Fig. 5.8D and 5.11B). These results, however, were not fully conclusive, due to the limited model domain. Similarly, based on the long-distance dispersal, connectivity between the Sofala Bank banana shrimps and other distant populations to the south, such as at Maputo Bay ($\sim$ 800 km from the Sofala Bank) and the Natal Bight (in South Africa, $\sim$ 1250 km further south) is possible. In the case where no strong eddy appeared near the shelf, there was no long-distance dispersal of simulated larvae, and as a consequence, nearly all larvae were retained on the shelf (Fig. 5.10A). Thus, absence of eddies decreased potential connectivity while promoting larval shelf retention. Further work is needed to clarify the role of eddy in connectivity between distant shrimp stocks in the region.

Another question related to the eddy-induced long-distance connectivity, for instance between Mozambique and Madagascar, is whether the shrimp larvae would survive in the open ocean during the journey. Offshore eddies are nutrient-rich at the surface (Weimerskirch et al., 2004; Tew-Kai and Marsac, 2009; Jose et al., 2014). Eddy associated nutrient-rich waters have enhanced primary production and, therefore, copepod production, providing favorable conditions for the feeding and survival of anchovy larvae entrained in eddy in the Kuroshio Current system (Nakata et al., 2000) and sardine larvae in the California Current system (Logerwell and Smith, 2001). Similarly, since pelagic shrimp larvae do not need to settle onto the sea bottom within the first 15 days, simulated larvae entrained in a nutrient-rich eddy and transported offshore might survive at the surface. In these offshore productive eddies, larvae may be exposed to high predation (Weimerskirch et al., 2004; Tew-Kai et al., 2009; Potier et al., 2014), but a small number of surviving larvae may be sufficient to ensure genetic connectivity.

Connectivity between distant populations or stocks of marine organisms is important for maintenance of these stocks, their resilience and recovery from various threats, including anthropogenic pressure (Jones et al., 2009; Robins et al., 2013). Similarly, connectivity between adjacent local stocks is also important. Here, the model results indicate that the connectivity between the northern and central regions of the bank was asymmetrical, with low northward

dispersal of simulated larvae and high southward dispersal (Figs. 5.7, 5.8, 5.10 and 5.11). This dominant southward connectivity between banana shrimp stocks near to one another is related to the propagation direction of the eddies. Similar model results were obtained for deep-sea hydrothermal vents in the East Pacific Rise (Adams and Flierl, 2010). As discussed before, larvae from the southern region, off Beira Bay, do not disperse much (Figs. 5.7, 5.8, 5.10 and 5.11). On the other hand, larvae from the north entrained into eddies were transported southwards on the outer shelf, bypassing Beira, and thus did not contribute to retention (i.e., low connectivity). Over the past 10 years, the banana shrimp stocks on the entire Sofala Bank have experienced a dramatic decline (de Sousa et al., 2013). It is suggested that, for the shrimp stock off Beira, which is relatively isolated from others on the Sofala Bank (and hence depends on local sources of larvae), recovery will be hard.

Based on the findings of consistently low connectivity and high simulated larval retention, Beira Bay is the best retention location for the banana shrimp larvae on the Sofala Bank. However, high retention does not necessarily mean high recruitment into the fishery. In fact, the banana shrimp catch off Beira is relatively low compared to other regions on the Sofala Bank; for this reason the shrimp stock off Beira is reserved for the semi-industrial fleets and not for industrial fleets (de Sousa et al., 2008). Bakun (1996) proposed that successful recruitment of marine organisms with pelagic larval stages depends on co-occurrence of three important processes: enrichment, concentration and retention. The former two are related to nutrient availability, which is not considered in the present study. Nevertheless, because Sofala Bank is an oligotrophic region, enrichment depends on allochthonous production carried by the Beira Bay rivers, with low river discharge compared to the Zambezi River (Fig. 3.4). This suggests a weak enrichment; thus the three processes proposed by Bakun (1996) are not preserved and consequently shrimp recruitment and catch are low. Further investigation is necessary to clarify the possible roles of these three processes for recruitment and catch of banana shrimp on the Sofala Bank, especially off Beira. Off Beira, the low connectivity with other stocks and the uncertainty of the importance of high larval retention to recruitment suggest that caution is needed when managing the banana shrimp stock in this region.

Lobel and Robinson (1986) showed that coral reef fish larvae entrained into eddies could return

to the natal reef inshore. Similarly here, Fig. 5.10 indicates that some of the simulated larvae advected by eddies, can sometimes eventually return to the bank, contributing to the shelf retention. However, the mean percentage of those larvae was low ($< 8\%$) compared to the mean percentage of those that stayed all the time on the bank. Considering that cold eddies increase mortality, the number of returning larvae might be even lower. Thus, the net contribution of the returned larvae to the shelf retention may be negligible compared to those that stayed on the shelf.

Many studies that investigated the temperature influence on penaeid shrimp focused on the optimum temperature for growth of postlarval stages (Chapter 1), while little attention has been given to lethargic effects. Penaeid shrimp mortality is believed to be greater at low temperatures than at high temperatures (Dall et al., 1990; Kumlu et al., 2010), but this effect is not yet determined for the banana shrimps on the Sofala Bank. For similar penaeid species elsewhere, many authors proposed a low lethal temperature below the optimum of 25°C (Wyban et al., 1995; Coman et al., 2002; Lopez-Martinez et al., 2003; Radhakrishnan, 2007; Kumlu et al., 2010; Wang Xingqiang and Ma, 2010) with massive mortality below 20°C. In this study, the influence of low lethal temperature (from 20 to 25°C) on shelf retention and dispersal of simulated larvae of banana shrimp was tested. Results show that assumed low lethal temperatures of $20 - 23$°C had little effect on simulated larval shelf retention, with high survival (Figs. 5.14 and Table 5.3). Therefore the hypothesis ($H_{5.2}$), that larvae die when encountering cooler temperature than 20°C is not supported for simulated banana shrimps on the Sofala Bank. This finding is explained by the simple fact that these low temperatures are rarely observed in hot tropical water, like on the Sofala Bank.

In contrast, significantly decreased larval survival was obtained for low lethal temperatures of $24 - 25$°C (Fig. 5.14 and Table 5.3), suggesting that the low lethal temperature for the larvae of banana shrimps on the Sofala Bank is around 24°C. There was also a strong seasonal effect, with low survival and retention extending over a large period in winter (Fig. 5.15) due to solar insolation. This finding is in agreement with: (1) low winter concentrations of mature females, especially for *M. monoceros* (Chapter 2), and (2) low winter catches of all banana shrimps on the bank (de Sousa et al., 2008). The model results show that decreased larval survival and

shelf retention also occurred in summer (Fig. 5.15), suggesting factors other than seasonal variability in temperature might be involved in larval mortality. The decreased larval survival episode observed in February (Fig. 5.15) coincided with a cool cyclonic eddy (not shown), causing larval mortality and thus decreasing shelf retention.

In summary the present model-based study shows that offshore eddy circulation partly controls the patterns of shelf retention and dispersal of simulated banana shrimp larvae on the Sofala Bank. Cyclonic eddies were identified as the main cause of decreased shelf retention. Since $4-6$ large anticyclonic eddies occur per year (on average), similar numbers events of reduced larval shelf retention could be expected. Larvae were dispersed long distances away from the Sofala Bank, suggesting that eddies may play an important role in the connectivity between distant shrimp populations or stocks. However, the role of mesoescale eddies in long-distance connectivity needs further investigation. The best location for larval retention was identified off Beira Bay, which is protected from the eddy circulation. Simulated larvae were affected by seasonal winter low temperatures. Cool eddies also appeared to impact simulated larval shelf retention.

Chapter 6

Factors influencing transport and coastal settlement of banana shrimp larvae

Abstract

An individual-based model (IBM) was developed to investigate the influences of environmental processes and larval behaviour on transport and coastal settlement of simulated banana shrimp larvae. Simulated larval shelf retention was positively correlated with larval coastal settlement ($r_{113} = 0.42$, $p < 0.001$). Exceptions included some elevated shelf retention, which was not associated with subsequent elevated settlement. This result indicates there are mechanisms that are favorable for shelf retention but unfavorable for coastal settlement. For some areas, there was no difference in simulated settlement success between larvae released in the actual spawning areas or in non-spawning areas. Simulated larvae released inshore had a significantly higher chance of settling at the coast than those released offshore. There was a tide-trapped, quasi-stationary larval pool in the offshore area off Beira Bay (to the south of $\sim 19°30'$S), promoting shelf retention but unfavorable for coastal settlement. The three best locations for simulated larval settlement were identified as: (1) northern, (2) central and (3) southern. These locations are in part explained by the influence of energetic offshore eddies and rings. The effects of diel vertical migration (DVM), tides and buoyant river plumes on simulated larval settlement were tested. All these factors significantly decrease the simulated larval settlement success, but the effect of DVM was not conclusive. Further investigation is necessary, considering a new IBM configuration that incorporates a selective tidal stream transport for postlarvae in the estuaries, to further clarify the role of DVM and tides on the settlement of banana shrimps.

6.1 Introduction

Many authors have suggested that marine organisms that have high larval retention also show high larval settlement success. For example, Shanks and Brink (2005) suggested that, for coastal species, all larvae are potentially retained near the coast and future settlement sites instead of being swept offshore. In the previous chapter (5) it was demonstrated that most simulated larvae were retained over the Sofala Bank. Whether they reach the coastal settlement areas remains an open question, which is addressed in the present chapter. It is hypothesised ($H_{6.1}$) that simulated larval coastal settlement is related to shelf retention, so that the locations and times of high (or low) shelf retention will result in subsequent high (or low) coastal settlement.

In marine organisms with a pelagic larval stage, patterns of larval transport and settlement may be important for subsequent distribution and abundance of juveniles recruiting into adult populations (Booth, 1992). This larval settlement distribution is not spatially homogeneous, which has implications for the adult population. For example, Gaines and Roughgarden (1985) demonstrated that the population structure of barnacles differs between locations of high and low larval settlement success. Larval settlement can also exhibit strong temporal variability (Roberts et al., 1991). Therefore it is hypothesised ($H_{6.2}$) that simulated larval settlement is not uniformly distributed over the entire coast of the Sofala Bank; instead, patches and times of high settlement success occur.

It is further hypothesised ($H_{6.3}$) that such patches and times of high settlement are not randomly distributed, but are related to environmental processes like tides and river discharge and larval behavior. The Sofala Bank is known to have the highest tidal amplitudes and tidal currents in the Mozambique Channel, particularly off Beira Bay (Chapters 3 and 4; Chevane, 2013), which is one of the world's hot spots for tidal generation (da Silva et al., 2009). However, the tidal influence on shrimp larval transport and settlement on the Sofala Bank is not known. It is thought that tides influence larval transport and settlement of many marine organisms around the world. Peliz et al. (2007) showed that river plumes influence larval transport. The coastal circulation over Sofala Bank is influenced by the plumes of the Zambezi (Nehama, 2012) and Beira Bay (Pungué and Buzi) Rivers (Chapters 3 and 4). The low-salinity plume front

changes the salinity and thus the water density, with potential implications for larval buoyancy, transport and settlement.

The aim of this chapter is to investigate transport and settlement of virtual larvae of banana shrimps along the coast of the Sofala Bank and identify the best locations for settlement. Similar to the preceding chapter (5), here an individual-based model approach is used. Especially, the potential influences of environmental processes such as offshore eddy activity, tides and river plumes on simulated larval settlement are investigated. Moreover, the influence of diel vertical migration on simulated larval transport and settlement is also investigated. Understanding these will help improve shrimp fisheries management.

6.2 Model and methods

6.2.1 IBM experiment configurations

An individual-based model (IBM) is used to simulate larval dispersal and coastal settlement of banana shrimp on the Sofala Bank. The IBM simulations were developed using a Lagrangian model, Ichthyop version 3.1, coupled to ROMS outputs as described in detail in chapter 5. The present chapter focuses on the fine resolution ROMS grid (Child) covering the entire Sofala Bank (Chapter 3). Detailed description and results of the Sofala Bank ROMS are discussed in chapters 3 and 4.

Coastal settlement

The release areas (Fig. 6.1A) are the same as in Chapter 5. Because banana shrimps settle into the coastal and estuarine areas (Dall et al., 1990), a narrow area along the entire Sofala Bank coast was defined for the investigation of settlement of simulated larvae (Fig. 6.1B). This area (hereafter called "settlement area") was defined by the 10 m isobath (purple line in Fig. 6.1). However, to allow movement of larvae within the area, a minimum of two grid cells were selected. In places where the 10 m isobath was found far offshore, a maximum of three grid cells were taken. Therefore the selected simulated settlement area varied between $2-3$ ROMS Child grid cells, i.e., $4-6$ km. The settlement area was first digitized in a GIS, considering the above mentioned criteria, and then imported into Ichthyop. Larvae which entered this area were considered as successfully settled from age of ten days, based on available information that larvae are not competent before a postlarval stage that corresponds ~ 10 days (Chapter 1).

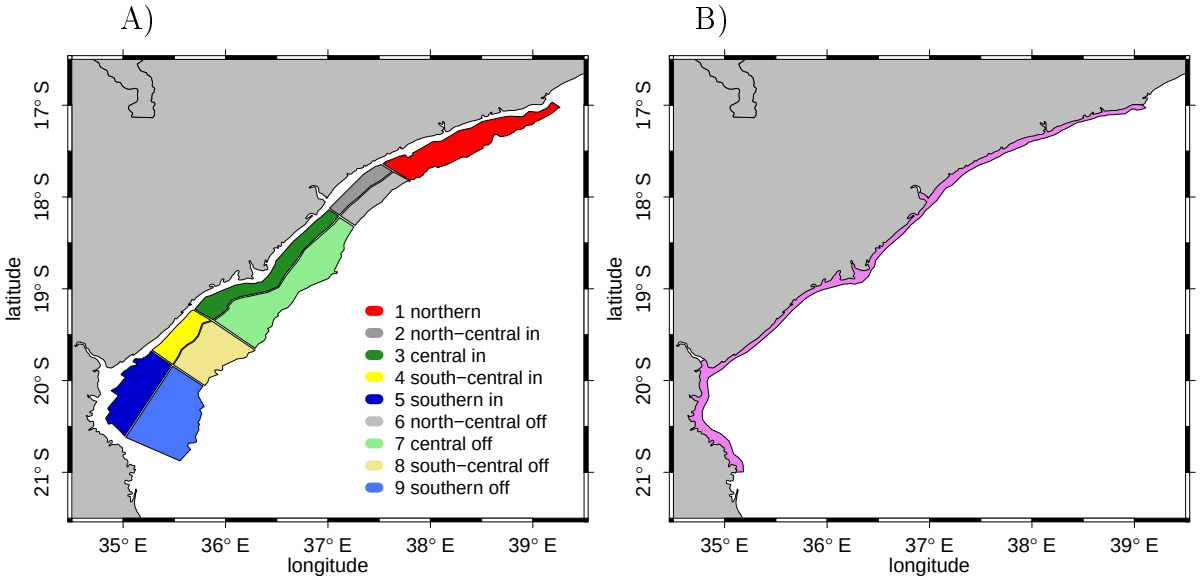

Figure 6.1: Map of the Sofala Bank showing (A) the release areas inshore (in) and offshore (off) as detailed in Chapter 5, and (B) the coastal settlement area used for the larval simulations.

Simulation experiments

Simulations consisted of randomly releasing 10000 virtual shrimp eggs within the release areas for one year and tracking their trajectories every 15 days. The simulation time step was set to 600 s (10 min) and the outputs recorded every three hours (i.e., every 18 time steps) or every hour in simulations including tides. There were five distinct simulation experiments:

Shelf retention – Consisted of Ichthyop coupled with the ROMS Child grid with tides, at hourly averaged ROMS outputs (ROMS-BSM-E4, Chapter 3). Successful simulated larval destination used here is shelf retention. This experiment is used to investigate the link between larval shelf retention and coastal settlement.

Coastal settlement (Reference) – Same as shelf retention experiment, but here the coastal settlement area is used for successful larvae.

DVM – Same as the reference experiment, but using Ichthyop with larval diel vertical migration (DVM, details about the implemented scheme are below).

Without tides (NoTides) – Same as the reference experiment, but using ROMS outputs without tides (ROMS-BSM-E3, Chapter 3).

River – Same as the reference experiment, but using ROMS outputs with river inputs (ROMS-BSM-E6, Chapter 3).

Note that the simulation experiments without tides and with river inputs used different ROMS outputs (ROMS-BSM-E3 and ROMS-BSM-E5, respectively) than those used for the former experiments (ROMS-BSM-E4). Thus caution is needed when comparing the reference experiment with the NoTides and River experiments.

Because banana shrimp larvae display diel vertical migration (DVM, Dall et al., 1990; Rothlisberg et al., 1995), DVM is implemented in the reference experiment to test its effects. The DVM scheme consisted of larvae migrating down to the sea bottom at sunrise (05:15 h) and up to the surface at sunset (18:00 h). This DVM scheme was only implemented for larvae older than 2 days because penaeid larvae start to display DVM behaviour when they reach the protozoeal stage, which corresponds to this age (Chapter 1). Larvae < 2 days (nauplius stage) simply drift at the surface by controlling their buoyancy, i.e., setting their density at 1 g cm^{-3}, which is less than that of sea water.

6.2.2 IBM output analyses

An independent samples t-test was conducted to compare the mean simulated larval settlement success obtained in the reference experiment with each of the DVM, NoTides and River experiments and also the larval shelf retention experiment. One-way analysis of variance and a post-hoc Tukey test were used to compare the mean simulated settlement from all nine release areas. Prior to performing these analyses, the assumptions of normality and equal variances were verified. Pearson's product-moment correlation was used to investigate strength of the relationship between the reference case and each experiment (retention, DVM, NoTides and River).

Relative difference was calculated as $((factor - Ref)/Ref) \times 100$, where Ref refers to the reference experiment and $factor$ to each of DVM, NoTides and River simulations. Because an infinite settlement difference would be obtained when $Ref = 0$ and $factor \neq 0$ (i.e., dividing by zero), the settlement difference was set to 100% in such cases.

To investigate a potential tidal cycle effect on the simulated larval settlement success, a wavelet analysis (Emery and Thomson, 2001) was applied to the daily time series of successfully settled larvae using the matlab toolbox developed by Torrence and Compo (1998). Prior to performing the wavelet analysis, the time series was normalized by subtracting the mean from the corresponding daily values and then divided by the standard deviation. The Morlet wavelet was chosen as the "mother" wavelet. The statistical significance test for wavelet power spectra was set at a 95% confidence level.

6.3 Results

6.3.1 Simulated larval coastal settlement.

The mean percentage of successfully settled larvae along the coast of the Sofala Bank (reference experiment [Ref.], 18%) was significantly less than the mean larval shelf retention (92%) (Table 6.1 and Fig. 6.2). This result was consistent throughout the time series (Fig. 6.2A). The simulated larval coastal settlement and larval shelf retention were significantly positively correlated ($r_{113} = 0.42$, $p < 0.001$), with exceptions (Fig. 6.2A and B). At times, simulated larval shelf retention was high yet coastal settlement was low (top left corner of Fig. 6.2B). There was no situation where shelf retention was low and coastal settlement high (bottom right corner of Fig. 6.2B).

Table 6.1: (A) t-test comparison between pairs of simulated coastal settlement for experiment with diffusion, tides and without DVM and rivers (mean = 18%, N = 115) (reference simulation, ref) and distinct experiments (factor): shelf retention, settlement without diffusion, settlement with DVM, settlement without tides and settlement with river input.

Mean Effect	t-value	DF	p	N Effect	Std.dev. Effect	F-ratio Variances	p Variances
Ref vs. Retention							
92	118.14	228	0.00	115	0.055	2.02	0.00021
Ref vs. NoDiffusion							
12	11.92	228	0.000000	115	0.034	1.26	0.21203
Ref vs. DVM							
10	18.63	228	0.00	115	0.028	1.92	0.00055
Ref vs. NoTides							
23	6.87	228	0.000000	115	0.070	3.30	0.00000
Ref vs. River							
16	5.11	228	0.000001	115	0.035	1.22	0.28988

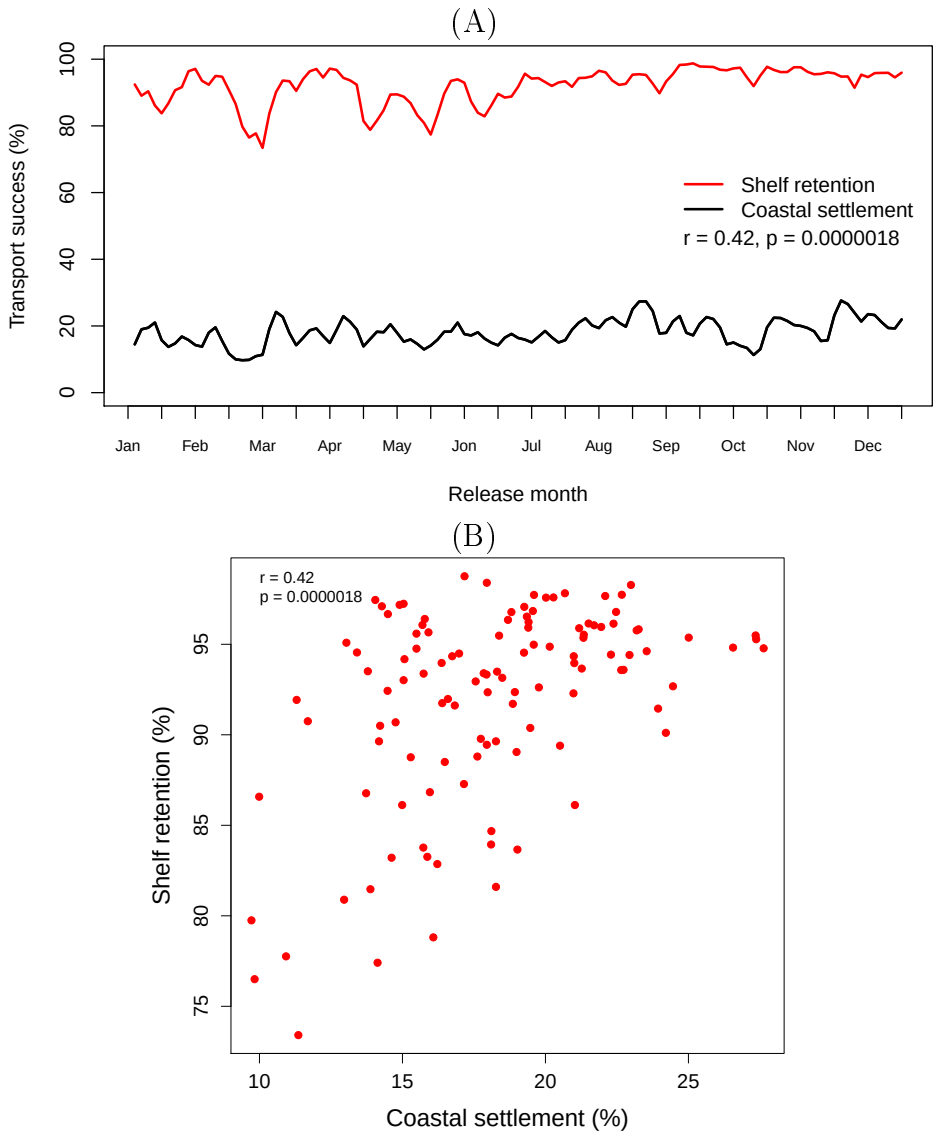

Figure 6.2: Comparison between time series of shelf retention and coastal settlement.

Fig. 6.3 shows that all nine release areas contributed to the settlement of simulated larvae along the coast of the Sofala Bank. Excluding the northernmost release area 1, there is a north-south declining trend in contributions to coastal settlement from the inshore areas 2 to 5 and also from the offshore areas 6 to 9 (Fig. 6.3). There were significantly different mean simulated larval settlements relative to the release areas (analysis of variance: $F_{8,1026} = 4.37$, $p < 0.001$). However, not all release areas were significantly different (Table. 6.2). Although not adjacent, the mean settlement from larvae originating from release area 1 (northern area) was not significantly different from those from release area 4 (south-central inshore area) (Table. 6.2A and B). For the inshore release areas, release area 2 (north-central area), which was the most successful release area with $\sim 52\%$ of the larvae settling, was not significantly different from release area

3092 3 (central release area), which was the second most successful release area ($\sim$ 49%). For the
3093 offshore release areas, the two southernmost release areas 8 and 9 (south-central and south-
3094 ern area, respectively) were not significantly different. These two release areas had the lowest
3095 larval coastal settlement of $< 2\%$. For pairs of adjacent inshore versus offshore release areas,
3096 they were all significantly different, with higher mean coastal settlement for the inshore release
3097 areas than those offshore (Table. 6.2A and C). Inshore area 5 and offshore area 6, though not
3098 adjacent, showed mean larval settlements that were not significantly different (Table. 6.2).

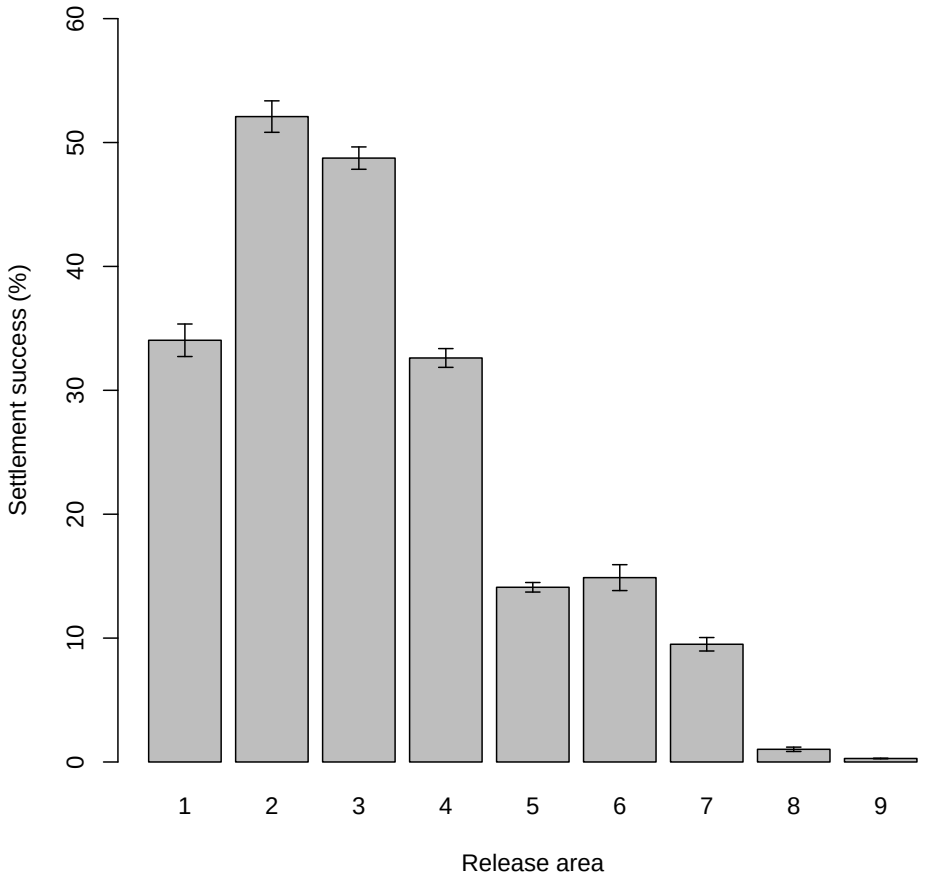

Figure 6.3: Mean ($\pm$s.e.) percentage of simulated larval coastal settlement on the Sofala Bank for the different release areas (as depicted in Fig. 6.1).

Table 6.2: (A) P-values of the post-hoc Tukey test for ANOVA comparing mean larval coastal settlement for all nine release areas. Red values indicate significant differences ($P < 0.05$). B) and C) schematic of the release areas (green) not significantly different and (red) different.

(A)

Release area	1 (34.0%)	2 (52.1%)	3 (48.8%)	4 (32.6%)	5 (14.1%)	6 (15.0%)	7 (95.4%)	8 (1.3%)	9 (0.28%)
1		< 0.001	< 0.001	0.950	< 0.001	< 0.001	< 0.001	< 0.001	< 0.001
2	< 0.001		0.116	< 0.001	< 0.001	< 0.001	< 0.001	< 0.001	< 0.001
3	< 0.001	0.116		< 0.001	< 0.001	< 0.001	< 0.001	< 0.001	< 0.001
4	0.950	< 0.001	< 0.001		< 0.001	< 0.001	< 0.001	< 0.001	< 0.001
5	< 0.001	< 0.001	< 0.001	< 0.001		0.998	0.004	< 0.001	< 0.001
6	< 0.001	< 0.001	< 0.001	< 0.001	0.998		< 0.001	< 0.001	< 0.001
7	< 0.001	< 0.001	< 0.001	< 0.001	0.004	< 0.001		< 0.001	< 0.001
8	< 0.001	< 0.001	< 0.001	< 0.001	< 0.001	< 0.001	< 0.001		0.999
9	< 0.001	< 0.001	< 0.001	< 0.001	< 0.001	< 0.001	< 0.001	0.999	

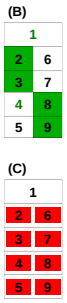

The density map of the origin of the settled larvae shows that they came from all over the Sofala Bank, except from an area in the south (with zero density), centred at $\sim 35°30'$E and between $19°30'$S and $20°$S (Fig. 6.4A). Interestingly, however, there was a small high density at the offshore edge of the south-central offshore release area (area 8). There were clear north−south and inshore−offshore gradients in the origin of the settled larvae (Fig. 6.4A), as already noticed (Fig. 6.3).

The latitudinal distribution of all settled larvae shows two peaks of > 20000 larvae (Fig. 6.4B). The first peak occurs at the northern portion of the bank between $17°15'$S and $17°45'$S and the second between $18°30'$S and $19°15'$S. Fewer (~ 13000) settled larvae were found between these two major peaks. A sharp decline in the numbers of settled larva is observed to the south of the second peak. However, a third (minor) peak with < 5000 settled larvae was found at $\sim 20°15'$S (Fig. 6.4B).

The density map of larval settlement from all nine release areas (labeled 9 in Fig. 6.4C) shows similar patterns to those in Fig. 6.4B, but for continuous spatial distribution instead of discrete latitude bins. When the larvae are released only from the actual spawning areas (i.e., areas 1, 3, 5 , 7, and 9, label 5 in Fig. 6.4C), the locations with high densities of settled larvae are enhanced, whereas the locations with low densities increase and a small location with nearly zero density appears at $\sim 19°20'$S. When considering only the northern release area (Fig. 6.4C label N), high density of settled larvae occurred at the northernmost limit of the bank,

decreasing towards the central region and reaching zero south of 19°S. When considering the central release areas (areas 3 and 7 labeled C in Fig. 6.4C), coastal settlement is obtained in the central region of the bank from ∼ 19°15′S to ∼ 17°45′S. When considering larvae released in the southern release areas (areas 5 and 9) only, relatively high density of settled larvae is found in the south between 20°45′S and 19°15′S, tending to zero in the north (Fig. 6.4C label S).

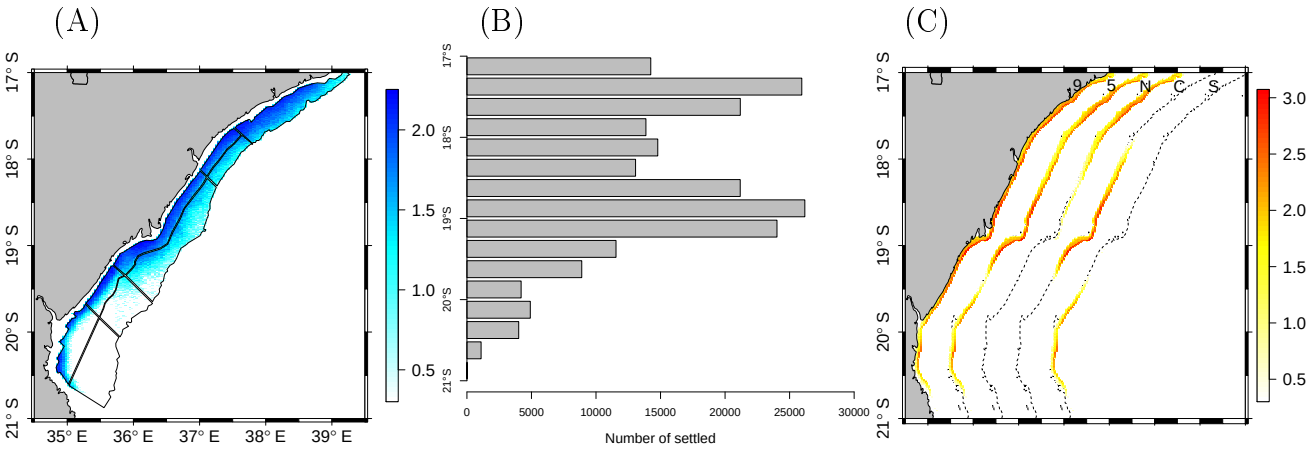

Figure 6.4: (A) Density map of the origin of the simulated larvae that settled for all nine release areas (delimited by the black lines). (B) Latitudinal distribution of the settled larvae every 0.25° between 17 − 21°S from all nine release areas. (C) Density map of the settled larvae for different sets of release areas: label 9 for all nine areas, 5 for the actual spawning areas inshore and offshore (i.e. areas 1, 3, 5 , 7, and 9), N for the northern area (1), C for the central areas (3 and 7) and S for the southern areas (5 and 9).

Influence of oceanic conditions on larval coastal settlement

To understand the link between larval coastal settlement, shelf retention and ocean circulation, four examples (snapshots) of simulated larval dispersal superimposed on averaged SSH and surface current velocity vectors are shown in Fig. 6.5: (1) both shelf retention and coastal settlement were low, e.g. on 20 February; (2) shelf retention was relatively high and the coastal settlement low, e.g. on 2 October; (3) both were high, e.g. on 17 November; and (4) explicitly chosen to illustrate how the few larvae that originated from the offshore edge of the south-central offshore release area settled, e.g. on 8 January.

On 20 February a large anticyclonic eddy was found over the shelf, associated with strong currents that reached the coast (Fig. 6.5, A1). Most of the simulated larvae entrained in the eddy were advected offshore (Fig. 6.5, A2, B2). At the end of the simulation, nearly all larvae from the northern release area had moved, and almost no larvae were found between $17-18°$S (Fig. 6.5, A1). The anticyclonic eddy generated a southwestward current, near the coast. During this process, a few larvae from the northern release area drifted southwestward and settled in the central area (Fig. 6.5, C1). There were only a few larvae from the central release areas that settled at the coast and those were mostly from the near inshore region (Fig. 6.5, C1). Settled larvae from the southern release areas were found separated into two subgroups, divided at $\sim 20°$S (Fig. 6.5, C1).

On 2 October there was no eddy activity despite a weak cyclonic eddy centred offshore off Beira Bay at $\sim 21°$S and $\sim 36°30'$E, and the general coastal circulation was weak (Fig. 6.5, A2). The southwestward drift, particularly for larvae from the northern release area, was absent (Fig. 6.5, B2, C2). Nearly all larvae from all release areas stayed on the shelf throughout the simulation, but only a few settled (Fig. 6.5, A−C2).

On 17 November there was a weak anticyclone/cyclone eddy pair dipole, with the anticyclonic eddy to the north, associated with relatively strong shelf circulation (Fig. 6.5, A3). There were a few larvae advected offshore, while most of them stayed on the shelf (Fig. 6.5, A3 and B3). There was a southwestward drift, and a large number of larvae settled at the coast (Fig. 6.5, C3).

Fig. 6.5A-C4, on 8 January, showed a pattern similar to that in Fig. 6.5A-C3, but with a stronger eddy field and offshore larval entrainment. There was a clear cyclonic eddy to the south that generated a northward shelf edge flow (Fig. 6.5, A4). This flow advected some larvae northwards, particularly those from the southern offshore release area (Fig. 6.5, B4), such that few of them settled in the central area (Fig. 6.5, C4). Fig. 6.5 shows that, for all four examples the larval shelf retention was generally high off Beira Bay, yet the coastal settlement was low.

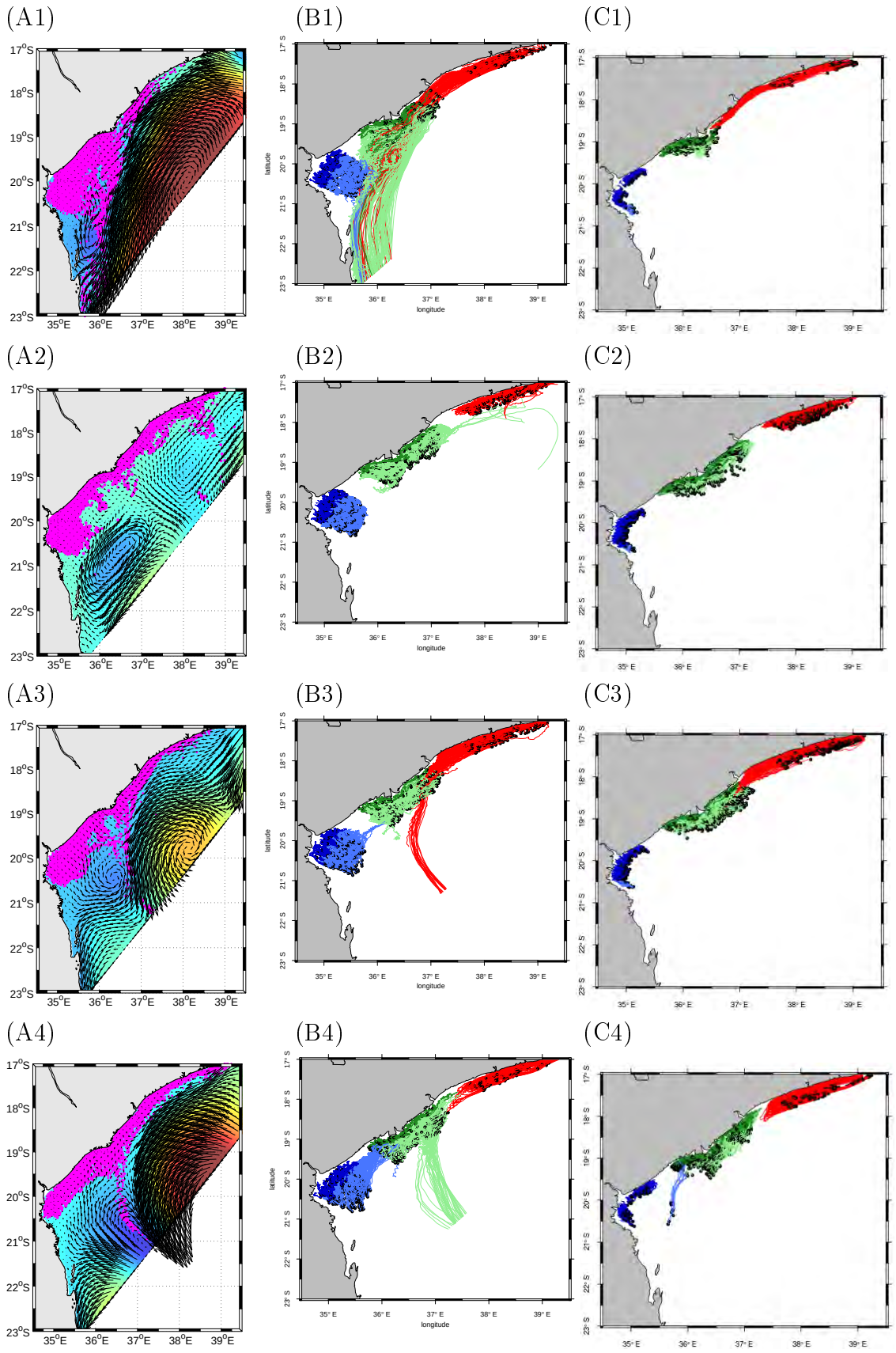

Figure 6.5: Snapshots of (A) larval distribution 15 days after release (pink dots) superimposed on the corresponding 15 days averaged ROMS-derived SSH (color shading, in cm) and surface currents (black arrows, cm s^{-1}). (B) Trajectories of all released larvae tracked for 15 days from (red) northern, (green) central and (blue) southern release areas. (C) Same as B but only for the settled larvae. For simulation starting on: (1) 20 February, (2) 2 October, (3) 17 November and (4) 8 January.

Snapshots of trajectories of randomly chosen larvae from each of the three selected release areas (northern, central and southern, respectively) tracked every hour for 15 days, show that larval from all three locations exhibited an oscillating movement (Fig. 6.6). Such a motion has a frequency of $\sim$ 6 hours, typical of the semi-diurnal tidal cycle observed in this region (Chapter 3). Larvae from the northern (Fig. 6.6A) and from the central (Fig. 6.6B) release areas were significantly displaced, whereas those from the southern area (Fig. 6.6C) did not move much, being trapped in place by the to-and-fro motion. These patterns are representative of coastal and inner-shelf regions; however, occasionally some larvae released offshore (i.e., on the shelf edge) in the south did move, as shown in Fig. 6.5, A−C1.

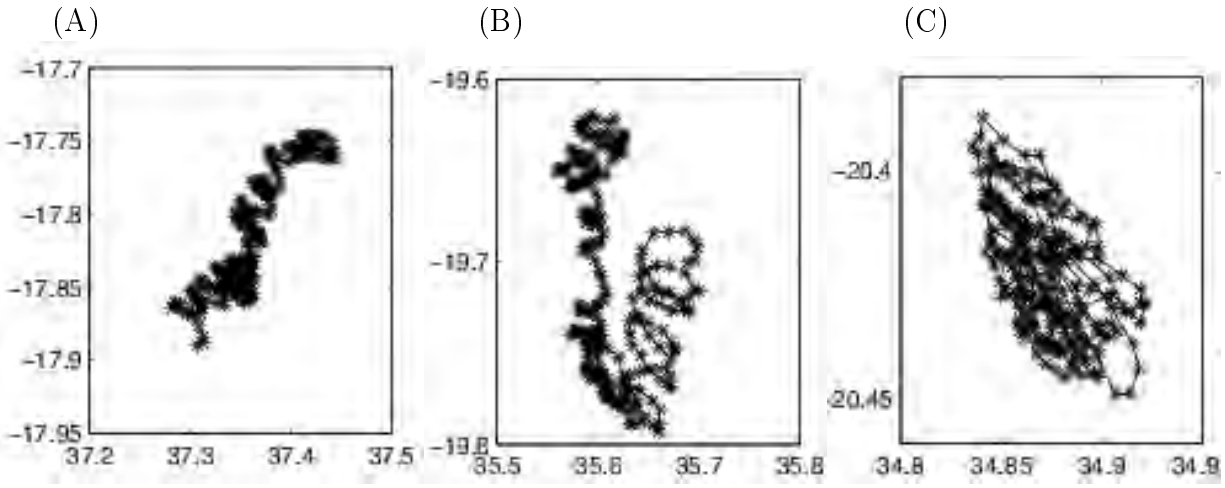

Figure 6.6: Snapshots of trajectories of randomly chosen single larvae from three selected release areas (A) northern, (B) central and (C) southern, tracked every hour for 15 days.

The distribution of the distance traveled by all settled larvae was skewed to the right, with the tail extending $>$ 400 km for the total distance traveled (Fig. 6.7A) and $\sim$ 350 km for the linear displacement (Fig. 6.7B). Such a tail corresponds to the small number of larvae that settled far from their release location. For the total distance traveled, the mode of the distribution was at$\sim$ 85 km (Fig. 6.7A), whereas for the linear displacement it was at $\sim$ 20 km (Fig. 6.7B).

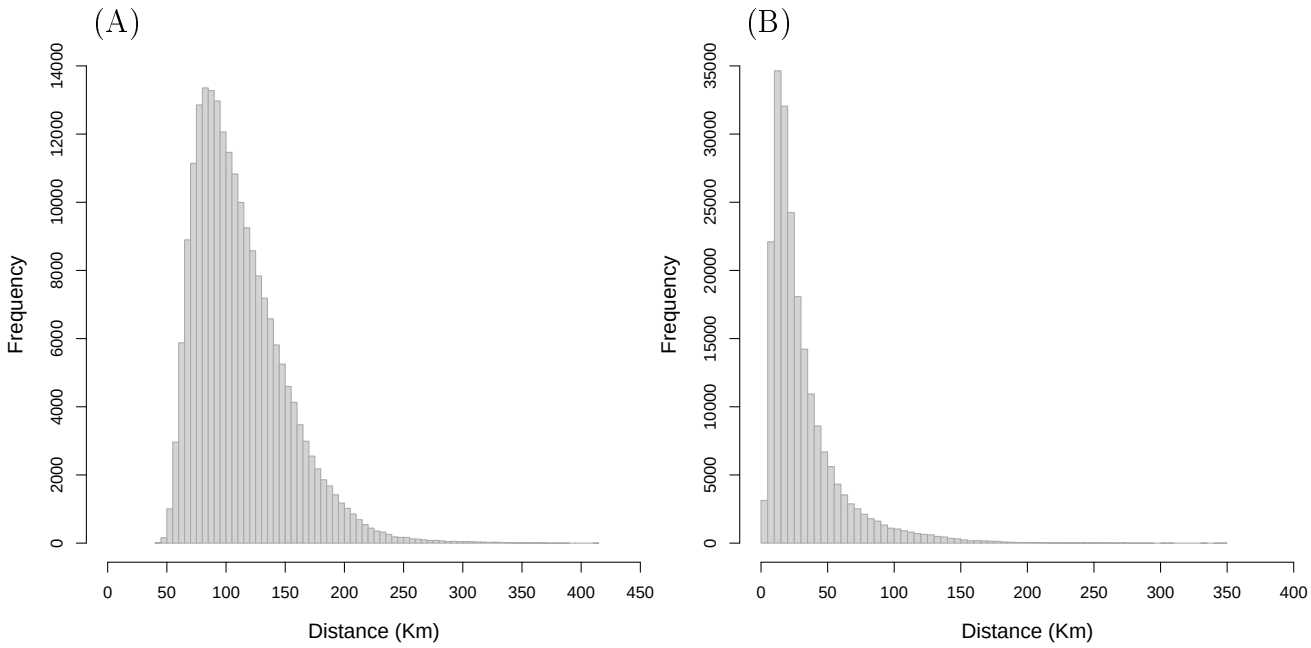

Figure 6.7: Frequency distributions of (A) total distance traveled (km) and (B) linear displacement (km) by all settled simulated larvae.

Morlet wavelet analysis of normalized daily time series of simulated larval coastal settlement shows low power (dark blue spectrum) over < 10 day periods (Fig. 6.8). There was high power (red spectrum), for a period of 14 to 16 days throughout the time series except in May $-$ June. This period of 14 days coincides with a semi-diurnal tidal cycle being dominant in the region. However, this period is only identified as significant in March and for two other short terms in late August and early November.

There were two significant high power spectra with periods of $30-32$ days in February$-$March and in September$-$October. The edges of these two periods were found in the region of the cone of influence. There was another significant high power period of $\sim$ 120 days from late April to November ($\sim$ 7 months), but most of it was in the region of the cone of influence (Fig. 6.8).

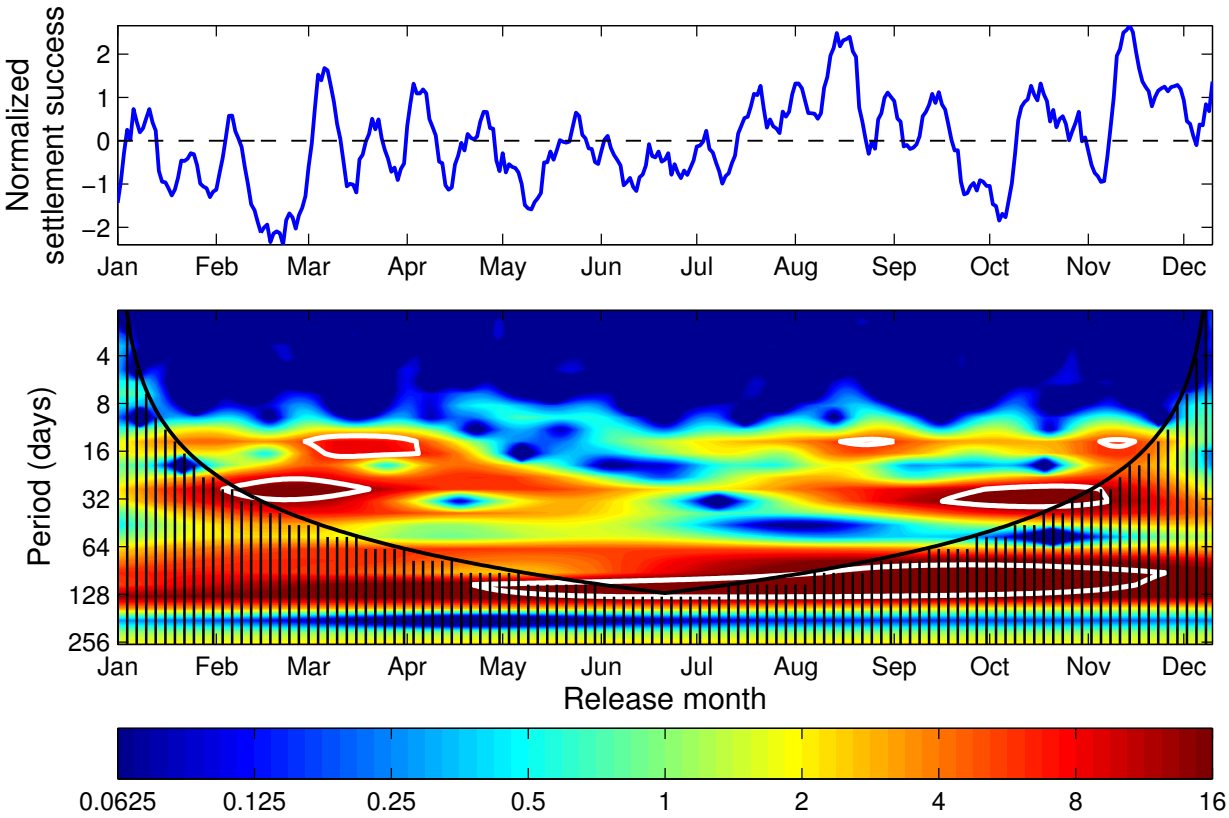

Figure 6.8: (Upper panel) Time series of normalized daily settled simulated larvae. (Same as the reference experiment depicted as black line in Fig. 6.2A, but normalized and for larvae released every day instead of every 3 days.) (Lower panel) the Morlet wavelet power spectrum. White line encloses the statistically significant region, with greater than 95% confidence level for red noise. Black lines indicate the region where edge effects of the finite time series become important, i.e. the cone of influence, region below thick black line.

6.3.2 Influence of DVM, tides and river input on larval settlement

Simulation experiment with DVM

There was a significant difference in mean larval settlement with and without DVM (Table. 6.1), with mean percentage with DVM (12%) being lower than without DVM (18%). This was consistent throughout the time series (not shown). The two time series were positively and significantly correlated ($r_{113} = 0.58$, $p < 0.001$).

Patterns of the origin and destination of settled larvae were qualitatively similar with and without DVM (Fig. 6.9A−C1). There were negative differences in the origin and destination of settled larvae with and without DVM all along the Sofala Bank, except at both the southernmost and northernmost edges (Fig. 6.9, A−C1).

Simulation experiment without tides

There was a significant increase in mean simulated larval settlement from the reference experiment with tides (18%) to the experiment without tides (23%) (Table. 6.1). The two experiments were significantly correlated ($r_{113} = 0.30$, $p < 0.001$).

The comparison between the experiments without and with tides shows that the difference in the origins of the settled larvae was generally positive, with larger differences offshore and to the south (Fig. 6.9, A2). Inshore, the differences were near zero or slightly negative, except in the southern region between $20° - 20°30'$S, where a large negative difference was obtained. These positive offshore and negative inshore differences contribute to a weaker inshore−offshore gradient in the origin of settled larvae without tides than with tides. The differences in larval settlement were mostly positive too, with largest differences in the south (Fig. 6.9, B2 and C2). There were negative differences at the northernmost limit and at 20°15′S.

Simulation experiment with river inputs

When river inputs were added to the reference simulation, there was a significant difference in the mean larval settlement (Table. 6.1), with a decreased mean percentage of settled larvae with river inputs (16%) than without river inputs (18%, reference). The two experiments were significantly correlated ($r_{df=113} = 0.38$, $p < 0.001$).

When the experiment with river inputs is compared to the reference experiment without river inputs, negative differences in the density of origin of settled larvae are obtained in a large area around the Zambezi River (between $17°30' - 19°$S) and another at the Beira Bay River ($\sim 20°$S) mouths (Fig. 6.9, A3). Fig. 6.9, A3 also shows that the differences tend to be positive offshore and negative inshore, which suggests that the inshore−offshore gradient in the origin of settled larvae is weaker with river inputs than without. There were large ($> 20\%$) negative differences in the same regions (Fig. 6.9, B3 and C3). Relative positive differences were obtained on the northernmost ($\sim 10\%$) and southernmost ($> 20\%$) portions of the bank. Smaller ($< 5\%$) negative or positive differences were found between the aforementioned regions.

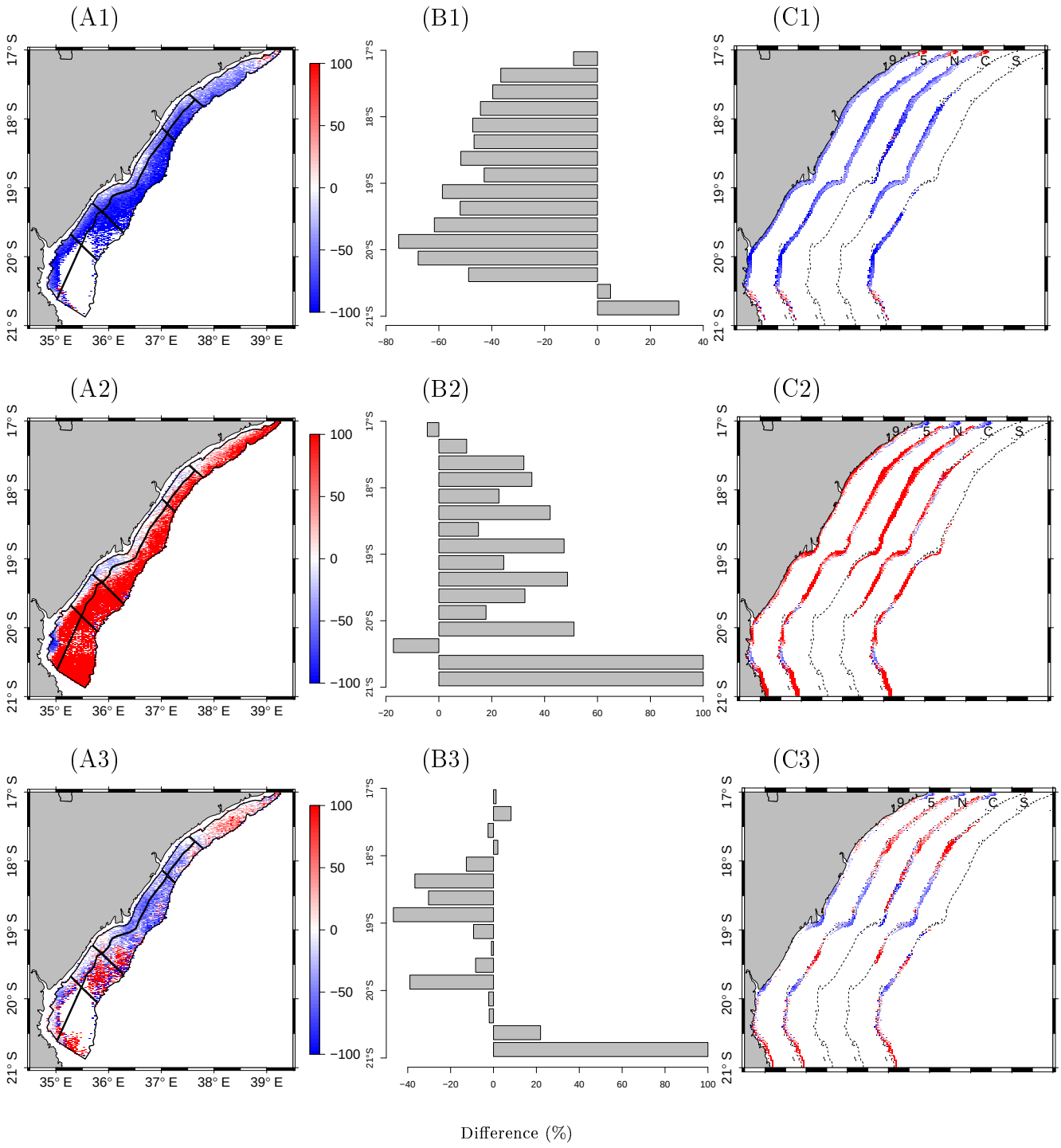

Figure 6.9: Same as in Fig. 6.4, but for relative difference (%) between the reference experiment and each factor experiment: (1) DVM; (2) NoTides and (3) River.

6.4 Discussion

This study shows that simulated larval dispersal and shelf retention of banana shrimp larvae on the Sofala Bank were significantly sensitive to changes in both spatial and temporal resolutions of the ROMS outputs, which were used to run the simulations (Appendix. F). This is congruent with recent studies that compared various sets of spatial and temporal resolutions of hydrodynamic model outputs that were used to run larval simulations (Blanke et al., 2012; Putman and He, 2013). Their studies showed that coarsening either spatial or temporal resolution slowed down (or increased travel time of) the simulated particles. Moreover, this promoted local retention of particles while it decreased connectivity with distant sites. Similarly, in the present study, the highest simulated larval shelf retention was obtained for the coarsest spatial and temporal resolution (Fig. F.1). Indeed, the simulated larval shelf retention decreased for finer spatial resolution, and decreased again with finer temporal resolution (Fig. F.1).

Putman and He (2013) compared trajectories of simulated particles with *in-situ* near-surface drifters. Their study demonstrated that coarsening the spatial resolution of the model output had less influence than coarsening the temporal resolution. Similarly, here it was shown that changing the spatial resolution from 6 to 2 km had a smaller effect on simulated larval shelf retention than changing the temporal resolution from 3 days to 1 hour. The high-resolution (hourly averaged) ROMS outputs resolved short-time coastal processes such as tides, eddy-associated filaments and meander currents (Chapter 4). Such processes were otherwise not well resolved nor preserved in the 3-day averaged ROMS outputs (Chapter 4). These important processes of the coastal regions are known to govern larval dispersal and retention. However, coarsening either spatial or temporal resolution did not affect the simulated larval dispersal and shelf retention patterns (Fig. F.1). Only the numbers of retained larvae changed, i.e., there was no qualitative effect. There is a positive correlation between simulated shelf retention using coarser and finer spatial−temporal resolution. Nevertheless, to simulate larval dispersal, the use of fine model resolution that preserves local processes is preferable (Putman and He, 2013).

This study shows that there is a positive correlation between simulated larval shelf retention and coastal settlement (Fig. 6.2). This supports the hypothesis ($H_{6.1}$) that high and low mean simulated larval shelf retention were linked with subsequent high and low mean coastal settlement, respectively. This result suggests that the influence of eddies on the shelf retention identified in Chapter 5 also generally applies to coastal settlement. At times, however, there was high shelf retention that was not necessarily associated with subsequent high coastal settlement. This suggests eddy conditions that are favorable for shelf retention but not for coastal settlement.

The mean simulated larval settlement (for all experiments) was relatively higher than expected. This quantitative discrepancy is explained by 30% of transport to the coast being caused by horizontal random diffusion, as illustrated in the results for an experiment without diffusion (Appendix. G). Since diffusion did not affect simulated larval dispersal and transport patterns, these study results can be qualitatively accepted (Fig. G.1). Moreover, horizontal diffusion has been recommended in many biophysical dispersal models (Rothlisberg et al., 1983; Peliz et al., 2007; Robins et al., 2013).

With respect to the relative contributions of the different release areas to the settled simulated larvae, there were some similarities when releasing inshore in the actual spawning areas and the non-spawning areas (Fig. 6.3). The mean contribution of the north-central release area (area 2, non-spawning) was not significantly different from that of the central release area (area 3, actual spawning). Similarly, the mean contribution of the northern release area (area 1, actual spawning) was not significantly different from the south-central release area (area 4, non-spawning). This result does not support the hypothesis that, by natural selection, adults (of migratory animals) reproduce in locations with favorable conditions to successful recruitment of their offspring (Putman et al., 2010). Indeed in the present study, the area that led to the highest simulated larval settlement (area 2, on average 52%) was a region where banana shrimp generally do not spawn (Chapter 2). In contrast, the lowest value was from an actual spawning area (area 5, in average $< 15\%$ of successful settled larvae). It appears that, regardless of the location of the release area, the contribution of the inshore area was larger than the adjacent offshore area. This result is consistent with the observed distributions of spawning, with higher

concentrations of mature females inshore than offshore (Chapter 2).

Interestingly, for all experiments with tidal forcing (Fig. 6.4A; Fig. 6.9, A1; and Fig. 6.9, A3), simulated larvae released off Beira Bay, at the south, did not settle much into the coastal region. Only $< 10\%$ of the simulated larvae originated from that area settled. Snapshots of larval trajectories (e.g. reference simulations, Figs. 6.5B−C, and 6.6) revealed that simulated larvae moved back and forth, with a semi-diurnal tidal frequency. During such movements, larvae that originated from the northern and central release areas displayed a considerable net displacement (Fig. 6.6A and B). In contrast, larvae from the southern release areas exhibited little displacement (Fig. 6.6C). This result indicates that larvae off Beira are trapped, nearly at the same place, by the strong sinusoidal tidal oscillation. It has been shown that the region off Beira has the largest tidal amplitudes and the strongest tidal currents on the Sofala Bank (Chevane, 2013 and Chapter 3). Consequently, the mean current is nearly zero (Chapter 3). This supports a tide-trapped, quasi-stationary larval pool (high retention), with little movement to the coast (low settlement). Similar results of tides retaining larvae were reported in other coastal ecosystems around the world, e.g. for scallops on Georges Bank (Tian et al., 2009a,b) and for polychaetes in the Bay of Mont Saint-Michel (Dubois et al., 2007). In their results, however, the tidal residual currents recirculate in a gyral motion promoting larval retention and future settlement in place. For the experiment without tides, the back and forth movement is not apparent (not shown), and more simulated larvae released off Beira settled (Fig. 6.9, A-C2).

There were three important regions for successful settlement of simulated banana shrimp larvae on the Sofala Bank: (1) a northern area centered at $\sim 17°30'\mathrm{S}$, (2) a central region off the Zambezi River mouth, centered at $\sim 19°\mathrm{S}$ and (3) a minor region, to the south off Beira Bay (Fig. 6.4B and C). This supports the hypothesis ($H_{6.2}$) that patches of high simulated larval settlement occur along the Sofala Bank coast. These three regions are particularly apparent when larvae are released from the actual spawning areas (label 5 in Fig. 6.4C). These three regions appeared consistently in all sets of experiments, although small variabilities were apparent (Fig. 6.9). These high settlement locations (latitudes) were not dependent on the number of larvae originally available. An attempt to weight the latitude bins for settlement by

the total number of larvae released at the latitude failed, because it requires the assumption that larvae settle at the same latitude at which they were released, which is not always the case. The best locations for larval settlement have been reported in other biophysical modelling studies, e.g. for lobsters in Australia (Feng et al., 2011).

Many factors have been proposed to influence larval transport and the settlement of marine organisms. Here, based on the results obtained in Chapter 5 and analyses of simulated dispersal patterns (Figs. 6.5 and 6.6), we can postulate the following: simulated larval settlement locations, particularly the northern and central regions, are primarily explained by the Mozambique Channel eddies and rings. Eddies or rings influencing larval dispersal, retention and settlement of marine organisms have been reported in many studies (e.g. Gutierrez et al., 2004; Adams and Flierl, 2010; Robins et al., 2013; Vaz et al., 2013). However, depending on the relative polarity of eddies, their strength and proximity to the shelf (Chapters 3 and 4), eddies can have different impacts on larval settlement success. On one hand, eddies induce a westward current that entrains simulated larvae towards the coast, favoring settlement (e.g. Fig. 6.5, A1 and A4). On the other hand, strong eddies induce strong currents that reach near the coastline, which can sweep most larvae away from the coastal settlement zone (e.g. Fig. 6.5, A2). Additionally, in the absence of eddies, the current velocities were weak and there was not much westward drift of larvae. Consequently, the numbers of simulated larvae reaching the coast and settling was low (e.g. Fig. 6.5, A3). Similarly, the third important settlement region is enclosed in the Beira Bay, thus protected from the influence of offshore eddies (Chapters 3 and 4). As result, there was not much westward drift of larvae and the subsequent simulated settlement was low compared to the northern and central regions.

Robins et al. (2013) also found high dispersal of larvae exposed to high-energy environments and, as a consequence, low coastal retention and settlement. Their study considered successful settlement as self-recruitment within 10 km of any release location. Thus, their settlement success was directly proportional to retention. Here we considered a settlement area distinct from the release areas, hence high retention did not necessarily lead to high settlement. Furthermore, Robins et al. (2013) noted that baroclinic currents associated with an oceanic gyre increased larval dispersal in tidally calm environments. Their result is congruent with the present study,

particularly, for the northern and central regions, where dynamic eddy and ring circulation dominates the relatively calm tidal current. In contrast, in the south, where the tidal currents are strong, the influence of eddies on simulated larval dispersal and settlement was weak.

A link between larval settlement and tides has been found in other biophysical modelling studies. For instance, Ayata et al. (2009) found high settlement success of *Sabellaria alveolata* larvae in an intertidal reef in the east of the bay of Mont Saint-Michel related to the neap−spring tidal cycle, particularly at neap-tides. In contrast, in the present study, although simulated larvae traveled with a semi-diurnal ($\sim$ 6 hours) tidal frequency (Fig. 6.6) due to strong flood-ebb tidal currents, tides alone were not identified as particularly important for simulated larval settlement on the Sofala Bank. Wavelet analysis does not show tidal influence, except the fortnightly ($\sim$ 14 days) period, which corresponds to the spring-neap tidal cycle, but was only observed for short terms (Fig. 6.8). Marinone et al. (2004) used a similar Lagrangian model approach to investigate larval dispersal of *Litopenaeus stylirostris* and *Farfantepenaeus californiensis* shrimps in the northern Gulf of California (they are penaeid shrimp species similar to banana shrimps). Although the dominant semi-diurnal tide amplifies in that region, they found no significant tidal effect on the number of larvae reaching the nursery areas. Therefore, the hypothesis ($H_{6.3}$) that patches of elevated simulated larval settlement is related to tides (alone) is not supported.

In the present study, the mean simulated larval settlement was, on average, higher for simulations without tides than with tides (Fig. 6.9, A-C2). When tide was removed from the reference experiment, a significant increase of settlement occurred for larvae released in offshore spawning areas (Fig. 6.9, A2). By contrast, larvae released inshore showed a relatively decreased settlement success (Fig. 6.9, A2). It has been shown that the interaction of barotropic tides with bottom topography induces vertical mixing in the water column (Dmitrenko, Igor A. and Kirillov, Sergey A. and Bloshkina, Ekaterina and Lenn, Yueng-Djern, 2012; Ffield and Gordon, 1996; Ragueneau et al., 1996), particularly on the Sofala Bank (Chevane, 2013), associated with baroclinic tides and internal waves (da Silva et al., 2009). It is suggested that such a vertical mixing acts as a barrier that inhibits larvae released offshore from moving towards the coast.

Many *in-situ* and model based studies suggest that larval behavior, such as diel vertical migra-

tion, enhances larval supply to suitable coastal and estuarine nursery areas (e.g. Rothlisberg et al., 1983). In contrast, Morgan et al. (2011), with *in-situ* observations of many plankton species, found that larval behavior did not substantially enhance larval retention and recruitment of crustaceans in Bodega Bay, North California. Here, diel vertical migration significantly decreased simulated larval settlement (Fig. 6.9, A-C1). The hypothesis ($H_{6.3}$) that diel vertical migration (alone) promotes settlement of simulated larvae of banana shrimps on the Sofala Bank is not supported. Larvae performing vertical migration spent 12.75 hours during the day at the sea bottom under calm current conditions, leading to weak net movement. The current field decreases vertically from a maximum at the surface to a minimum at depth (Chapter 3). At night, larvae spent 11.25 hours at the surface exposed to both flood-tide and the subsequent reversed ebb-tide, particularly off Beira Bay, thus not enhancing larval transport to the coast.

In order to enhance larval transport towards the coast and hence promote larval settlement, larval behavior could alternatively be a combination of diel vertical migration and tidal migration. This would involve selective tidal stream transport such that larvae only stay at the surface during the night flood tide (but not during ebb), thus favoring unidirectional larval transport towards the coast (Rothlisberg et al., 1983; Forbes and Benfield, 1986; Hill, 1991; Rothlisberg et al., 1995; Marinone et al., 2004; Criales et al., 2007; Queiroga et al., 2007). It has been suggested that larvae of penaeid shrimps change from a diel vertical migration behavior to a tidal vertical migration at postlarval, stage to enter into the estuaries (Rothlisberg et al., 1983; Dall et al., 1990; Rothlisberg et al., 1995; Criales et al., 2007). This study did not attempt to simulate postlarvae as they start to develop swimming abilities and the passive drift hypothesis is no longer applicable. Moreover, estuarine inlets were not represented in the ROMS outputs (as it is a coastal model). Thus, a selective tidal stream transport or tidal activity when postlarvae reach the estuaries was not considered here.

Penn (1975) argued that, regardless of tidal activity, shrimp larvae performing diel vertical migration would have a net inshore transport, promoting settlement during one half of the year (and net offshore transport for the other half). He suggested a mechanism in which larvae would move more inshore at night than offshore during the day, due to a night flood tide-dominant half of the yearly cycle (ebb tide dominated other half). This hypothesis is not supported in

the results, possibly because of the strong impact of the eddy circulation. Further investigation is necessary to clarify the roles of possible larval behavior to settlement success.

Most of the studies that have investigated the influence of rivers on penaeid shrimp focused on the effect of low salinity on larval development (e.g. survival), particularly for postlarvae (e.g. Kutty et al., 1971; Kumlu, 1998). Little attention has been given to the influences of the river plume on transport and settlement of shrimps in early larval stages. Peliz et al. (2007) showed that patterns of simulated crab larval dispersal change significantly with river plumes, promoting offshore dispersal. Similarly, in this study, simulated larval transport and settlement of banana shrimps are sensitive to river inputs. The mean simulated larval settlement was significantly lower for the experiment with river inputs than without rivers, especially near the main river mouths (Fig. 6.9, A-C3). There is a positive inshore−offshore gradient in the relative differences in the origin of settled larvae with and without river inputs. This result indicates that the influence of river inputs is coastal, which corroborates with plume structure (Chapter. 3 and 4).

The Beira Bay and the Zambezi River buoyant plume, radiate relatively strong currents in all directions from their river mouths (Chapter. 4). This promotes larval dispersal away from the river mouths, and consequently reduces the chance of larvae settling near the river mouths. On the other hand, the river plume increases the along-shore larval dispersal and settlement (excursion) to both sides of the river mouth, particularly to the north in the case of the Zambezi River (positive difference in Fig. 6.9, C3 label C). Moreover, the Zambezi River surface buoyant plume and the associated low-salinity front represent a barrier for pelagic larvae released at the north to settle further south (negative difference in Fig. 6.9, C3 label N). These are supported by a bidirectional plume that dominates northwards in the propagation direction of the Kelvin wave (Chapter 3−3.4 and Nehama, 2012). Since the hydrodynamic model used to couple the IBM underestimate the offshore extent of the river plumes, caution needs to be exercised when interpreting the influence of the plumes on the simulated larval settlement.

In summary the simulated larval shelf retention was positively correlated with simulated larval coastal settlement. However, high shelf retention was occasionally associated with low coastal settlement. Most of the simulated settled larvae come from the inshore region and there was no

difference between release in the actual or the non-spawning areas. Three important locations for simulated larval settlement were identified: (1) northern, (2) central and (3) southern. The settled larvae mainly drifted southwestwards, traveling on average $\sim$ 85 km. The simulated larval transport is primarily controlled by the highly energetic offshore eddy activity of the Mozambique Channel. The results indicate that, in the absence of such eddies, there is no movement, consequently the coastal settlement is low. This mechanism was not previously proposed for penaeid shrimps, particularly not for banana shrimp on the Sofala Bank, although it has been proposed for other marine organisms in similar high energetic regions around the world. This study indicates that, contrary to what was previously believed, tide alone is not particularly important for simulated penaeid shrimp settlement. In fact, a tide-induced larval pool, favorable for shelf retention yet unfavorable for coastal settlement, was identified. In the case of the diel vertical migration experiment, the mean simulated settlement was lower with DVM than without DVM. A selective tidal stream transport for postlarvae not explicitly incorporated in the simulations should further clarify the role of DVM in larval coastal settlement. Buoyant river plumes and associated low-salinity fronts are critical processes in larval settlement patterns. They promote dispersal, while being unfavorable for settlement, particularly in the vicinity of river mouths.

Chapter 7

Synthesis and conclusion

Due to limited observational data in the study area, the Sofala Bank of Mozambique, the present thesis is mostly based on numerical models. A high-resolution two-way nested coastal ocean circulation model of the Sofala Bank was developed. Comparisons between this circulation model, available observational data and literature agree reasonably well. These model outputs were used to set up a coupled biophysical, individual-based model for early life stages of banana shrimps on the Sofala Bank. At present, no observational data are available to evaluate the biophysical model outputs directly. The biophysical model was based on spawning patterns identified from both commercial and research data, analyzed within this thesis. The results of the two models and the biological data are synthesized in the following sections, focusing on processes of ocean circulation and structure and their putative effects on early life-history stages of banana shrimps on the Sofala Bank.

Sofala Bank circulation

Since 2000, there have been a number of studies on the complex, passing offshore eddy activity of the Mozambique Channel (Chapter 1). However, there is little information about the influences of these mesoscale eddies on the shelf and coastal regions. The Mozambique Channel system is unique because of the absence of a western boundary current like the Kuroshio, East Australia

Current, Gulf Stream, Brazil Current and Agulhas Current. Therefore, the eddy and mean-flow interactions observed in the major western boundary current systems do not apply to the Mozambique Channel. Recent observational studies by Roberts et al. (2014) and Ternon et al. (2014) surveyed episodic events of eddies and, from these, suggested that eddies may influence the shelf circulation. They recommended that long-time observations are needed for confirmation of this influence. In the absence of long-term observational data, the present study uses seven years of high-resolution model outputs and presents new insights on eddy-induced shelf circulation on the Sofala Bank.

Firstly, the model results presented here confirm that offshore eddies influence the shelf circulation and their impact can reach as far as near the coast. The nature of the eddy influence depends on the eddy's strength and proximity to the shelf (or coast). Secondly, offshore mesoscale eddy activity impacts river plume structures, more precisely, their direction. This influence is particularly strong for the Zambezi River, which is highly exposed to offshore eddy activity. The river plumes themselves influence the coastal circulation within the buoyant plume. On the other hand, eddies have limited influence off Beira Bay ($\sim 20°$S), where tidal currents dominate the circulation. These influences of eddies contrast with the limited role that the wind-induced coastal circulation appears to have on the Sofala Bank circulation. This bank is characterized by weak winds of the transition from the East Africa monsoons to the trade wind regime, which explains their weak influence.

The main processes of the ocean circulation identified in this thesis allow the development of a conceptual model of the circulation on the Sofala Bank, especially in relation to the complex mesoscale eddy field, river plumes and tides (Fig. 7.1). Because of the variable and complex nature of the Mozambique Channel eddies, it is difficult to ascribe a single, clear cartoon illustrating the key processes of the Sofala Bank circulation. Therefore, a series of cartoons that highlights different situations and distinct processes is presented. The model results indicate that strong cyclonic eddies close to the shelf induce strong equatorward currents over most of the shelf except off Beira Bay, where a strong tidal current dominates (Fig. 7.1A). In this situation, the cyclonic eddy-induced shelf current is coincidentally in the same direction as the dominant northward Zambezi River plume. There was little evidence that the eddy influences

this plume direction. The northward plumes are simply explained by the Coriolis force that, for the southern hemisphere, deflects the river input to the left of the river mouth. In addition, the Coriolis force keeps the northward plume attached to the coast, resulting in a coastal plume that extends as far as the Licungo River mouth. The Zambezi River plume results in a circulation that is distinct from that outside the plume. The plume recirculates into a small coastal anticyclonic eddy at the river mouth, the bulge plume circulation, similar to that observed in other river plumes (Chao and Boicourt, 1986; Horner-Devine, 2009).

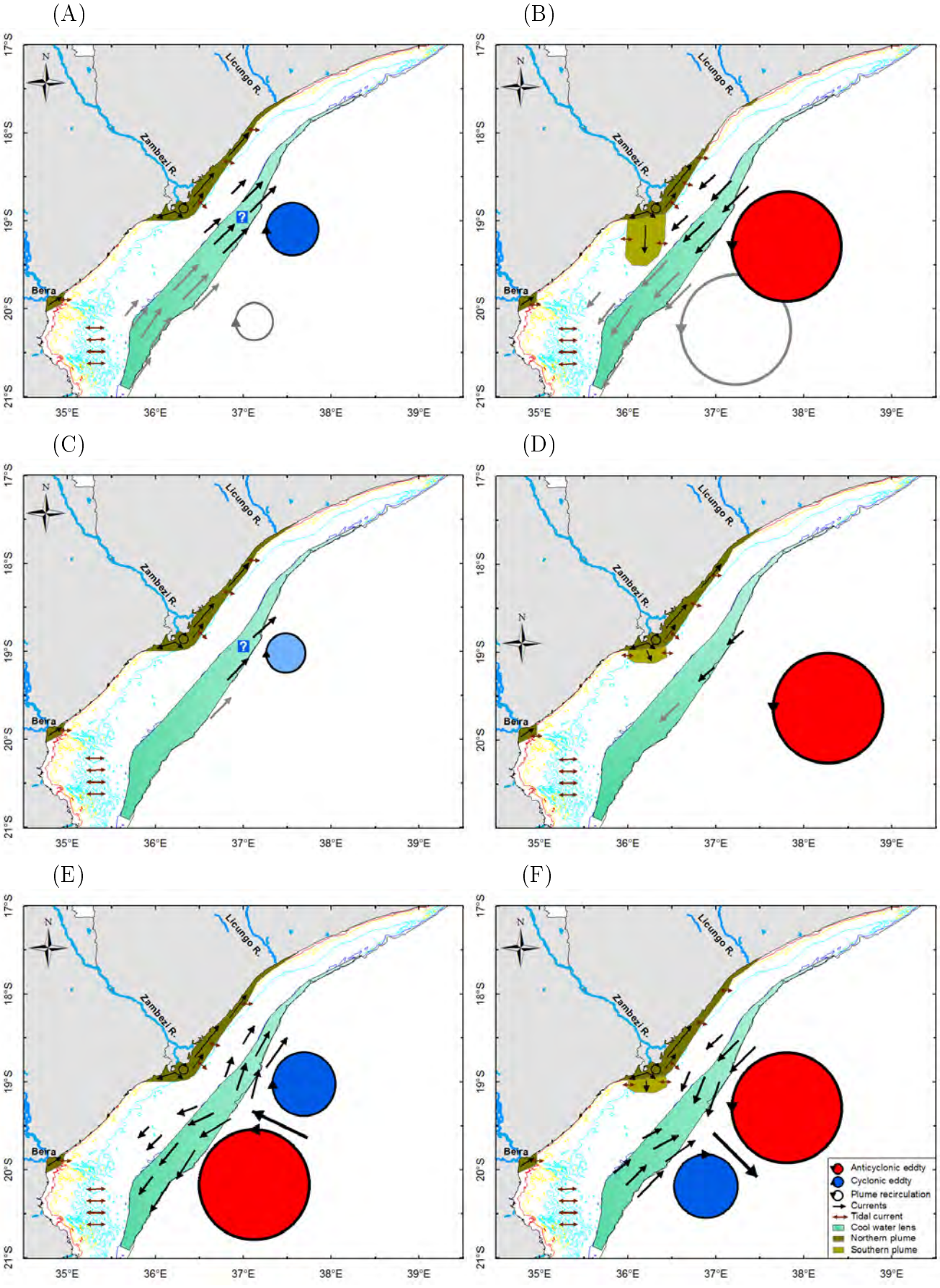

Figure 7.1: Fig 7.1. A conceptual model of the processes of circulation of the Sofala bank, especially in relation to offshore passing mesoscale eddies, river plume and tides. ? – uncertainty in the link between the cyclonic eddy and the cool water lens.

Anticyclonic eddies induce a poleward current (Fig. 7.1B). Such eddies erode the northward–directed coastal plume, separating the small plume of the Licungo River from the Zambezi plume. A southward plume appears to the south of the Zambezi River mouth. The Coriolis force keeps the southward plume detached from the coast, in contrast to the coastal northward plume. Note that while the northward plume can appear alone (Fig. 7.1A, C and E), the southward plume does not (Fig. 7.1B, D and F); the southward plume occurs simultaneously with the northward plume, resulting in a bi-directional plume similar to that observed for the Columbia River (Hickey et al., 2005). The predominately northward plume of the Beira Bay rivers remains unaffected by the presence of eddies, being far onshore and protected from their influence.

Eddy strength and proximity to the shelf play fundamental roles in determining their impacts on the coast. Strong eddies close to the coast impact the coastal circulation significantly whereas weak, early–generated or decaying eddies close to the shelf (e.g., Fig. 7.1C) or strong eddies far offshore (e.g., Fig. 7.1D) have little impact on the coastal circulation and river plumes. In these scenarios the eddy influences are limited to the shelf-break.

The eddy field of the Mozambique Channel is more complex than the occurrence of just a single eddy. Instead, a continuous train of eddies with different rotations (dipole or tripole) is often observed (Schouten et al., 2003; Tew-Kai and Marsac, 2009; Roberts et al., 2014). Such a train of eddies is generally characterized by two distinct types of dipoles (1) with the cyclone to the north and (2) with the anticyclone to the north. Provided the dipole is sufficiently strong and close to the coast, for the dipole with the cyclone to the north there is a strong shoreward current (Fig. 7.1E). When this current reaches the shelf it diverges into two branches, one northward and the other southward. In contrast, for the eddy dipole with the anticyclone to the north, a southward and northward current meet between the two eddies, generating a strong offshore current (Fig. 7.1F). The southward current of the anticyclone induces a southward Zambezi plume, but the northward current of the cyclone inhibits the plume from expanding further south. Again, in the dominant tidal region off Beira, the eddy dipoles have little influence on the circulation and river plume.

Another important oceanographic feature of the Sofala Bank identified in this thesis is the surface, cool water (decrease by $\sim 1°C$) lens between the mid-shelf and shelf-break (Fig. 7.1). The model results revealed that although the surface cooling is enhanced for the simulations with tides, it still occurs in the simulations without tides. The cooling also coincides with the onshore edge of the avenue of propagating eddies, following the 200 m isobath on the Mozambican slope (Hancke et al., 2014). Vertical sections show that the poleward currents generated by anticyclonic eddies interact with the shelf-slope to raise the isotherms, stratifying the water column and bring deep, cool water up to mid-depths. Onshore, tides acting on the stratified water column generate internal tides and short waves, which lead to vertical movement and mixing, bringing the cool water to the surface.

The role of cyclonic eddies on the cool water lens is not fully understood (? in Fig.7.1A and C). Although deep cool water can be upwelled in the core of a cyclonic eddy, the cyclone edge interaction with the shelf generates an equatorward current that results in downwelling of the isotherms, thus no cool water is made available sufficiently close to the surface for the tidal mixing to bring it there. A model circulation experiment without eddies could clarify the general influence that cyclonic eddies have on the cool water lens. Tides constantly influence the cool water lens by moving it offshore and back shoreward at a tidal frequency, i.e., ~ 6 hours for the semi-diurnal tides observed on the bank. A similar tidal influence is found on the rivers plumes.

In summary, this thesis shows that offshore eddies in highly energetic regions, such as the Mozambique Channel, can strongly modulate the shelf and coastal circulation and structures by creating variable currents in space and time when the eddies interact with the shelf. This is hypothesized to be important for coastal ecosystems and fisheries by entrainment of pelagic larvae of marine organisms to areas that are potentially unfavorable to their growth and survival. However, the effect of offshore eddies is likely low when there is a strong background current, such as caused by tides in the case of the southern Sofala Bank or, by extension, jet currents of the Gulf Stream and Kuroshio.

Larval transport, retention and settlement of banana shrimps

The results presented in this thesis provide important insights into the processes related to spawning, dispersal, transport, retention and settlement of simulated larvae of banana shrimp species in a shelf environment affected by a highly energetic and complex eddy system. The specific hypotheses listed in the introduction (Chapter 1) and described at the beginning of each relevant chapter (2, 4, 5 and 6) have been tested and accepted or rejected in the corresponding chapters. The present section focuses on the main hypothesis of this thesis, namely that eddies can transport shrimp larvae offshore to regions where they are unable to survive and are thus lost. The individual-based model (IBM) results indicate that simulated larvae may be transported offshore by passing mesoscale eddies (Chapters 5 and 6), therefore supporting the main hypothesis. Conditions which are favorable to this transport offshore have been identified, which have resulted in the development of a conceptual model of early life history dynamics of banana shrimps on the Sofala Bank (Fig. 7.2), detailed below.

The first element to consider is spawning. Similar to other tropical regions in the world, spawning of the two banana shrimp species occurs year-round on the Sofala Bank, but increases at certain periods (Fig. 7.2). For *Fenneropenaeus indicus*, two periods of increased spawning activity are identified, a minor one in late-summer and autumn and an other in late-winter and spring, with optimal environmental conditions for larval development during summer. This can explain why the peak of recruitment into the fishery in March-May comes from the second, increased, spawning activity period of the year (de Sousa et al., 2006, 2013). For *Metapenaeus monoceros*, spawning increases in summer and decreases in winter in relation to cool temperatures. A similar decrease is observed at the inter-annual scale for years following a severe winter. This implies that severe winters result in low recruitment into the fishery and, consequently, low catches of *M. monoceros*. Simulated larval retention on the Sofala Bank supports this statement, with massive simulated mortality at assumed low lethal temperatures of $23 - 25°C$ in winter, but not in summer, except in the presence of cool cyclonic eddies.

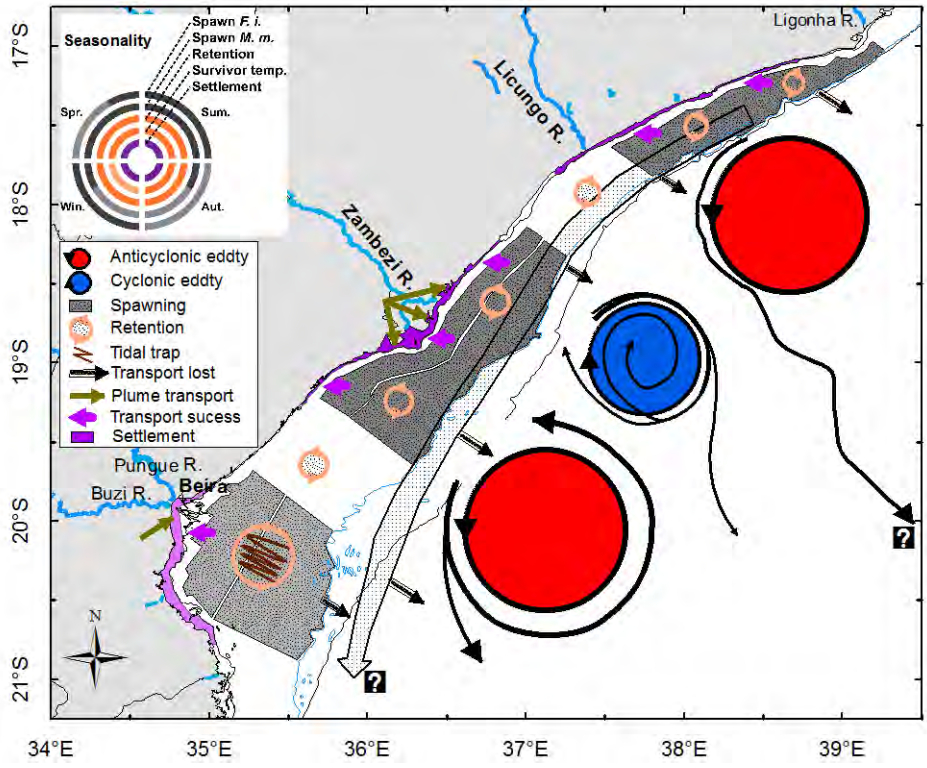

Figure 7.2: A conceptual model of early life stages of banana shrimps (*F. indicues* and *M. monoceros*) on the Sofala Bank. ? indicates unsure on final destination to the east and south. The schematic rings (top left) indicate the processes/factors temporal variability (seasonality). Light colors indicate weak/decreased patterns and dark colors strong/increased ones.

Three principal spawning areas (northern, central and southern) were identified for banana shrimps on the Sofala Bank, based on high abundances of mature females, using the annual research cruise survey data (Chapter 2). Note that these data are limited to the summer and do not provide information about the seasonality in spawning locations. However, considering that banana shrimps spawn year-round, these spawning areas can be potentially used throughout the year. There was little inter-annual variability in spawning areas. All three areas are located close to river mouths. However, no relation with environmental factors, especially low salinity that could explain that distribution, was found. It is hypothesized that the link between spawning areas and rivers is related to substratum type and associated organic matter content. Sediment samples are needed to test this hypothesis. The hypothesis suggesting that adult shrimps naturally select these locations for spawning to ensure favorable environmental conditions for successful larval transport into the coastal and estuarine nursery grounds, promoting settlement, is not supported. Simulated larvae originating from both spawning and non-spawning areas

have a similar chance of being retained and settling, according to the IBM results. However, simulated larvae originating from the offshore spawning locations, particularly those from the central and northern locations, which are more exposed to the offshore circulation, were found to have significantly less chance of settling into coastal areas.

Retention of simulated larvae in the spawning areas, as well as over the entire continental shelf, is generally high year-round, without evidence of seasonality. However, at times, episodes of decreased shelf retention occur, as a consequence of larvae being transported to the south or offshore by passing mesoscale eddies (Fig. 7.2). Conversely, these eddies occasionally provide mechanisms for westward transport of larvae towards the coast, promoting their settlement. In the absence of eddies, although shelf retention is high (Chapter 5), coastal settlement is much lower (Chapter 6) because of weak shoreward transport of larvae to the coast. Regions protected from offshore eddies have high shelf retention, but low coastal settlement year round. This is particularly true for the semi-enclosed region off Beira Bay. Moreover, simulated larvae released there were trapped in the strong tidal current, and hence were unable to contribute to coastal settlement. Interestingly, the field data indicate that the southern spawning area off Beira has the lowest intensity and the highest inter-annual variability in spawning compared to the other two areas. The southern region off Beira is supposedly the best location for shelf retention, but with such low subsequent coastal settlement, this spawning area was the worst among the three for the simulated banana shrimps on the Sofala Bank.

Three main settlement locations (northern, central and southern) were identified along the coast of the Solafa Bank, based on the biophysical model (Chapter 6). These areas are essentially adjacent to the main spawning areas, all of them being located around the river mouths (Fig. 7.2). The river outflow slightly decreased the simulated coastal settlement success within the buoyant plume compared to the simulations without rivers. It is found that the plume can (1) prevent the simulated larvae released in other regions from entering the vicinity of the river mouths and (2) disperse larvae, both offshore and alongshore. However, alongshore transport of larvae can increase coastal settlement in other regions. For example, the Zambezi River plume increases settlement to the adjacent northern region. Neither diel vertical migration nor tides alone were found to enhance settlement success. Alternatively, it has been proposed that a

selective tidal stream transport combining diel vertical migration and tidal migration, i.e., larvae migrate to the surface only during night flood tides, is needed (Rothlisberg et al., 1983; Dall et al., 1990; Hill, 1991; Criales et al., 2007). This mechanism, which is supposedly important for postlarval stages to enter into estuaries, was not considered in the present biophysical model. A biophysical model incorporating estuary inlet and selective tidal stream transport is needed to clarify the role of tides and vertical migration, but this would require the development of an estuarine circulation model with higher spatial resolution.

Regarding larval transport, it is difficult to propose general pathways due to the highly variable and dynamic nature of the eddy fields. No recurrent pathways were identified (Fig. 7.2), but instead a variety of pathways, even in the presence of apparently similar eddy fields. The timing of larval release relative to the eddy type (cyclone, anticyclone or dipole), position, proximity to the shelf, and strength, all play a role in determining the simulated larval trajectory. Larvae released a few days apart in the same eddy field occasionally had completely different trajectories. However, three notable aspects of transport were identified: (1) onshore, promoting settlement; (2) southwards, favoring both retention and loss; and (3) offshore, favoring loss. Larvae trapped in the edge of eddies occasionally had the chance to return to the shelf, contributing to shelf retention and, potentially, subsequent settlement. However, these occasions and numbers were few. Other larvae transferred into the eddy core, especially cyclones, were lost.

Long-distance dispersal was sometimes observed for simulated larvae entrained in the eddy circulation or between eddies for their entire pelagic larval duration. A number of simulated larvae were found exiting the model domain at the easternmost limit close to Madagascar. Others were found exiting the domain within a few days at the southernmost limit, transported towards Maputo Bay and the Natal Bight further, south in South Africa. Due to limited model spatial coverage, the present IBM was unable to determine whether these larvae (? in Fig. 7.2) could reach other regional shrimp populations like Madagascar, Maputo Bay and Natal Bight. An IBM that covers a larger domain is needed to investigate the long-distance connectivity between the shrimp stocks in the region. On the other hand, there is likely some connectivity between the local stocks on the Sofala Bank, especially between the northern and

central release areas. This connectivity is unidirectional, southwards, in the same direction as eddy propagation. In contrast, there is very low simulated connectivity between these two areas and the southern spawning area, which is protected from the influence of offshore eddies. Hence, the southern area is relatively isolated on the bank, which raises questions about its self-persistence. The maintenance and recovery of this particular shrimp stock might depend strongly on its own spawning stock and capability to self-recruit, which are both relatively low.

In summary, the present thesis confirms that offshore passing eddies transport simulated larvae of banana shrimps offshore, decreasing shelf retention and coastal settlement, supporting the main hypothesis of this study. But it also shows that eddies can provide a means of onshore transport of larvae to settlement areas, compared with periods without eddies, an unanticipated result. This focus on the role of eddies in processes of larval transport, retention, and settlement, although clearly important for inter- and intra-annual variability, is unlikely to explain the observed continuous decline in banana shrimps catches on the Sofala Bank and in other similar regions around the world. Caution needs to be exercised when interpreting these results because the IBM experiments were based on climatological forcing.–

Recommendations for management and future research

The present section proposes recommendations for further research and management that could improve our understanding of the system and monitoring of the stocks of banana shrimps. Although some recommendations were made throughout the thesis, they are regrouped here. The climatological monthly winds used for the ROMS lack fine temporal resolution required to reproduce the wind-driven coastal currents accurately. To fully understand the role played by wind on the Sofala Bank circulation and ecosystem, an inter-annual ocean model configuration incorporating both realistic winds and the eddy field is needed.

The Sofala Bank is a key, historic fishing ground for penaeid shrimps and other commercially important marine resources in Mozambique and in the southwest Indian Ocean in general. However, besides the CTD data collected during annual summer research cruises, there is no other environmental data collection to help understand population and stock dynamics. There

is an urgent need to develop monitoring programs to collect mid- to long-term time series of relevant environmental data, like shallow water moorings to measure sea temperature, salinity, currents, etc. Besides potentially correlating with marine resources data, these environmental data would also be useful to increase our general knowledge of the oceanography of the bank and for evaluation of model, like the one developed in this thesis. It is also necessary to expand the CTD cruise stations to the northern Sofala Bank to cover all the fishing grounds.

The data for female ovarian maturity stages from the IIP annual research cruise survey have been combined as immature (stages I and II) and mature (stages III and IV) since 2007 (Chapter 2). Considering that these banana shrimps return to stage II after spawning, it could be more appropriate to consider stage I alone rather than combining stages I and II to investigate non-spawning individuals. In addition, to investigate spawning both temporally and spatially, it would be more relevant to use the very last maturity stage IV, just before or ready to spawning, rather than the combined stages III and IV. This indicates that the data can be used for a wider range of applications when disaggregated than when combined, and therefore it is recommended to return to the old (before 2007) four-stages data record. The cruise data, which is the only comprehensive georeferenced biological shrimp data from the Sofala Bank, is very valuable but limited to summer. Data covering other seasons are needed to investigate the seasonal variability of banana shrimp spawning on the bank.

Under continuously low recruitment into the fishery, since 2008 an increase in fishery closure from about three to six months has been implemented as a tool to prevent growth overfishing of shrimps and to test ways of decreasing fishing effort (de Sousa et al., 2009; Brito, 2010). In addition, closures during full moon periods and at the mid-season in July-August, when the lowest catch rates are attained in the fishery, have also been proposed as a profitability strategy that would reduce fuel and operating costs (Brito, 2010). This may pose challenges to the ability to monitor the shrimp resource by compromising the available traditional logbook data records from one long fishing season. As a result, additional research cruise surveys should be considered during these new fishery closure periods to avoid potential gaps in the datasets.

This is the first time that an individual-based model has been developed for the Sofala Bank. The model has progressively evolved from being a simple passive drift approach into incorporating additional factors like tides, rivers, larval behavior, etc., one at a time. Each time a new factor was added to the model, the results were analysed to identify its effect. This approach is necessary but time consuming, which prevented consideration of all these factors combined and testing of the potential influences of many others, like the selective tidal stream, Stokes drift, spatio-temporal variability in the spawning stocks and temperature-dependent growth or mortality. These remain aspects requiring further investigation. Even after considering all these remain aspects, the IBM approach only deals with the early life stages and a full life cycle modelling approach is also recommended for future research. Similarly, field studies on the full life cycle of the banana shrimps on the Sofala Bank is also recommended to validate the model results.

Field studies for sediment substratum type and organic content are needed to investigate the spawning preference of shrimps for the riverine environment. In addition, more studies to test the three simulated recruitment locations and the impact of eddies are needed. For example, one could try to correlate time series of satellite sea surface anomaly with historical catch, considering a 6 months lag covering the period from larval dispersal to recruitment into the fishery and other complexity about the catch. Due to the influence of remote forcing on the banana shrimps, it could also be interesting to correlate the catch with atmospheric tropical cyclones that impact the Sofala Bank every year, and with large scale climatic drivers like the El Niño Southern Oscillation Index and the Indian Ocean Dipole.

The offshore transport and loss of larvae challenge the traditional view of the life cycle of penaeid shrimps, in which offshore spawned larvae are transported shoreward to the coastal and estuarine nursery grounds. This general view is used in the management of many shrimp fisheries around the world, including the Sofala Bank. When managing this resource, it should also be considered that a large quantity of shrimp larvae may be lost in the event of large, strong, anticyclonic eddies close to the coast, with potential negative impacts on recruitment and catches. Since it takes about six to nine months for the larvae to recruit into the fishery, large strong eddies close to the coast can be monitored, for example using satellite altimetry

observations, and their detrimental effects on recruitment anticipated. Similarly, periods of absence of eddy activity also need to be carefully monitored. Another aspect that needs to be taken into consideration is the extreme winters, which can result in low summer reproductive outputs for *M. monoceros*. Finally, this thesis provides maps of three spawning areas (based on field data) and three coastal settlement areas (based on process-oriented models) for the two banana shrimp species on the Sofala Bank. These maps can assist in the integrated management of human activities on the bank.

References

Adams, D. K. and Flierl, G. R. (2010). Modeled interactions of mesoscale eddies with the East Pacific Rise: Implications for larval dispersal. *Deep Sea Research Part I: Oceanographic Research Papers*, 57(10):1163–1176.

Aktaş, M. and Kumlu, M. (1999). Gonadal maturation and spawning of *Penaeus semisulcatus* (Penaeidae: Decapoda). *Turkish Journal of Zoology*, 23:61–66.

Aktaş, M., Kumlu, M., and Eroldoğan, O. T. (2003). Off-season maturation and spawning of Penaeus semisulcatus by photoperiod, and/or temperature and eyestalk ablation in subtropical conditions. *Aquaculture*, 228(1-4):361–370.

Amanat, Z. and Qureshi, N. A. (2011). Ovarian Maturation Stages and Size at Sexual Maturity of Penaeus indicus (H. Milne Edwards, 1937) in the Lagoon Water of Sonmiani Bay, Balochistan. *Pakistan Journal of Zoology*, 43(3):447–459.

Anger, K. (2001). *The Biology of Decapod Crustacean Larvae*. Crustacean Issues 14. A.A. Balkema Publishers, The Netherlands.

Ayata, S. D., Ellien, C., Dumas, F., Dubois, S., and Thiebaut, E. (2009). Modelling larval dispersal and settlement of the reef-building polychaete Sabellaria alveolata: Role of hydroclimatic processes on the sustainability of biogenic reefs. *Continental Shelf Research*, 29(13):1605–1623.

Ayub, Z. and Ahmed, M. (2002). Maturation and spawning of four commercially important penaeid shrimps of Pakistan. *Indian journal of marine sciences*, 31(2):119–124.

Backeberg, B. C., Johannessen, J. A., Bertino, L., and Reason, C. J. C. (2008). The greater Agulhas Current system: An integrated study of its mesoscale variability. *Journal of Operational Oceanography*, 1(1):29–44.

Backeberg, B. C. and Reason, C. J. C. (2010). A connection between the South Equatorial Current north of Madagascar and Mozambique Channel Eddies. *Geophysical Research Letters*, 37(4):L04604.

Badawi, H. K. (1975). On maturation and spawning in some penaeid prawns of the Arabian Gulf. *Marine Biology*, 32(1):1–6.

Bailey, K. M., Stabeno, P. J., and Powers, D. A. (1997). The role of larval retention and transport features in mortality and potential gene flow of walleye pollock. *Journal of Fish Biology*, 51:135–154.

Bakun, A. (1996). *Patterns in the ocean. Ocean Processes and marine population dynamics. University of California Sea Grant, California, in cooperation with Centro de Investigaciones Biologicas de Noroeste, La Paz* .

Barbosa, F. M. A., Cuambe, C. C., and Bandeira, S. O. (2001). Status and distribution of mangroves in Mozambique. *South African Journal of Botany*, 67(3):393–398.

Barlow, R., Lamont, T., Morris, T., Sessions, H., and van den Berg, M. (2014). Adaptation of phytoplankton communities to mesoscale eddies in the Mozambique Channel. *Deep Sea Research Part II: Topical Studies in Oceanography*, 100(0):106 – 118. The Mozambique Channel: Mesoscale Dynamics and Ecosystem Responses.

Barnier, B., Siefridt, L., and Marchesiello, P. (1995). Thermal forcing for a global ocean circulation model using a three-year climatology of ECMWF analyses. *Journal of Marine Systems*, 6(4):363 – 380.

Baxter, K. N. (1963). Abundance of postlarval shrimp-one index of future shrimping success. In *Proc. Gulf Caribb. Fish. Inst*, volume 15, pages 79–87.

Bell, G. I. and Pratt, L. J. (1992). The Interaction of an Eddy with an Unstable Jet. *Journal of Physical Oceanography*, 22(11):1229–1244.

Benchoucha, S., Berraho, A., Bazairi, H., Katara, I., Benchrifi, S., and Valavanis, V. D. (2008). Salinity and temperature as factors controlling the spawning and catch of *Parapenaeus longirostris* along the Moroccan Atlantic Ocean. In Valavanis, V. D., editor, *Essential Fish Habitat Mapping in the Mediterranean*, volume 203 of *Developments in Hydrobiology*, pages 109–123.

Berg, M., Agasøster, M., Grammeltvedt, E., and Gas, T.-N. (2012). Natural gas in east africa. *Department of Petroleum Engineering and Applied Geophysics, NTNU.*

Bernal, M., Stratoudakis, Y., Coombs, S., Angelico, M. M., de Lanzó s, A. L., Porteiro, C., Sagarminaga, Y., Santos, M., Uriarte, A., Cunha, E., Valdés, L., and Borchers, D. (2007). Sardine spawning off the European Atlantic coast: Characterization of and spatio-temporal variability in spawning habitat. *Progress in Oceanography*, 74(2-3):210–227. Ecological Functioning of the Iberian Seas: A synthesis of {GLOBEC} Research in Spain and Portugal.

Biastoch, A., Böning, C. W., and Lutjeharms, J. R. E. (2008). Agulhas leakage dynamics affects decadal variability in Atlantic overturning circulation. *Nature*, 456:489–492.

Biastoch, A. and Krauss, W. (1999). The role of mesoscale eddies in the source regions of the Agulhas Current. *Journal of Physical Oceanography*, 29:2303–2317.

Blanke, B., Bonhommeau, S., Grima, N., and Drillet, Y. (2012). Sensitivity of advective transfer times across the North Atlantic Ocean to the temporal and spatial resolution of model velocity data: Implication for European eel larval transport. *Dynamics of Atmospheres and Oceans*, 55–56(0):22–44.

Booth, D. J. (1992). Larval settlement patterns and preferences by domino damselfish Dascyllus albisella Gill. *Journal of Experimental Marine Biology and Ecology*, 155(1):85–104.

Brito, A. (2010). Lunar cycles, catchability of penaeid shrimps and implications for management of the shrimp fishery on Sofala bank in Mozambique. *Western Indian Ocean Journal of Marine Science*, 9(1):75–89.

Brito, A. and Abdula, S. (2007). Relatório de cruzeiro de investigação de camarão no Banco de Sofala realizado de 29 de Janeiro a 17 de Fevereiro de 2007. Relatório de cruzeiro, Unpublished report Instituto Nacional de Investigação Pesqueira, Beira. (In Portuguese).

Brito, A. and Pena, A. (2007). Population Structure and Recruitment of Penaeid Shrimps from the Pungué River Estuary to the Sofala Bank Fishery, Mozambique. *Western Indian Ocean Journal of Marine Science*, 6(1):147–158.

Brito, A. J.and Dias, N., Rodrigues, M., and Thuzine, A.and Volstad, J. (1998). Relatório de cruzeiro de investigação de camarão no Banco de Sofala, realizado de 2 a 24 de Fevereiro de 1998. Relatório de cruzeiro nÂ° 41, Unpublished report of Instituto Nacional de Investigação Pesqueira, Maputo. (In Portuguese).

Burla, M., Baptista, A. M., Zhang, Y., and Frolov, S. (2010). Seasonal and interannual variability of the Columbia River plume: A perspective enabled by multiyear simulation databases. *Journal of Geophysical Research: Oceans*, 115(C2):n/a–n/a.

Burrows, M. T., Schoeman, D. S., Buckley, L. B., Moore, P., Poloczanska, E. S., Brander, K. M., Brown, C., Bruno, J. F., Duarte, C. M., Halpern, B. S., Holding, J., Kappel, C. V., Kiessling, W., O'Connor, M. I., Pandolfi, J. M., Parmesan, C., Schwing, F. B., Sydeman, W. J., and Richardson, A. J. (2011). The Pace of Shifting Climate in Marine and Terrestrial Ecosystems. *Science*, 334(6056):652–655.

Cai, S., Su, J., Gan, Z., and Liu, Q. (2002). The numerical study of the South China Sea upper circulation characteristics and its dynamic mechanism, in winter. *Continental Shelf Research*, 22(15):2247–2264.

Calderon-Aguilera, L. E., Marinone, S. G., and Aragón-Noriega, E. A. (2003). Influence of oceanographic processes on the early life stages of the blue shrimp (*Litopenaeus stylirostris*) in the Upper Gulf of California. *Journal of Marine Systems*, 39(1-2):117–128.

Casey, K. S. and Cornillon, P. (1999). A Comparison of Satellite and In Situ−Based Sea Surface Temperature Climatologies. *Journal of Climate*, 12(6):1848–1863.

Chao, S. Y. and Boicourt, C. B. (1986). Onset of Estuarine Plume. *Journal of Physical Oceanography*, 16:2137–2149.

Chevane, C. M. (2013). General characteristics of modelled tides on the Sofala Bank, Mozambique. Master's thesis, Department of oceanography - University of Cape Town, South Africa.

Cloern, J. E., Foster, S. Q., and Kleckner, A. E. (2014). Phytoplankton primary production in the world's estuarine-coastal ecosystems. *Biogeosciences*, 11(9):2477–2501.

Coman, G. J., Crocos, P. J., Preston, N. P., and Fielder, D. (2002). The effects of temperature on the growth, survival and biomass of different families of juvenile Penaeus japonicus Bate. *Aquaculture*, 214(1 - 4):185–199.

Coull, K. A., Johnstone, R., and Rogers, S. I. (1998). Fisheries sensitivity maps in British waters. Published and distributed by UKOOA Ltd, Aberdeen.

Criales, M. M., Browder, J. A., Mooers, C. N. K., Robblee, M. B., Cardenas, H., and Jackson, T. L. (2007). Cross-shelf transport of pink shrimp larvae: interactions of tidal currents, larval vertical migrations and internal tides. *Marine Ecology Progress Series*, 345:167–184.

Criales, M. M. and Lee, T. N. (1995). Larval distribution and transport of penaeoid shrimps during the presence of the Tortugas Gyre in May-June 1991. *Fishery Bullentin*, 93(417-482).

Cripe, G. M. (1994). Induction of maturation and spawning of pink shrimp, Penaeus duorarum, by changing water temperature, and survival and growth of young. *Aquaculture*, 128(3-4):255–260.

Cristo, M. and Mascarenhas, V. (1986). Escala macroscópica de maturacão de ciclo sexual das espécies *P. indicus* e *M. monoceros*. *Revista Investigação Pesqueira*, 15:1–44. Instituto de Investigação Pesqueira, Maputo. (In Portuguese).

Crocos, P. J. and Kerr, J. (1983). Maturation and spawning of the banana prawn Penaeus merguiensis de Man (Crustacea : Penaeidae) in the Gulf of Carpentaria, Australia. *Journal of Experimental Marine Biology and Ecology*, 69(1):37–59.

Crocos, P. J. and Kerr, J. D. (1986). Factors affecting induction of maturation and spawning of the tiger prawn, *Penaeus esculentus* (Haswell), under laboratory conditions. *Aquaculture*, 58(3-4):203–214.

Crocos, P. J. and van der Velde, T. D. (1995). Seasonal, spatial and interannual variability in the reproductive dynamics of the grooved tiger prawn *Penaeus semisulcatus* in Albatross Bay, Gulf of Carpentaria, Australia: the concept of effective spawning. *Marine Biology*, 122(4):557–570.

Cronin, M. and Watts, D. R. (1996). Eddy-Mean Flow Interaction in the Gulf Stream at 68°W. Part I: Eddy Energetics. *Journal of Physical Oceanography*, 26(10):2107–2131.

Cuif, M., Kaplan, D. M., Lefevre, J., Faure, V. M., Caillaud, M., Verley, P., Vigliola, L., and Lett, C. (2014). Wind-induced variability in larval retention in a coral reef system: A biophysical modelling study in the South-West Lagoon of New Caledonia. *Progress in Oceanography*, 122:105 – 115.

da Costa, R. C. and Fransozo, A. (2004). Reproductive biology of the shrimp *Rimapenaeus constrictus* (Decapoda, Penaeidae) in the Ubatuba region of Brazil. *Journal of Crustacean Biology*, 24(2):274–281.

Da Silva, A., Young-Molling, C., and Levitus, S. (1994). Atlas of Surface Marine Data 1994, vol. 1, Algorithms and Procedures, NOAA Atlas NESDIS, vol. 6, Natl. *Oceanic and Atmos. Admin., Silver Spring, Md.*

da Silva, J. C. B., New, A. L., and Magalhaes, J. M. (2009). Internal solitary waves in the Mozambique Channel: Observations and interpretation. *Journal of Geophysical Research: Oceans*, 114(C5):1–12.

Dall, W., Hill, B., Rothlisberg, P., and Staples, D. (1990). *The Biology of the Penaeidae (Advances in Marine Biology, Vol. 27)*. Elsevier Academic Press, London.

de Freitas, A. (1986). Selection of nursery areas by six southeast African Penaeidae. *Estuarine, Coastal and Shelf Science*, 23(6):901–908.

de Freitas, A. J. (1972). Chave simplificada para identificação dos peneideos da baia de Lourenco Marques. Missão de Bioceaonologia e Pescas de Moçambique. *Biomar.*, 2:1–5. (In Portuguese).

de Freitas, A. J. (2011). The Penaeoidea of southeast Africa IV – The Family Penaeidae: Genus *Penaeus*. Investigational report no. 59:130pp, Oceanographic Research Institute, Durban, South Africa. http://www.saambr.org.za/uploads/files/oriinvrep59.PDF.

De Grave, S., Pentcheff, N. D., Ahyong, S. T., Chan, T.-Y., Crandall, K. A., Dworschak, P. C., Felder, D. L., Feldmann, R. M., Fransen, C. H. J. M., Goulding, L. Y. D., Lemaitre, R., Low, M. E. Y., Martin, J. W., Ng, P. K. L., Schweitzer, C. E., Tan, S. H., Tshudy, D., and Wetzer, R. (2009). A classification of living and fossil genera of decapod Crustaceans. *The Raffles Bulletin of Zoology, Supplement*, 21:1–109.

de Ruijter, W. P. M., Ridderinkhof, H., Lutjeharms, J. R. E., Schouten, M. W., and Veth, C. (2002). Observations of the flow in the Mozambique Channel. *Geophysical Research Letters*, 29(10):1502–1504.

de Sousa, L. P., Abdula, S., de Sousa, B. P., Penn, J., and Howell, D. (2013). *The shallow water shrimp at Sofala Bank Mozambique 2013*. Unpublished report Instituto Nacional de Investigação Pesqueira, Maputo.

de Sousa, L. P., Brito, A., Abdula, S., Howell, D., and Penn, J. (2006). *The shallow water shrimp at Sofala Bank Mozambique 2006*. Unpublished report Instituto Nacional de Investigação Pesqueira, Maputo.

de Sousa, L. P., Brito, A., Abdula, S., Penn, J., and Howell, D. (2008). *O Camarao do Banco de Sofala 2008*. Unpublished report Instituto Nacional de Investigação Pesqueira, Maputo. (In Portuguese).

de Sousa, L. P., Brito, A., Abdula, S., Penn, J., and Howell, D. (2009). *O Camarao do Banco de Sofala 2009*. Unpublished report Instituto Nacional de Investigação Pesqueira, Maputo. (In Portuguese).

Debreu, L., B. E. (2008). Two-way embedding algorithms: a review. *Ocean Dynamics*, 58:415–428.

Debreu, L., Marchesiello, P., Penven, P., and Cambon, G. (2012). Two-way nesting in split-explicit ocean models: Algorithms, implementation and validation. *Ocean Modelling*, 49-50:1–21.

DeLancey, L. B., Jenkins, J. E., Maddox, M. B., Whitaker, J. D., and Wenner, E. L. (2005). Field Observations on White Shrimp, *Litopenaeus setiferus*, during Spring Spawning Season in South Carolina, U.S.A., 1980-2003. *Journal of Crustacean Biology*, 25(2):212–218.

Di Lorenzo, E., Foreman, M., and Crawford, W. (2005). Modelling the generation of the Haida Eddies. *Deep-Sea Research II*, 52:853–873.

DiMarco, S. F., Chapman, P., Jr., W. D. N., Hacker, P., Donohue, K., Luther, M., Johnson, G. C., and Toole, J. (2002). Volume transport and property distributions of the Mozambique Channel. *Deep Sea Research Part II: Topical Studies in Oceanography*, 49(7 - 8):1481 – 1511. World Ocean Circulation Experiment.

Diop, H., Keithly Jr., W. R., Kazmierczak Jr., R. F., and Shaw, R. F. (2007). Predicting the abundance of white shrimp (Litopenaeus setiferus) from environmental parameters and previous life stages. *Fisheries Research*, 86(1):31–41.

Dmitrenko, Igor A. and Kirillov, Sergey A. and Bloshkina, Ekaterina and Lenn, Yueng-Djern (2012). Tide-induced vertical mixing in the Laptev Sea coastal polynya. *Journal of Geophysical Research: Oceans*, 117(C9):1–19.

Doney, S. C., Ruckelshaus, M., Emmett Duffy, J., Barry, J. P., Chan, F., English, C. A., Galindo, H. M., Grebmeier, J. M., Hollowed, A. B., Knowlton, N., Polovina, J., Rabalais,

3931 N. N., Sydeman, W. J., and Talley, L. D. (2012). Climate Change Impacts on Marine
3932 Ecosystems. *Annual Review of Marine Science*, 4(1):11–37. PMID: 22457967.

3933 Downing, J. A., Van Leeuwen, H., and Di Paolo, L. A. (2000). Substratum patch selection
3934 in the lacustrine mussels *Elliptio complanata* and *Pyganodon grandis grandis*. *Freshwater*
3935 *Biology*, 44(4):641–648.

3936 Dredge, M. C. L. (1985). Importance of estuarine overwintering in the life cycle of the banana
3937 prawn, *Penaeus merguiensis*. In Rothlisberg, P. C., Hill, B. J., and Staples, D. J., editors,
3938 *Second Australian National Prawn Seminar, NPS2*, pages 115–123, Cleveland, Australia.

3939 Dubois, S., Comtet, T., Retiere, C., and Thiebaut, E. (2007). Distribution and retention
3940 of Sabellaria alveolata larvae (Polychaeta: Sabellariidae) in the Bay of Mont-Saint-Michel.
3941 *Marine Ecology Progress Series*, 346:243–254.

3942 Egbert, G. and Erofeeva, S. (2002). Efficient inverse modeling os barotropic ocean tides. *J.*
3943 *Atmos. Oceanic Technol.*, 19(2):183–204.

3944 Ehrhardt, N. M. and Legault, C. M. (1999). Pink Shrimp, Farfantepenaeus duorarum, Recruit-
3945 ment Variability as an Indicator of Florida Bay Dynamics. *Estuaries*, 22(2):pp. 471–483.

3946 Ellis, J. R., Milligan, S. P., Readdy, L., Taylor, N., and Brown, M. J. (2012). Spawning and nurs-
3947 ery grounds of selected fish species in UK waters. Science series technical report no. 147:56pp,
3948 Cefas Lowestoft. http://www.cefas.defra.gov.uk/publications/techrep/TechRep147.pdf.

3949 Emery, W. J. and Thomson, R. E. (2001). *Data analysis methods in physical oceanography.*
3950 Elsevier, Amsterdam, 2nd rev edition.

3951 Falcieri, F. M., Benetazzo, A., Sclavo, M., Russo, A., and Carniel, S. (2014). Po River plume
3952 pattern variability investigated from model data. *Continental Shelf Research*, 87:84–95.
3953 Oceanography at coastal scales.

3954 FAO (1997). Review of the state of world aquaculture. FAO Fisheries Circular No. 886, Rev.1,
3955 FAO Fisheries Department, Rome.

3956 FAO (2000). *The State of World Fisheries and Aquaculture 2000.* FAO, Rome.

3957 FAO (2005). Global Forest Resource Assessment 2005: Thematic Study on Mangroves, Mozam-
3958 bique. Country profile, FAO, Forestry Department, Rome.

3959 FAO (2010). *The State of World Fisheries and Aquaculture 2010.* FAO, Rome.

3960 FAO (2012). *The State of World Fisheries and Aquaculture 2012.* FAO, Rome.

3961 Fatoyinbo, T. E. and Simard, M. (2013). Height and biomass of mangroves in Africa from
3962 ICESat/GLAS and SRTM. *International Journal of Remote Sensing*, 34(2):668–681.

Fatoyinbo, T. E., Simard, M., Washington-Allen, R. A., and Shugart, H. H. (2008). Landscape-scale extent, height, biomass, and carbon estimation of Mozambique's mangrove forests with Landsat ETM+ and Shuttle Radar Topography Mission elevation data. *Journal of Geophysical Research: Biogeosciences*, 113(G2):n/a–n/a.

Feliks, Y. (2004). Nonlinear Dynamics and Chaos in the Sea and Land Breeze. *Journal of Atmospheric Sciences*, 61:2169–2187.

Feng, M., Caputi, N., Penn, J., Slawinski, D., de Lestang, S., Weller, E., and Pearce, A. (2011). Ocean circulation, Stokes drift, and connectivity of western rock lobster (Panulirus cygnus) population. *Canadian Journal of Fisheries and Aquatic Sciences*, 68(7):1182–1196.

Ffield, A. and Gordon, A. L. (1996). Tidal Mixing Signatures in the Indonesian Seas. *Journal of Physical Oceanography*, 29(9):1924–1937.

Fiedler, P. C. (1986). Offshore entrainment of anchovy spawning habitat, eggs, and larvae by a displaced eddy in 1985. *Calif. Coop. Ocean. Fish. Invest. Rep*, 27:144–152.

Fischer, W., Sousa, I., Silva, C., Freitas, A. D., Poutiers, J., Schneider, W., Borges, T., Féral, J., and Massinga, A. (1990). *Fichas FAO de identificação de espécies para actividades de pesca. Guía de campo das espécies comerciais marinhas e de águas salobras de Moçambique*. FAO, Roma. Publicação preparada em collaboração com o Instituto de Investigação Pesqueira de Moçambique, com financiamento do Projecto PNUD/FAO MOZ/86/030 e de NORAD.

Flather, R. (1976). A tidal model of the northwest European continental shelf. *Memoires de la Society Royal des Sciences de Liegr 6 series*, 10:141–161.

Fong, D. A. and Geyer, W. R. (2002). The Alongshore Transport of Freshwater in a Surface-Trapped River Plume. *Journal of Physical Oceanography*, 32(3):957–972.

Forbes, A. and Benfield, M. (1986). Tidal behaviour of post-larval penaeid prawns (Crustacea: Decapoda: Penaeidae) in a southeast African estuary. *Journal of Experimental Marine Biology and Ecology*, 102(1):23 – 34.

Forbes, A. T. and Demetriades, A. N. (2005). A review of the commercial, shallow water penaeid prawn resource of South Africa: status, fisheries, aquaculture and management. Unpublished specialist report prepared for ezemvelo kzn wildlife, Marine and Estuarine Research, South Africa. http://www.saambr.org.za/uploads/files/oriinvrep59.PDF.

Gaines, S. and Roughgarden, J. (1985). Larval settlementrate: a leading determinant of structure in an ecological community of the marine intertidal zone. *Proceedings of the National Academy of Sciences of the USA*, 82:3707–3711.

Galindo-Bect, M. S., Glenn, E. P., Page, H. M., Fitzsimmons, K., Galindo-Bect, L. A., Hernandez-Ayon, J. M., Petty, R. L., Garcia-Hernandez, J., and Moore, D. (2000). Penaeid

shrimp landings in the upper Gulf of California in relation to Colorado River freshwater discharge. *Fishery Bulletin*, 98(1):222–225.

Gammelsrod, T. (1992). Variation in shrimp abundance on Sofala Bank, Mozambique, and its relation to the Zambezi River runoff. *Estuarine, Coastal and Shelf Science*, 35:91–103.

García, S. (1988). Tropical penaeid prawns. *Fish population dynamics: the implications for management*, pages 219–249.

García-Berdeal, I., Hickey, B. M., and Kawase, M. (2002). Influence of wind stress and ambient flow on a high discharge river plume. *Journal of Geophysical Research: Oceans*, 107(C9):13–1–13–24.

Garvine, R. W. (1987). Estuary Plume and Fronts in Shelf waters: A Layer Model. *Journal of Physical Oceanography*, 17:1877–1896.

Geyer, W. (1995). Tide-induced mixing in the Amazon frontal zone. *Journal of Geophysical Research*, 100(2):2341–2353.

Giri, C., Ochieng, E., Tieszen, L. L., Zhu, Z., Singh, A., Loveland, T., Masek, J., and Duke, N. (2011). Status and distribution of mangrove forests of the world using earth observation satellite data. *Global Ecology and Biogeography*, 20(1):154–159.

Gracia, A. (1991). Spawning Stock-Recruitment Relationships of White Shrimp in the Southwestern Gulf of Mexico. *Transactions of the American Fisheries Society*, 120(4):519–527.

Greenberg, D. A., Dupont, F., Lyard, F. H., Lynch, D. R., and Werner, F. E. (2007). Resolution issues in numerical models of oceanic and coastal circulation. *Continental Shelf Research*, 27(9):1317–1343. Recent Developments in Physical Oceanographic Modelling: Part {IV}.

Griffiths, F. B. and Wadley, V. A. (1986). A synoptic comparison of fishes and crustaceans from a warm-core eddy, the East Australian Current, the Coral Sea and the Tasman Sea. *Deep Sea Research Part A. Oceanographic Research Papers*, 33(11-12):1907–1922.

Gudmundsson, G. H. (2006). Fortnightly variations in the flow velocity of Rutford Ice Stream, West Antarctica. *Nature*, 444|21/28:1063–1064.

Gutierrez, O., Marinone, S., and Pares-Sierra, A. (2004). Lagrangian surface circulation in the Gulf of California from a 3D numerical model. *Deep Sea Research Part II: Topical Studies in Oceanography*, 51:659–672. Oceanography of the Eastern Pacific: Volume {III}.

Haidvogel, D. B. and Beckmann, A. (1999). *Numerical ocean circulation modeling* , volume 2. Imperial College Press.

Haidvogel, D. B., Wilkin, J. L., and Young, R. (1991). A Semi-spectral Primitive Equation Ocean Circulation Model Using Vertical Sigma and Orthogonal Curvilinear Horizontal Coordinates. *Journal of Computational Physics*, 94(1):151–185.

Halo, I., Backeberg, B., Penven, P., Ansorge, I., Reason, C., and Ullgren, J. E. (2014). Eddy properties in the Mozambique Channel: A comparison between observations and two numerical ocean circulation models. *Deep Sea Research Part II: Topical Studies in Oceanography*, 100(0):38 – 53. The Mozambique Channel: Mesoscale Dynamics and Ecosystem Responses.

Halo, I. F. M. (2012). *The Mozambique Channel eddies: characteristics and mechanisms of formation*. PhD thesis, Department of oceanography - University of Cape Town, South Africa.

Hancke, L., Roberts, M. J., and Ternon, J. F. (2014). Surface drifter trajectories highlight flow pathways in the Mozambique Channel. *Deep Sea Research Part II: Topical Studies in Oceanography*, 100(0):27 – 37. The Mozambique Channel: Mesoscale Dynamics and Ecosystem Responses.

Harley, C. D. G., Randall Hughes, A., Hultgren, K. M., Miner, B. G., Sorte, C. J. B., Thornber, C. S., Rodriguez, L. F., Tomanek, L., and Williams, S. L. (2006). The impacts of climate change in coastal marine systems. *Ecology Letters*, 9(2):228–241.

Hedstrom, K. S. (1997). SCRUM Manuel. Technical report, Institute of Marine and Coastal Sciences, Rutgers University, USA.

Hetland, R. (2004). Water mass structure of wind forced river plume. *Journal of Physical Oceanography*, pages 1–32.

Hickey, B., Geier, S., Kachel, N., and MacFadyen, A. (2005). A bi-directional river plume: The Columbia in summer. *Continental Shelf Research*, 25(14):1631–1656.

Hickey, B. M., Kudela, R. M., Nash, J. D., Bruland, K. W., Peterson, W. T., MacCready, P., Lessard, E. J., Jay, D. A., Banas, N. S., Baptista, A. M., Dever, E. P., Kosro, P. M., Kilcher, L. K., Horner-Devine, A., Zaron, E. D., McCabe, R. M., Peterson, J. O., Orton, P. M., Pan, J., and Lohan, M. C. (2010). River Influences on Shelf Ecosystems: Introduction and Synthesis. *Journal of Geophysical Research*, 115:1–26.

Hijmans, R. J. (2014). *geosphere: Spherical Trigonometry*. R package version 1.3-8.

Hill, A. E. (1991). Vertical migration in tidal currents. *Marine Ecology Progress Series*, 75:39–54.

Hoang, T., Lee, S. Y., Keenan, C. P., and Marsden, G. E. (2002). Effect of temperature on spawning of Penaeus merguiensis. *Journal of Thermal Biology*, 27(5):433–437.

Hobday, A. J. and Pecl, G. (2014). Identification of global marine hotspots: sentinels for change and vanguards for adaptation action. *Reviews in Fish Biology and Fisheries*, 24(2):415–425.

Hoegh-Guldberg, O. and Bruno, J. F. (2010). The Impact of Climate Change on the World's Marine Ecosystems. *Science*, 328(5985):1523–1528.

Holdway, D. A. (2002). The acute and chronic effects of wastes associated with offshore oil and gas production on temperate and tropical marine ecological processes. *Marine Pollution Bulletin*, 44(3):185–203.

Holland, W. R. and Rhines, P. B. (1980). An Example of Eddy-Induced Ocean Circulation. *Journal of Physical Oceanography*, 10(7):1010–1031.

Horner-Devine, A. (2009). The bulge circulation in the Columbia River plume. *Continental Shelf Research*, 29:234–251.

Hossain, M. Y. and Ohtomi, J. (2008). Reproductive Biology of the Southern Rough Shrimp Trachysalambria curvirostris (Penaeidae) in Kagoshima Bay, Southern Japan. *Journal of Crustacean Biology*, 28(4):607–612.

Huang, R. and Dewar, W. (1996). Haline Circulation: Bifurcation and Chaos. *Journal of Physical Oceanography*, 26:2093–2106.

Huggett, J. A. (2014). Mesoscale distribution and community composition of zooplankton in the Mozambique Channel. *Deep Sea Research Part II: Topical Studies in Oceanography*, 100(0):119 – 135. The Mozambique Channel: Mesoscale Dynamics and Ecosystem Responses.

Hughes, D. A. (1966). Investigations of the 'Nursery Areas' and Habitat Preferences of Juvenile Penaeid Prawns in Mozambique. *Journal of Applied Ecology*, 3(2):349–354.

Ibaibarriaga, L., Irigoien, X., Santos, M., Motos, L., Fives, J. M., Franco, C., Lago de Lanzós, A., Acevedo, S., Bernal, M., Bez, N., et al. (2007). Egg and larval distributions of seven fish species in north-east Atlantic waters. *Fisheries Oceanography*, 16(3):284–293.

Ivanov, B. G. and Hassan, A. M. (1976). Penaeid Shrimps (Decapoda, Penaeidae) Collected off East Africa by the Fishing Vessel "Van Gogh", 1. Solenocera ramadani sp. nov., and Commercial Species of the Genera Penaeus and Metapenaeus. *Crustaceana*, 30(3):241–251.

Jackson, C. J., Rothlisberg, P. C., and Pendrey, R. C. (2001). Role of larval distribution and abundance in overall life-history dynamics: a study of the prawn *Penaeus semisulcatus* in Albatross Bay, Gulf of Carpentaria, Australia. *Marine ecology. Progress series*, 213:241–252.

Jakobsson, M., Macnab, R., Mayer, L., Anderson, R., Edwards, M., Hatzky, J., Schenke, H. W., and Johnson, P. (2008). An improved bathymetric portrayal of the Arctic Ocean: Implications for ocean modeling and geological, geophysical and oceanographic analyses. *Geophysical Research Letters*, 35(7):L07602.

Jayawardane, P. A. A. T., McLusky, D. S., and Tytler, P. (2002). Reproductive biology of Penaeus indicus (H. Milne Edward, 1837) from the western coastal waters of Sri Lanka. *Asian Fisheries Science*, 15:315–328.

Jiang, Z., Huang, Y., Xu, X., Liao, Y., Shou, L., Liu, J., Chen, Q., and Zeng, J. (2010). Advance in the toxic effects of petroleum water accommodated fraction on marine plankton. *Acta Ecologica Sinica*, 30(1):8–15.

Jin, B., Wang, G., Liu, Y., and Zhang, R. (2010). Interaction between the East China Sea Kuroshio and Ryukyu Current as revealed by self-organizing map. *Journal of Geophysical Research*, 115:1–7.

Johnesen, E., Krakstad, J. O., Ostrowski, M., Serigstad, B., Stromme, T., Alvheim, O., Olsen, M., Zaera, D., Andre, E. R., Dias, N., de Sousa, L. P., de Sousa, B. P., Malauene, B. S., and Abdula, S. (2008). Survey of the living marine resources of Mozambique. Ecosystem survey and special studies. Cruise reports "Dr. Fridtjof Nansen". Technical Report FAO-NORAD PROJECTNO: GCP/INT/003/NOR, Institute of Marine Research (IMR), Bergen.

Jones, A. C., Dimitriou, D. E., Ewald, J. J., and Tweedy, J. H. (1970). Distribution of Early Developmental Stages of Pink Shrimp,Penaeus Duorarum, in Florida Waters. *Bulletin of Marine Science*, 20(3):634–661.

Jones, G. P., Almany, G. R., Russ, G. R., Sale, P. F., Steneck, R. S., van Oppen, M. J. H., and Willis, B. L. (2009). Larval retention and connectivity among populations of corals and reef fishes: history, advances and challenges. *Coral Reefs*, 28:307 – 325.

Jose, Y. S., Aumont, O., Machu, E., Penven, P., Moloney, C. L., and Maury, O. (2014). Influence of mesoscale eddies on biological production in the Mozambique Channel: Several contrasted examples from a coupled ocean-biogeochemistry model. *Deep Sea Research Part II: Topical Studies in Oceanography*, 100(0):79 – 93. The Mozambique Channel: Mesoscale Dynamics and Ecosystem Responses.

Kaartvedt, S., Klevjer, T. A., and Aksnes, D. L. (2012). Internal wave-medeated shading cause frequent vertical migration in fishes. *Marine Ecology Progress Series*, 452:1–10.

Kachel, N. B., Jr., G. L. H., Salo, S. A., Schumacher, J. D., Stabeno, P. J., and Whitledge, T. E. (2002). Characteristics and variability of the inner front of the southeastern Bering Sea. *Deep Sea Research Part II: Topical Studies in Oceanography*, 49(26):5889–5909. Ecology of the {SE} Bering Sea.

Kasai, A., Rippeth, T. P., and Simpson, J. H. (1999). Density and flow structure in the Clyde Sea front. *Continental Shelf Research*, 19(14):1833–1848.

Kir, M. and Kumlu, M. (2008). Effect of temperature and salinity on low thermal tolerance of *Penaeus semisulcatus* (Decapoda: Penaeidae). *Aquaculture Research*, 39(10):1101–1106.

Kohonen, T. (2001). *Self-Organizing Maps*. Springer-Verlag, Berlin, 3 edition. Number 30 in Springer Series in Information Sciences.

Kolasinski, J., Kaehler, S., and Jaquemet, S. (2012). Distribution and sources of particulate organic matter in a mesoscale eddy dipole in the Mozambique Channel (south-western Indian Ocean): Insight from C and N stable isotopes. *Journal of Marine Systems*, 96-97(0):122–131.

Kongkeo, H. (2005). *Penaeus monodon* Cultured Aquatic Species Information Programme. In *FAO Fisheries and Aquaculture Department*. Online, http://www.fao.org/fishery/culturedspecies/Penaeus_monodon/en, upload on 29 July 2005, last visited August 2012.

Kumlu, M. (1998). The Effect of Salinity on Larval Growth and Survival of *Penaeus indicus* (Decapoda: Penaeidae). *Turkish Journal of Zoology*, 22(2):163–167.

Kumlu, M., Avsar, D., and Eroldogan, T. (1999). Some Biological Aspects of Penaeid Shrimps Inhabiting Yumurtalik Bight in İskenderun Bay (North-Eastern Mediterranean). *Turkish Journal of Zoology*, 23:53–59.

Kumlu, M., Eroldogan, O. T., Aktaş, M., and Saglamtimur, B. (2001). Larval growth, survival and development of *Metapenaeus monoceros* (fabricius) cultured in different salinities. *Aquaculture Research*, 32(2):81–86.

Kumlu, M. and Jones, D. A. (1995). Salinity tolerance of hatchery-reared postlarvae of *Penaeus indicus* H. Milne Edwards originating from India. *Aquaculture*, 130(2-3):287–296.

Kumlu, M., Türkmen, S., Kumlu, M., and Eroldoğan, O. T. (2011). Off-season maturation and spawning of the Pacific white shrimp Litopenaeus vannamei in sub-tropical conditions. *Turkish Journal of Fisheries and Aquatic Sciences*, 11:15–23.

Kumlu, M., TÃŒrkmen, S., and Kumlu, M. (2010). Thermal tolerance of Litopenaeus vannamei (Crustacea: Penaeidae) acclimated to four temperatures. *Journal of Thermal Biology*, 35(6):305 – 308.

Kutty, M. N., Murugapoopathy, G., and Krishnan, T. S. (1971). Influence of salinity and temperature on the oxygen consumption in young juveniles of the Indian prawn *Penaeus indicus*. *Marine Biology*, 11(2):125–131.

Lamont, T., Barlow, R. G., Morris, T., and van den Berg, M. A. (2014). Characterisation of mesoscale features and phytoplankton variability in the Mozambique Channel. *Deep Sea Research Part II: Topical Studies in Oceanography*, 100(0):94 – 105. The Mozambique Channel: Mesoscale Dynamics and Ecosystem Responses.

Large, W. G., McWilliams, J. C., and Doney, S. C. (1994). Oceanic vertical mixing: A review and a model with a nonlocal boundary layer parameterization. *Rev. Geophys.*, 32:363–403.

Law, C. (2011). Northern Mozambique True Wildcat Exploration Success. *Houston Geological Society Bulletin*. Abstract.

Laxminarayana, A., M., P. S., Surendran, K. K., and Sasidharan, C. S. (1995). *Backyard hatchery technology for the white prawn, Penaeus indicus*. Central Institute of Brackishwater Aquaculture (CIBA). Bulletin No. 8.

Le Reste, L. and Marcille, J. (1976). Biologie de la crevette *Penaeus indicus* H. Milne Edwards à Madagascar : croissance, recrutement, migrations, reproduction, mortalité : contribution à l'étude d'une baie eutrophique tropicale. *Cahiers ORSTOM.Série Océanographie*, 14(2):109–127. (In french).

Ledesma, D. (2013). East Africa Gas-Potential for Export. *Oxford Institute for Energy Studies*.

Lehmann, M. K., Fennel, K., and He, K. (2009). Statistical validation of a 3-D bio-physical model of the western North Atlantic. *Biogeosciences*, 6:1961–1974.

Lett, C., Veitch, J., van der Lingen, C. D., and Hutchings, L. (2007). Assessment of an environmental barrier to transport of ichthyoplankton from the southern to the northern Benguela ecosystems. *Marine Ecology Progress Series*, 347:247–259.

Lett, C., Verley, P., Mullon, C., Parada, C., Brochier, T., Penven, P., and Blanke, B. (2008). A Langrangian tool for modelling ichthyoplankton dynamics. *Enviromental Modelling & Software*, 23:1210–1214.

Levin, L. A. (2006). Recent Progress in Understanding Larval Dispersal: New Directions and Digressions. Integrative and Comparative Biology. *Integrative and Comparative Biology*, 46(3):282 – 297.

Lie, H. J. (1989). Tidal fronts in the southeastern Hwanghae (Yellow Sea). *Continental Shelf Research*, 9(6):527–546.

Limouzy-Paris, C. B., Graber, H. C., Jones, D. L., Röpke, A. W., and Richards, W. J. (1997). Translocation of larval coral reef fishes via sub-mesoscale spin-off eddies from the Florida Current. *Bulletin of Marine Science*, 60(3):966–983.

Liu, Y., MacCready, P., and Hickey, B. M. (2009a). Columbia River plume patterns in summer 2004 as revealed by a hindcast coastal ocean circulation model. *Geophysical Research Letters*, 36:L02601.

Liu, Y., MacCready, P., Hickey, B. M., Dever, E. P., Kosro, P. M., and Banas, N. S. (2009b). Evaluation of a coastal ocean circulation model for the Columbia River plume in summer 2004. *Journal of Geophysical Research*, 114:1–23.

Liu, Y. and Weisberg, R. H. (2005). Patterns of current variability in the West Florida shelf using the self-organizing map. *Journal of Geophysical Research*, 110:1–12.

Liu, Y., Weisberg, R. H., and Mooers, C. N. K. (2006). Performance evaluation of the self-organizing map for feature extraction. *Journal of Geophysical Research*, 111:C05018.

Liu, Y., Weisberg, R. H., and Yuan, Y. (2008). Patterns of upper layer circulation variability in the South China Sea from satellite altimetry using the self-organizing map. *Acta OCeanologica Sinica*, 27:129–144.

Lobel, P. S. and Robinson, A. R. (1986). Transport and entrapment of fish larvae by ocean mesoscale eddies and currents in Hawaiian waters. *Deep Sea Research Part A. Oceanographic Research Papers*, 33(4):483–500.

Logerwell, E. A., Lavaniegos, B., and Smith, P. E. (2001). Spatially-explicit bioenergetics of Pacific sardine in the Southern California Bight: are mesoscale eddies areas of exceptional prerecruit production? *Progress in Oceanography*, 49(1-4):391–406. Pacific climate variability and marine ecosystem impacts.

Logerwell, E. A. and Smith, P. E. (2001). Mesoscale eddies and survival of late stage Pacific sardine (Sardinops sagax) larvae. *Fisheries Oceanography*, 10(1):13–25.

Lohrenz, S. E., Fahnenstiel, G. L., Redalje, D. G., Lang, A. G., dagg dagg dagg dagg, M. J., Whitledge, T. E., and Dortch, Q. (1999). Nutrients, irradiance, and mixing as factors regulating primary production in coastal waters impacted by the mississippi River plume. *Continental Shelf Research*, 19:1113–1141.

Lopez-Martinez, J., Arreguin-Sanchez, F., Hernandez-Vazquez, S., Garcia-Juarez, A. R., and Valenzuela-Quinonez, W. (2003). Interannual variation of growth of the brown shrimp Farfantepenaeus californiensis and its relation to temperature. *Fisheries Research*, 61(1 - 3):95 – 105.

López-Martínez, J., Rábago-Quiroz, C., Nevárez-Martínez, M. O., García-Juárez, A. R., Rivera-Parra, G., and Chávez-Villalba, J. (2005). Growth, reproduction, and size at first maturity of blue shrimp, Litopenaeus stylirostris (Stimpson, 1874) along the east coast of the Gulf of California, Mexico. *Fisheries Research*, 71(1):93–102.

Lorenz, E. (1963). Deterministic Nonperiodic Flow. *Journal of Atmospheric Sciences*, 20:130–141.

Lutjeharms, J. R. E. (2006). *The Agulhas Current*. Springer-Praxis Books.

MacCready, P., Banas, N. S., Hickey, B. M., Dever, E. P., and Liu, Y. (2009). A model study of tide- and wind-induced mixing in the Columbia River Estuary and Plume. *Continental Shelf Research*, 29:278–291.

Macia, A. (2004). Juvenile Penaeid Shrimp Density, Spatial Distribution and Size Composition in four adjacent habitats within a Mangrove-Fringed Bay on Inhaca Island, Mozambique. *Western Indian Ocean Journal of Marine Science*, 3(2):163–178.

Main, K. L. and Fulks, W. (1990). The Culture of Cold-Tolerant Shrimp. In *Proceedings of an Asian-U.S. Workshop on Shrimp Culture, Honolulu, HI, 1989*, page 215, Hawaii. The Oceanic Institute.

Malauene, B. S., Shillington, F. A., Roberts, M. J., and Moloney, C. L. (2014). Cool, elevated chlorophyll-a waters off northern Mozambique. *Deep Sea Research Part II: Topical Studies in Oceanography*, 100(0):68 – 78. The Mozambique Channel: Mesoscale Dynamics and Ecosystem Responses.

Marchesiello, P., Debreu, L., and Couvelard, X. (2009). Spurious diapycnal mixing in terrain-following coordinate models: advection problem and solutions. *Submitted: J. Phys. Oceanogr.*

Marchesiello, P., McWilliams, J. C., and Shchepetkin, A. (2003). Equilibrium Structure and Dynamics of the California Current System. *Journal of Physical Oceanography*, 33:753–783.

Marinone, S., Gutierrez, O., and Pares-Sierra, A. (2004). Numerical simulation of larval shrimp dispersion in the Northern Region of the Gulf of California. *Estuarine, Coastal and Shelf Science*, 60(4):611 – 617.

Mason, E., Molemaker, J., Shchepetkin, A. F., Colas, F., McWilliams, J. C., and Sangra, P. (2010). Procedures for offline grid nesting in regional ocean models. *Ocean Modelling*, 35(1-2):1–15.

Maximenko, N. and Niiler, P. (2006). Mean surface circulation of the global ocean inferred from satellite altimeter and drifter data. In Danesy, D., editor, *Proceedings of the Symposium on 15 years of Progress in Radar Altimetry 13-18 March 2006, Venice, Italy*, page 614, Noordwijk, Netherlands. Eurpean Space Agency, ESA Publications Division.

Maximenko, N., Niiler, P. P., Rio, M., Melnichenko, O., Centurioni, L., Chambers, D., Zlotnicki, V., and Galperin, B. (2009). Mean Dynamic Topography of the Ocean Derived from Satellite and Drifting Buoy Data Using Three Different Techniques. *Journal of Atmospheric and Oceanic Technology*, 26:1910–1919.

McCabe, R. M., MacCready, P., and Hickey, B. M. (2009). Ebb-Tide Dynamics and Spreading of a Large River Plume. *Journal of Physical Oceanography*, 39:2839–2856.

Miao, S. and Tu, S. (1995). Modeling thermal effect on growth of chinese shrimp, *Penaeus chinensis* (Osbeck). *Ecological Modelling*, 80(2-3):187–196.

Minagawa, M., Yasumoto, S., Ariyoshi, T., Umemoto, T., and Ueda, T. (2000). Interannual, seasonal, local and body size variations in reproduction of the prawn Penaeus (Marsupenaeus) japonicus (Crustacea: Decapoda: Penaeidae) in the Ariake Sea and Tachibana Bay, Japan. *Marine Biology*, 136(2):223–231.

Morgan, S. G., Fisher, J. L., and Largier, J. L. (2011). Larval retention, entrainment, and accumulation in the lee of a small headland: Recruitment hot spots along windy coasts. *Limnology and Oceanography*, 56(1):161–178.

Mullon, C., Cury, P., and Penven, P. (2002). Evolutionary individual-based model for the recruitment of anchovy (engraulis capensis) in the southern benguela. *Canadian Journal of Fisheries and Aquatic Sciences*, 59(5):910–922.

Munga, C. N., Mwangi, S., Ong'anda, H., Ruwa, R., Manyala, J., Groeneveld, J. C., Kimani, E., and Vanreusel, A. (2013). Species composition, distribution patterns and population structure of penaeid shrimps in Malindi-Ungwana Bay, Kenya, based on experimental bottom trawl surveys. *Fisheries Research*, 147:93–102.

Nakata, H., Kimura, S., Okazaki, Y., and Kasai, A. (2000). Implications of meso-scale eddies caused by frontal disturbances of the kuroshio current for anchovy recruitment. *ICES Journal of Marine Science*, 57:143–152.

Nehama, F. P. J. (2012). *Modelling the Zambezi River plume using the Regional Oceanic Modelling System*. PhD thesis, Department of oceanography - University of Cape Town, South Africa.

Nehring, D., Hagen, E., da Silva, J. A., Schemainda, R., Wolf, G., Michelchen, N., Kaiser, W., Postel, L., Gosselck, F., Brenning, U., Kuhner, E., Arlt, G., Siegel, H., Gohs, L., and Bublitz, G. (1987). Results of oceanological stuies in the Mozambique Channel in February-March 1980. *Beitrage Zur Meereskunded*, 56:51–63.

Neves, R., Coelho, H., Taborda, R., and Pina, P. (2003). Physical processes and modelling at ocean margins. In Wefer, G., Billett, D., Hebbeln, D., JÃžrgensen, B., SchlÃŒter, M., and van Weering, T., editors, *Ocean Margin Systems*, pages 99–123. Springer Berlin Heidelberg.

Niamaimandi, N., Aziz, A., Siti Khalijah, D., Che Roos, S., and Kiabi, B. (2008). Reproductive biology of the green tiger prawn (Penaeus semisulcatus) in coastal waters of Bushehr, Persian Gulf. *ICES Journal of Marine Science: Journal du Conseil*, 65(9):1593–1599.

Nieto, K., McClatchie, S., Weber, E. D., and Lennert-Cody, C. E. (2014). Effect of mesoscale eddies and streamers on sardine spawning habitat and recruitment success off Southern and central California. *Journal of Geophysical Research: Oceans*, 119(9):6330–6339.

Nikurashin, M. and Ferrari, R. (2010a). Radiation and dissipation of internal waves generated by geostrophic motions impinging on small-scale topography: application to the southern ocean. *Journal of Physical Oceanography*, 40:2025–2042.

Nikurashin, M. and Ferrari, R. (2010b). Radiation and dissipation of internal waves generated by geostrophic motions impinging on small-scale topography: theory. *Journal of Physical Oceanography*, 40:1055–1074.

Nikurashin, M. and Ferrari, R. (2013). Overturning circulation driven by breaking internal waves in the deep ocean. *Geophysical Research Letters*, 40(12):3133–3137.

Nikurashin, M., Vallis, G. K., and Adcroft, A. (2013). Routes to energy dissipation for geostrophic flows in the Southern Ocean. *Nature Geoscience*, 6:48–51.

Omta, A. W., Llido, J., Garcon, V., Kooijman, S. A. L. M., and Dijkstra, H. A. (2009). The interpretation of satellite chlorophyll observations: the case of the Mozambique Channel. *Deep-Sea Research I*, 56:974–988.

Oozeki, Y., Takasuka, A., Kubota, H., and Barange, M. (2007). Characterizing Spawning Habitats of Japanese Sardine, Sardinops Melanostictus, Japanese Anchovy, Engraulis Japonicus, and Pacific Round Herring, Etrumeus Teres, in the Northwestern Pacific. *California Cooperative Oceanic Fisheries Investigations Report*, 48:191–203.

Ospina-Álvarez, A., Bernal, M., Catalán, I. A., Roos, D., Bigot, J.-L., and Palomera, I. (2013). Modeling Fish Egg Production and Spatial Distribution from Acoustic Data: A Step Forward into the Analysis of Recruitment. *PLoS ONE*, 8(9):e73687.

Parado-Estepa, F. D., Ferraris, R. P., Ladja, J. M., and Jesus, E. G. D. (1987). Responses of intermolt *Penaeus indicus* to large fluctuations in environmental salinity. *Aquaculture*, 64(3):175–184.

Paris, C. B., Cherubin, L. M., and Cowen, R. K. (2007). Surfing, spinning, or diving from reef to reef: effects on population connectivity. *Marine Ecology Progress Series*, 347:285–300.

Peliz, A., Marchesiello, P., Dubert, J., Marta-Almeida, M., Roy, C., and Queiroga, H. (2007). A study of crab larvae dispersal on the Western Iberian Shelf: Physical processes. *Journal of Marine Systems*, 68:215 – 236.

Penn, J. W. (1975). The influence of tidal cycles on the distributional pathway of Penaeus latisulcatus Kishinouye in Shark Bay, Western Australia. *Australian Journal of Marine and Freshwater Research*, 26:93–102.

Penn, J. W. (1986). Spawning and fecundity of the western king prawn *Penaeus latisulcatus* Kishinouye in Western Australia waters. *Australian Journal of Marine and Freshwater Research*, 31:21–35.

Penn, J. W. and Caputi, N. (1986). Spawning stock-recruitment relationships and environmental influences on the tiger prawn (*Penaeus esculentus*) fishery in Exmouth Gulf, Western Australia. *Australian Journal of Marine and Freshwater Research*, 37:491–505.

Penn, J. W., Watson, R. A., Caputi, N., and Hall, N. (1997). Protecting vulnerable stocks in multi-species prawn fisheries. In *Developing and Sustaining World Fisheries Resources. The State of Science and Management. 2nd World Fisheries Congress*, pages 122–129.

Penven, P., Debreu, L., Marchesiello, P., and McWilliams, J. C. (2006a). Evaluation and application of the ROMS 1-way embedding procedure to the central california upwelling system. *Ocean Modelling*, 12:157–187.

Penven, P., Halo, I., Pous, S., and Marie, L. (2014). Cyclogeostrophic balance in the Mozambique Channel. *Journal of Geophysical Research: Oceans*, 119(2):1054–1067.

Penven, P., Lutjeharms, J. R. E., and Florenchie, P. (2006b). Madagascar: A pacemaker for the agulhas current system? *Geophysical Research Letters*, 33(17):L17609.

Penven, P., Marchesiello, P., Debreu, L., and Lefevre, J. (2008). Software tools for pre- and post-processing of oceanic regional simulations. *Environmental Modelling and Software*, 23(5):660–662.

Pineda, J., Hare, J. A., and Sponaugle, S. (2007). Recent Progress in Understanding Larval Dispersal: New Directions and Digressions. Integrative and Comparative Biology. *Oceanography*, 20(3):22 – 39.

Poloczanska, E. S., Brown, C. J., Sydeman, W. J., Kiessling, W., Schoeman, D. S., Moore, P. J., Brander, K., Bruno, J. F., Buckley, L. B., Burrows, M. T., Duarte, C. M., Halpern, B. S., Holding, J., Kappel, C. V., O/'Connor, M. I., Pandolfi, J. M., Parmesan, C., Schwing, F., Thompson, S. A., and Richardson, A. J. (2013). Global imprint of climate change on marine life. *Nature Climate Change*, 3(10):919–925.

Ponce-Palafox, J., Martinez-Palacios, C. A., and Ross, L. G. (1997). The effects of salinity and temperature on the growth and survival rates of juvenile white shrimp, *Penaeus vannamei*, Boone, 1931. *Aquaculture*, 157(1-2):107–115.

Porri, F., Jackson, J. M., der Meden, C. E. V., Weidberg, N., and McQuaid, C. D. (2014). The effect of mesoscale oceanographic features on the distribution of mussel larvae along the south coast of South Africa. *Journal of Marine Systems*, 132(0):162–173.

Potier, M., Bach, P., Ménard, F., and Marsac, F. (2014). Influence of mesoscale features on micronekton and large pelagic fish communities in the Mozambique Channel. *Deep Sea Research Part II: Topical Studies in Oceanography*, 100(0):184 – 199. The Mozambique Channel: Mesoscale Dynamics and Ecosystem Responses.

Primavera, J. H. (1985). A review of maturation and reproduction in closed thelycum penaeids. In Taki, Y., Primavera, J. H., and Llobrera, J. A., editors, *Proceedings of the First International Conference on the Culture of Penaeid Prawns/Shrimps, 4-7 December 1984, Iloilo City, Philippines*, pages 47–64. Aquaculture Department, Southeast Asian Fisheries Development Center.

Primavera, J. H. (1998). Mangroves as Nurseries: Shrimp Populations in Mangrove and Non-mangrove Habitats. *Estuarine, Coastal and Shelf Science*, 46(3):457–464.

Pritchard, D., Bamba, A., and Rilla, F. (2009). Ramsar Advisory Missions-No. 62: Marromeu Complex Ramsar Site, Mozambique (2009). Mission report, The Ramsar Convention.

Putman, N. F. and He, R. (2013). Tracking the long-distance dispersal of marine organisms: sensitivity to ocean model resolution. *Journal of the Royal Society, Interface*, 10(81):1–11.

Putman, N. F., Shay, T. J., and Lohmann, K. J. (2010). Is the Geographic Distribution of Nesting in the Kemp's Ridley Turtle Shaped by the Migratory Needs of Offspring? *Integrative and Comparative Biology*, 50(3):305–314.

Qiu, B. and Chen, S. (2010). Eddy-mean flow interaction in the decadally modulating Kuroshio Extension system. *Deep Sea Research Part II: Topical Studies in Oceanography*, 57(13-14):1098–1110. North Pacific Oceanography after WOCE: A Commemoration to Nobuo Suginohara.

Qiu, B. and Miao, W. (2000). Kuroshio Path Variations South of Japan: Bimodality as a Self-Sustained Internal Oscillation. *Journal of Physical Oceanography*, 30(8):2124–2137.

Quartly, G., de Cuevas, B., and Coward, A. (2013). Mozambique channel eddies in gcms: A question of resolution and slippage. *Ocean Modelling*, 63(0):56 – 67.

Quartly, G. D. and Srokosz, M. A. (2004). Eddies in the southern Mozambique Channel. *Deep-Sea Research II*, 51(1-3):69–83.

Queiroga, H. and Blanton, J. (2004). Interactions Between Behaviour and Physical Forcing in the Control of Horizontal Transport of Decapod Crustacean Larvae. volume 47 of *Advances in Marine Biology*, pages 107 – 214. Academic Press.

Queiroga, H., Cruz, T., dos Santos, A., Dubert, J., Gonzalez-Gordillo, J. I., Paula, J., Peliz, A., and Santos, A. M. P. (2007). Oceanographic and behavioural processes affecting invertebrate larval dispersal and supply in the western Iberia upwelling ecosystem. *Progress in Oceanography*, 74(2–3):174–191. Ecological Functioning of the Iberian Seas: A synthesis of {GLOBEC} Research in Spain and Portugal.

Qureshi, N. A. and Amanat, Z. (2014). Reproductive biology and size at sexual maturity of Penaeus merguiensis (de Man, 1887) from the Sonmiani Bay Lagoon, Balochistan, Pakistan. *JAPS, Journal of Animal and Plant Sciences*, 24(2):503–511.

Racotta, I. S., Palacios, E., and Ibarra, A. M. (2003). Shrimp larval quality in relation to broodstock condition. *Aquaculture*, 227:107–130.

Radhakrishnan, E. V. (2007). Penaeus indicus. Cultured Aquatic Species Information Programme. *online*. In: FAO Fisheries and Aquaculture Department. last visited March 2014.

4402 Ragueneau, O., Queguiner, B., and Treguer, P. (1996). Contrast in Biological Responses to
4403 Tidally-induced Vertical Mixing for Two Macrotidal Ecosystems of Western Europe. *Estu-*
4404 *arine, Coastal and Shelf Science*, 42(5):645 – 665.

4405 Richardson, A., Risien, C., and Shillington, F. A. (2003). Using self-organizing maps to identify
4406 patterns in satellite imagery. *Progress in Oceanography*, 59:223–239.

4407 Ridderinkhof, H. and de Ruijter, W. P. M. (2003). Moored current observations in the Mozam-
4408 bique Channel. *Deep-Sea Research II*, 50:1933–1955.

4409 Ridderinkhof, H., van der Werf, P. M., Ullgren, J. E., van Aken, H. M., van Leeuwen, P. J.,
4410 and de Ruijter, W. P. M. (2010). Seasonal and interannual variability in the Mozam-
4411 bique Channel from moored current observations. *Journal of Geophysical Research: Oceans*,
4412 115(C6):C06010.

4413 Ridgway, K. R., Dunn, J. R., and Wilkin, J. L. (2002). Ocean Interpolation by Four-Dimensional
4414 Weighted Least Squares-Application to the Waters around Australasia. *Journal of Atmo-*
4415 *spheric and Oceanic Technology*, 19(9):1357–1375.

4416 Rio, M. H., Guinehut, S., and Larnicol, G. (2011). New CNES-CLS09 global mean dynamic
4417 topography computed from the combination of GRACE data, altimetry, and in situ mea-
4418 surements. *Journal of Geophysical Research: Oceans*, 116(C7):n/a–n/a.

4419 Rio, M.-H., Schaeffer, P., Lemoine, J.-M., and Hernandez, F. (2005). Estimation of the ocean
4420 Mean Dynamic Topography through the combination of altimetric data, in-situ measure-
4421 ments and GRACE geoid. In *From global to regional studies, Proceedings of the GOCINA*
4422 *international workshop*.

4423 Roberts, D., Rittschof, D., Holm, E., and Schmidt, A. (1991). Factors influencing initial larval
4424 settlement: temporal, spatial and surface molecular components. *Journal of Experimental*
4425 *Marine Biology and Ecology*, 150(2):203–221.

4426 Roberts, M. J., Ternon, J.-F., and Morris, T. (2014). Interaction of dipole eddies with the
4427 western continental slope of the Mozambique Channel. *Deep Sea Research Part II: Topical*
4428 *Studies in Oceanography*, 100(0):54 – 67. The Mozambique Channel: Mesoscale Dynamics
4429 and Ecosystem Responses.

4430 Robertson, L., Bray, W., and Lawrence, A. (1991). Reproductive Response of *Penaeus*
4431 *stylirostris* to Temperature Manipulation. *Journal of the World Aquaculture Society*,
4432 22(2):109–117.

4433 Robins, P. E., Neill, S. P., Gimenez, L., Jenkins, S. R., and Malham, S. K. (2013). Physical
4434 and biological controls on larval dispersal and connectivity in a highly energetic shelf sea.
4435 *Limnology and Oceanography*, 58(2):505–524.

Rönnbäck, P., Macia, A., Almqvist, G., Schultz, L., and Troell, M. (2002). Do Penaeid Shrimps have a Preference for Mangrove Habitats? Distribution Pattern Analysis on Inhaca Island, Mozambique. *Estuarine, Coastal and Shelf Science*, 55(3):427–436.

Ronquillo, J. D., Saisho, T., and McKinley, R. S. (2006). Early developmental stages of the tiger prawn, *Penaeus semisulcatus* de Haan (Crustacea, Decapoda, Penaeidae). *Hydrobiologia*, 560:175–196.

Rothlisberg, P., Church, J., and Fandry, C. (1995). A mechanism for near-shore concentration and estuarine recruitment of post-larval Penaeus plebejus hess (Decapoda, Penaeidae). *Estuarine, Coastal and Shelf Science*, 40(2):115 – 138.

Rothlisberg, P. C. (1982). Vertical migration and its effect on dispersal of penaeid shrimp larvae in the Gulf Carpentaria, Australia. *Fishery Bulletin*, 80(2):541–554.

Rothlisberg, P. C., Church, J. A., and Forbes, A. M. G. (1983). Modelling the advection of vertically migrating shrimp larvae. *Journal of Marine Research*, 41:511–538.

Rozas, L. P. and Minello, T. J. (2011). Variation in penaeid shrimp growth rates along an estuarine salinity gradient: Implications for managing river diversions. *Journal of Experimental Marine Biology and Ecology*, 397(2):196–207.

Sætre, R. and da Silva, A. J. (1982). Water mass and circulation of the Mozambique Channel. Revista de Investigação pesqueira. Technical Report 3, Instituto de Desenvolvimanto Pesqueiro, Maputo.

Sætre, R. and da Silva, A. J. (1984). The circulation of the Mozambique Channel. *Deep-Sea Research I*, 31:485–508.

Sánchez-Velasco, L., Lavín, M. F., Jiménez-Rosenberg, S. P. A., Godínez, V. M., del Angel, E. S., and Hernández-Becerril, D. U. (2013). Three-dimensional distribution of fish larvae in a cyclonic eddy in the Gulf of California during the summer. *Deep Sea Research Part I: Oceanographic Research Papers*, 75(0):39 – 51.

Schmitz, Jr., W. J. (1984). Abyssal eddy kinetic energy in the North Atlantic. *Journal of Marine Research*, 42(3):509–536.

Schouten, M. W., de Ruijter, W. P. M., and van Leeuwen, P. J. (2002). Upstream control of Agulhas Ring shedding. *Journal of Geophysical Research*, 107(C8):3109–3120.

Schouten, M. W., de Ruijter, W. P. M., van Leeuwen, P. J., and Ridderinkhof, H. (2003). Eddies and variability in the Mozambique Channel. *Deep-Sea Research II*, 50:1987–2003.

Segtnan, O. (2006). Simulating the circulation in the Mozambique Channel by use of a numerical ocean model. Master's thesis, Geophysical Institute - University of Bergen, Norway.

Shanks, A. L. and Brink, L. (2005). Upwelling, downwelling, and cross-shelf transport of bivalve larvae: test of a hypothesis. *Marine Ecology Progress Series*, 302:1–12.

Sharifi, M., Georgakakos, K., and Rodriguez-Iturbe, I. (1990). Evidence of Deterministic Chaos in Pulse of Storm Rainfall. *Journal of the Atmospheric Sciences*, 47(7):888–893.

Shchepetkin, A. F. and McWilliams, J. C. (2005). The regional ocean modeling system (ROMS): A split-explicit, free-surface, topography-following-coordinate oceanic model. *Ocean Modell.*, 9:347–404.

Siegel, D. A., Mitarai, S., Costello, C. J., Gaines, S. D., Kendall, B. E., Warner, R. R., and Winters, K. B. (2008). The stochastic nature of larval connectivity among nearshore marine populations. *Proceedings of the National Academy of Sciences*, 105(26):8974–8979.

Sinnott, R. W. (1984). Virtues of the Haversine. *Sky and Telescope*, 68(2):159.

Snover, M. L. (2008). Ontogenetic Habitat Shifts in Marine Organisms: Influencing Factors and the Impact of Climate Variability. *Bulletin of Marine Science*, 83(1):53–67.

Song, Y. and Haidvogel, D. (1994). A semi-implicit ocean circulation model using a generalized topography following coordinate system. *Journal of Computational Physics*, 115:228–248.

Sorte, C. J. B., Williams, S. L., and Carlton, J. T. (2010). Marine range shifts and species introductions: comparative spread rates and community impacts. *Global Ecology and Biogeography*, 19(3):303–316.

Sponaugle, S., Lee, T., Kourafalou, V., and Pinkard, D. (2005). Florida Current frontal eddies and the settlement of coral reef fishes. *Limnology and Oceanography*, 50(4):1033–1048.

Stabeno, P. J., Bond, N. A., Kachel, N. B., Salo, S. A., and Schumacher, J. D. (2001). On the temporal variability of the physical environment over the south-eastern Bering Sea. *Fisheries Oceanography*, 10(1):81–98.

Staples, D. J. and Heales, D. S. (1991). Temperature and salinity optima for growth and survival of juvenile banana prawns *Penaeus merguiensis*. *Journal of Experimental Marine Biology and Ecology*, 154(2):251–274.

Stockwell, D. A., Whitledge, T. E., Zeeman, S. I., Coyle, K. O., Napp, J. M., Brodeur, R. D., Pinchuk, A. I., and Hunt, G. L. (2001). Anomalous conditions in the south-eastern bering sea, 1997: nutrients, phytoplankton and zooplankton. *Fisheries Oceanography*, 10(1):99–116.

Ternon, J. F., Roberts, M. J., Morris, T., Hancke, L., and Backeberg, B. (2014). In situ measured current structures of the eddy field in the Mozambique Channel. *Deep Sea Research Part II: Topical Studies in Oceanography*, 100(0):10 – 26. The Mozambique Channel: Mesoscale Dynamics and Ecosystem Responses.

Tew-Kai, E. and Marsac, F. (2009). Patterns of variability of sea surface chlorophyll in Mozambique Channel: A quantitative approach. *Journal of Marine Systems*, (77):77–88.

Tew-Kai, E., Rossi, V., Sudre, J., Weimerskirch, H., Lopez, C., Hernandez-Garcia, E., Marsac, F., and Garcon, V. (2009). Top marine predators track Lagrangian coherent structures. *Proceedings of the National Academy of Sciences*, 106(20):8245–8250.

Tian, R. C., Chen, C., Stokesbury, K. D. E., Rothschild, B. J., Cowles, G. W., Xu, Q., Hu, S., Harris, B. P., and Marino II, M. C. (2009a). Dispersal and settlement of sea scallop larvae spawned in the fishery closed areas on Georges Bank. *ICES Journal of Marine Science*, 66:2155–2164.

Tian, R. C., Chen, C., Stokesbury, K. D. E., Rothschild, B. J., Cowles, G. W., Xu, Q., Hu, S., Harris, B. P., and Marino II, M. C. (2009b). Modeling the connectivity between sea scallop populations in the Middle Atlantic Bight and over Georges Bank. *Marine Ecology Progress Series*, 380:147–160.

Torrence, C. and Compo, G. P. (1998). A Practical Guide to Wavelet Analysis. *Bulletin of the American Meteorological Society*, 79:61–78.

Turkmen, G. (2007). Experimental commercial growout of *Penaeus semisulcatus* (Decapoda: Penaeidae). *Israeli Journal of Aquaculture−Bamidgeh*, 59(1):52–57.

Turner, R. E. and Brody, M. S. (1983). *Habitat suitability index models: northern Gulf of Mexico brown shrimp and white shrimp.* U.S. Department of the Interior, Fish and Wildlife Service. FWS/OBS-82/10.54:24pp.

Turok, I. (2013). Securing the resurgence of African cities. *Local Economy*, 28(2):142–157.

Twatwa, N. M., Van Der Lingen, C. D., Drapeau, L., Moloney, C. L., and Field, J. G. (2005). Characterising and comparing the spawning habitats of anchovy engraulis encrasicolus and sardine sardinops sagax in the southern benguela upwelling ecosystem. *African Journal of Marine Science*, 27(2):487–499.

Ullgren, J., Aken, H., Ridderinkhof, H., and de Ruijter, W. P. M. (2012). The hydrography of the Mozambique Channel from six years of continuous temperature, salinity and velocity observation. *Deep-Sea Research I*, 69:36–50.

Valiela, I. (1995). *Marine Ecological Processes.* Springer Verlag, New York.

van der Lingen, C. D., Hutchings, L., Merkle, D., van der Westhuizen, J. J., and Nelson, J. (2001). Comparative spawning habitats of anchovy (Engraulis capensis) and sardine (Sardinops sagax) in the southern Benguela upwelling ecosystem. In Kruse, G. H., Bez, N., Booth, T., Dorn, M., Hills, S., Lipcius, R. N., Pelletier, D., Roy, C., Smith, S. J., and Witherell, D., editors, *Spatial processes and Management of Marine Populations*, pages 185–209. University of Alaska Sea Grant. Report No. AK-SG -01-02, Fairbanks.

Vance, D. J., Haywood, M. D. E., Heales, D. S., Kenyon, R. A., and Loneragan, N. R. (1998). Seasonal and annual variation in abundance of postlarval and juvenile banana prawns *Penaeus merguiensis* and environmental variation in two estuaries in tropical northeastern Australia: a six year study. *Marine Ecology Progress Series*, 163(1):21–36.

Vandermeirsch, F. O., Carton, X. J., and Morel, Y. G. (2003). Interaction between an eddy and a zonal jet: Part I. One-and-a-half-layer model. *Dynamics of Atmospheres and Oceans*, 36(4):247 – 270.

Vaz, A. C., Richards, K. J., Jia, Y., and Paris, C. B. (2013). Mesoscale flow variability and its impact on connectivity for the island of Hawai'i. *Geophysical Research Letters*, 40(2):332–337.

Veitch, J., Penven, P., and Shillington, F. (2010). Modeling Equilibrium Dynamics of the Benguela Current System. *Journal of Physical Oceanography*, 40:1942–1964.

Veitch, J. A., Penven, P., and Shillington, F. A. (2009). The Benguela: a laboratory for comparative studies. *Prog. Oceanogr.*, In Press, Corrected Proof.

Vesanto, J., Himberg, J., Alhoniemi, E., and Parhankangas, J. (2000). SOM Toolbox for Matlab 5. Tech. rep., Helsinki University of Technology, Helsinki, Finland.

Wang Xingqiang, Kappalli Sudha, M. C. and Ma, S. (2010). Effects of Low Salinity and Low Temperature on Survival, Growth, and Energy Budget of Juvenile Exopalaemon carinicauda. *Journal of Shellfish Research*, 29(4):1035 – 1041.

Waterman, S. and Jayne, S. R. (2011). Eddy-Mean Flow Interactions in the Along-Stream Development of a Western Boundary Current Jet: An Idealized Model Study. *Journal of Physical Oceanography*, 41(4):682–707.

Wehrens, R. and Buydens, L. M. C. (2007). Self- and Super-organizing Maps in R: The kohonen Package. *Journal of Statistical Software*, 21(5):1–19.

Weimerskirch, H., Le Corre, M., Jaquemet, S., Potier, M., and Marsac, F. (2004). Foraging strategy of a top predator in tropical water: great frigatebirds in the Mozambique Channel. *Marine Ecology Progress Series*, 275:297–308.

Weisberg, R. H. and He, R. (2003). Local and deep-ocean forcing contributions to anomalous water properties on the West Florida Shelf. *Journal of Geophysical Research: Oceans*, 108(C6):3184.

Williams, A. B. (1958). Substrates as a factor in shrimp distribution. *Limnology and Oceanography*, 3(3):283–290.

Woillez, M., Poulard, J.-C., Rivoirard, J., Petitgas, P., and Bez, N. (2007). Indices for capturing spatial patterns and their evolution in time, with application to european hake (merluccius

merluccius) in the bay of biscay. *ICES Journal of Marine Science: Journal du Conseil*, 64(3):537–550.

Wunsch, C. and Ferrari, R. (2004). Vertical mixing, energy, and the general circulation of the oceans. *Annual Review of Fluid Mechanics*, 36(1):281–314.

Wyban, J., Walsh, W. A., and Godin, D. M. (1995). Temperature effects on growth, feeding rate and feed conversion of the Pacific white shrimp (Penaeus vannamei). *Aquaculture*, 138(1-4):267 – 279.

Xu, Y., Chai, F., Rose, K. A., C., M. N., and Chavez, F. P. (2013). Environmental influences on the interannual variation and spatial distribution of Peruvian anchovy (Engraulis ringens) population dynamics from 1991 to 2007: A three-dimensional modeling study. *Ecological Modelling*, 264:64–82.

Yano, I. (1995). Final oocyte maturation, spawning and mating in penaeid shrimp. *Journal of Experimental Marine Biology and Ecology*, 193(1-2):113–118. Behavioural Ecology of Decapod Crustaceans: An Experimental Approach.

Ye, Y. (2000). Is recruitment related to spawning stock in penaeid shrimp fisheries? *ICES Journal of Marine Science: Journal du Conseil*, 57(4):1103–1109.

Yin, Y., Lin, X., Li, Y., and Zeng, X. (2014). Seasonal variability of Kuroshio intrusion northeast of Taiwan Island as revealed by self-organizing map. *Chinese Journal of Oceanology and Limnology*, pages 1–8.

Zacharia, S. and Kakati, V. S. (2004). Optimal salinity and temperature for early developmental stages of Penaeus merguiensis De man. *Aquaculture*, 232(1-4):373–382.

Zeng, X., Pielke, R., and Eykholt, R. (1993). Chaos Theory and Application to the Atmosphere. *Bulletin of the American Meteorological Society*, 74(4):631–644.

Zheng, L. and Weisberg, R. H. (2012). Modeling the west Florida coastal ocean by downscaling from the ocean, across the contonental shelf and into the estuaries. *Ocean Modelling*, 48:10–29.

Zwolinski, J. P., Oliveira, P. B., Quintino, V., and Stratoudakis, Y. (2010). Sardine potential habitat and environmental forcing off western Portugal. *ICES Journal of Marine Science: Journal du Conseil*, 67(8):1553–1564.

Appendices

Appendix A

Maturity stages and size relationship

Females of banana shrimps dominated the research survey catch data during the closed season months of January and February 2003 – 2010. The average proportion of females was 56% ($n = 14,309$) and of males was 44% ($n = 11,256$) for *F. indicus*; and for *M. monoceros*, females were 59% ($n = 16,123$) and males were 41% ($n = 11,382$). A similar pattern of dominant females was also observed every month (March–November) of the fishing season *2000-2003*. Banana shrimp females were larger than males (Fig. A.1). Since large numbers of small males were caught, it is assumed there was no gear/net size selectivity.

The mean carapace length of banana shrimp females increases with development of ovarian maturity stages, with the largest change from stage I to II (Fig A.2). There were significant differences in mean carapace length between the four stages for *F. indicus* (one-way ANOVA $F_{DF=3,\,14.5} = 4171.9,\ p < 0.001$) and *M. monoceros* (one-way ANOVA $F_{DF=3,\,16.1} = 2659.6,\ p < 0.001$). Tukey analysis ($P < 0.001$) confirmed differences across all four stages for the two species. However, the size ranges among the four maturity stages overlap for both *F. indicus* (Fig. A.1A) and *M. monoceros* (Fig. A.1B), suggesting no strict size – maturity stage association during the study period.

Females of *F. indicus* (Fig. A.2B) were larger than those of *M. monoceros* (Fig. A.2C) for all four stages. Consistently, females of *F. indicus* (Fig. A.3A) reached maturity larger than *M. monoceros* (Fig. A.3B). The estimated size of carapace length at first maturity for *F. indicus* was 32.3 mm ($R^2 = 0.987, DF = 38, P = 0.0001$, Fig. A.3A) and for *M. monoceros* 29.5 mm ($R^2 = 0.972, DF = 35, P < 0.0001$, Fig. A.3B).

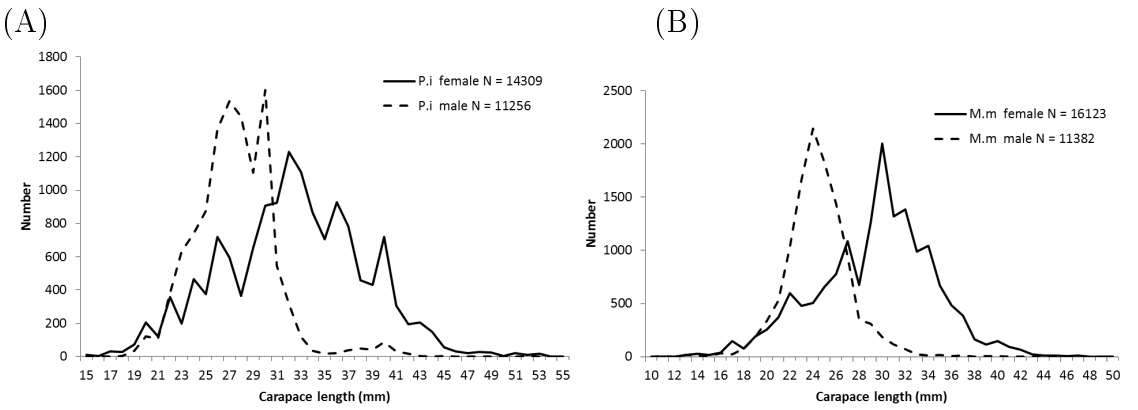

Figure A.1: Size (carapace length, mm) frequency comparisons of males and females of (A) *F. indicus* and (B) *M. monoceros* from research survey January/February 2003 – 2006 on the Sofala Bank. The total number (N) of each sex is shown in the top right corner.

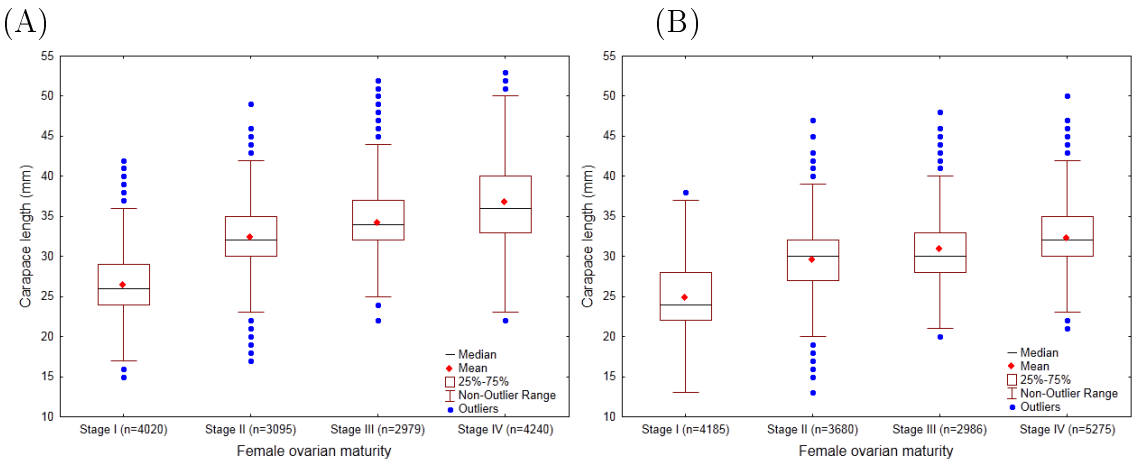

Figure A.2: Carapace length (mm) at different female maturity stages of (A) *F. indicus* and (B) *M. monoceros* from research survey January/February 2003 – 2006 on the Sofala Bank. The number (n) of individuals at each stage is shown in brackets in the x axis.

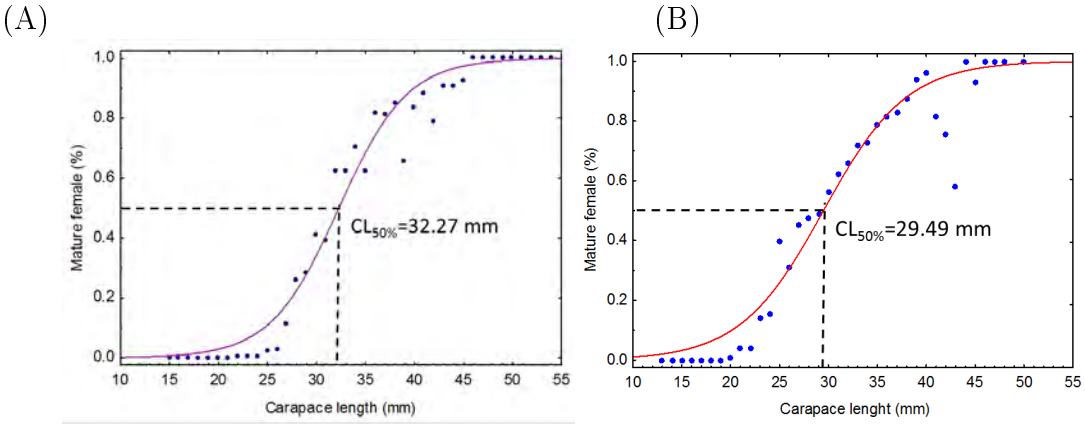

Figure A.3: Relationship between the proportion of mature females and their size (carapace length – CL, mm) for (A) F. indicus and (B) M. monoceros from research survey data during January/February 2003 – 2006 on the Sofala Bank. Dots indicate observed values and the line is the best-fitted logistic regression $S = 1/(1+e^{-b\times(CL-CL_{50})})$. Size at maturity is defined as the size at which half (50%) of the female population reaches maturity.

Appendix B

Seasonal cycle model-observation comparison

Modeled seasonally averaged shelf-bottom (18 m depth) temperature agrees with UTR observations at the Mozambique Island and Zambia reef sites. The only difference was identified in summer to the north, i.e. Mozambique Island mooring. This discrepancy can be explained by two facts. One, monthly climatology QuicksCat winds lacked temporal high-resolution that could allow the model to reproduce a significant Angoche upwelling. Synoptic, partly wind-induced upwelling is found off Angoche during the summer months (Malauene et al., 2014). This coincided with the summer decreased temperature observed at the Mozambique Island UTR site. Secondly the station site is located out of the Child domain on the northernmost edge of the Parent grid, which could be associated with the boundary problems. Since the general circulation propagates from the north (upstream field dynamics), which is missing, it is important to reproduce local processes like the Angoche upwelling.

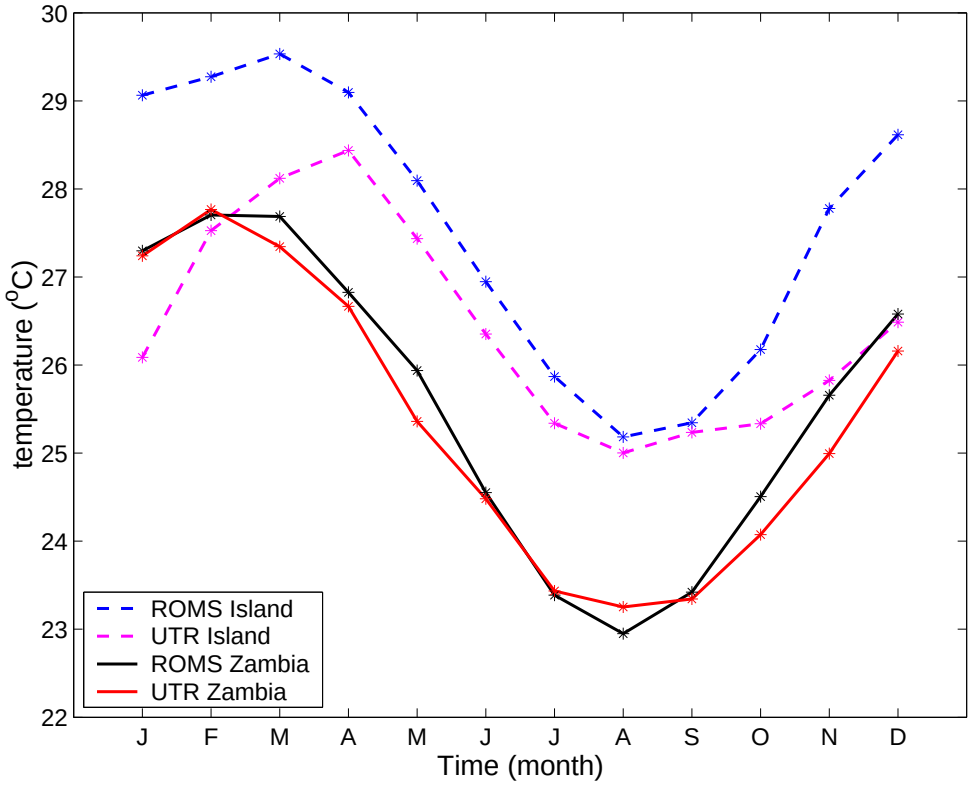

Figure B.1: Comparison model-observation monthly averaged temperature at 18 m depth at the UTR sites off Mozambique Island in the north on the model domain (blue and pink lines) and off Zambia reef, Inhambane Province to the south on the domain.

Appendix C

A sequential event of cool water lens

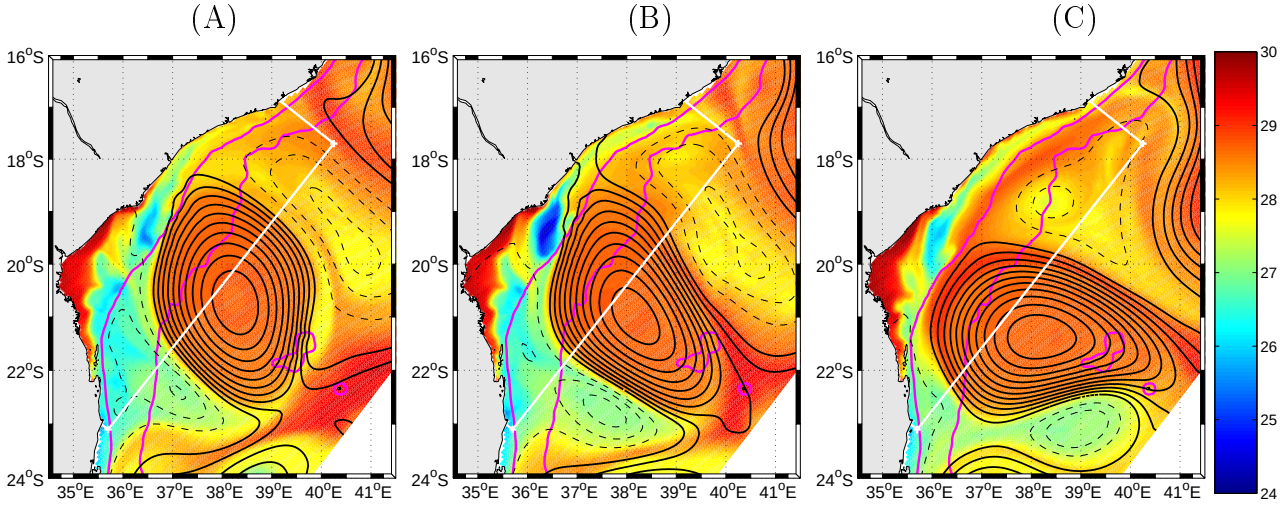

Figure C.1: Result of model simulation with tides (ROMS-BSM-E6) showing a sequence event of cool water lens and eddies. (G, H and I) snapshots of 3-days averaged model SST (color) superimposed by SSH (lines: solid line for positive values and dashed lines for negative) every five days from 15 January model-year 4. Pink lines indicate the 200 and 2000 m bathymetry contours.

Appendix D

Influence of eddy-induced SST on larval shelf retention

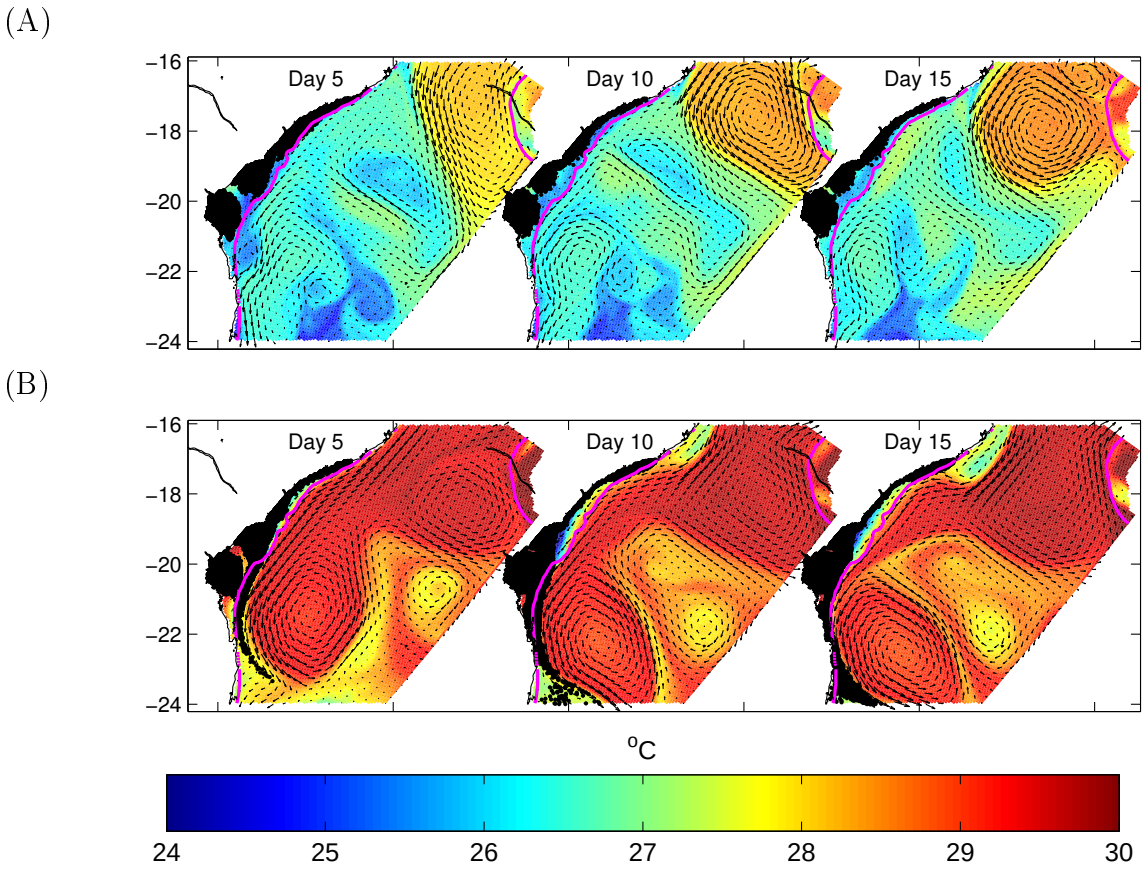

Figure D.1: Results of the experiment E1 showing snapshots of larval distribution (black dots) superimposed on the corresponding ROMS−derived surface current vectors (arrows, in cm s^{-1}) and SST (color shading, in °C) on the Sofala Bank. Labels indicate larvae five, ten and 15 days after release on (A) 5 November and (B) 2 February model year 5.

(A)

(B)

(C)

(D)

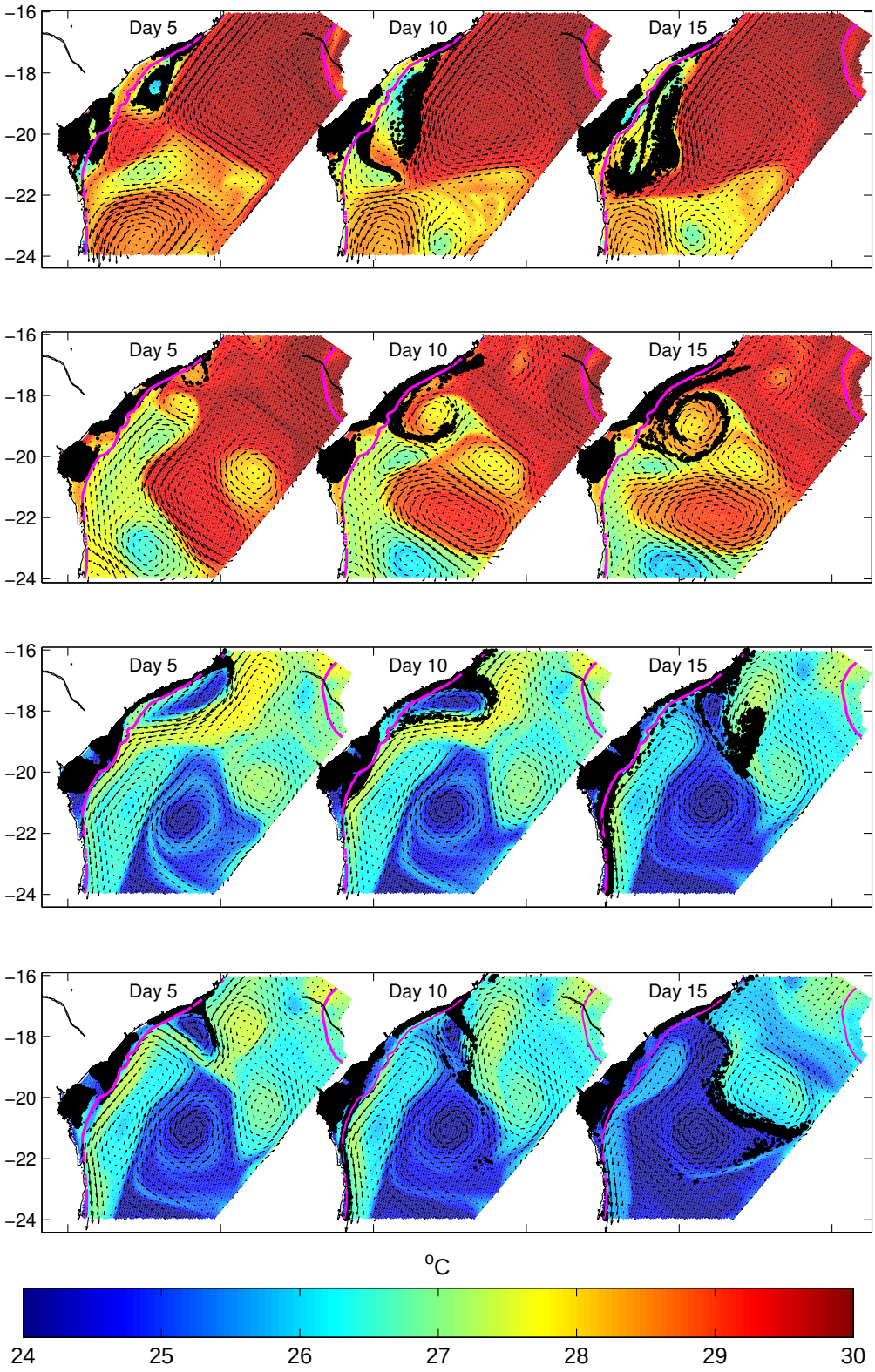

Figure D.2: Some as Fig. D.1 but on and (A) 26 February, (B) 17 March, (C) 29 May, (D) 5 June.

Appendix E

Cross-correlation between simulated larval retention and offshore circulation

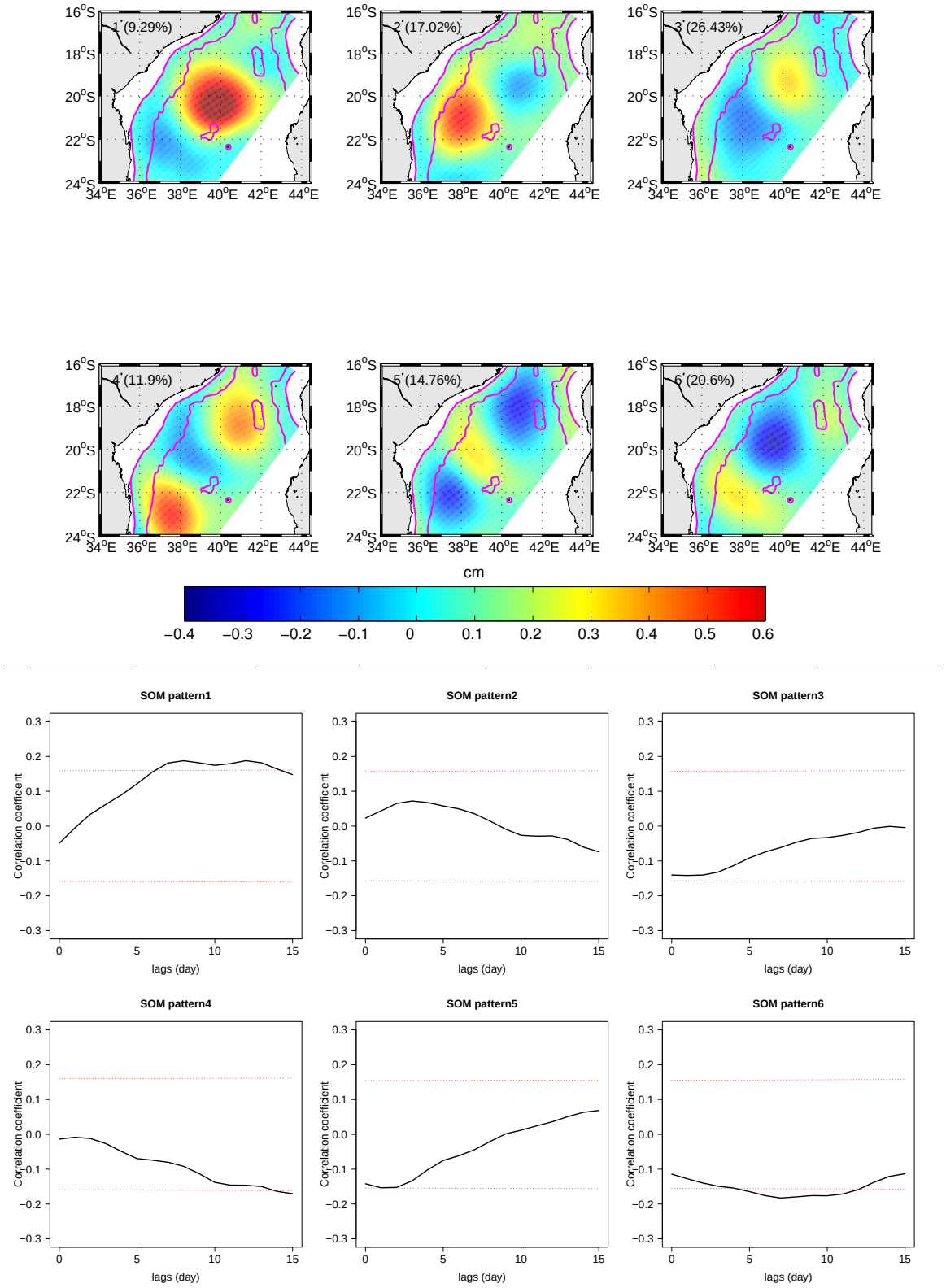

Figure E.1: (A) 2×3 SOM map for the SSH anomaly from ROMS-BSM-E2 years $4-10$. Number in the top left corner indicate the SOM pattern (unit) and the percentage the frequency of occurrence of that pattern. (B) Correlations at different lag periods (cross-correlations) for time series of simulated larval shelf retention (Fig. 5.5) and Euclidian distances to each SOM pattern. Dashed red lines indicates the 95% confidence level.

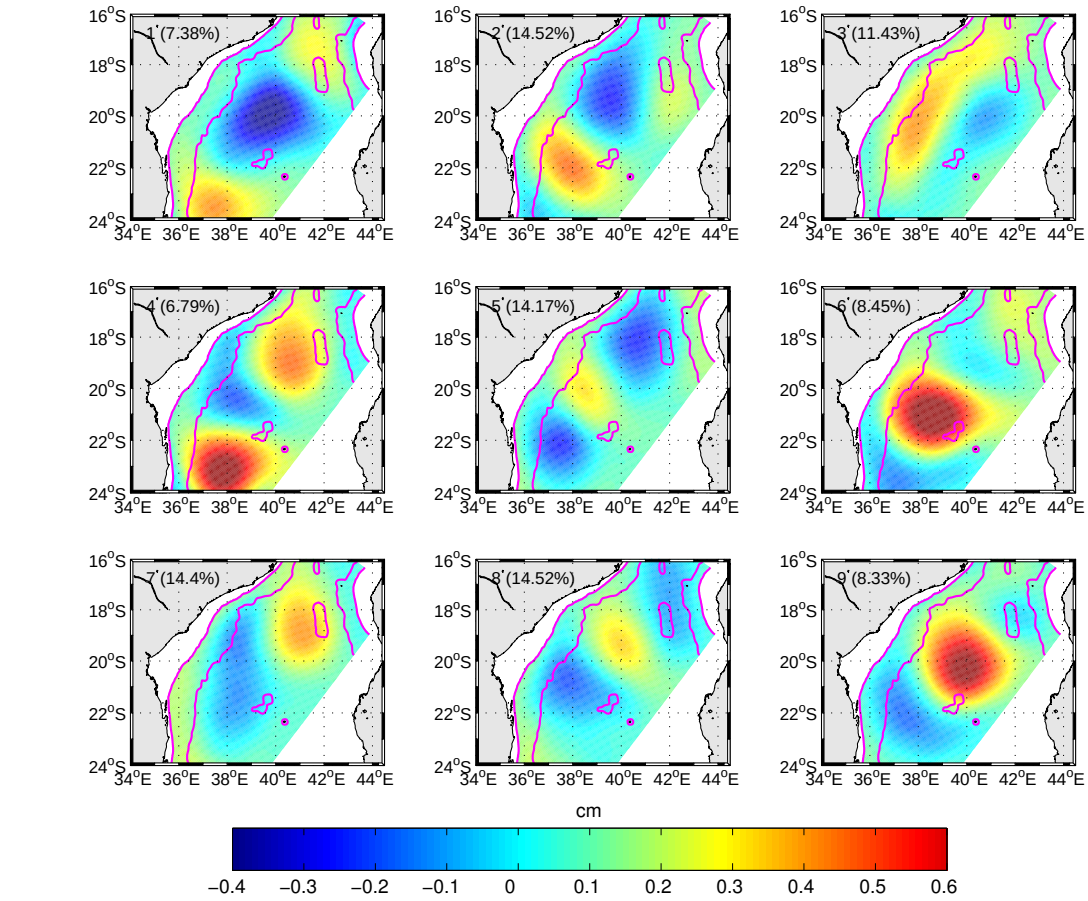

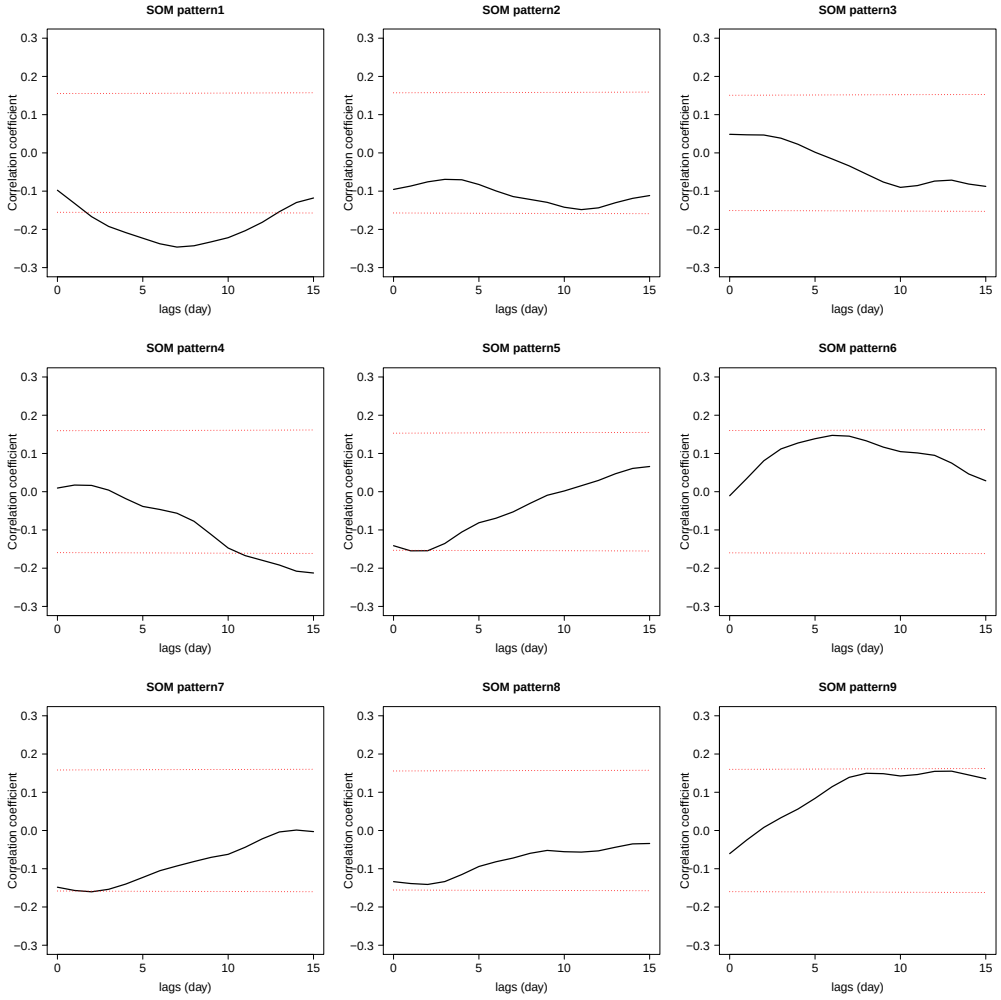

Figure E.2: Same as Fig. E.1, but for 3×3 SOM.

Appendix F

Sensitivity of simulated larval shelf retention to temporal and spatial resolution of the inputs

To test the effect of spatial and temporal resolution on simulated larval shelf retention and consequently larval settlement, three different IBM experiment configurations were developed:

Parent 3-day – Consisted of Ichthyop coupled with ROMS Parent grid with tides at 3-day averaged outputs (ROMS-BSM-E3, Chapter 3). Successful simulated larval destination used here is shelf retention. Eggs were released every three days for one year and their trajectories tracked for 15 days.

Child 3-day – Same as Parent 3-day experiment, but coupled with ROMS Child grid.

Child hourly – Same as Child 3-day experiment, but using hourly averaged ROMS outputs.

A set of three simulated shelf retention experiments using different spatial (2 vs. 6 km) and temporal (1−hour vs. 3−day) resolutions (Fig. F.1A) resulted in significantly different mean percentage of shelf retention (analysis of variance: $DF = 2, 342$, $F = 61.9$, $p < 0.001$). Post-hoc Tukey tests showed that there were significant differences across all three experiments (Fig. F.1b). Although significantly different, increasing spatial resolution from 6 km (Parent grid) to 2 km (Child grid) only resulted in slightly lower simulated shelf retention (Fig. F.1A). A larger change in simulated shelf retention occurred when increasing the input temporal resolution from every three days to every hour. Increasing both spatial and temporal resolution of the ROMS inputs resulted in a consistent diminution of the simulated larval shelf retention throughout the

time series. Although simulated levels of shelf retention were different in the three experiments, patterns of successive peaks and troughs along the timeseries were similar, suggesting a similar influence of eddies on shelf retention in the three experiments.

(A)

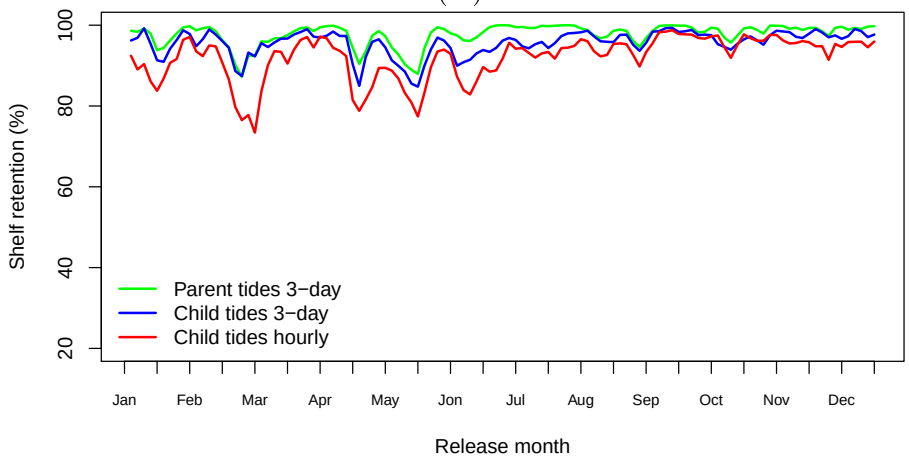

(B)

Simulation	Parent 3-day (98%)	Child 3-day (96%)	Child 1-hourly (92%)
Parent 3-day		< 0.001	< 0.001
Child 3-day	< 0.001		< 0.001
Child 1-hourly	< 0.001	< 0.001	

Figure F.1: (A) Comparison between simulated shelf retention from different ROMS spatial and temporal resolutions at: 6 km and every 3−day (Parent 3−day), 2 km and every 3−day (Child 3−day) and 2 km and every 1−hour (Child 1−hour). (B) Post-hoc Tukey test from ANOVA comparisons on the three experiments. Red values indicate significant differences ($P < 0.05$).

Appendix G

Simulation experiment without diffusion

When horizontal diffusion was removed from the reference simulation (Fig. G.1) there was a significant difference in the mean larval successful settlement (t-test: $t_{228} = 1.26$, $p < 0.001$), with decreased mean percentage for the experiment without diffusion (12%) compared with that with diffusion (18%). The larval settlement without diffusion was consistently less than with diffusion throughout the time series (Fig. G.1A). There was a positive, strong and significant linear correlation ($r_{113} = 0.9$, $p < 0.001$) between the time series with and without diffusion. The larval settlement without diffusion shows a fluctuation similar to that with diffusion, with the trough and peaks occurring simultaneously in the two time series (Fig. G.1A).

The density map of the origin of the successfully settled larvae for the experiment without diffusion shows high values in the inshore region along the entire coast and low values were found offshore (Fig. G.1B). There was nearly zero density on the offshore edge of the central release area and no density was observed offshore to the south of 19°S (Fig. G.1B). The latitudinal distribution of larval successful settlement without diffusion shows three peaks in which the number of larvae declined from high in the north to low in the south (Fig. G.1C). There was almost no settlement at the two southernmost latitude bins. Fig. G.1D shows three main region (northern, central and southern) of high density of successfully settled larvae without diffusion for larvae released from all nine and from five release areas. For larvae released just from the northern (label N) or from the central (label C) or on the southern (label S) release areas, successfully settled larvae were found limited to the vicinity of the respective release areas.

Negative differences in the origin of the successfully settled larvae between the experiments with and without diffusion were observed all over the bank except in the south (Fig. G.1E). Large differences were mostly found offshore and to the south whereas low differences were found to the north and inshore, particularly in the central region. There were negative differences in larval successful settlement between the two experiments (Fig. G.1F and G). These differences were always more that 20% and large on the central and southern Sofala Bank.

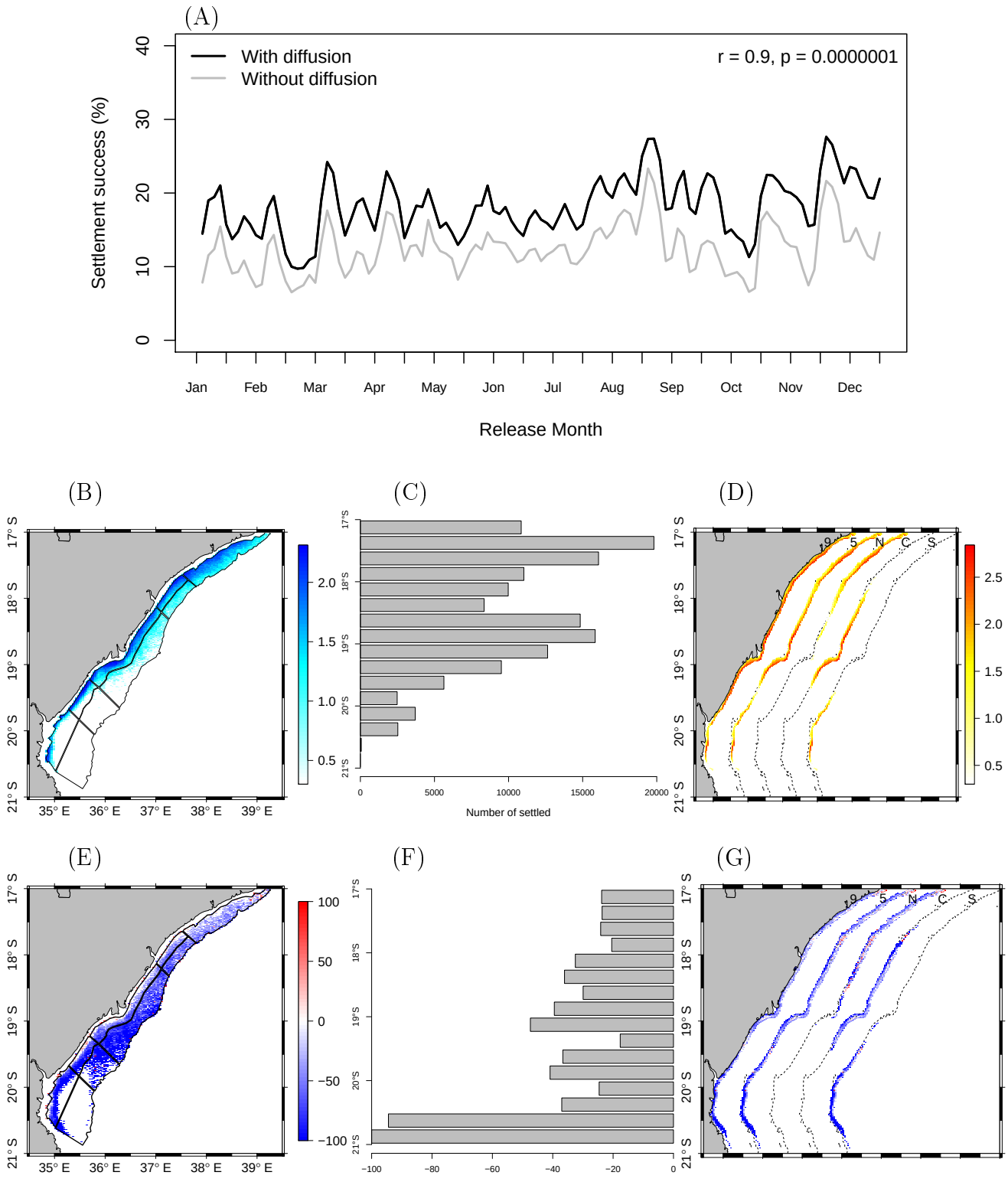

Figure G.1: Effect of horizontal diffusion on simulated larval settlement (A) comparison between time series of larval settlement with (Reference) and without diffusion. (B) Density map of the origin of the successfully settled larvae from all nine release areas. (C) Settled latitude every 0.25° between 17−21°S from all nine release areas. (D) Density map of the larvae successful settlement from different release areas: 9 for all nine releases areas, 5 for the actual spawning areas including the offshore version, N for the northern release areas, C for the central release areas and S for the southern release areas. (E), (F) and (G) same as (B), (C) and (D), respectively, but for relative difference (%) between the experiment without and with diffusion.